Synthèse et formulation d'encres polymères pour couche active de cellules solaires organiques

Laurie Parrenin

université de BORDEAUX

THÈSE PRÉSENTÉE

POUR OBTENIR LE GRADE DE

DOCTEUR DE

L'UNIVERSITÉ DE BORDEAUX

ÉCOLE DOCTORALE DES SCIENCES CHIMIQUES

SPÉCIALITÉ : Polymères

Par Laurie PARRENIN

Synthèse et formulation d'encres polymères pour la couche active de cellules solaires organiques

Sous la direction de : Dr Éric CLOUTET et Prof. Georges HADZIIOANNOU

Soutenue le 14 octobre 2016

Membres du jury :

Dr SCHMITT Véronique, CRPP, Université de Bordeaux	Président
Dr BOURGEAT-LAMI Elodie, C2P2, CPE Lyon	Rapporteur
Dr REYNAUD Stéphanie, IPREM/EPCP, Université de Pau et des Pays de l'Adour	Rapporteur
Dr BOURRIGAUD Sylvain, GRL, Arkema	Examinateur
Dr BROCHON Cyril, LCPO, Université de Bordeaux	Invité
Dr PAVLOPOULOU Eleni, LCPO, Université de Bordeaux	Invité

- Remerciements -

En tout premier lieu je remercie tous les membres du jury : Dr Elodie Bourgeat-Lami, Dr Sylvain Bourrigaud, Dr Cyril Brochon, Dr Eric Cloutet, Prof. Georges Hadziioannou, Dr Eleni Pavlopoulou, Dr Stéphanie Reynaud et Dr Véronique Schmitt pour avoir accepté de juger ce travail.

Je tiens à remercier les deux directeurs du laboratoire successifs Prof. Cramail et Prof. Lecommandoux pour m'avoir accueillie chaleureusement au sein du LCPO.

Mes remerciements sont ensuite tournés vers mes deux directeurs de thèse Prof. Georges Hadziioannou et Dr Eric Cloutet pour m'avoir encadrée tout en me laissant une certaine part d'autonomie, pour leurs précieux conseils, pour leur soutien et pour m'avoir permis de présenter mes travaux aux quatre coins du monde. Merci également à Cyril Brochon pour sa bonne humeur et ses conseils (scientifiques et culinaires !), ainsi qu'à Guillaume Fleury pour son aide sur les neutrons et la rédaction de publications. Je souhaite également remercier Eleni Pavlopoulou pour les nombreuses heures passées dans son bureau pour des discussions scientifiques et personnelles. Enfin merci à Luca Muccioli et Angelos Giannakopoulos pour les simulations de mes particules et leur temps.

Un immense merci à Gildas pour l'intégration de mes particules dans des cellules solaires, « quand on persiste, on finit par y arriver » ! Un grand merci à l'IMS et particulièrement à Laurence Vignau pour la caractérisation des cellules solaires.

Un grand merci à tout le personnel administratif sans qui le laboratoire ne tournerait pas rond, en particulier merci à Aude Manson, Dominique Gouzerh, Claude Le Pierres, Dominique Richard, Loïc Peltrault et bien sûr Catherine Roulinat.

Merci à toutes les personnes qui s'occupent des caractérisations, notamment Anne-Laure Wirotius pour la RMN, Gilles Pecastaing pour les nombreuses heures devant l'AFM, Gérard Dimier pour les analyses thermiques et Mélanie Bousquet pour la SEC, toute l'organisation du B8, les commandes mais par pour les croix !

Enfin merci à toutes les personnes non-permanentes, thésards et post-doc avec qui j'ai partagé ces trois années. Merci à Guillaume Garbay pour « la synthèse pour les nuls », les discussions autour de ma paillasse (et parfois la tienne, mais beaucoup la mienne !), les brainstormings autour de croissants et de PAINS AU CHOCOLAT, les voyages en conf (on a même rencontré Kanye West à Biarritz !), bref merci pour tout ! Merci à tous ceux qui ont partagé mon bureau : Anna, Yiannis, Jon, Nicoletta, Konstantinos pour votre bonne humeur et votre soutien. Merci à Dimitrios avec qui j'ai partagé le labo pour tous tes conseils. Merci à Mumtaz pour la synthèse et ton optimisme « ça va marcher » ! Merci à Najim pour toutes les formations sur les machines ainsi qu'à Mikaël pour les dispositifs.

Un grand merci au personnel du CAES qui a su me remonter le moral avec la qualité des plats du midi et bien sûr aux personnes avec qui j'ai partagé ces repas !

Merci à Camille pour les minutes potins, à Pierre pour les blagues Basques du vendredi après-midi et à Amélie pour ton soutien, tes conseils et tous les moments passés à décompresser hors labo.

Merci à ma famille, mes parents et mon frère qui m'ont toujours soutenue.

Merci à mes amies de la Yaute.

Pour finir, merci Clément pour ta présence et ton soutien indéfectible.

- Liste des abréviations -

^{1}H-RMN	Résonance magnétique nucléaire du proton
AFM	Microscopie à Force Atomique
Ag	Argent
Al	Aluminium
BHJ	Bulk-heterojunction ou hétéro-jonction volumique
Ca	Calcium
c-AFM	Microscopie à Force Atomique conductrice
$CDCl_3$	Chloroforme deutéré
$CHCl_3$	Chloroforme
CMC	Concentration micellaire critique
Đ	Dispersité
DLS	Diffusion dynamique de la lumière
Eg	Energie de la bande interdite
EtOH	Ethanol
FF	Facteur de forme
FTIR	Infra-rouge par Transformée de Fourier
GRIM	Métathèse de Grignard
HO	Orbitale moléculaire la plus haute occupée
ITO	Oxyde d'indium-étain
J_{sc}	Courant de court-circuit
M_n	Masse molaire moyenne en nombre
MoO_3	Oxyde de Molybdène
M_w	Masse molaire moyenne en masse

$Ni(dppp)Cl_2$	1,3-bis(diphenylphosphino)propane dichloronickel (II)
NPs	Nanoparticules
OPV	Photovoltaïque Organique
$PC_{71}BM$	[6,6]-phenyl C_{71} butyric acid methyl ester ($PC_{71}BM$)
PCDTBT	Poly(N- 9'-heptadecanyl-2,7-carbazole-alt-5,5-4,7-di-2-thienyl-2',1',3'-benzothiadiazole) (PCDTBT)
PCE	Rendement de conversion énergétique
$Pd(PPh_3)_4$	Tetrakis(triphenylphosphine)palladium(0))
PL	Photoluminescence
PVP	Poly(N-vinylpyrrolidone)
RI	Détécteur réfractométrique
R_s	Résistance en série
R_{sh}	Résistance en parallèle (« shunt »)
SANS	Diffusion des Neutrons aux Petits Angles
SDS	Sodium Dodecyl Sulfate
SEC	Chromatographie d'exclusion Stérique
^{t}BuOK	*Tert* Butoxyde de Potassium
TEM	Microscopie à Transmission Electronique
T_g	Température de transition vitreuse
TGA	Analyse Thermo-Gravimétrique
THF	Tetrahydrofurane
UV-vis	Spectroscopie ultra-violet-visible
V_{oc}	Tension de circuit ouvert
Wt%	Pourcentage massique
ZnO	Oxyde de zinc

- Table des matières -

Introduction générale

La société est confrontée à une crise énergétique majeure qui ne cesse de s'accentuer depuis de nombreuses années. Les énergies fossiles comme le pétrole, le gaz et le charbon, se raréfient tandis que la demande mondiale en énergie n'a jamais été aussi forte et continue de croitre. Les dernières estimations prévoient ainsi que cette dernière devrait doubler d'ici à 2050, passant de 13 000 à 26 000 GW. Les énergies fossiles sont de nos jours indispensables, puisqu'elles assurent 85% des besoins mondiaux en énergies primaires. Malheureusement elles présentent de nombreux inconvénients comme leur coût en constante augmentation mais aussi et surtout la pollution qui est engendrée par la combustion du pétrole et du charbon produisant du dioxyde de carbone libéré dans l'atmosphère. Leur exploitation participe donc à l'accroissement de l'effet de serre et de toutes ses conséquences (fonte des glaces, inondations, cyclones etc..).

Sans abandonner le questionnement du nucléaire il convient d'assurer les futurs besoins énergétiques de notre société et de développer des sources d'énergie alternatives plus respectueuses de l'environnement et peu couteuses.

L'énergie solaire semble être une solution adaptée en raison de ses nombreux avantages comme son caractère inépuisable et son abondance qui témoignent de son fort potentiel. En effet, l'énergie solaire frappant la surface de la Terre en deux heures (soit 640 EJ) est supérieure à la consommation énergétique mondiale de l'année 2016 de toutes sources confondues.[1] Des panneaux photovoltaïques permettraient ainsi d'exploiter ce fort potentiel en transformant cette énergie solaire en électricité.

Le premier panneau solaire, d'un rendement de 6% déjà prometteur, a été fabriqué par les laboratoires Bell Telephone en 1954. Les nombreux efforts de recherches ont permis par la suite d'atteindre des rendements de l'ordre de 25% en employant notamment le silicium comme matériau photoactif. Ce dernier est utilisé dans la plupart des panneaux solaires actuels. Il a cependant de nombreux inconvénients, le plus important étant son coût de fabrication ainsi que l'utilisation de procédés peu respectueux de l'environnement liés à sa purification et à sa mise en œuvre.

Parmi les alternatives au silicium, les cellules solaires organiques offrent de nombreux avantages en termes de coût et de fabrication (comme la possibilité de travailler en solution et donc en impression) mais aussi en raison de leur légèreté et flexibilité.

L'efficacité de conversion de l'énergie solaire en électricité des cellules organiques reste à l'heure actuelle bien moindre comparée à celle obtenue pour les cellules inorganiques mais les progrès croissants de la recherche dans ce domaine afin de combler ce retard sont encourageants. En effet l'efficacité de conversion a augmenté de 0,001%[2] en 1975 à 1%[3] en 1986 et plus récemment à 13,2% en 2016 pour une cellule à multi-jonctions par la société Heliatek.[4]

La plupart des cellules solaires organiques sont composées d'une couche dite active de type hétérojonction en volume avec un mélange entre un matériau donneur d'électrons (le plus souvent un polymère semi-conducteur) et un matériau accepteur d'électrons (le plus souvent un dérivé du fullerène) prise en « sandwich » entre deux électrodes.

La plupart du temps, une séparation de phase entre les deux matériaux (donneur et accepteur d'électrons) est observée menant à des domaines riches en donneurs d'électrons et des domaines riches en accepteurs d'électrons au sein de la couche active. La taille de ces domaines doit être proche de la longueur de diffusion d'un exciton (l_D) afin de minimiser la recombinaison des charges.

Habituellement les deux matériaux sont mélangés dans un bon solvant (qui est capable de solubiliser les deux espèces) et la solution ainsi fabriquée est déposée sur un substrat. Après évaporation du solvant, un film est formé constituant ainsi la couche active de la cellule. Le problème majeur de l'industrie du photovoltaïque concerne le processus de fabrication de ce type de cellule puisqu'il fait intervenir des solvants toxiques et inflammables, le plus souvent chlorés et/ou aromatiques. En effet les polymères conjugués, utilisés dans les cellules OPV (Organic PhotoVoltaic), ne sont quasiment solubles que dans ces solvants.[5] Une étude lancée par ProcessOne montre que 16 millions de litres de chlorobenzène sont nécessaires pour produire 1 GW d'une cellule solaire.[6] Ces chiffres ne peuvent qu'appuyer la tendance actuelle à se tourner vers la chimie « verte » et des solutions alternatives. Pour le moment l'application des cellules solaires organiques à grande échelle (correspondant à quelques GW) n'est donc pas une approche viable et l'utilisation de solvants alternatifs est plus que nécessaire.[7]

Les solutions envisagées pour contourner ces difficultés sont d'une part l'augmentation de la solubilité des matériaux utilisés en solvants non-halogénés/non-

aromatiques tels que eau ou alcools *via* l'adjonction de chaînes solubilisantes le long du squelette π-conjugué[7–9] et d'autre part la préparation de ces polymères sous forme de dispersions colloïdales en milieux non toxiques/non polluants. C'est dans le contexte de développement d'encres de polymères semi-conducteurs destinées à être enduites pour la fabrication grande échelle de cellules photovoltaïques que se situent ces travaux de thèse. En fait, cette thèse est intégrée de façon plus large dans un projet de site aquitain coordonné par Arkema, à savoir le projet ISOCEL (Innovative Solar CELls) soutenu par l'ADEME. Ce projet regroupe de nombreux acteurs académiques et industriels de différentes filières complémentaires et a pour but de mettre en place une filière industrielle de modules photovoltaïques compétitive et durable.

Le premier chapitre de ce manuscrit est consacré à une recherche bibliographique sur les différentes voies envisagées pour préparer et mettre en forme les polymères semi-conducteurs, essentiellement pour des applications cellules solaires organiques.

Le deuxième chapitre portera sur la synthèse d'un polymère à faible largeur de bande (le PCDTBT : poly[N-9'-heptadecanyl-2,7-carbazole-*alt*-5,5-4,7-di-2-thienyl-2',1',3'-benzothiadiazole]) par polycondensation (couplage de Suzuki) en dispersion en milieu alcool.

La préparation de particules composites à base de PCDTBT et de molécules acceptrices d'électron telles que le $PC_{71}BM$ (un dérivé du fullerène) *via* un procédé de miniemulsion post-polymérisation sera quant à elle décrite dans le troisième chapitre.

Ces mêmes particules composites ont été obtenues en utilisant un copolymère à blocs de type P3HT-*b*-PEO comme stabilisant stérique et seront décrites dans le chapitre 4.

De manière plus exploratoire le dernier chapitre sera dédié à la technique de nanoprécipitation pour préparer ce même système PCDTBT:$PC_{71}BM$ en l'absence de stabilisant.

Nous avons choisi de présenter tous les chapitres en anglais en vue de leur soumission sous forme de publications. Quant à la partie expérimentale, celle-ci est décrite à la fin de chaque chapitre.

References

[**1**] J. Tsao, N. Lewis, G. Crabtree, *Solar FAQ's: US Department of Energy*, **2006**.

[**2**] C. W. Tang, A. C. Albrech, *J. Chem. Phys.*, **1975**, *62*, 2139.

[**3**] C. W. Tang, *Appl. Phys. Lett.*, **1986**, *48*, 183.

[**4**] Heliatek, "Heliatek record efficiency," can be found under http://www.heliatek.com/en/heliafilm/technical-data, **2016**.

[**5**] T. R. Andersen, T. T. Larsen-Olsen, B. Andreasen, A. P. L. Böttiger, J. E. Carlé, M. Helgesen, E. Bundgaard, K. Norrman, J. W. Andreasen, M. Jørgensen, *ACS Nano*, **2011**, *5*, 4188.

[**6**] T. R. Andersen, T. T. Larsen-Olsen, B. Andreasen, A. P. L. Böttiger, J. E. Carlé, M. Helgesen, E. Bundgaard, K. Norrman, J. W. Andreasen, M. Jørgensen, F. C. Krebs, *ACS Nano*, **2011**, *5*, 4188.

[**7**] R. Søndergaard, M. Helgesen, M. Jørgensen, F. C. Krebs, *Adv. Energy Mater.*, **2011**, *1*, 68.

[**8**] M. Chayer, K. Faïd, M. Leclerc, *Chem. Mater.*, **1997**, *9*, 2902.

[**9**] F. Tran-Van, M. Carrier, C. Chevrot, *Synth. Met.*, **2004**, *142*, 251.

Chapitre I
Eco-conception de polymères π-conjugués

- Liste des abréviations du chapitre I -

AA	*p*-anisaldehyde
ACN	Acetonitrile
ADMET	Acyclic Diene METathesis
Ag	Argent
Al	Aluminium
AM	Nombre d'air masse
BC	Bande de conduction
BHJ	Bulk-heterojunction ou hétéro-jonction volumique
BV ou LUMO	Orbitale moléculaire la plus basse vacante
Ca	Calcium
c-AFM	Microscopie à Force Atomique conductrice
CB	Chlorobenzène
CTAB	Hexadecyl triethylammonium bromide
DIO	Diiodooctane
DMF	Dimethylformamide
DMN	1,2-dimethyl-naphtalene
DMSO	Dimethylsulfoxyde
DPP	Diketopyrrolopyrrole
DPP-SVS	Poly(diketopyrrolopyrrole-selenophene vinylene selenophene)
DTAC	Dodecyltrimethylammonium chloride
Eg	Energie de la bande interdite
EQE	Efficacité quantique externe
EtOH	Ethanol

F8BT	Poly(9,9'-dioctylfluorene-*co*-bis-N,N'-(4-butylphenyl)-bis-N,N'-phenyl-1,4 phenylenediamine) (PFB) and poly(9,9-dioctylfluorene-co-benzothiadiazole)
F8EDOT	Poly[(9,9-dioctylfluorenyl-2,7-diyl)-alt-(3,4-ethylenedioxythiophene-2,5-diyl)]
F8TMT2	Poly[(9,9-dioctylfluorenyl-2,7-diyl)-alt- (3,3',4,4'-tetrametylbithiophene-2,5'-diyl)]
FF	Facteur de forme
HO ou HOMO	Orbitale moléculaire la plus haute occupée
ICBA	Indene-C_{60} bisadduct
IQE	Efficacité quantique interne
ITO	Oxyde d'indium-étain
J_{sc}	Courant de court-circuit
Me-LPPP	Methyl substituted ladder-type poly(*p*-phenylene)
MeOH	Méthanol
NPs	Nanoparticules
o-DCB	*ortho*-dichlorobenzene
OFET	Transistor Organique à Effet de Champs
OLED	Diode électroluminescente organique
OPV	Photovoltaïque Organique
P2VP	Poly(2-vinylpyridine)
P3DDUT	Poly[3-[2-(N-dodecylcarbamoyloxy)ethyl]thiophene-2,5-diyl]
P3HT	Poly(3-hexylthiophene)
P3HT-*b*-PEO	Poly(3-hexylthiophene)-*block*-poly(ethyleneoxide)
PBDPP	Poly(benzodithiophène-diketopyrrolopyrrole)
$PC_{71}BM$	[6,6]-phenyl C_{71} butyric acid methyl ester ($PC_{71}BM$)
PCBM	[6,6]-Phenyl C_{61} butyric acid methyl ester

PCDTBT	Poly(N- 9'-heptadecanyl-2,7-carbazole-alt-5,5-4,7-di-2-thienyl-2',1',3'-benzothiadiazole) (PCDTBT)
PCE	Rendement de conversion énergétique
PCz-DTBTA	Poly[(N-90-heptadecanyl-2,7-carbazole)-alt-(4,7-bis(20-thienyl)-2-dodecyl-2,1,3-benzotriazole)](PCz-DTBTA),
$Pd(PPh_3)_4$	Tetrakis(triphenylphosphine)palladium(0))
$PdCl_2$	1,3-bis[2,6-bis-(diphenylmethyl)-4-methylphényl]imidazole-2-ylidène)
PDPPNBr	Poly[2,5-bis(2-octyldodecyl)-3,6-bis(thiophen-2-yl)-pyrrolo[3,4-c]pyrrole-1,4-dione-alt-2,5-bis[6-(N,N,N-trimethylammonium)hexyl]-3,6-bis(thiophen-2-yl)-pyrrolo[3,4-c]pyrrole-1,4-dione]
PDPP-TNT	Poly{3,6-dithiophene-2-yl-2,5-di(2-octyldodecyl)-pyrrolo [3,4-c] pyrrole-1,4-dione-alt-naphthalene}
PDTP-DFBT	Poly[2,7-(5,5-bis-(3,7-dimethyloctyl)-5H-dithieno[3,2-b:2',3'-d]pyran)-alt-4,7-(5,6-difluoro-2,1,3-benzothiadiazole)]
PDTSTPD	Poly[(5,6-dihydro-5-octyl-4,6-dioxo-4*H*-thieno[3,4-*c*]pyrrole-1,3-diyl)[4,4-bis(2-ethylhexyl)-4*H*-silolo[3,2-*b*:4,5-*b'*;]dithiophene-2,6-diyl]]
PECz-DPQx	Poly(quinoxaline-4,5-ethylene-2,7-carbazole)
PEDOT :PSS	Poly(3,4-éthylènedioxythiophène):poly(styrène sulfonate)
PEO	Poly(oxide d'éthylène)
PF	Polyfluorène
PF8BT	Poly(9,9-dioctylfluorène)
PF8BT	Poly(9,9-dioctylfluorène-*alt*-benzothiadiazole)
PF8T2	Poly(9,9-dioctylfluorène-*alt*-bithiophène)
PF8TAA	Poly-(9,9-dioctylfluorène-*alt*-4-sec-butylphényldiphenylamine)
PF-DTBTA	Poly[9,9-dioctyl-2,7-fluorène-*alt*-(4,7-bis(20-thienyl)-2-dodécyl-2,1,3-benzotriazole)]
PFDTBTP	Poly[9,9-dioctylfluorenyl-2,7-dyil-*co*-10,12-bis(thiophene-2-yl)-3,6-dioxooctyl-11-thia-9,13-diaza-cyclopenta[b]triphenylène)
PffBT4T-2OD	Poly[(5,6-difluoro-2,1,3-benzothiadiazol-4,7-diyl)-*alt*-(3,3'''-di(2-octyldodécyl)-2,2';5',2'';5'',2'''-quaterthiophen-5,5'''-diyl)]

PFFO	2,7-poly(9,9-dialkylfluorène-*co*-fluorenone)
PFN	Poly[(9,9-*bis*(3'-(N,N-diméthylamino)propyl)-2,7-fluorène)-*alt*-2,7-(9,9–dioctylfluorène)]
PIDTT-DFBT	Poly(indacenodithiophène-thieno[3,2-b]thiophène-difluorobenzothiadiazole
PL	Photoluminescence
PMMA	Poly(methacrylate de méthyle)
PPh-DTBTA	Poly[(2,5-dioctyl-1,4-phenylène)-*alt*-(4,7-bis-(20-thienyl)-2-dodécyl-2,1,3-benzotriazole)]
PPV	Poly(*p*-phénylènevinylène)
PSBTBT	Poly[(4,4'-bis(2-ethylhexyl)dithieno[3,2-*b*:2'3'-d]silole)-2,6-diyl-*alt*-(2,1,3-benzothiadiazole)-4,7-diyl]
PT	Polythiophène
PTB7	Poly[(4,8-bis[(2-éthylhexyl)oxy]benzo[1,2-*b*:4,5-b']dithiophène-2,6-diyl)(3-fluoro-2-[(2-ethylhexyl)carbonyl]thieno[3,4-*b*]thiophènediyl)]
PTB7-Th	Poly[4,8-bis(5-(2-ethylhexyl)thiophen-2-yl)benzo[1,2-b:4,5-b']dithiophène-*alt*-3-fluorothieno[3,4-b]thiophène-2-carboxy-late]
PTBT-DPP	Poly(dithienothiophene-diketopyrrolopyrrole)
PVA	Poly(alcool vinylique)
PV-*co*-PVA	Poly(1-vinylpyrrolidone-*co*-vinyl acetate)
PVP	Poly(N-vinylpyrrolidone)
PVPVA	Poly(vinyl alcool-*co*-vinyl acetate)
R_s	Résistance en série
R_{sh}	Résistance en parallèle (« shunt »)
SANS	Diffusion des Neutrons aux Petits Angles
sc-CO_2	Dioxyde de carbone supercritique
SDS	Sodium Dodecyl Sulfate
STXM	Microscope à rayons-X par balayage à Transmission
THF	Tetrahydrofurane

TiOx	Oxyde de titane
TMB	Trimethylbenzene
TNT	Trinitrotoluene
TQ1	Poly[2,3-bis-(3-octyloxyphenyl)quinoxaline-5,8-diyl-*alt*-thiophène-2,5-diyl]
TTAB	Tetradecyltrimethylammonium bromide
UV-O_3	Traitement de surface à l'ultra-violet-ozone
V_{oc}	Tension de circuit ouvert
ZnO	Oxyde de zinc

- CHAPITRE I -

Eco-conception de polymères π-conjugués

Table of Contents

I.1. Généralités sur les cellules solaires

I.1.1. Introduction

Edmond Becquerel est à l'origine de la découverte en 1839 de l'effet photovoltaïque en constatant l'apparition d'un courant électrique entre deux bornes plongées dans une solution électrolytique sous exposition lumineuse. Plus d'un siècle plus tard, les laboratoires *Bell Telephone* réalisent la première cellule solaire photovoltaïque à base de silicium. Les progrès s'enchaînent alors et permettent rapidement d'utiliser cette technologie dans de nombreux objets de la vie courante nécessitant une faible puissance comme les calculatrices par exemple.

Les cellules les plus courantes sont de nature inorganique dont l'efficacité de conversion de l'énergie solaire en électricité est très bonne. Ainsi les cellules photovoltaïques basées sur le silicium cristallin, largement plébiscitées pendant de nombreuses années et représentant encore actuellement près de 90% des ventes, permettent une conversion de l'ordre de 25 % et un temps de vie de ces panneaux jusqu'à 20 ans.[1] Malheureusement, leur coût de fabrication est très élevé et leur fabrication requiert des conditions très peu respectueuses de l'environnement, comme par exemple de chauffer jusqu'à 1100°C.[2]

Des recherches ont donc été menées afin de trouver des solutions alternatives à ces cellules « traditionnelles » telles que des composés organiques comme agents photoactifs. De telles cellules organiques offrent des perspectives intéressantes en raison de leur fort coefficient d'absorption. Ce dernier permet ainsi d'utiliser une plus faible épaisseur de film pour absorber la lumière par rapport au silicium. Cette propriété ouvre la voie au développement de dispositifs flexibles ultrafins, au coût de fabrication réduit et offrant une plus grande légèreté.[3,4] Il est alors possible d'envisager le développement de produit nomades en intégrant par exemple ces systèmes à des vêtements ou dans des vitrages.

I.1.2. Les cellules solaires photovoltaïques organiques

La découverte en 1977 des polymères π-conjugués par Shirakawa, MacDiarmid et Heeger a révolutionné l'industrie des semi-conducteurs.[5] Ces nouveaux matériaux innovants combinent à la fois les propriétés des semi-conducteurs mais aussi les propriétés mécaniques et chimiques plus polyvalentes liées aux polymères.

Une cellule solaire photovoltaïque organique comprend une couche dite active (qui absorbe la lumière du soleil) prise en sandwich entre deux électrodes. Les électrodes doivent être conductrices pour permettre le transport des charges (les électrons et les trous) et l'une des deux doit être transparente pour laisser passer la lumière du soleil vers la couche active. L'oxyde d'indium-étain (ITO) par exemple remplit très bien ces deux conditions. Des métaux tels que le calcium (Ca), l'aluminium (Al) ou encore l'argent (Ag) sont principalement utilisés pour l'autre électrode.

Une cellule contient souvent plus de trois couches où des couches interfaciales améliorent le transport des charges et les contacts électriques avec les électrodes. Les matériaux les plus utilisés sont le poly(3,4-éthylènedioxythiophène):poly(styrène sulfonate) (PEDOT :PSS) ou encore les oxydes métalliques (Zn, Ti, Mo etc…).

Dans ce chapitre nous ne considérons que des polymères ou molécules organiques à squelette π-conjugué comme matériaux photoactifs pour la couche principale des dispositifs. Les critères de bon fonctionnement de ces dispositifs sont abordés ci-après.

I.1.3. Fonctionnement d'une cellule solaire organique

I.1.3.1 L'effet photovoltaïque

Lors d'une première étape, la lumière du soleil pénètre dans la cellule par l'électrode transparente. Le matériau actif absorbe alors des photons conduisant au transfert d'un électron de l'orbitale moléculaire la plus haute occupée (HO ou HOMO) vers l'orbitale moléculaire la plus basse vacante (BV ou LUMO) laissant un trou dans sa HO (étape 1 figure 1 et 2). Cette paire électron-trou, appelée exciton est liée par interaction électrostatique.

Cet exciton peut être dissocié si un second matériau dont les niveaux HO (HOMO) et BV (LUMO) sont plus bas que le premier est présent. Le plus souvent il s'agit d'un dérivé du

fullerène. La dissociation de l'exciton est la deuxième étape qui consiste au passage de l'électron du niveau BV (LUMO) du premier matériau vers le niveau BV (LUMO) du second (étape 3 figure 1 et 2). On appelle donneur d'électron le premier matériau et accepteur d'électron le second.

Les excitons peuvent diffuser à travers le matériau sur une longueur d'environ 10-20 nm pour les polymères[6] (longueur de diffusion d'un exciton l_D). Pour les matériaux organiques, l'exciton ne peut se dissocier qu'à l'interface donneur / accepteur (étape 2 figure 2) ; il faut donc que l'exciton soit généré à une distance de l'interface inférieure à la longueur de diffusion pour qu'il y ait dissociation.

Les électrons et les trous sont ensuite conduits vers la cathode et l'anode respectivement (étape 4 figure 1 et 2). Les métaux des électrodes se doivent d'être bien choisis pour que les niveaux de Fermi de la cathode et de l'anode soient respectivement proches les niveaux HO (HOMO) du donneur et BV (LUMO) de l'accepteur respectivement afin de limiter la barrière énergétique que les porteurs de charges doivent franchir.

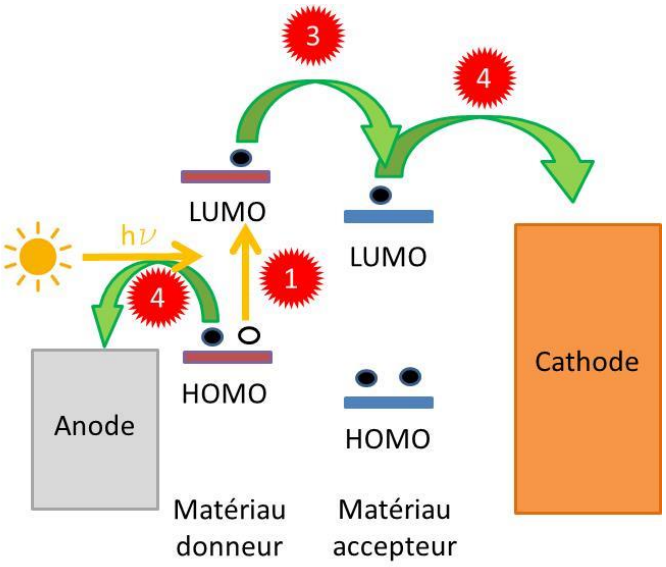

Figure 1 : Schéma des transferts d'électrons et de trous lors d'une absorption lumineuse hv. Les principales étapes sont : la création d'un exciton (1), la séparation de l'exciton (3) et le transport des porteurs de charges aux électrodes (4)

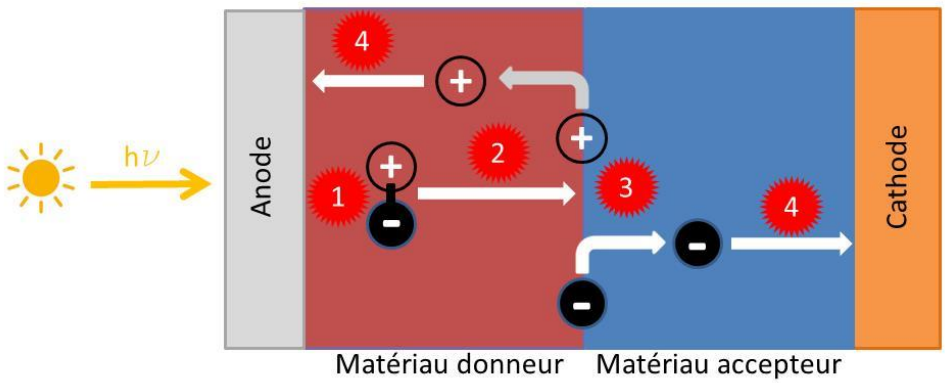

Figure 2 : Schéma de l'interface donneur/accepteur d'électrons mettant en jeu des transferts de charges après absorption lumineuse hv. Les principales étapes sont : la création d'un exciton (1), la diffusion de l'exciton vers une interface (2), la séparation de l'exciton (3) et le transport des porteurs de charges aux électrodes (4).

I.1.3.2 Les caractéristiques d'une cellule

La figure 3 représente la courbe caractéristique de la densité de courant en fonction de la tension (V) d'une cellule solaire sous illumination. Les courbes courant-tension permettent de définir les paramètres photovoltaïques caractéristiques de la cellule comme le courant de court-circuit (J_{sc}), la tension de circuit ouvert (V_{oc}) et le facteur de forme (FF). Les résistances en parallèle (« shunt » R_{sh}) et en série (R_s) peuvent aussi être définies comme l'inverse de la pente en V=0 et J=0 respectivement.[7–9]

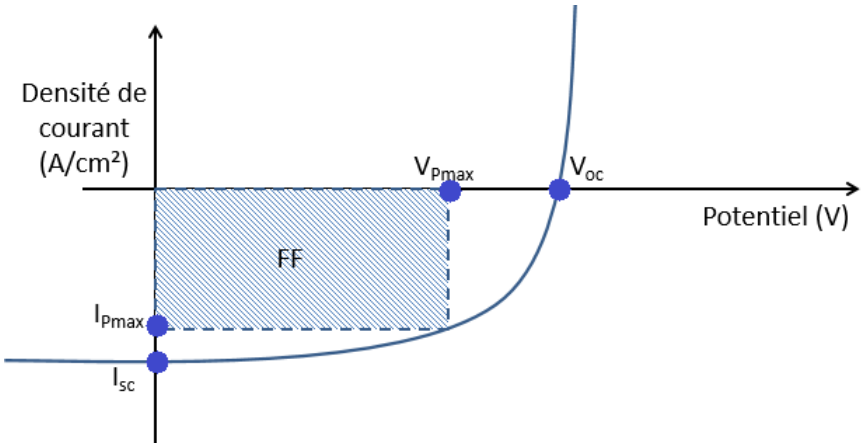

Figure 3 : Courbe courant-tension d'une cellule photovoltaïque sous illumination

Le courant de court-circuit (J_{sc}) correspond au courant maximum qui passe dans le dispositif sous illumination quand la tension est nulle. Il est lié à la mobilité et à la durée de vie des porteurs de charges.[10]

La tension en circuit-ouvert (V_{oc}) est la tension maximale que peut produire un dispositif à courant nul. Elle dépend de la différence entre la HO (HOMO) du donneur et la BV (LUMO) de l'accepteur.[11]

La résistance en parallèle (R_{sh}) est liée à la perte des charges par piégeage ou recombinaison.

La résistance en série (R_s) traduit la résistance de la couche active et la résistance de contact entre les électrodes et la couche active.[12]

Le facteur de forme (FF) permet d'évaluer la qualité de la cellule en comparant la plus grande collection de charges possible pour une cellule parfaite par rapport à la quantité de charges réellement collectées. Ce facteur traduit la compétition entre le transport des charges et leur recombinaison.[13]

$$FF = \frac{I_{Pmax} V_{Pmax}}{I_{sc} V_{oc}}$$

L'efficacité de conversion (ou rendement η) est défini comme le rapport entre la puissance maximale délivrée par la cellule ($I_{Pmax} V_{Pmax}$) et la puissance lumineuse incidente (P_{in}).

$$\eta = \frac{FF\ V_{oc} I_{sc}}{P_{in}}$$

Pour obtenir la courbe figure 3, les cellules sont mises à la lumière d'un simulateur solaire d'une masse d'air de 1,5 ce qui correspond à la lumière reçue du soleil à notre latitude, la puissance est alors égale à 100 mW/m².[14] En effet, la couche d'ozone absorbe une certaine partie du rayonnement solaire. Ainsi, le rayonnement solaire au sol n'est pas le même sur toute la surface de la planète et dépend de l'épaisseur d'atmosphère traversée.

I.1.4. Vers l'utilisation de solvants non-halogénés/non-aromatiques

Comme nous l'avons vu précedemment, les cellules solaires photovoltaïques organiques offrent de nombreux avantages par rapport aux cellules « traditionnelles ». Toutefois, le principal frein à leur industrialisation est l'utilisation de solvants chlorés et/ou aromatiques qui sont toxiques et inflammables. L'objet de l'étude bibliographique qui suit est de répertorier les solutions proposées pour trouver de nouveaux solvants non halogénés, pour augmenter la solubilité des matériaux utilisés dans la couche active en solvants non-halogénés/non-aromatiques et pour préparer ces polymères sous forme de dispersions colloïdales en milieux non toxiques/non polluants. En vue d'une future publication cette étude est rédigée en anglais.

I.2. Toxic solvent free processing of conjugated polymers

Main polymerization routes of conjugated polymers

Π-conjugated polymers can be synthesized by different routes: the precursor route for the synthesis of polyacetylene[15] or poly(*p*-phenylene vinylene),[16] the oxidative polymerization for the synthesis of poly(thiophene) or poly(pyrrole)[17] and the cross-coupling polymerization route which is very efficient to create a carbon-carbon bond between two molecules with the use of metallic catalyst just to quote a few.

The most common coupling reactions involve a hetero-coupling (or cross-coupling) in which one or two molecules react in the presence of a metallic catalyst in order to form a third molecule. The $Pd(PPh_3)_4$ (tetrakis(triphenylphosphine)palladium(0)) is used a lot for these reactions. Several couplings are extensively used for the synthesis of conjugated polymers : the Suzuki coupling[18] (for the synthesis of poly(*p*-phenylene)[19] or poly(fluorene) or more recently poly(N- 9'-heptadecanyl-2,7-carbazole-*alt*-5,5-4,7-di-2-thienyl-2',1',3'-benzothiadiazole) (PCDTBT) reaching 7.5% efficiency[20]), the Stille coupling[21] (for the synthesis of poly(*p*-phenylene), poly(*p*-phenylene vinylene) and poly(phenylenethiophene)[22] and more recently poly(benzodithiophene-diketopyrrolopyrrole) (PBDPP) reaching efficiency of 6.18%[23], the Heck coupling[24] (for the synthesis of poly(*p*-phenylene vinylene)[25]), the Ullmann coupling[26] (for the synthesis of poly(pyrrole)[27] and poly(thiophene)[28]), the Sonogashira coupling (for the synthesis of poly(phenyleneethylene)(PPE)[29]), the Kumada coupling[30] (for the synthesis of poly(thiophene)[31] and the Negishi coupling[32] (for the synthesis of poly(3-alkylthiophene)[33,34]). Thanks to the accomplishment of such synthetic pathways, three Professors R.F. Heck, E.-I. Negishi and A. Suzuki were awarded in 2010 receiving the Nobel prize in chemistry.[35]

Π-conjugated polymers can also be synthesized by other ways such as metal-free polymerizations via Siegrist polycondensation,[36] Wittig-Horner polycondensation,[37] Knoevenagel polycondensation[38] and the Gilch polycondensation for the synthesis of PPV[39] just to quote a few.

Main solvents used for the synthesis and processing of conjugated polymers

Solvents can be used at various stages of the semiconducting polymer life, from the synthesis, to the purification and processing into devices. Most common solvents used for the synthesis routes described above are toluene, dimethylformamide (DMF), tetrahydrofurane (THF), dimethylsulfoxide (DMSO), acetonitrile (ACN) or diethyl ether.

Semiconducting polymers usually require purification steps in order to get rid of impurities, catalysts, monomers, etc. They are often purified using Soxhlet apparatus for example to decrease the amount of metallic residues which may interfere in the polymer properties[40] and to fractionate the different molar mass which has a huge impact on the efficiencies. For example for the PCDTBT, the efficiency goes from 2.42% for a quantity of 2570 ppm of residual catalyst to 4.55% for a quantity of 0.1 ppm,[41] same for the molar mass : from 10 kDa with an efficiency of 2.26% it increases to 4.15% for 22 kDa.[42] These purification processes use extensive amount of solvents such as halogenated ones and/or aromatics that are considered as toxic for human or environment.

Later, for their integration into devices, semiconducting polymers are conditioned in solvents that allow the formation of thin films. For Organic Photovoltaic (OPV) devices, the p-type conjugated polymer as electron donor is mixed with an electron acceptor, usually a n-type fullerene derivative, into an organic solvent which allows, after deposition, the formation of an intimate blend.[7] Solvent annealing is often required to improve the morphology. Laboratory methods are now succeeding to obtain domain size around 20 nm which is close to the exciton diffusion length.[43] However these methods are not viable from an industrial point of view for several reasons.

Most of the π-conjugated polymers are usually soluble in halogenated solvents which are hazardous for human health and environment.[44] The solvents which are mostly used are chloroform, dichloromethane, chlorobenzene (CB), dichlorobenzene, trichlorobenzene because they allow the formation of thin and homogeneous films.[45] The most used being chlorobenzene and *ortho*-dichlorobenzene (*o*-DCB) because they have high boiling points, appropriate viscosity and good solubility for conjugated polymers. To achieve better efficiency, additives can also be used such as diiodooctane or chloronaphtalene.

Lab-scale coating techniques are usually drop-casting and spin-coating even if the later may lead to big material loss. Other techniques such as roll-to-roll, ink jet printing, spray coating and doctor blade were developed for large area but still put forward at industrial scale. It can be noted that whatever the process, the technician will be in contact with toxic solvents which may cause dramatic consequence on his health.[44]

Polymerization, purification and film formation process lead to the consumption of liters of toxics solvents which is not viable for the production of devices in large area.[45] Moreover these solvents do not exist in the nature so they are more expensive to produce.

The main challenge today is to transfer the lab-technologies to large-scale production, especially the substitution of chlorinated solvents by environmentally friendly solvents. The commercialization will be viable when the photovoltaic organic would be compatible with the printing manufacturing. Thus, although the researchers have made a breakthrough since the beginning of the organic solar cell, reaching now decent efficiencies for their industrialization, they have to concentrate their efforts toward the use of environmentally friendly techniques and scalable depositions.

There are several solutions to tackle this issue: finding new solvent, increasing the polymer and fullerene solubility or preparing the photoactive materials under the form of colloids as detailed here after.

Alternatives routes to handle π-conjugated polymers: use of non-halogenated solvents

There is a consensus on the replacement of chlorinated and other hazardous solvents. For instance Hansen or Hoy parameters can be a good indication for this challenge to find out which solvent could replace them. First, methylbenzene derivatives such as toluene, xylene and trimethylbenzene (TMB) were chosen because they allow similar properties than their halogenated counterpart. Moreover they are obtained by simple distillation of the crude oil and they are biodegradable. However fullerene derivatives used for solar cells are poorly soluble in them, leading to macroscopic phase separation and low efficiencies.[46] In 2011, Park *et al* used the Hansen parameter of dichlorobenzene to find a mixture of solvents which could mimic the interaction between the P3HT, the acceptor and the *o*-DCB. A mixture of mesitylene and acetophenone (80:20) led to a power cell efficiency of 3.38% versus 3.92% for the *o*-DCB.[47]

Mesitylene mixed with tetraline, anisole or xylene was used to produce ink-jet printed solar cells with PCE of 2.8% versus 3.5% for the halogenated counterpart (mixture between chlorobenzene and trichlorobenzene) for poly[9,9-dioctylfluorenyl-2,7-dyil-*co*-10,12-bis(thiophene-2-yl)-3,6-dioxooctyl-11-thia-9,13-diaza-cyclopenta[b]triphenylene) (PFDTBTP) (see figure 4).[48] Slightly improved efficiencies were achieved using *o*-xylene, 1,2,4-trimethylbenzene and 1,2-dimethyl-naphtalene (DMN) compared to devices using *o*-DCB up to 7% for poly(indacenodithiophene-thieno[3,2-b]thiophene-difluorobenzothiadiazole (PIDTT-DFBT):$PC_{71}BM$ (see figure 4).[46] Similar efficiencies were also obtained for P3HT:PCBM devices using *o*-xylene, indan and tetraline (1:1:1) which shows good performances for inkjet printing from small active area to big ones (up to 92 cm^2) compared to spin-coated layer from chlorobenzene solution.[49]

Chloronaphtalene, a well-known additive was also replaced by his non-chlorinated counterpart : methylnaphthalene and xylene as a solvent were used to spin-coat Poly[(5,6-dihydro-5-octyl-4,6-dioxo-4*H*-thieno[3,4-*c*]pyrrole-1,3-diyl)[4,4-bis(2-ethylhexyl)-4*H*-silolo[3,2-*b*:4,5-*b'*;]dithiophene-2,6-diyl]] (PDTSTPD); a 6.2% efficiency was reached with 2wt% of methylnaphthalene and 3wt% of diiodooctane (DIO) (against 7.5% for chlorinated solvents).[50] *p*-anisaldehyde (AA) was also used as eco-friendly additive using *o*-xylene as solvent enabling

to reach higher efficiencies compared to halogenated based devices. For instance PTB7/$PC_{71}BM$ based solar cells in *o*-xylene using AA as additive reached 7.4% efficiency compared to 7.0%. These results were also transposable to other low-band gap polymer such as poly[4,8-bis(5-(2-ethylhexyl)thiophen-2-yl)benzo[1,2-b:4,5-b']dithiophene-*alt*-3-fluorothieno[3,4-b]thiophene-2-carboxy-late] (PTB7-Th) which achieved 8.3% compared to 7.5%, poly[2,7-(5,5-bis-(3,7-dimethyloctyl)-5H-dithieno[3,2-b:2',3'-d]pyran)-*alt*-4,7-(5,6-difluoro-2,1,3-benzothia diazole)] (PDTP-DFBT) which achieved 4.7% compared to 4.0%, and Poly[(5,6-difluoro-2,1,3-benzothiadiazol-4,7-diyl)-*alt*-(3,3'''-di(2-octyldodecyl)-2,2';5',2'';5'',2'''-quaterthiophen-5,5'''-diyl)] (PffBT4T-2OD) which achieved 9.0% compared to 7.7% (see figure 4).[51]

Diketopyrrolopyrrole (DPP) based OPV devices were also created using a mixture of non-halogenated solvent. The innovation is the use of Dr Blade for the coating without the need of additives or postdeposition treatments. Better efficiencies from non-halogenated inks compared to those deposited from halogenated ones were obtained (6.1% for thiophene:tetralin and 5.6% for xylene:tetralin against 5.1% and 4.9% for chloroform:*o*-dichlorobenzene).[52]

PCDTBT based solar cells using non-halogenated solvents was also investigated. A mixture between acetone and carbon disulphide leads to 6.75% of efficiency which is 20% better than cells made from chlorobenzene. This is explained by an increase in holes and electron carriers mobility.[53]

DPP derivatives using a mixture of toluene and diphenyl ether reached 12.5 $cm^2.V^{-1}.s^{-1}$ for the hole mobility when integrated as OFET and 6.5% efficiency when integrated as a solar cell which was better than with halogenated solvent (5.8%).[54]

Despite all the attempts and solvent alternative in π-conjugated polymer processing and development there is still a long way to go. Beside it is noteworthy that the use of non-halogenated solvent does not necessarily mean non-toxicity, as reported by Heremans and coll.[52] This issue could be discussed elsewhere.

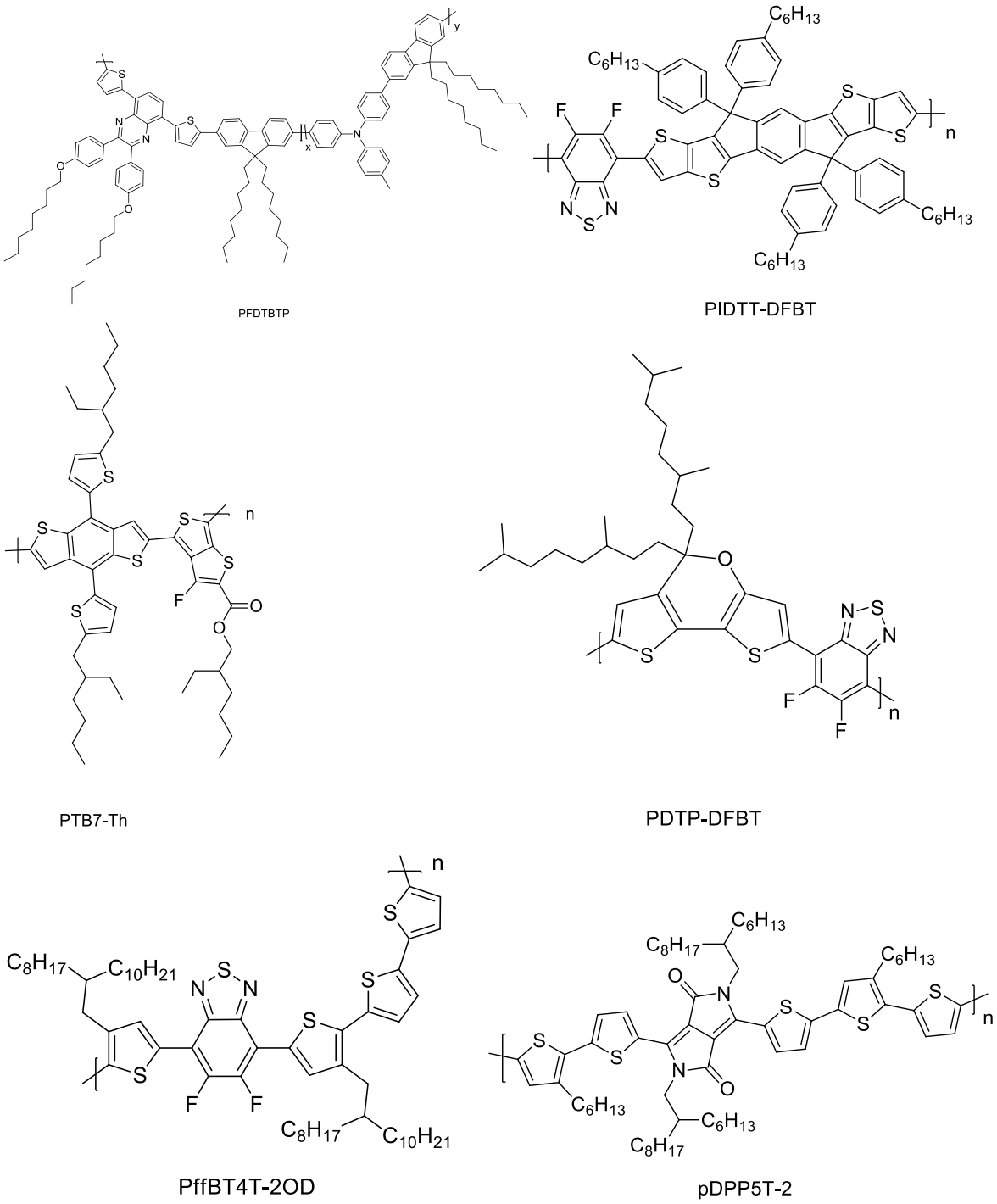

Figure 4 : Polymers used for the preparation of solar cells from non-halogenated solvents[46,48,51]

Synthesis of π-conjugated polymers in polar media

Homogeneous conditions

This part summarizes the use of ionic moieties as one approach to develop π-conjugated polymers in polar media. An ionic group such as sulfonic acid, carboxylic acid, ammonia or hydroxyl for example can be grafted onto the main backbone to allow solubility in water or alcohol of the resulting compound.

Even if very poor efficiencies have been obtained so far, poly(thiophene) has been functionalized with pendant sulfonated groups and ammonia, allowing water solubility (see figure 5). Films with these two polymers blended with modified carbon nanotubes reached an efficiency around 10^{-4} %.[55]

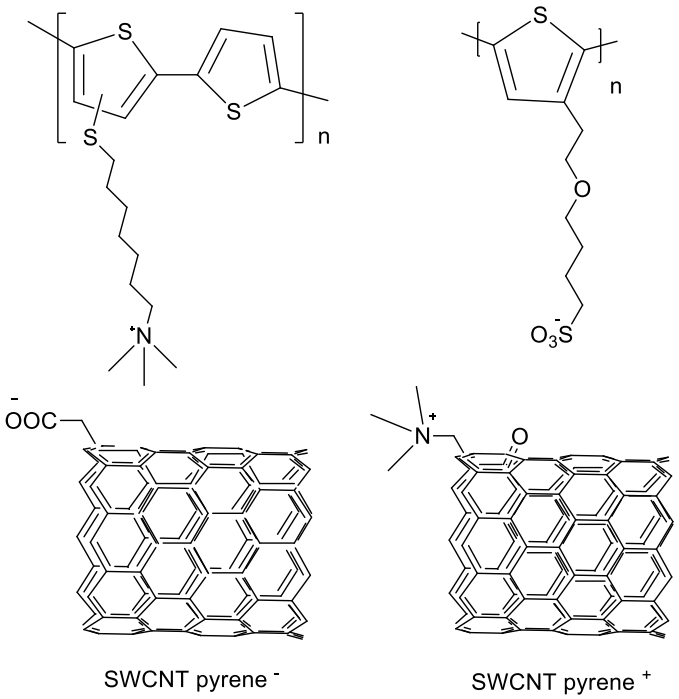

Figure 5 : Modified polythiophene and carbon nanotubes with ionic moieties for further processing in polar media[55]

Low efficiencies were also obtained in the group of Reynolds by using a mixture between several polyelectrolyte and modified Phenyl-C_{61}-butyric acid methyl ester (PCBM) in water (see figure 6). Several layers were deposited to achieve a maximum efficiency of 0.04%.[56]

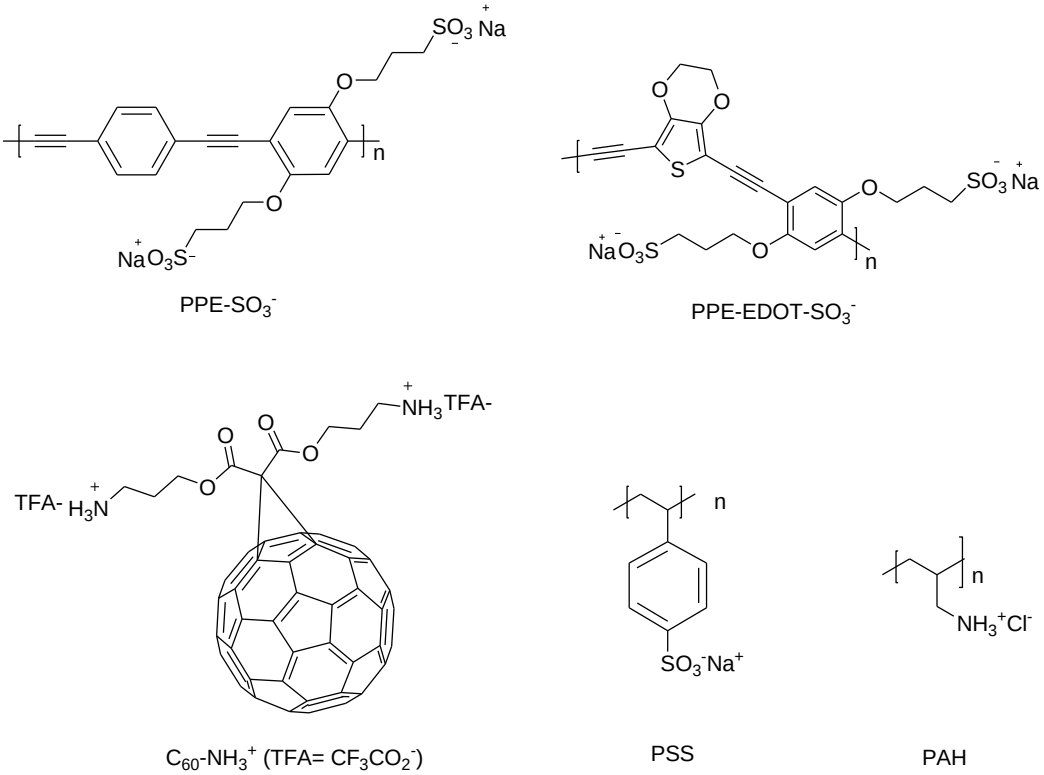

Figure 6 : Polyelectrolytes and modified PCBM synthetized by Reynolds *and coll* for further processing in water[56]

In 2011, an innovative methodology was proposed by Krebs *and coll* for the processing of all the layers in an aqueous environment. The active layer was composed of modified poly(thiophene). The authors used an ester function linked to the thiophene unit which ensures water solubility. After the deposition, a 200°C heating leads to the withdrawal of the ester and then its decarboxilation after the second step at 300°C (see figure 7). They also synthesized a fullerene derivative soluble in water which permits to reach an efficiency around 0.5%.[57]

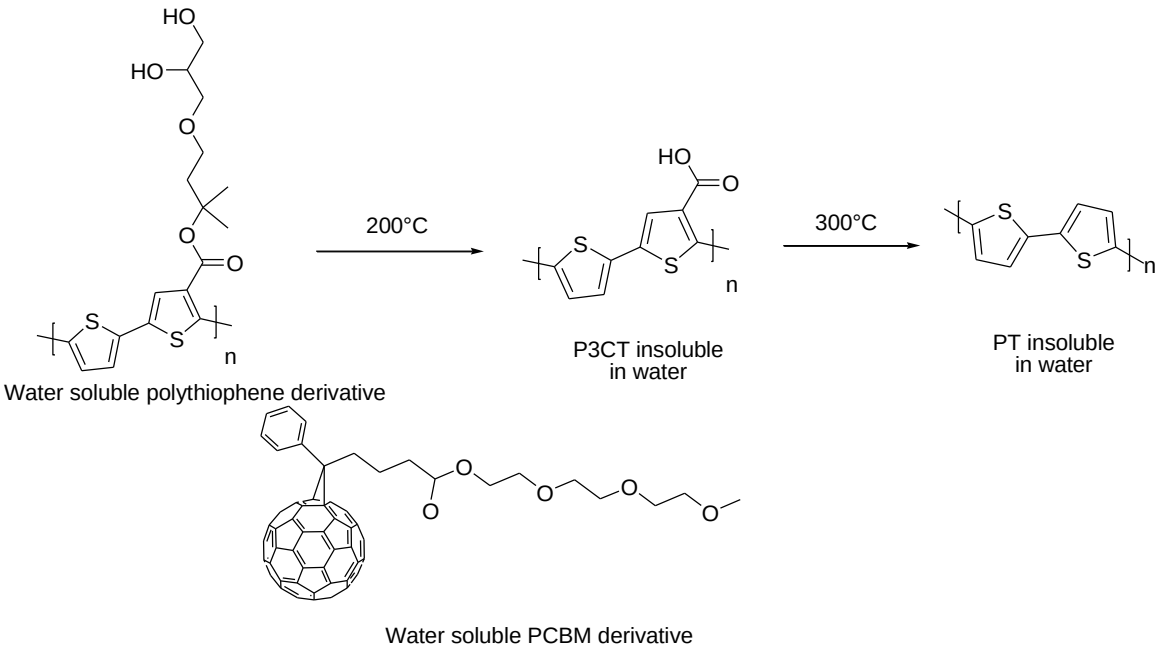

Figure 7 : Water soluble modified polythiophene and PCBM synthesized by Krebs'group, after annealing the polymer became insoluble due to the withdrawal of water soluble functions[57]

Lots of other groups developed water or alcohol soluble polymers but they did not report their integration into solar cells. For instance Zhu *and coll* synthesized a water soluble polymer by Heck coupling which showed a photocurrent generation of 5.5 µA.cm^{-2} (see figure 8).[58]

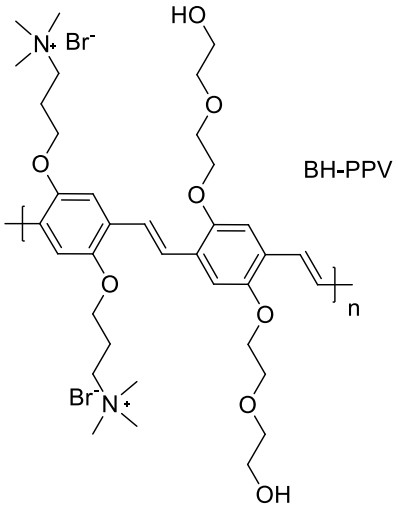

Figure 8: Water soluble modified PPV thanks to the ether, alcohol and quaternary ammonium functions synthesized by Zhu and coll[58]

Other uses of polyelectrolyte

Conjugated polyelectrolytes have the advantages of combining electrons and ions conduction in one component so they have been used extensively in biological or chemical sensing.[59–62] For instance, they can find application as interface layers for electron or hole conduction in various optoelectronic devices.

Poly[(9,9-bis(3'-(N,N-dimethylamino)propyl)-2,7-fluorene)-*alt*-2,7-(9,9–dioctylfluorene)] Polyfluorene grafted with N,N dimethylamino (PFN, see figure 9) (with a small amount of acid to protonate the amine) has been extensively used as interlayer to block holes[63–68] between the active layer and the cathode which allows to improve the photovoltaic performance. For example Cao *and coll* reached efficiencies of poly[(4,8-bis[(2-ethylhexyl)oxy]benzo[1,2-*b*:4,5-b']dithiophene-2,6-diyl)(3-fluoro-2-[(2-ethylhexyl)carbonyl]thieno[3,4-*b*]thiophenediyl)] (PTB7) up to 8.37% and 6.79% for PCDTBT.[64] By using PFN and Al as electrode, the efficiencies of quinoxaline-containing poly(4,5-ethylene-2,7-carbazole) (PECz-DPQx) based solar cells reached 6.07% instead of 4.52% for Ca:Al and 3.99% for Al sole.[68] For poly[9,9-dioctyl-2,7-fluorene-*alt*-(4,7-bis(20-thienyl)-2-dodecyl-2,1,3-benzotriazole)] (PF-DTBTA), poly[(N-90-heptadecanyl-2,7-carbazole)-*alt*-(4,7-bis(20-thienyl)-2-dodecyl-2,1,3-benzotriazole)](PCz-DTBTA), and poly[(2,5-dioctyl-1,4-phenylene)-*alt*-(4,7-bis-(20-thienyl)-2-dodecyl-2,1,3-benzotriazole)] (PPh-DTBTA), the use of PFN interlayer increased the efficiency up to 80% more for PCz-DTBTA devices (2.75% *vs* 1.51% for Al sole).[67]

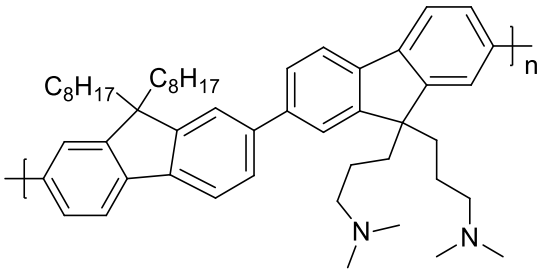

PFN

Figure 9 : Chemical structure of polyfluorene grafted with N,N dimethylamino (PFN). This polymer is mostly use as hole blocking interlayer

A methanol-soluble n-type polyelectrolyte was also used as electron transport layer because poly[2,5-bis(2-octyldodecyl)-3,6-bis(thiophen-2-yl)-pyrrolo[3,4-c]pyrrole-1,4-dione-alt-2,5-bis[6-(N,N,N-trimethylammonium)hexyl]-3,6-bis(thiophen-2-yl)-pyrrolo[3,4-c]pyrrole-

1,4-dione] (PDPPNBr, see figure 10) presents high electron mobility. This polymer allows to increase the efficiency of a P3HT-based solar cell up to 25%.[69]

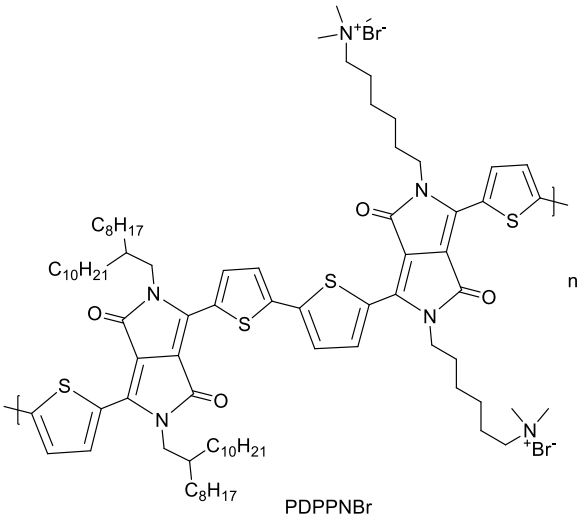

Figure 10 : Methanol soluble poly[2,5-bis(2-octyldodecyl)-3,6-bis(thiophen-2-yl)-pyrrolo[3,4-c]pyrrole-1,4-dione-alt-2,5-bis[6-(N,N,N-trimethylammonium)hexyl]-3,6-bis(thiophen-2-yl)-pyrrolo[3,4-c]pyrrole-1,4-dione] (PDPPNBr) used as electron transport layer[69]

The use of water or alcohol soluble organic materials may be a first approach to stop the use of toxic solvents; however, the ionic groups or counter-ions in the polymer backbone are potential traps for the charge carriers. Other groups' researches were conducted in adding non-charged groups allowing solubility in environmentally-friendly solvents (for example alcohols). PCDTBT and [6,6]-phenyl C_{71} butyric acid methyl ester ($PC_{71}BM$) were modified by introducing a tertiary amine group on the pendant chains (see figure 11). Unfortunately, the solar cells made from these two molecules in butanol solution didn't present any photovoltaic response due to the presence of hole traps.[70]

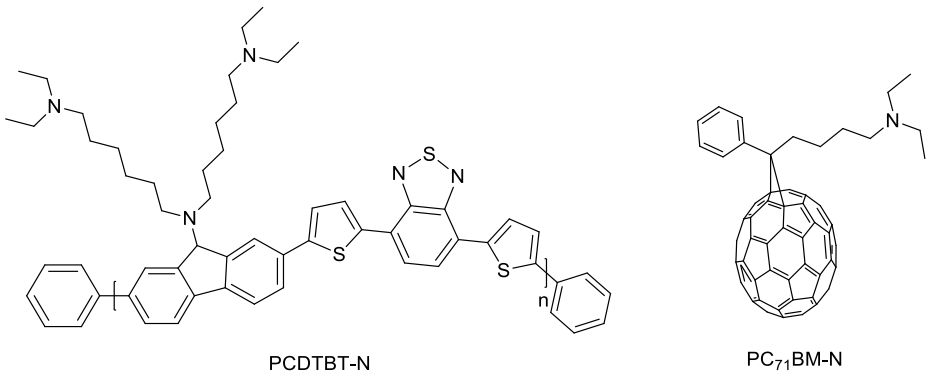

Figure 11 : Modified poly[N-9'-heptadecanyl-2,7-carbazole-*alt*-5,5-4,7-di-2-thienyl-2',1',3'-benzothiadiazole] (PCDTBT) and [6,6]-phenyl C_{71} butyric acid methyl ester ($PC_{71}BM$) using tertiary amine groups allowing solubility in butanol[70]

Heterogeneous conditions: dispersion techniques

Another way to improve the processability would be to prepare the active material under the form of colloids. Polymer (and electron acceptor) particles would then be dispersed in a non-toxic medium like alcohol or water. Extensive studies were developed to study the synthesis of conjugated polymers and their properties in bulk or in thin film whereas very few studies were dedicated to nanoparticles of conjugated polymers.

The main motivation to create particles of conjugated polymer is to go beyond the processing problems. Industries have developed aqueous dispersions like PEDOT:PSS under the commercial name of Baytron P®/ Clevios P® or polyaniline under the commercial name of Ormecon®. Films prepared from these dispersions allow a conductivity superior to 10^3 S. cm^{-1}, which can find application in Organic Light Emitting Diode (OLED) as hole injection layer or replace ITO as electrode.

For the photovoltaic application, the main interest in developing photoactive particles, such as particles composed of both electron-donor and electron-acceptor moieties lies in the fact that the size of the particles could fit with the domain size required in efficient bulk heterojunction solar cells, thus, the phase separation dimension[71,72] can be controlled which rules the device efficiency. The other advantage of using nanoparticles is that the efficiency does not depend on the deposition (evaporation rate, speed of deposition and temperature) unlike for bulk-heterojunction (BHJ) but only on the size and composition of the nanoparticles which is set during the synthesis. This allows an easier transition towards large scale deposition.

Nanoparticles of photoactive polymer can find applications in optoelectronics, or in the medical field[73,74] such as imaging[75] or cell labelling[76] and delivery[74] because they are non-cytotoxic. They can be elaborated by post-polymerization process also known as secondary dispersion or directly by dispersion polymerization in a heterogeneous media.

Polymerization processes

Dispersion

Polymerizations in dispersed media have the advantage to not only be restricted to polymers soluble in organic media and offer a large range in particles size. The dispersion polymerization requires the monomer to be soluble in the medium and the polymer to be insoluble, the aggregation of insoluble growing chains leads to a macroscopic precipitation of the polymer. This precipitation can be controlled by the addition of a stabilizer which is soluble in the medium, so a polymer dispersion with a submicrometric size can be obtained (see figure 12).

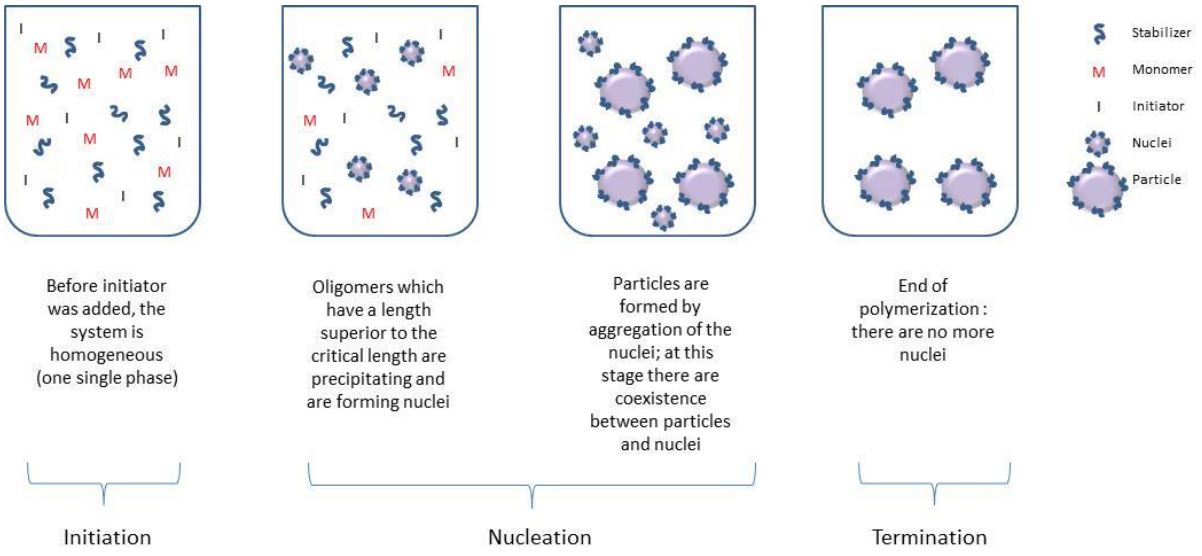

Figure 12 : Principle of dispersion polymerization in case of chain growth mechanism

The steric stabilizer is usually another polymer, soluble in the medium, which can be physically adsorbed or chemically grafted to the growing polymer. Finally, “hairy” particles are obtained, that are colloidally stable and do not aggregate. A high molar mass stabilizer is usually preferred because the particles will be better covered.[77] The most used water soluble steric stabilizers are poly(2-vinylpyridine) (P2VP)[78], poly(vinyl alcool) (PVA)[79], poly(vinyl alcool-*co*-vinyl acetate) (PVPVA)[80], poly(ethyleneoxide) (PEO)[81], poly(N-vinylpyrrolidone) (PVP)[82–87], or some proteins.[88] Amphiphilic block (co)polymers can also be used as stabilizers, allowing particles stabilization by physical adsorption, for example poly(styrene)-*b*-poly(ethyleneoxide) (PS-*b*-PEO)[89–91] has been used a lot. The main drawback of this method is the addition of

insulating matter to stabilize semi-conducting particles which can be detrimental to charge transport for example after integration into devices.

The first conjugated polymer synthesized by dispersion polymerization was polyacetylene[92] followed by polypyrrole or polyaniline for example. Later, polymers with interesting luminescence properties were synthesized under the form of particles such as poly(phenylenevinylene), poly(phenyleneethylene) and poly(fluorene). Most of the conducting polymers synthesized by dispersion polymerization were made by oxidative coupling[93] such as pyrrole[94,95] or aniline[96–98] or poly(3,4-ethylenedioxythiophene) (PEDOT).[77]

The team of Kuehne was the first to propose a new method for the preparation of polyfluorene and polythiophene nanoparticles in an alcohol (see figure 13). The first demonstration of a Suzuki coupling dispersion polymerization took place in 2013 where monodispersed particles were produced thanks to two stabilizers, a block-copolymer poly(1-vinylpyrrolidone-*co*-vinyl acetate) (PVPVA) and a non-ionic surfactant Triton™ X-45. The particles were monodisperse (dispersity index < 4%) due to the use of a very high stabilizer concentration PVPVA coupled to a surfactant. The authors also showed that this kind of particles can be used for photonic crystals.[80]

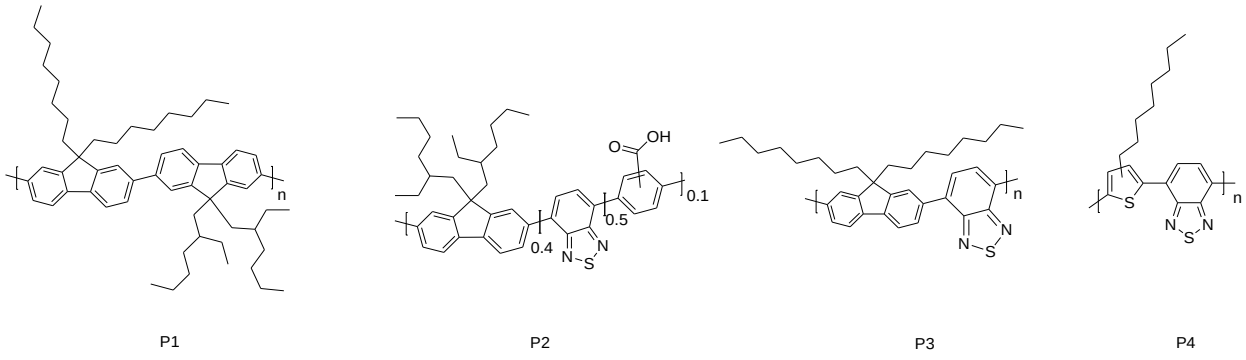

Figure 13 : First polymers synthesized by Suzuki-coupling dispersion polymerization in polar medium: Poly(dioctylfluorene-*alt*-diethylhexylfluorene) (P1), Poly(dioctylfluorene-*alt*-benzothiadiazole) (P2), Poly(diethylhexyl-*co*-benzothiadiazole-*co*-benzoic acid) (P3), Poly(thiophene-*alt*-benzothiadiazole) (P4) [80]

Fluorene and azobenzene-based polymers were also synthesized by dispersion polymerization. These particles react with light thanks to the azobenzene moiety which can change from *cis* to *trans* conformation (see figure 14). They can find applications in photonic or labelling for biomedical.[99]

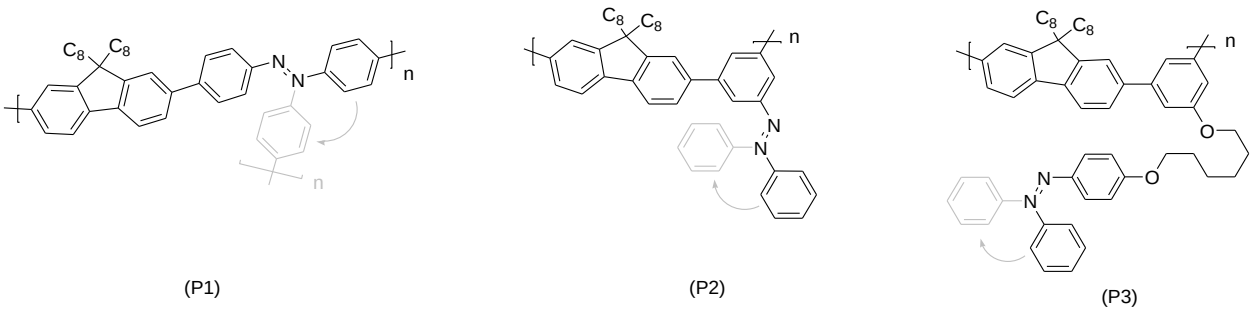

Figure 14 : Incorporation of azobenzene moieties into polyfluorene : azobenzene unit along the Polymer Backbone (P1), Perpendicular to the Polymer Chain (P2), and Electronically Decoupled from the Polymer Backbone by Means of an Alkyl-Spacer (P3) synthesized by Suzuki-coupling dispersion polymerization in polar medium[99]

Successful Heck coupling[100] and Sonogashira coupling (see figure 15) by dispersion polymerization were developed in 2015 following the same methodology. Using the acetylene moieties on the surface of the particles, thiol-yne reaction was carried out and the particles were used as fluorescent probe for imaging.[101]

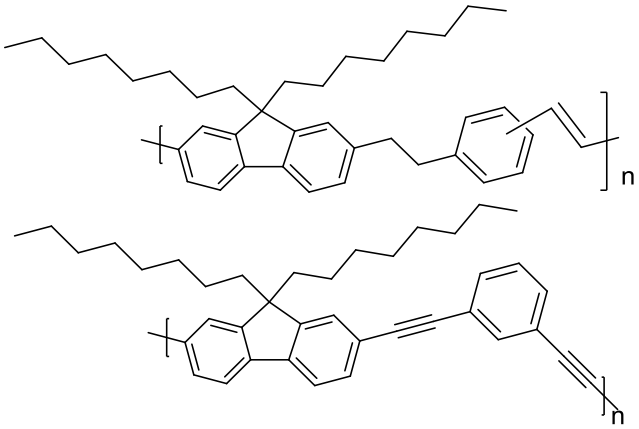

Figure 15 : Poly(fluorine-*alt*-divinyl benzene) synthesized by Heck coupling[100] and poly(fluorine-*alt*-diacetylene phenylene) synthesized by Sonogashira coupling[101] using dispersion polymerization in polar medium

The three coupling reactions described previously (Suzuki, Heck and Sonogashira) took place in alcohol: the propan-1-ol which can be addressed as environmentally-friendly solvent for a green approach to organic photovoltaic. In 2015, we adopted a similar methodology for the synthesis of PCDTBT particles in alcohol, unfortunately despite the good optical properties, the low molar mass of the polymer was an obstacle toward the integration in solar cells with good efficiency.[102]

Emulsion

In emulsion polymerization, the monomers need to have a low solubility in the dispersant medium. The growth of the polymer chains induces the nucleation of hydrophobic particles stabilized by surfactant adsorption. The polymerization keeps going inside the particles, where the monomer has to diffuse from the monomer droplets (which act as reservoir) through the aqueous phase (see figure 16).[103]

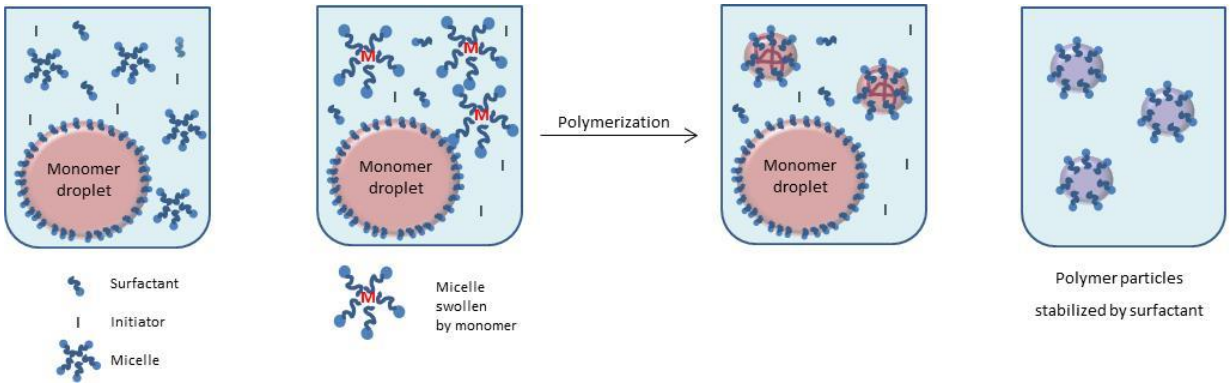

Figure 16 : Principle of emulsion polymerization using surfactant above the CMC in case of chain growth mechanism

Unfortunately emulsion polymerizations have been mainly restricted to chain growth polymerizations[104–106] and only few authors were interested in transferring cross-coupling polymerization to emulsion.

Three luminescent polyfluorene derivatives were synthesized under the form of particles by Suzuki coupling emulsion polymerization. As conventional Suzuki-coupling uses toluene and water as solvents, this coupling seems to be very suitable for an oil-in-water emulsion. The particles' fluorescence was tunable depending on the monomers used. Tween 80, a non-ionic surfactant widely used in the food industry, was used as stabilizer because ionic surfactants can be affected by the alkaline salt used in the reaction. The particles also showed biocompatibility with cells so it opens a large range of applications from labelling, drug delivery to OLED.[107]

Particles of poly(9,9-dioctylfluorene) (PF8), poly(9,9-dioctylfluorene-*alt*-benzothiadiazole) (PF8BT), poly-(9,9-dioctylfluorene-*alt*-4-sec-butylphenyldiphenylamine) (PF8TAA) and poly(9,9-dioctylfluorene-*alt*-bithiophene) (PF8T2) were also synthesized by emulsion polymerization using Suzuki coupling. The emulsion was xylene-in-water and the stabilizer was Triton™ X-102 which is here again, non-ionic. For this reaction, a new catalyst

(1,3-bis[2,6-bis-(diphenylmethyl)-4-methylphenyl]imidazole-2-ylidene) $PdCl_2$(triethylamine) was synthesized and allowed performing the reaction at room temperature. Depending on the polymer, different shapes were obtained: rod-like structures (PF8 and PF8T2) or spherical particles (PF8BT and PF8TAA) and they can be integrated in devices such as Organic Field Effect Transistor (OFET), OPV or photonic devices.[108]

Porous polymer nanospheres from Tris(4-bromophenyl)amine and Benzene-1,4-diboronic acid monomers were synthesized by a toluene-in-water emulsion polymerization via Suzuki coupling without surfactant (see figure 17). At the end of the reaction, 200 nm porous nanoparticles were obtained with high surface area and good H_2 absorption. Due to its low cytotoxicity and good optical properties the nanoparticles can be used as fluorescence marker in bioimaging.[109]

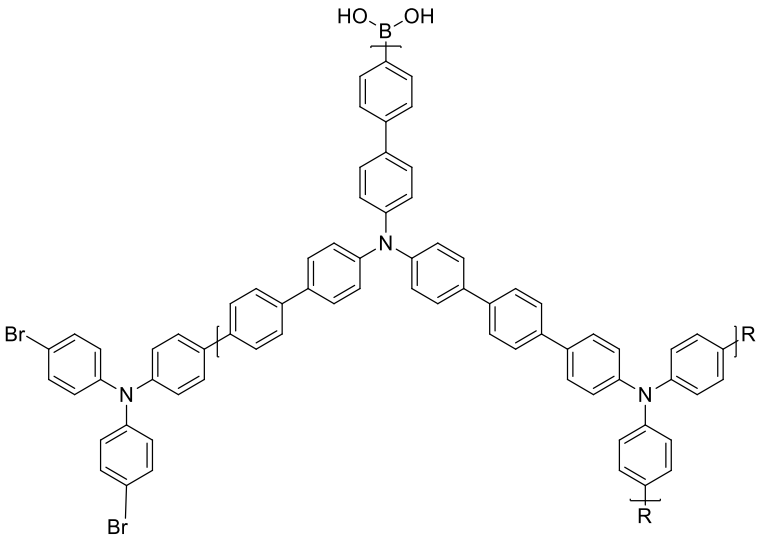

Figure 17 : Polymer composed of phenyl and triphenylamine subunits used in the fabrication of porous nanospheres by emulsion polymerization[109]

Miniemulsion

Another oil-in-water process is sometimes preferred: the mini-emulsion polymerization. At first, the monomer droplets becoming individual nanoreactors are created by a strong shearing, the polymerization takes place inside the droplets so the monomer does not need to diffuse through the aqueous phase. This leads to polymer particles which are the exact copy of the initial miniemulsion (see figure 18).[103] Classically, this process needs the use of a hydrophobic molecule.

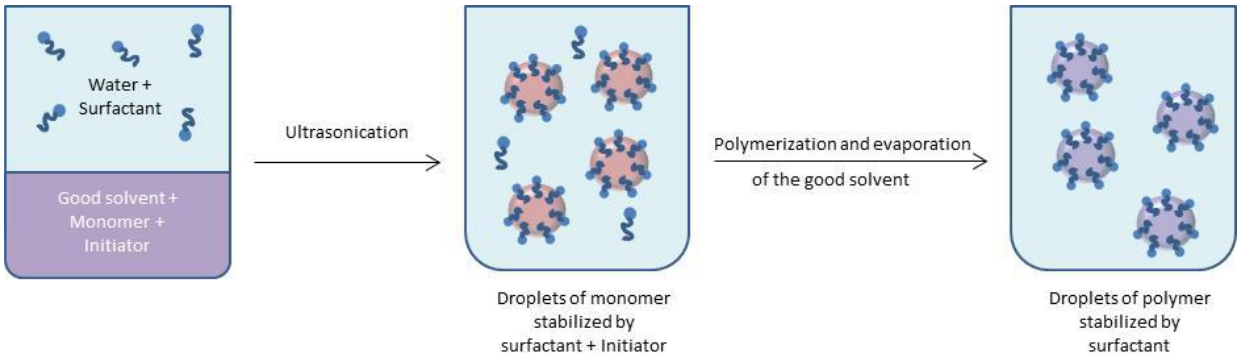

Figure 18 : Principle of miniemulsion polymerization in chain growth methodology using solid monomer

The first step-growth polymerization in miniemulsion was reported in 2007 by the team of Mecking for the synthesis of PPV derivative (see figure 19). PPV was synthesized from p-divinylbenzenes by ADMET (Acyclic Diene METathesis) polymerization using two different catalysts: Grubbs second generation and Hoveyda-Grubbs second generation. Dodecyltrimethylammonium chloride (DTAC) was found to be a good stabilizer unlike SDS which results in a failed polymerization. Lower yields and molar masses were obtained compared to the polymerizations in non-aqueous environment probably due to a partial catalyst decomposition.[110]

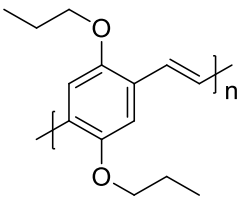

Figure 19 : PPV derivative synthesized by miniemulsion polymerization[110]

Poly(arylene diethynylene) was synthesized using mini-emulsion polymerization via Glaser coupling. Its emission wavelength was adjusted by incorporating a dye.

Tetradecyltrimethylammonium bromide (TTAB) was used as surfactant and 30 nm particles were obtained. The advantage of this coupling is the use of only one monomer which avoid the stoichiometric problems of A_2 + B_2 condensations (in the Suzuki coupling for example) leading to high molar masses up to 50 kDa.[111]

The Sonogashira coupling was also transferred to miniemulsion: nanocomposite particles were created by incorporating Titane dioxide (TiO_2) and cadmium selenide (CdSe) into the poly(arylene ethynylene) particles made by a toluene-in-water miniemulsion stabilized by sodium dodecyl sulfate (SDS) which leads to molar mass around 70 kDa.[112] Poly(arylene ethynylene) nanoparticles were also synthesized through this coupling by miniemulsion polymerization in aqueous environment with dyes covalently linked to the polymer. Nanoparticles of 60-120 nm and high molar masses of 200 kDa were obtained. The dye incorporation enables a bathochromic adjustment of the particles'emission color. Those particles were proved to be suitable as probes for cell imaging with a biocompatibility.[113] Particles of poly(*p*-phenylene ethynylene) (PPE) were synthesized using 1,2,4-tribromobenzene as a cross linker (see figure 20). In standard conditions, the reaction mixture gelled after a short time but when surfactant (SDS) coupled with ultrasonic bath are used, particles with a size between 50-200 nm can be obtained. The particle size can be tuned from nm to mm depending on the presence of surfactant and the mixing conditions. The networks are highly luminescent and comparable to linear PPE without any electronic defect.[114]

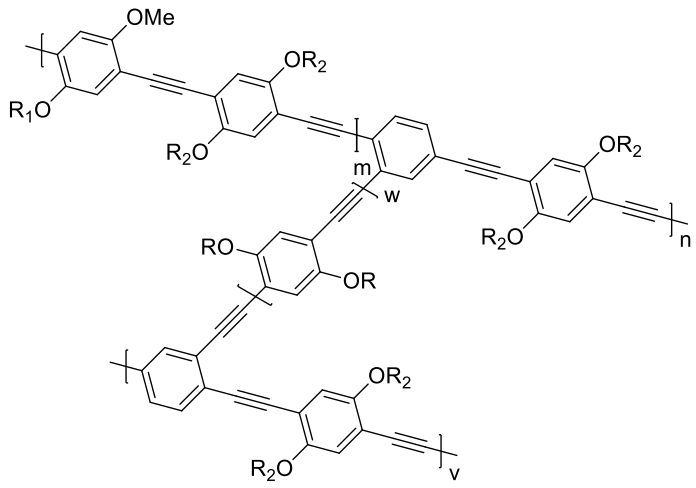

Figure 20 : 3D conjugated network based on PPE[114]

This coupling by miniemulsion polymerization allows the formation of microporous nanoparticles which could find applications in optoelectronic as antenna for the collection of photons. The size was ranging from 30 to 60 nm and efficient energy transfer from nanoparticles to surface bound dye molecule Rhodamine 6G was demonstrated (see figure 21).[115]

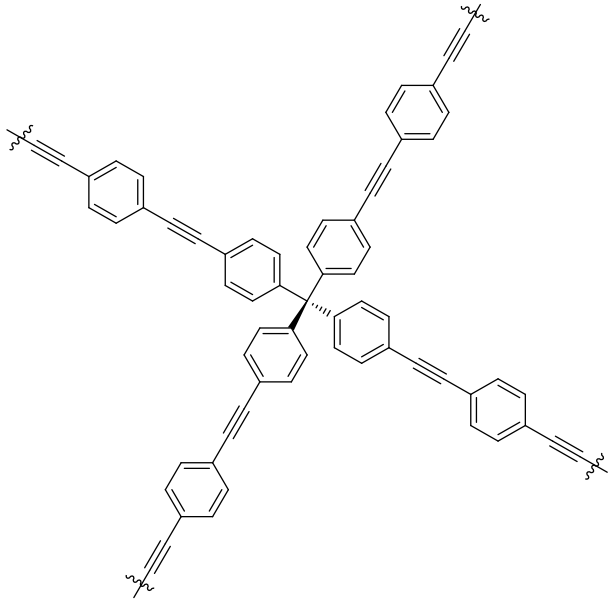

Figure 21 : Microporous nanoparticles based on p-phenylene ethynylene subunits by Sonogashira miniemulsion polymerization[115]

Nanoparticles of poly(*p*-phenylene ethynylene) showing excellent catalytic activity for Suzuki-Miyaura reaction were also synthesized using cross-linked conjugated polymer.[116]

Recently, Zhang's team developed conjugated microporous polymer nanoparticles of different sizes and morphologies (rod-shape, spherical, ring-shape, see figure 22) for photocatalytic activity. Using Suzuki or Sonogashira polycondensations in oil-in-water miniemulsion, stable nanoparticles in organic solvent as well as water were obtained. By playing on the nature of the monomers (phenyl cross-linker A_3-type and co-monomer B_2-type using fluorene, benzothiadiazole or biphenyl), the shape of the nanoparticles can be controlled. The nanoparticles (NPs) present high photocatalytic activity demonstrated by the reduction of oxygen degradation and photooxidation of N,N,N,N'-tetramethyl-p-phenylenediamine.[117]

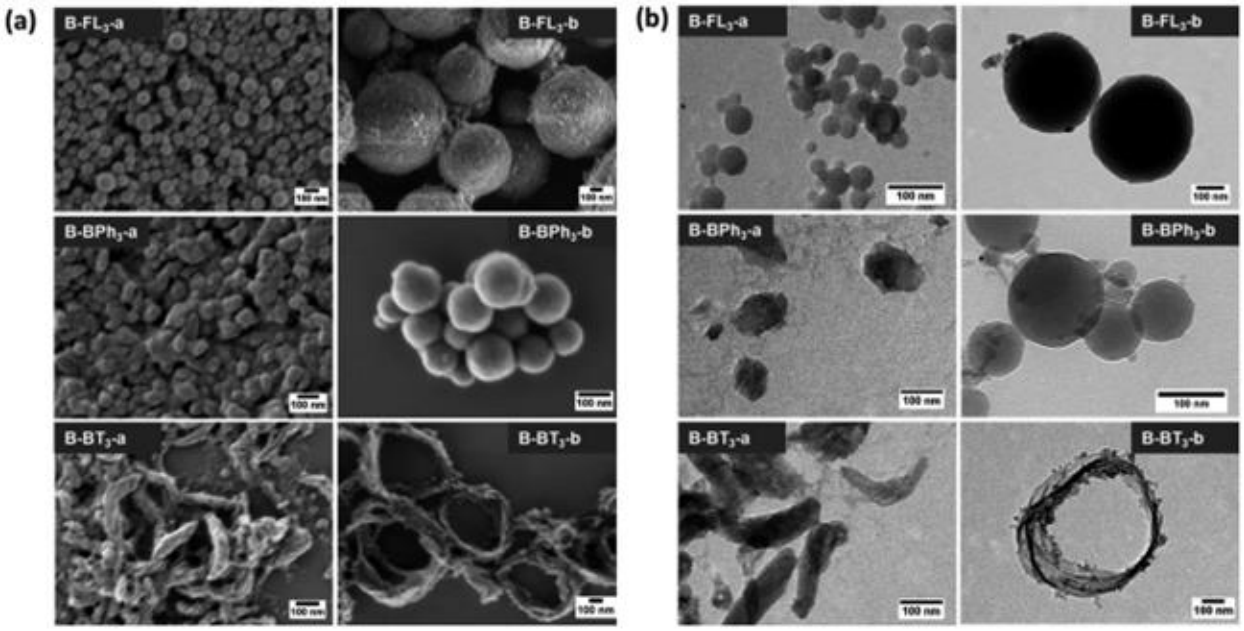

Figure 22 : (a) SEM and (b) TEM images of NPs with different shapes and morphologies obtained by miniemulsion polymerization of microporous poly(phenyl-*co*-fluorene), poly(phenyl-*co*-biphenyl) and poly(phenyl-*co*-benzothiadiazole) polymers[117]

As miniemulsion is a method of choice for the preparation of highly dispersed hybrid materials, Mecking *and coll* synthesized in 2012 a polyfluorene particle from bifunctional monomer 2-(4,4,5,5-tetramethyl-1,3,2-dioxaborolan-2-yl)-7-bromo-9,9-dioctylfluorene with quantum dots using a Suzuki-coupling mini-emulsion polymerization. SDS was used to stabilize the particles and less base than what is usually proposed was used, due to the sensitivity of SDS to the ionic strength. The size of the particles was around 40 nm for a high molar mass of 23 kDa. The application of these hybrid materials is quantum optics due to the energy transfer phenomena between the two compounds.[118]

Hyperbranched polymer nanoparticles were also prepared by Suzuki coupling miniemulsion polymerization in order to keep the spherical morphology in organic solvent and even after complete removal of the surfactant. The particle size was varied between 60 to 460 nm by playing on the amount of surfactant. The surfactant used was CTAB (hexadecyl triethylammonium bromide) which stabilized the toluene-in-water miniemulsion. The polymer displays a blue emission in solution and as solid. These particles were used to detect picric acid in water. As fluorescent probe, the particles present a high fluorescence quenching due to efficient photo-induced electron transfer with a linear detection range, much higher than its linear counterpart (figure 23).[119]

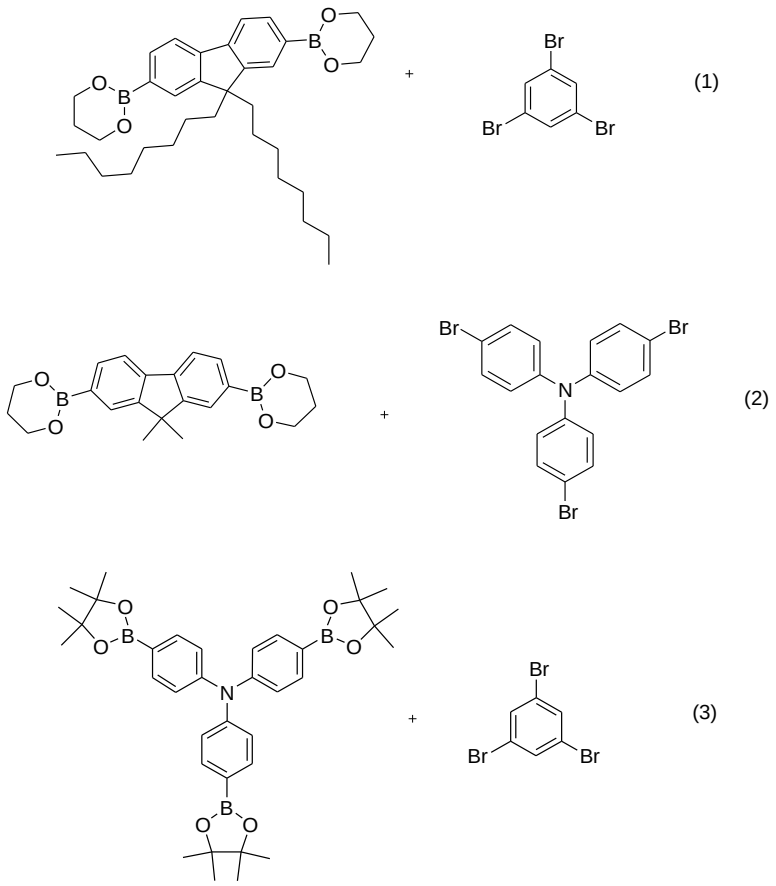

Figure 23 : Monomers involved in the synthesis of hyperbranched polymer nanoparticles: 9,9-dioctylfluorene-2,7-diboronic acid bis(1,3-propanediol)ester and 1,3,5-tribromobenzene (1), 2,7-bis(4,4,5,5-tetramethyl-[1,3,2]dioxaborolane)-9,9-dimethyl-fluorene and tris(4-bromophenyl)amine (2) and tris{4-(4,4,5,5-tetramethyl-[1,3,2]dioxaborolane)phenyl}amine and 1,3,5-tribromobenzene (3)[119–121]

2,7-bis(4,4,5,5-tetramethyl-[1,3,2]dioxaborolane)-9,9-dimethyl-fluorene and tris(4 bromophenyl)amine as cross-linker produced particles with a size of 20-60 nm which can, as before, be dispersed in organic solvents. This hyperbranched polymer exhibits nice sensitivity for the detection of nitroaromatics for example. Its efficiency was also better than those of linear counterpart.[120] Another hyperbranched polymer with a higher specific surface area was synthesized leading to higher sensitivity as low as 0.5 ng mm² for trinitrotoluene (TNT) probably due to easier diffusion of the analyte which is 20 times more sensitive than the linear counterpart (figure 23).[121]

Post-polymerization processes

Post-polymerization processes show some advantages through the use of synthesized π-conjugated polymer as raw materials. Indeed key parameters can be predictively set such as the molar mass, the chain functionality and the structure of the raw polymer. Then, a process can be carried out in order to design polymer particles with a controlled size and size distribution.

Nanoprecipitation

Nanoprecipitation is a post-polymerization method to form hydrophobic particles. It is a universal process because any polymer which is soluble in a solvent can be used. The polymer solution is then dispersed in a big quantity of bad solvent under vigorous stirring.[122] Then, the good solvent is evaporated and leaves conjugated polymer particles dispersed in water or alcohol (see figure 24). This method is based on the difference of solubility of the polymer between good and bad solvents that have to be miscible. The latter characteristic allows the production of nanoparticles in one step. The main advantage of this technique relies in the absence of stabilizer which could be detrimental towards the application (traps in electronic organic or disturbance of the charge transport for example).

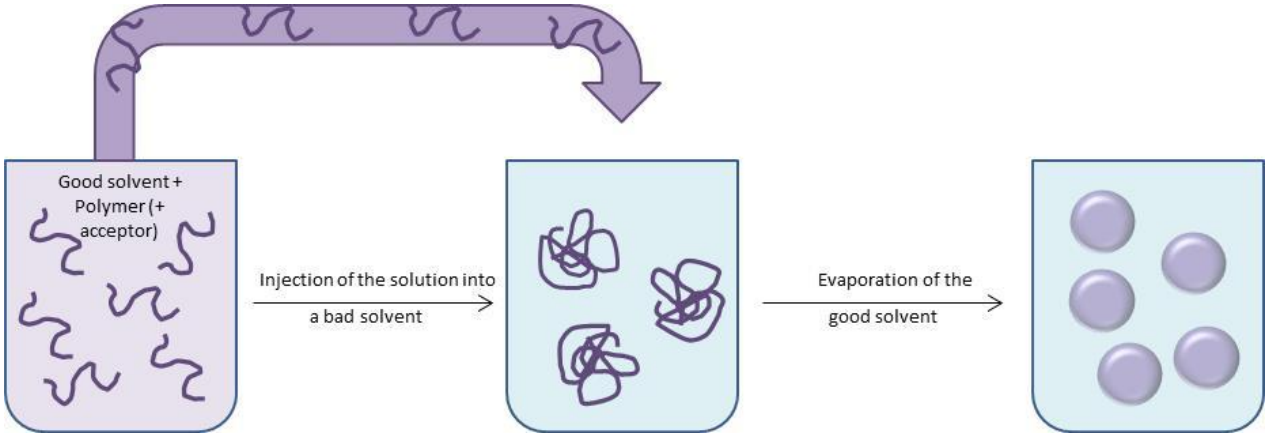

Figure 24 : Principle of the nanoprecipitation post-polymerization process

This process was first reported in 2006 by McNeill *and coll* for the synthesis of polyfluorene particles of 5-10 nm. The driving force for the particles formation was attributed to the hydrophobic interactions and the π-π stacking. Indeed, the polymer chains want to minimize the contact towards water, so they form spheres which have minimum contact towards the exterior.[123]

The nanoparticles'size and shape depend on physical conditions of the process such as the rate of mixing, the injection mode (addition of polymer solution in the bad solvent or contrary, abrupt addition or slow etc) and on chemical conditions like concentrations, dilution volume etc.[124] The couple of solvents used (bad and good) has also an impact on the morphology of the particles. For example in the case of poly[(9,9-dioctylfluorenyl-2,7-diyl)-*alt*-(3,3',4,4'-tetrametylbithiophene-2,5'-diyl)] (F8TMT2) the couple methanol/THF leads to well-defined spheres whereas the couple acetone/THF leads to fused or deformed spheres (see figure 25).[125] The assembly geometry also depends on the polymer: for F8T2, the nanoprecipitation led to irregular aggregates whereas well-shaped spheres were obtained when using Poly[(9,9-dioctylfluorenyl-2,7-diyl)-*alt*-(3,4-ethylenedioxythiophene-2,5-diyl)] (F8EDOT). Similarly, Li *et al* never obtained the same size by using different polymers in same concentrations.[126]

Polymer	Chemical Structure	M_n,[a] M_w/M_n,[a] DP[b]	Solvent/Vapor[c]	Assembling Geometry	d_w (σ) /μm	Corresponding Figure and Table
F8T2	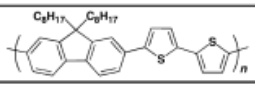	26600, 2.66, 48	$CHCl_3$/MeOH	Irregular Aggregates	–	Figure S6 Table S5
F8TMT2	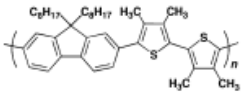	31800, 2.46, 52	CH_2Cl_2/MeOH $CHCl_3$/MeOH THF/MeOH $CHCl_3$/Acetone CH_2Cl_2/Acetone	Well-Shaped Spheres	2.7 (0.39) 2.4 (1.2) 1.9 (0.73) 1.5 (0.61) 1.9 (0.59)	Figure 1, Table 3
F8EDOT	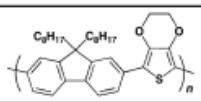	27000, 3.81, 51 13800, 2.03, 26 6300, 1.43, 12	$CHCl_3$/MeOH	Well-Shaped Spheres	0.61 (0.18) 0.44 (0.09)[d] 2.2 (0.78) 4.5 (2.1)	Figure 2, Table 4 Figure 4 Figure S10b Figure S10a

Figure 25 : Polymers poly[(9,9-dioctylfluorenyl-2,7-diyl)-*alt*-bithiophene] (F8T2), poly[(9,9-dioctylfluorenyl-2,7-diyl)-*alt*-(3,3',4,4'-tetrametylbithiophene-2,5'-diyl)] (F8TMT2) and poly[(9,9-dioctylfluorenyl-2,7-diyl)-*alt*-(3,4-ethylenedioxythiophene-2,5-diyl)] F8EDOT and geometry of the assembling obtained using different solvents by nanoprecipitation[125]

The molar mass has also an impact on the particle size, bigger the molar mass is (longer chains) bigger will be the size of the particles. For instance the size of P3HT particles ranged from 50 to 600 nm by tuning its molar mass and concentration.[122]

The size of poly[3-[2-(N-dodecylcarbamoyloxy)ethyl]thiophene-2,5-diyl] (P3DDUT) nanoparticles (see figure 26) was controlled by playing on the concentration of the solution injected, going from 0.1 to 1 wt%, sizes from 40 and 140 nm were obtained. The temperature

is another parameter to control: for a fixed concentration the size varied from 140 to 420 nm for a water temperature from 20 to 80°C.[127]

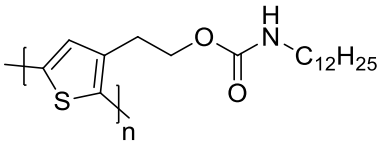

Figure 26 : poly[3-[2-(N-dodecylcarbamoyloxy)ethyl]thiophene-2,5-diyl] (P3DDUT) polymer involved in the formation of nanoparticles by nanoprecipitation

Other parameters such as the ratio of good/bad solvent[128] or the way of mixing[129] can be tuned to control the size of the particles.

The advantages of nanoprecipitation are its versatility: whatever polymer can be used as soon as appropriate solvent is found; no extensive purification is needed after the particles formation, the solution can be used right away and no stabilizer is used.

However for a successful nanoprecipitation, the polymer solution has to be very diluted: for P3HT, a concentration higher than 2.5wt% leads to macroscopic precipitates at the surface of water as soon as the polymer solution was added.[122] Moreover, as none stabilizer is used, the particles are not stable and aggregate pretty fast.

Due to their low concentration, high brightness, high photostability and low toxicity conjugated nanoparticles (so called polymer-dot or PDot) were used a lot for cell labelling,[76,124] fluorescent imaging,[130–133] as well as probe for metallic detection,[134] temperature sensor[135] and oxygen sensing.[136] They were also used for organic electronics as reported by several authors motivated by the absence of stabilizer which could be detrimental for the solar cells. The team of Dastoor firstly reported this methodology in 2011 to produce an active layer from P3HT NP in ethanol reaching low efficiency of 0.018%.[137] The best efficiencies using NP made by nanoprecipitation were reported by Colsmann and coll[138] for the system P3HT: indene-C_{60} bisadduct (ICBA) reaching 3.5% of efficiency in ethanol. However the active layer processing involved 25 spin-coating to overcome the low concentration of the solution which may be a brake from an industrial point of view. Large scale deposition techniques were also used to deposit the active layer reaching 3.5% efficiency using Dr Blade on the same system and 2.9% using ink-jet printing.[139]

Miniemulsion post-polymerization

The miniemulsion post-polymerization is another post-polymerization method to create a large range of polymer nanoparticles with a surfactant quantity relatively low compare to microemulsions. The polymer is first dissolved into a good solvent which is immiscible to water and this solution is added to a water solution with appropriate surfactant.[140] The mixture is then sonicated until a homogenous droplet size is reached (see figure 27). Finally, the good solvent is evaporated in order to form solid nanospheres in water with a diameter between 30 and 300 nm according to the experimental conditions.

As before, the strength of this process is its versatility because whatever material can be processed into particles as long as they are soluble into non water miscible solvent. Typically chloroform is used for π-conjugated polymers, the advantage being its low boiling point. This allows its evaporation without excess heating which could damage the material.

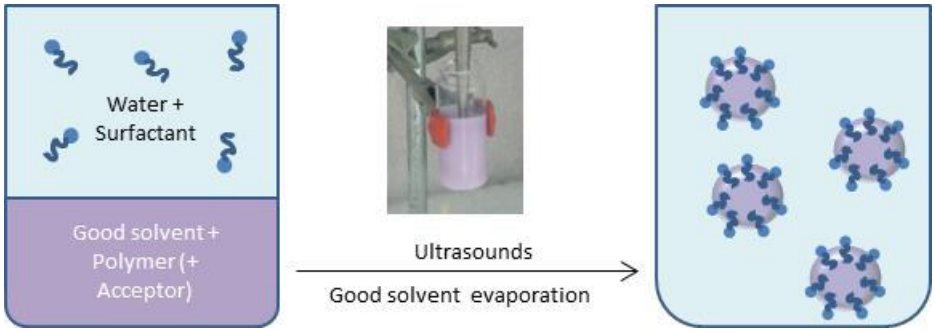

Figure 27 : Principle of miniemulsion post-polymerization process

The use of particles dispersed in water for OPV application presents several advantages: as before, the size of the particles could permit the control of the active layer morphology. In this way, the size of the particles rules the size of the domains, smaller they are, more interface there will be so better the exciton could separate because it will reach an interface before recombination. Contrary to what people can think, the size of the domains does not need to be the exact value of the exciton diffusion length: indeed it can be larger as McNeill *et al* showed for poly(9,9'-dioctylfluorene-*co*-bis-N,N'-(4-butylphenyl)-bis-N,N'-phenyl-1,4 phenylenediamine) (PFB) and poly(9,9-dioctylfluorene-*co*-benzothiadiazole) (F8BT) PFB:F8BT blend. Different length scale phase separation were obtained from less than 10 nm to 40 nm and surprisingly, phase separation of 20 nm provided the best efficiency which is way larger than the exciton diffusion length.[141] Moreover the use of water allows getting rid

of chlorinated solvents during deposition, waste treatment and recycling are no longer needed.

The use of this technique for other applications such as OLED[142–144] for example will not be discussed here.

The size of the particles can be adjusted by playing on different parameters. For example, by using an ultrasonic bath instead of an ultrasounds probe, the size of 2,7-poly(9,9-dialkylfluorene-*co*-fluorenone) (PFFO) particles increased to 149 nm against 45 nm for the probe. The polymer concentration is also an important parameter to take into account for the final particles size. A higher concentration will lead to bigger particles: for example for a 15g/L solution of polymer, the particles'size was 45 nm whereas it was 5.1 nm for a concentration of 0.7 g/L.[145,146] Other important parameters are the surfactant quantity and the time of sonication.[147] Smaller particle size can be obtained by using higher surfactant concentration because more surfactant molecules are available to stabilize a larger number of droplets. The size of the particles went from 38 nm for a SDS concentration of 0.017 M to 150 nm for a SDS concentration of 0.003M.[148] The size-dispersity is not an important parameter for OPV application. Indeed with a relatively broad size distribution, the small particles can fill the gap between the bigger ones and a more uniform film can be obtained.[149]

For photovoltaic applications the polymer (electron donor) can be solubilized with an electron acceptor such as PCBM in order to create composite particles which will act as full active-layer components. The suspensions obtained after the miniemulsion post-polymerization can be concentrated by dialysis; this process also allows washing away the remaining surfactant in the medium because it can act as trap and decrease the solar cell efficiency.

This technique was firstly used in 2002 for semi-conducting polymers. Methyl substituted ladder-type poly(*p*-phenylene) (Me-LPPP) and polyfluorene derivatives (polyfluorene and polycyclopentadithiophenes) (see figure 28) NP were synthesized and controllable particle size between 70 and 250 nm were obtained. The importance of annealing to reach homogeneous layer was underlined.[150]

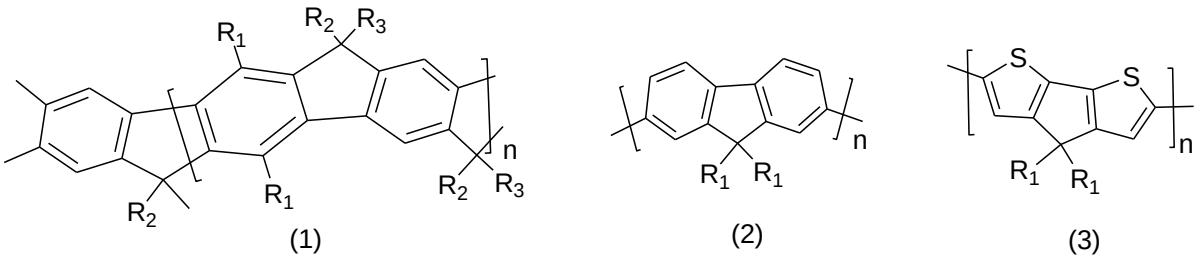

Figure 28 : (1) Me-LPPP: ladder-type poly(*p*-phenylene), (2) PF: polyfluorene derivative and (3) PCPDT : polycyclopentadithiophene derivative synthesized as NP by miniemulsion post-polymerization in 2002.[150]

The annealing step is indeed very important to remove water from the film and to agglomerate the particles in order to form a continuous film. After thermal annealing one can also notice that the quenching of the fluorescence is bigger which indicates a better contact between the electron acceptor and electron donor.[151]

Nanoparticles from a blend of two fluorescent polymers: PFB as electron-donor and F8BT as electron acceptor (see figure 29) were synthesized from chloroform and xylene solution in water. Particle size of 49 nm and 53 nm respectively were reported reaching comparable external quantum efficiencies (EQE refers to ratio of the number of charge carriers collected by the solar cell to the number of incident photons) with peak value around 1.7% once integrated into the active layer of a solar cell. *A contrario*, in BHJ using chloroform and xylene, different efficiencies were obtained (from 0.25 to 4%). This result is very important and shows that the efficiencies do not depend on the solvent used but mainly on the size of the particles.[152]

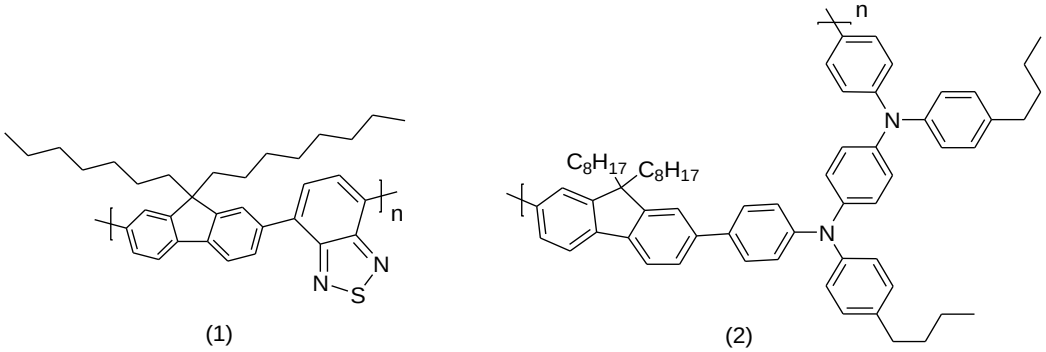

Figure 29 : (1) F8BT : poly(9,9-dioctylfluorene-*co*-benzothiadiazole) and (2) PFB : poly(9,9'-dioctylfluorene-*co*-bis-N,N'-(4-butylphenyl)-bis-N,N'-phenyl-1,4 phenylenediamine) used for NP preparation from xylene or chloroform solutions[152]

So far, the best efficiency using NP made by miniemulsion post-polymerization was reported in 2016 with poly[2,3-bis-(3-octyloxyphenyl)quinoxaline-5,8-diyl-*alt*-thiophene-2,5-diyl] (TQ1) blended with $PC_{71}BM$. Similar efficiencies than BHJ devices were reached for the

NP based devices (2.54% against 2.58%). Thermal annealing at mild temperature was used in order to optimize the morphology.[153]

NP of poly{3,6-dithiophene-2-yl-2,5-di(2-octyldodecyl)-pyrrolo [3,4-c] pyrrole-1,4-dione-*alt*-naphthalene} (PDPP-TNT) blended with $PC_{71}BM$ showed almost double efficiency in water compared to chloroform dispersion due to macroscopic phase segregation in the latter (1.99% *vs* 1.05%). Annealing at 130°C during 10 min was emphasized promoting NP connectivity while too much heating (130°C during 60 min) led to gross phase segregation.[154]

Large scale deposition techniques were also used to create the active layer from inks made by miniemulsion post-polymerization. Roll-to-roll process was used to deposit NP of poly[4,8-bis(2-ethylhexyloxy)benzo(1,2-b:4,5-b0)dithiophene-*alt*-5,6-bis(octyloxy)-4,7-di(thiophen-2-yl)(2,1,3-benzothiadiazole)-5,50-diyl] (P1), poly[(4,40-bis(2-ethylhexyl)dithieno[3,2-b:20,30-d]silole)-2,6-diyl-*alt*-(2,1,3-benzothiadiazole)-4,7-diyl] (P2), and poly[2,3-bis-(3-octyloxyphenyl)quinoxaline-5,8-diyl-*alt*-thiophene-2,5-diyl] (P3) (see figure 30) blended with PCBM. Even if low efficiencies were obtained (0.07, 0.55 and 0.15% respectively) the use of this process is very innovative because it is very common in industry unlike the usual laboratory technics (spin-coating for example).[45]

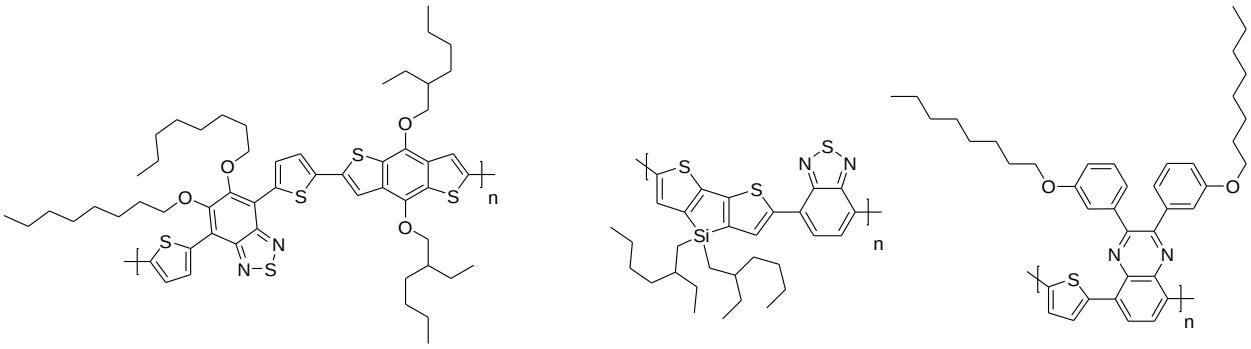

Figure 30 : (P1): poly[4,8-bis(2-ethylhexyloxy)benzo(1,2-b:4,5-b0)dithiophene-*alt*-5,6-bis(octyloxy)-4,7-di(thiophen-2-yl)(2,1,3-benzothiadiazole)-5,50-diyl], (P2): poly[(4,40-bis(2-ethylhexyl)dithieno[3,2-b:20,30-d]silole)-2,6-diyl-*alt*-(2,1,3-benzothiadiazole)-4,7-diyl] and (P3): poly[2,3-bis-(3-octyloxyphenyl)quinoxaline-5,8-diyl-*alt*-thiophene-2,5-diyl] polymers used for the preparation of NP-based active layer deposited by roll-to-roll[45]

For future industrialization, big batches production weas also studied: a 100mL P3HT:PCBM NP ink was created. Even if the efficiencies were relatively low: up to 0.29% (for a

single slot-die coating) and 0.03% (for a double slot-die coating), this result is very encouraging from a prospective point of view.[155]

NP of poly(dithienothiophene-diketopyrrolopyrrole) (P(TBT-DPP)) and ICBA deposited by Dr Blade were reported with a domain size around 100 nm compared to domains in the order of 500 nm for conventional BHJ (see figure 31 image AFM). 2.16% efficiency for the NP was reached against 0.44 % for chloroform based BHJ. This result can be explained by the higher charge transportation in the case of NP due to closer contact between the two compounds compared to conventional BHJ devices.[146]

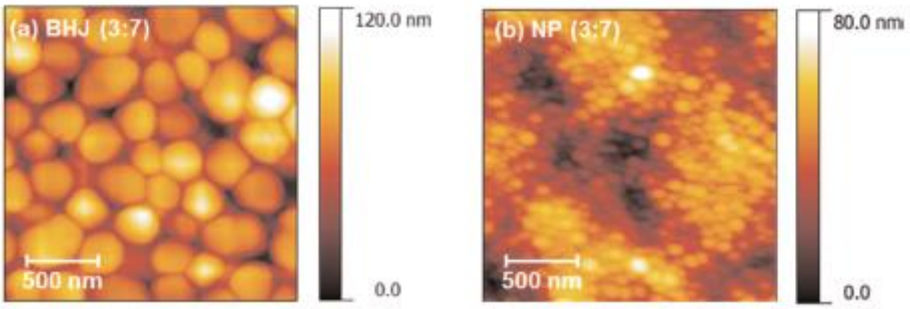

Figure 31 : AFM images of poly(dithienothiophene-diketopyrrolopyrrole) (P(TBT-DPP)) and indene-C_{60} bisadduct (ICBA) films deposited by Dr Blade BHJ (left) and NP (right)[146]

Low efficiencies reported above can be due to the use of surfactant, SDS being the most used. The latter negatively charged creates interface layers disrupting the transport of charges. Chung *and coll* proposed to replace the SDS by a non-ionic stabilizer based on ethoxy and carbonated chains (C_nE_m) which could be taken away by post washing due to the lower inter-surfactant interactions. Using this new surfactant, NP of poly(diketopyrrolopyrrole-selenophene vinylene selenophene) (DPP-SVS) led to a charge-carrier mobility of 2.5 $cm^2 V^{-1} s^{-1}$ (versus 10^{-3} $cm^2 V^{-1} s^{-1}$ with SDS) (see figure 32).[156]

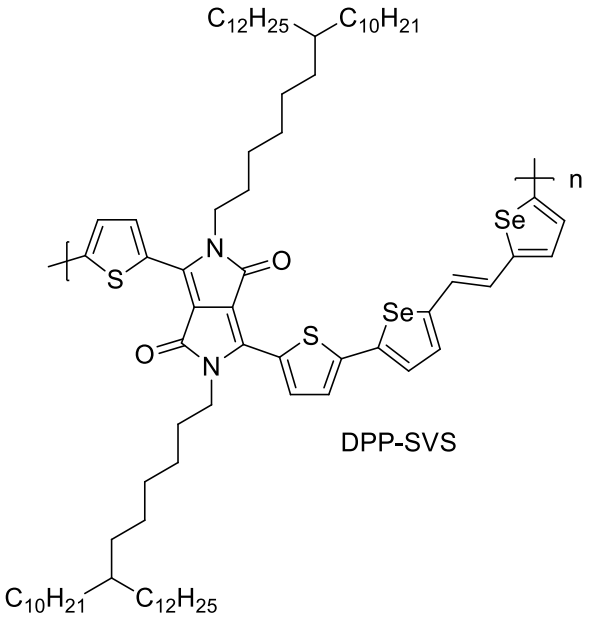

Figure 32 : poly(diketopyrrolopyrrole-selenophene vinylene selenophene) (DPP-SVS) used for the preparation of NP using ethoxyl and carbonated moieties as non-ionic stabilizer

Solar cells efficiencies integrating nanoparticles reported in the literature

The table below displays the different systems based on photoactive nanoparticles as reported from the literature. This ranking includes the nature of the polymer and the acceptor, the method of NP synthesis, the "green" solvent used and the deposition technique.

Table 1 : Summary of the solar cell efficiency using nanoparticles in the active layer

Year	Polymer:acceptor	Method for the synthesis of NP	Solvent	Deposition technique	Efficiency (%)	Reference
2004	P3HT:PCBM	MEPP	Water	SC	1.32E-05	**151**
2005	PPE-SO_3^-:C_{60}-NH_3^+	H	Water	SC	4.10E-02	**56**
2009	1:SWCNT-pyrene$^-$	H	Water	DC	8.21E-04	**55**
2011	P3HT:PCBM	NP	EtOH	SC	1.80E-02	**137**
2011	P1:PCBM	MEPP	Water	R2R	0.07	**45**
2011	P2:PCBM	MEPP	Water	R2R	0.55	**45**
2011	P3:PCBM	MEPP	Water	R2R	0.15	**45**
2012	P3HT:PCBM	MEPP	Water	SDC	0.29	**157**
2012	PFB:F8BT	MEPP	Water	SC	0.39	**158**
2012	PFB:F8BT	MEPP	Water	SC	0.82	**159**
2013	P3HT:ICBA	MEPP	Water	SC	2.50	**160**
2014	P3HT:PCBM	MEPP	Water	SC	0.85	**161**
2014	P3HT:PCBM	MEPP	Water	SC	1.20	**162**
2014	P3HT:PCBM	MEPP	Water	SC	1.94	**163**
2014	PDPP-TNT:$PC_{71}BM$	MEPP	Water	SC	1.99	**154**
2014	P3HT:ICBA	NP	EtOH	SC	3.50	**138**
2014	P3HT:ICBA	NP	MeOH	SC	4.10	**138**
2015	PSBTBT:PCBM	MEPP	Water	SC	1.30	**164**
2015	P(TBT-DPP):ICBA	MEPP	Water	DB	2.16	**146**
2016	PFB:F8BT	MEPP	Water	SC	0.39	**165**
2016	P3HT:PCBM	MEPP	Water	SC	0.46	**165**
2016	TQ1:$PC_{71}BM$	MEPP	Water	SC	2.54	**153**
2016	P3HT:ICBA	NP	EtOH	IJ	2.90	**139**
2016	P3HT:ICBA	NP	EtOH	DB	3.50	**139**
2016	P3HT:ICBA	NP	EtOH	SC	4.20	**166**
2016	P3HT:ICBA	NP	EtOH	SC	4.30	**139**

Legend of Table 1

Polymer:acceptor

1 *: poly{trimethyl-[7-(3-thienylsulfanyl)heptyl]ammonium iodide-co-thiophene}*

SWCNT-pyrene$^-$ *: single-walled carbon nanotubes functionalized with 1-pyrenebutyric acid*

P1 *: poly[4,8-bis(2-ethylhexyloxy)benzo(1,2-b:4,5-b')dithio-phene-alt-5,6-bis(octyloxy)-4,7 di(thiophen-2-yl)(2,1,3-benzothiadiazole)-5,5'-diyl]*

P2 *: poly[(4,4'-bis(2-ethyl-hexyl)-dithieno[3,2-b:2',3'-d]silole)-2,6-diyl-alt-(2,1,3-benzothiadiazole)-4,7-diyl]*

P3 *: poly[2,3-bis-(3-octyloxyphenyl)-quinoxaline-5,8-diyl-alt-thiophene-2,5-diyl]*

PDPP-TNT *: poly{3,6-dithiophene-2-yl-2,5-di(2-octyldodecyl)-pyrrolo[3,4-c]-pyrrole-1,4-dione-alt-naphthalene}*

P(TBT-DPP) *: poly[{2,6-(4,8-didodecylbenzo[1,2-b:4,5-b']dithiophene)}-alt-{5,5-(2,5-bis(2-butyloctyl)-3,6-dithiophen-2-yl-2,5dihydropyrrolo[3,4-c]57pyrrole-1,4-dione)}]*

PSBTBT *: poly[4,8-bis(2-ethylhexyloxy)benzo(1,2-b:4,5-b')dithiophene-alt-5,6-bis(octyloxy)-4,7 di(thiophen-2-yl)(2,1,3-benzothiadiazole)-5,5'-diyl]*

TQ1 *: Poly[2,3-bis-(3-octyloxyphenyl)quinoxaline-5,8-diyl-alt-thiophene-2,5-diyl]*

Method of synthesis

MEPP *: Mini-Emulsion Post-Polymerization*

H *: Homogeneous synthesis*

NP *: NanoPrecipitation*

Deposition technique

SC *: Spin-coating*

DC *: Dip-coating*

R2R *: Roll-to-roll*

SDC *: Sloe-die coating*

IJ *: Ink-jet*

DB *: Dr Blade*

Conclusion

Among main solvents, chlorinated are extensively used for the processing of π-conjugated polymers. It represents a real issue in terms of human health and environment. We have shown that water or alcohol soluble polyelectrolytes are not a right outcome due to low efficiency of the solar cells once they are integrated into solar cells. The other solution is the use of conjugated nanoparticles which are very promising materials and could find application in various area such as bioimaging and biosensing, optoelectronic, photonics etc. The processes to make nanoparticles are very adaptable and are being used for a wide range of polymers.

As a matter of photovoltaic application direct synthesis of π-conjugated polymer in more environmentally-friendly solvent following heterogeneous conditions (dispersion techniques) appears to be the greenest hopeful approach for large and extended development of electronic inks, ready for already available printing facilities for large scale production of optoelectronics. It is still a long way to find acceptable alternatives in order to get fully printed large surface organic solar cells.

I.3. Problématique du projet de recherche

Les premiers résultats obtenus dans la littérature montrent que l'utilisation de nanoparticules pour la fabrication de couches actives de cellules photovoltaïques semble être une bonne alternative aux solutions halogénées/chlorées, toxiques pour l'homme et l'environnement. L'obtention de particules de polymère permet d'envisager un meilleur contrôle de la morphologie de la couche active en ajustant leur taille et leur composition.

Parmi les nombreux polymères conjugués existants, nous avons choisi de nous intéresser au poly[N- 9'-heptadecanyl-2,7-carbazole-*alt*-5,5-(4,7-di-2-thienyl-2',1',3'-benzothiadiazole] (PCDTBT). Ce polymère dispose en effet d'une faible bande interdite facilitant l'absorption d'une grande partie des photons disponibles. Ce polymère a été synthétisé pour la première fois par l'équipe de Mario Leclerc[167] et peut atteindre des rendements de conversion jusqu'à 7,2%[168] associé au $PC_{71}BM$ comme accepteur d'électrons. Sa température de transition vitreuse relativement élevée a aussi attiré notre attention (Tg~130°C) puisque cette valeur est plus appropriée aux températures d'usage des panneaux photovoltaïques qui peuvent atteindre jusqu'à 85°C sur le toit. Une température de transition vitreuse trop basse (comme celle du P3HT Tg~12°C[169]) risquerait d'entraîner une ségrégation de phase macroscopique et donc de diminuer drastiquement les performances de la cellule.[153,170] En outre, ce polymère est synthétisé *via* un couplage de Suzuki qui n'est pas sensible à un environnement aqueux et de nombreuses équipes ont déjà réussi à transférer cette synthèse vers des conditions hétérogènes.[80,99,107–109,117–121]

Le principal objectif de ce travail de thèse a ainsi consisté à préparer des encres « prêtes à l'emploi » pour la couche active de cellules solaires organiques à base d'un couple donneur/accepteur. Le choix s'est porté sur le système PCDTBT/$PC_{71}BM$ en milieu alcool ou aqueux. Deux voies principales ont été envisagées, à savoir directement par des procédés de synthèse en milieux hétérogènes ou indirectement *via* des techniques de dispersions post-polymérisation. Ces méthodologies sont décrites dans les chapitres deux à cinq.

Le deuxième chapitre exposera la synthèse du PCDTBT en dispersion dans le propan-1-ol. Une étude systématique des paramètres de la synthèse sur la taille des particules obtenues sera développée. Les propriétés optiques des particules seront évaluées pour vérifier si ces dernières pourraient se substituer au polymère synthétisé de façon classique.

Nous montrerons que ces particules atteignent des masses molaires relativement faibles empêchant leur utilisation en remplacement du polymère synthétisé de façon classique, puisque la masse molaire a un fort impact sur le rendement de conversion des cellules solaires.

Le troisième chapitre décrira la mise en forme du polymère et du $PC_{71}BM$ *via* un procédé de mini-émulsion post-polymérisation permettant d'obtenir des particules stabilisées par un tensioactif (le SDS). Cette approche permet d'obtenir des NP de propriétés identiques au polymère synthétisé de façon classique (absorption, émission, niveaux énergétiques etc…) et d'obtenir des rendements de conversion modestes *via* le dépôt à la tournette de la couche active en milieu aqueux.

Le quatrième chapitre dépeindra la synthèse d'un copolymère à blocs basé sur du poly(3-hexylthiophène)-*bloc*-poly(oxyde d'éthylène) (P3HT-*b*-PEO) spécifiquement façonné pour stabiliser des particules de PCDTBT et de $PC_{71}BM$ afin de limiter la quantité de composés isolants et chargés (comme le SDS) qui pourraient perturber le transport des charges. Le dépôt des NP ainsi obtenues fait appel à des technologies d'impression par spray en raison des concentrations de matières actives dispersées dans l'eau.

Le cinquième chapitre portera sur une voie originale d'obtention de particules sans stabilisant par nano-précipitation d'une solution de polymère ou de système donneur/accepteur dans l'eau. Comme dans le chapitre précédent c'est la technique du spray qui sera utilisée pour le dépôt de la couche active.

I.4. Références

[1] T. J. and J. H. and P. Kuivalainen, *Phys. Scr.*, **2002**, *2002*, 96.
[2] J. C. Muller, in *Doss. BE 8579*, **2007**, p. Les techniques de l'ingénieur.
[3] C. Li, M. Liu, N. G. Pschirer, M. Baumgarten, K. Müllen, *Chem. Rev.*, **2010**, *110*, 6817.
[4] K. M. Coakley, M. D. McGehee, *Chem. Mater.*, **2004**, *16*, 4533.
[5] C. K. Chiang, C. R. Fincher, Y. W. Park, A. J. Heeger, H. Shirakawa, E. J. Louis, S. C. Gau, A. G. MacDiarmid, *Phys. Rev. Lett.*, **1977**, *39*, 1098.
[6] J. J. M. Halls, K. Pichler, R. H. Friend, S. C. Moratti, A. B. Holmes, *Appl. Phys. Lett.*, **1996**, *68*.
[7] S. Günes, H. Neugebauer, N. S. Sariciftci, *Chem. Rev.*, **2007**, *107*, 1324.
[8] L. Protin, S. Astier, *Les Tech. l'ingénieur*, **1997**, d3360.
[9] P. Destruel, I. Seguy, *Les Tech. l'ingénieur*, **2004**, RE 25.
[10] S. E. Shaheen, C. J. Brabec, N. S. Sariciftci, F. Padinger, T. Fromerz, J. C. Hummelen, *Appl. Phys. Lett.*, **2001**, *78*, 841.
[11] F. Padinger, R. Rittberger, N. S. Sariciftci, *Adv. Funct. Mater.*, **2003**, *13*, 85.
[12] P. Schilinsky, U. Asawapirom, U. Scherf, M. Biele, C. Brabec, *J. Chem. Mater.*, **2005**, *17*, 2175.
[13] M.-S. Kim, B.-G. Kim, J. Kim, *ACS Appl. Mater. Interfaces*, **2009**, *1*, 1264.
[14] S. Gunes, H. Neugebauer, N. S. Sariciftci, *Chem. Rev.*, **2007**, *107*, 1324.
[15] J. H. Edwards, W. J. Feast, *Polymer (Guildf).*, **1980**, *21*, 595.
[16] Wessling, Zimmermann, *Polyacetylene*, **1972**, 3401152.
[17] A. Malinauskas, *Polymer (Guildf).*, **2001**, *42*, 3957.
[18] N. Miyaura, A. Suzuki, *Chem. Rev.*, **1995**, *95*, 2457.
[19] M. Rehahn, A.-D. Schlüter, G. Wegner, W. J. Feast, *Polymer (Guildf).*, **1989**, *30*, 1060.
[20] Y. Sun, C. J. Takacs, S. R. Cowan, J. H. Seo, X. Gong, A. Roy, A. J. Heeger, *Adv. Mater.*, **2011**, *23*, 2226.
[21] D. Milstein, J. K. Stille, *J. Am. Chem. Soc.*, **1978**, *100*, 3636.
[22] Z. Bao, W. Chan, L. Yu, *Chem. Mater.*, **1993**, *5*, 2.
[23] S. Zhang, L. Ye, Q. Wang, Z. Li, X. Guo, L. Huo, H. Fan, J. Hou, *J. Phys. Chem. C*, **2013**, *117*, 9550.
[24] R. F. Heck, *J. Am. Chem. Soc.*, **1969**, *91*, 6707.
[25] A. Greiner, W. Heitz, *Die Makromol. Chemie, Rapid Commun.*, **1988**, *9*, 581.
[26] F. Ullmann, J. Bielecki, *Berichte der Dtsch. Chem. Gesellschaft*, **1901**, *34*, 2174.
[27] L. Groenendaal, H. W. I. Peerlings, J. L. J. van Dongen, E. E. Havinga, J. A. J. M. Vekemans, E. W. Meijer, *Macromolecules*, **1995**, *28*, 116.
[28] M. Pomerantz, H. Yang, Y. Cheng, *Macromolecules*, **1995**, *28*, 5706.
[29] K. Sonogashira, Y. Tohda, N. Hagihara, *Tetrahedron Lett.*, **1975**, *16*, 4467.
[30] K. Tamao, K. Sumitani, M. Kumada, *J. Am. Chem. Soc.*, **1972**, *94*, 4374.
[31] R. D. McCullough, S. Tristram-Nagle, S. P. Williams, R. D. Lowe, M. Jayaraman, *J. Am. Chem. Soc.*, **1993**, *115*, 4910.
[32] S. Baba, E. Negishi, *J. Am. Chem. Soc.*, **1976**, *98*, 6729.
[33] T. A. Chen, R. D. Rieke, *J. Am. Chem. Soc.*, **1992**, *114*, 10087.
[34] T.-A. Chen, X. Wu, R. D. Rieke, *J. Am. Chem. Soc.*, **1995**, *117*, 233.
[35] E. Negishi, *Angew. Chemie Int. Ed.*, **2011**, *50*, 6738.
[36] B. de Boer, U. Stalmach, P. F. van Hutten, C. Melzer, V. V. Krasnikov, G. Hadziioannou, *Polymer (Guildf).*, **2001**, *42*, 9097.
[37] Y. Liu, S. Xu, J. Li, Y. Xin, G. Zhao, B. Ye, S. Cao, *Polym. Adv. Technol.*, **2008**, *19*, 793.
[38] S. C. Moratti, R. Cervini, A. B. Holmes, D. R. Baigent, R. H. Friend, N. C. Greenham, J. Grüner, P. J. Hamer, *Synth. Met.*, **1995**, *71*, 2117.
[39] H. G. Gilch, W. L. Wheelwright, *J. Polym. Sci. Part A-1 Polym. Chem.*, **1966**, *4*, 1337.
[40] Ö. Usluer, M. Abbas, G. Wantz, L. Vignau, L. Hirsch, E. Grana, C. Brochon, E. Cloutet, G. Hadziioannou, *ACS Macro Lett.*, **2014**, *3*, 1134.
[41] A. Katsouras, N. Gasparini, C. Koulogiannis, M. Spanos, T. Ameri, C. J. Brabec, C. L. Chochos, A. Avgeropoulos, *Macromol. Rapid Commun.*, **2015**, *36*, 1778.
[42] S. Beaupré, M. Leclerc, *J. Mater. Chem. A*, **2013**, *1*, 11097.
[43] D. E. Markov, E. Amsterdam, P. W. M. Blom, A. B. Sieval, J. C. Hummelen, *J. Phys. Chem. A*, **2005**, *109*, 5266.
[44] A. M. Ruder, *Ann. N. Y. Acad. Sci.*, **2006**, *1076*, 207.
[45] T. R. Andersen, T. T. Larsen-Olsen, B. Andreasen, A. P. L. Böttiger, J. E. Carlé, M. Helgesen, E. Bundgaard,

K. Norrman, J. W. Andreasen, M. Jørgensen, F. C. Krebs, *ACS Nano*, **2011**, *5*, 4188.
[**46**] C.-C. Chueh, K. Yao, H.-L. Yip, C.-Y. Chang, Y.-X. Xu, K.-S. Chen, C.-Z. Li, P. Liu, F. Huang, Y. Chen, W.-C. Chen, A. K.-Y. Jen, *Energy Environ. Sci.*, **2013**, *6*, 3241.
[**47**] C.-D. Park, T. A. Fleetham, J. Li, B. D. Vogt, *Org. Electron.*, **2011**, *12*, 1465.
[**48**] A. Lange, W. Schindler, M. Wegener, K. Fostiropoulos, S. Janietz, *Sol. Energy Mater. Sol. Cells*, **2013**, *109*, 104.
[**49**] T. M. Eggenhuisen, Y. Galagan, E. W. C. Coenen, W. P. Voorthuijzen, M. W. L. Slaats, S. A. Kommeren, S. Shanmuganam, M. J. J. Coenen, R. Andriessen, W. A. Groen, *Sol. Energy Mater. Sol. Cells*, **2015**, *134*, 364.
[**50**] B. R. Aïch, S. Beaupré, M. Leclerc, Y. Tao, *Org. Electron.*, **2014**, *15*, 543.
[**51**] C. Sprau, F. Buss, M. Wagner, D. Landerer, M. Koppitz, A. Schulz, D. Bahro, W. Schabel, P. Scharfer, A. Colsmann, *Energy Environ. Sci.*, **2015**, *8*, 2744.
[**52**] J. G. Tait, T. Merckx, W. Li, C. Wong, R. Gehlhaar, D. Cheyns, M. Turbiez, P. Heremans, *Adv. Funct. Mater.*, **2015**, *25*, 3393.
[**53**] J. Griffin, A. J. Pearson, N. W. Scarratt, T. Wang, A. D. F. Dunbar, H. Yi, A. Iraqi, A. R. Buckley, D. G. Lidzey, *Org. Electron.*, **2015**, *21*, 216.
[**54**] Y. Ji, C. Xiao, Q. Wang, J. Zhang, C. Li, Y. Wu, Z. Wei, X. Zhan, W. Hu, Z. Wang, R. A. J. Janssen, W. Li, *Adv. Mater.*, **2015**, n/a.
[**55**] V. Sgobba, A. Troeger, R. Cagnoli, A. Mateo-Alonso, M. Prato, F. Parenti, A. Mucci, L. Schenetti, D. M. Guldi, *J. Mater. Chem.*, **2009**, *19*, 4319.
[**56**] J. K. Mwaura, M. R. Pinto, D. Witker, N. Ananthakrishnan, K. S. Schanze, J. R. Reynolds, *Langmuir*, **2005**, *21*, 10119.
[**57**] R. Søndergaard, M. Helgesen, M. Jørgensen, F. C. Krebs, *Adv. Energy Mater.*, **2011**, *1*, 68.
[**58**] H. Li, Y. Li, J. Zhai, G. Cui, H. Liu, S. Xiao, Y. Liu, F. Lu, L. Jiang, D. Zhu, *Chem. Eur. J.*, **2003**, *9*, 6031.
[**59**] F. Xia, X. Zuo, R. Yang, Y. Xiao, D. Kang, A. Vallée-Bélisle, X. Gong, A. J. Heeger, K. W. Plaxco, *J. Am. Chem. Soc.*, **2010**, *132*, 1252.
[**60**] A. Satrijo, T. M. Swager, *J. Am. Chem. Soc.*, **2007**, *129*, 16020.
[**61**] D. T. McQuade, A. H. Hegedus, T. M. Swager, *J. Am. Chem. Soc.*, **2000**, *122*, 12389.
[**62**] H.-A. Ho, M. Leclerc, *J. Am. Chem. Soc.*, **2004**, *126*, 1384.
[**63**] Z. He, C. Zhong, S. Su, M. Xu, H. Wu, Y. Cao, *Nat Phot.*, **2012**, *6*, 591.
[**64**] Z. He, C. Zhong, X. Huang, W.-Y. Wong, H. Wu, L. Chen, S. Su, Y. Cao, *Adv. Mater.*, **2011**, *23*, 4636.
[**65**] Y.-M. Chang, C.-Y. Leu, *J. Mater. Chem. A*, **2013**, *1*, 6446.
[**66**] R. Xia, D.-S. Leem, T. Kirchartz, S. Spencer, C. Murphy, Z. He, H. Wu, S. Su, Y. Cao, J. S. Kim, J. C. deMello, D. D. C. Bradley, J. Nelson, *Adv. Energy Mater.*, **2013**, *3*, 718.
[**67**] L. Zhang, C. He, J. Chen, P. Yuan, L. Huang, C. Zhang, W. Cai, Z. Liu, Y. Cao, *Macromolecules*, **2010**, *43*, 9771.
[**68**] Z. He, C. Zhang, X. Xu, L. Zhang, L. Huang, J. Chen, H. Wu, Y. Cao, *Adv. Mater.*, **2011**, *23*, 3086.
[**69**] L. Hu, F. Wu, C. Li, A. Hu, X. Hu, Y. Zhang, L. Chen, Y. Chen, *Macromolecules*, **2015**, *48*, 5578.
[**70**] C. Duan, W. Cai, B. B. Y. Hsu, C. Zhong, K. Zhang, C. Liu, Z. Hu, F. Huang, G. C. Bazan, A. J. Heeger, Y. Cao, *Energy Environ. Sci.*, **2013**, *6*, 3022.
[**71**] T. Kietzke, D. Neher, K. Landfester, R. Montenegro, R. Guntner, U. Scherf, *Nat Mater*, **2003**, *2*, 408.
[**72**] K. Landfester, R. Montenegro, U. Scherf, R. Güntner, U. Asawapirom, S. Patil, D. Neher, T. Kietzke, *Adv. Mater.*, **2002**, *14*, 651.
[**73**] C. Wu, D. T. Chiu, *Angew. Chemie Int. Ed.*, **2013**, *52*, 3086.
[**74**] Y.-H. Chan, P.-J. Wu, *Part. Part. Syst. Charact.*, **2015**, *32*, 11.
[**75**] L. Feng, L. Liu, F. Lv, G. C. Bazan, S. Wang, *Adv. Mater.*, **2014**, *26*, 3926.
[**76**] N. A. A. Rahim, W. McDaniel, K. Bardon, S. Srinivasan, V. Vickerman, P. T. C. So, J. H. Moon, *Adv. Mater.*, **2009**, *21*, 3492.
[**77**] M. Mumtaz, A. de Cuendias, J.-L. Putaux, E. Cloutet, H. Cramail, *Macromol. Rapid Commun.*, **2006**, *27*, 1446.
[**78**] S. P. Armes, M. Aldissi, S. Agnew, S. Gottesfeld, *Langmuir*, **1990**, *6*, 1745.
[**79**] J. Stejskal, P. Kratochvíl, M. Helmstedt, *Langmuir*, **1996**, *12*, 3389.
[**80**] A. J. C. Kuehne, M. C. Gather, J. Sprakel, *Nat Commun*, **2012**, *3*, 1088.
[**81**] V. Schmitt, C. Cattelet, F. Leal-Calderon, *Langmuir*, **2004**, *20*, 46.
[**82**] C. M. Tseng, Y. Y. Lu, M. S. El-Aasser, J. W. Vanderhoff, *J. Polym. Sci. Part A Polym. Chem.*, **1986**, *24*, 2995.
[**83**] H. Bamnolker, S. Margel, *J. Polym. Sci., Part A Polym. Chem.*, **1996**, *34*, 1857.
[**84**] S. Shen, E. D. Sudol, M. S. El-Aasser, *J. Polym. Sci. Part A Polym. Chem.*, **1993**, *31*, 1393.

[**85**] D. Wang, V. L. Dimonie, E. D. Sudol, M. S. El-Aasser, *J. Appl. Polym. Sci.*, **2002**, *84*, 2692.
[**86**] Q. Ye, Z. Zhang, H. Jia, W. He, X. Ge, *J. Colloid Interface Sci.*, **2002**, *253*, 279.
[**87**] E. Bourgeat-Lami, J. Lang, *J. Colloid Interface Sci.*, **1998**, *197*, 293.
[**88**] A. Benichou, A. Aserin, N. Garti, *J. Dispers. Sci. Technol.*, **2002**, *23*, 93.
[**89**] G. L. Jialanella, E. M. Firer, I. Piirma, *J. Polym. Sci. Part A Polym. Chem.*, **1992**, *30*, 1925.
[**90**] F. Corcos, E. Bourgeat-Lami, C. Novat, J. Lang, *Colloid Polym. Sci.*, **1999**, *277*, 1142.
[**91**] J.-L. Mura, G. Riess, *Polym. Adv. Technol.*, **1995**, *6*, 497.
[**92**] B. Vincent, *Polym. Adv. Technol.*, **1995**, *6*, 356.
[**93**] J. Pecher, S. Mecking, *Chem. Rev.*, **2010**.
[**94**] T. K. Mandal, B. M. Mandal, *J. Polym. Sci. Part A Polym. Chem.*, **1999**, *37*, 3723.
[**95**] R. B. Bjorklund, B. Liedberg, *J. Chem. Soc. Chem. Commun.*, **1986**, 1293.
[**96**] J. Stejskal, P. Kratochvíl, S. P. Armes, S. F. Lascelles, A. Riede, M. Helmstedt, J. Prokeš, I. Křivka, *Macromolecules*, **1996**, *29*, 6814.
[**97**] S. P. Armes, M. Aldissi, *J. Chem. Soc. Chem. Commun.*, **1989**, 88.
[**98**] K. Mallick, M. J. Witcomb, A. Dinsmore, M. S. Scurrell, *Macromol. Rapid Commun.*, **2005**, *26*, 232.
[**99**] N. Anwar, T. Willms, B. Grimme, A. J. C. Kuehne, *ACS Macro Lett.*, **2013**, *2*, 766.
[**100**] S. Ciftci, A. J. C. Kuehne, *Macromolecules*, **2015**, *48*, 8389.
[**101**] N. Anwar, A. Rix, W. Lederle, A. J. C. Kuehne, *Chem. Commun.*, **2015**, *51*, 9358.
[**102**] L. Parrenin, C. Brochon, G. Hadziioannou, E. Cloutet, *Macromol. Rapid Commun.*, **2015**, *36*, 1816.
[**103**] J.-C. Daniel, C. Pichot, *Les Latex Synthétiques*, Lavoisier, **2006**.
[**104**] J. Huber, S. Mecking, *Angew. Chemie Int. Ed.*, **2006**, *45*, 6314.
[**105**] S. Mecking, A. Held, F. M. Bauers, *Angew. Chemie Int. Ed.*, **2002**, *41*, 544.
[**106**] S. Mecking, *Colloid Polym. Sci.*, **2006**, *285*, 605.
[**107**] R. Wang, C. Zhang, W. Wang, T. Liu, *J. Polym. Sci. Part A Polym. Chem.*, **2010**, *48*, 4867.
[**108**] D. Muenmart, A. B. Foster, A. Harvey, M.-T. Chen, O. Navarro, V. Promarak, M. C. McCairn, J. M. Behrendt, M. L. Turner, *Macromolecules*, **2014**, *47*, 6531.
[**109**] L. Zhang, T. Lin, X. Pan, W. Wang, T.-X. Liu, *J. Mater. Chem.*, **2012**, *22*, 9861.
[**110**] J. Pecher, S. Mecking, *Macromolecules*, **2007**, *40*, 7733.
[**111**] M. C. Baier, J. Huber, S. Mecking, *J. Am. Chem. Soc.*, **2009**, *131*, 14267.
[**112**] C. Jung, M. Krumova, S. Mecking, *Langmuir*, **2014**, *30*, 9905.
[**113**] J. Pecher, J. Huber, M. Winterhalder, A. Zumbusch, S. Mecking, *Biomacromolecules*, **2010**, *11*, 2776.
[**114**] E. Hittinger, A. Kokil, C. Weder, *Angew. Chemie Int. Ed.*, **2004**, *43*, 1808.
[**115**] A. Patra, J.-M. Koenen, U. Scherf, *Chem. Commun.*, **2011**, *47*, 9612.
[**116**] P. Zhang, Z. Weng, J. Guo, C. Wang, *Chem. Mater.*, **2011**, *23*, 5243.
[**117**] B. C. Ma, S. Ghasimi, K. Landfester, F. Vilela, K. A. I. Zhang, *J. Mater. Chem. A*, **2015**, *3*, 16064.
[**118**] C. Negele, J. Haase, A. Leitenstorfer, S. Mecking, *ACS Macro Lett.*, **2012**, *1*, 1343.
[**119**] H. Li, X. Wu, B. Xu, H. Tong, L. Wang, *RSC Adv.*, **2013**, *3*, 8645.
[**120**] X. Wu, H. Li, Y. Xu, B. Xu, H. Tong, L. Wang, *Nanoscale*, **2014**, *6*, 2375.
[**121**] X. Wu, H. Li, B. Xu, H. Tong, L. Wang, *Polym. Chem.*, **2014**, *5*, 4521.
[**122**] H. Shimizu, M. Yamada, R. Wada, M. Okabe, *Polym. J*, **2007**, *40*, 33.
[**123**] C. Wu, C. Szymanski, J. McNeill, *Langmuir*, **2006**, *22*, 2956.
[**124**] X. Zhang, J. Yu, C. Wu, Y. Jin, Y. Rong, F. Ye, D. T. Chiu, *ACS Nano*, **2012**, *6*, 5429.
[**125**] T. Adachi, L. Tong, J. Kuwabara, T. Kanbara, A. Saeki, S. Seki, Y. Yamamoto, *J. Am. Chem. Soc.*, **2013**, *135*, 870.
[**126**] X. Xu, Z. Xu, S. Ye, Y. Liu, M. Wu, L. Li, *Part. Part. Syst. Charact.*, **2015**, n/a.
[**127**] N. Kurokawa, H. Yoshikawa, N. Hirota, K. Hyodo, H. Masuhara, *ChemPhysChem*, **2004**, *5*, 1609.
[**128**] H. Yabu, T. Higuchi, K. Ijiro, M. Shimomura, *Chaos*, **2005**, *15*, 047505.
[**129**] F. Bally, D. K. Garg, C. A. Serra, Y. Hoarau, N. Anton, C. Brochon, D. Parida, T. Vandamme, G. Hadziioannou, *Polymer (Guildf).*, **2012**, *53*, 5045.
[**130**] C. Wu, C. Szymanski, Z. Cain, J. McNeill, *J. Am. Chem. Soc.*, **2007**, *129*, 12904.
[**131**] C. Szymanski, C. Wu, J. Hooper, M. A. Salazar, A. Perdomo, A. Dukes, J. McNeill, *J. Phys. Chem. B*, **2005**, *109*, 8543.
[**132**] J. Xu, Y. Zhou, G. Cheng, S. Liu, M. Dong, C. Huang, *Luminescence*, **2015**, *30*, 451.
[**133**] C.-G. Qian, S. Zhu, P.-J. Feng, Y.-L. Chen, J.-C. Yu, X. Tang, Y. Liu, Q.-D. Shen, *ACS Appl. Mater. Interfaces*, **2015**, *7*, 18581.
[**134**] E. S. Childress, C. A. Roberts, D. Y. Sherwood, C. L. M. LeGuyader, E. J. Harbron, *Anal. Chem.*, **2012**, *84*, 1235.

[**135**] F. Ye, C. Wu, Y. Jin, Y.-H. Chan, X. Zhang, D. T. Chiu, *J. Am. Chem. Soc.*, **2011**, *133*, 8146.
[**136**] C. Wu, B. Bull, K. Christensen, J. McNeill, *Angew. Chemie Int. Ed.*, **2009**, *48*, 2741.
[**137**] D. Darwis, D. Elkington, E. Sesa, N. Cooling, G. Bryant, X. Zhou, W. Belcher, P. Dastoor, in *AIP Conf. Proc.*, **2011**, pp. 120.
[**138**] S. Gärtner, M. Christmann, S. Sankaran, H. Röhm, E.-M. Prinz, F. Penth, A. Pütz, A. E. Türeli, B. Penth, B. Baumstümmler, A. Colsmann, *Adv. Mater.*, **2014**, *26*, 6653.
[**139**] S. Sankaran, K. Glaser, S. Gärtner, T. Rödlmeier, K. Sudau, G. Hernandez-Sosa, A. Colsmann, *Org. Electron.*, **2016**, *28*, 118.
[**140**] P. Sarrazin, D. Chaussy, L. Vurth, O. Stephan, D. Beneventi, *Langmuir*, **2009**, *25*, 6745.
[**141**] C. R. McNeill, S. Westenhoff, C. Groves, R. H. Friend, N. C. Greenham, *J. Phys. Chem. C*, **2007**, *111*, 19153.
[**142**] T. P. and H. P. and G. M. and S. G. and C. G. and F. P. W. and S. P. and R. M. and M. B. and J. R. R. and U. S. and K. L. and E. J. W. List, *Jpn. J. Appl. Phys.*, **2005**, *44*, 479.
[**143**] E. Fisslthaler, S. Sax, U. Scherf, G. Mauthner, E. Moderegger, K. Landfester, E. J. W. List, *Appl. Phys. Lett.*, **2008**, *92*, 1.
[**144**] T. Piok, S. Gamerith, C. Gadermaier, H. Plank, F. P. Wenzl, S. Patil, R. Montenegro, T. Kietzke, D. Neher, U. Scherf, K. Landfester, E. J. W. List, *Adv. Mater.*, **2003**, *15*, 800.
[**145**] O. Pras, D. Chaussy, O. Stephan, Y. Rharbi, P. Piette, D. Beneventi, *Langmuir*, **2010**, *26*, 14437.
[**146**] N. A. D. Yamamoto, M. E. Payne, M. Koehler, A. Facchetti, L. S. Roman, A. C. Arias, *Sol. Energy Mater. Sol. Cells*, **2015**, *141*, 171.
[**147**] Y.-X. Nan, X.-L. Hu, T. T. Larsen-Olsen, B. Andreasen, T. Tromholt, J. W. Andreasen, D. M. Tanenbaum, H.-Z. Chen, F. C. Krebs, *Nanotechnology*, **2011**, *22*, 475301.
[**148**] O. Ghazy, *Macromol. Symp.*, **2015**, *352*, 25.
[**149**] O. A. Ghazy, *Adv. Polym. Technol.*, **2015**, *34*, 1.
[**150**] K. Landfester, R. Montenegro, U. Scherff, R. Güntner, U. Asawapirom, S. Patil, D. Neher, T. Kietzke, *Adv. Mater.*, **2002**, *14*, 651.
[**151**] T. Kietzke, D. Neher, M. Kumke, R. Montenegro, K. Landfester, U. Scherf, *Macromolecules*, **2004**, *37*, 4882.
[**152**] T. Kietzke, D. Neher, K. Landfester, R. Montenegro, B. Guntner, U. Scherf, *Nat. Mater.*, **2003**, *2*, 408.
[**153**] N. P. Holmes, M. Marks, P. Kumar, R. Kroon, M. G. Barr, N. Nicolaidis, K. Feron, A. Pivrikas, A. Fahy, A. D. de Z. Mendaza, A. L. D. Kilcoyne, C. Müller, X. Zhou, M. R. Andersson, P. C. Dastoor, W. J. Belcher, *Nano Energy*, **2016**, *19*, 495.
[**154**] B. Vaughan, E. L. Williams, N. P. Holmes, P. Sonar, A. Dodabalapur, P. C. Dastoor, W. J. Belcher, *Phys. Chem. Chem. Phys.*, **2014**, *16*, 2647.
[**155**] T. T. Larsen-Olsen, B. Andreasen, T. R. Andersen, A. P. L. Böttiger, E. Bundgaard, K. Norrman, J. W. Andreasen, M. Jørgensen, F. C. Krebs, *Sol. Energy Mater. Sol. Cells*, **2012**, *97*, 22.
[**156**] J. Cho, K. H. Cheon, H. Ahn, K. H. Park, S.-K. Kwon, Y.-H. Kim, D. S. Chung, *Adv. Mater.*, **2015**, 5587.
[**157**] T. T. Larsen-Olsen, T. R. Andersen, B. Andreasen, A. P. L. Böttiger, E. Bundgaard, K. Norrman, J. W. Andreasen, M. Jørgensen, F. C. Krebs, *Sol. Energy Mater. Sol. Cells*, **2012**, *97*, 43.
[**158**] A. Stapleton, B. Vaughan, B. Xue, E. Sesa, K. Burke, X. Zhou, G. Bryant, O. Werzer, A. Nelson, A. L. David Kilcoyne, L. Thomsen, E. Wanless, W. Belcher, P. Dastoor, *Sol. Energy Mater. Sol. Cells*, **2012**, *102*, 114.
[**159**] B. Vaughan, A. Stapleton, B. Xue, E. Sesa, X. Zhou, G. Bryant, W. Belcher, P. Dastoor, *Appl. Phys. Lett.*, **2012**, *101*.
[**160**] S. Ulum, N. Holmes, M. Barr, A. L. D. Kilcoyne, B. Bin Gong, X. Zhou, W. Belcher, P. Dastoor, *Nano Energy*, **2013**, *2*, 897.
[**161**] K. Feron, S. Ulum, E. Sesa, B. B. Gong, W. J. Belcher, X. Zhou, C. . Fell, P. C. Dastoor, *J. Appl. Phys.*, **2014**, *116*, 124502.
[**162**] N. P. Holmes, S. Ulum, P. Sista, K. B. Burke, M. G. Wilson, M. C. Stefan, X. Zhou, P. C. Dastoor, W. J. Belcher, *Sol. Energy Mater. Sol. Cells*, **2014**, *128*, 369.
[**163**] M. Bag, T. S. Gehan, L. A. Renna, D. D. Algaier, P. M. Lahti, D. Venkataraman, *RSC Adv.*, **2014**, *4*, 45325.
[**164**] H. F. Dam, N. P. Holmes, T. R. Andersen, T. T. Larsen-Olsen, M. Barr, A. L. D. Kilcoyne, X. Zhou, P. C. Dastoor, F. C. Krebs, W. J. Belcher, *Sol. Energy Mater. Sol. Cells*, **2015**, *138*, 102.
[**165**] B. Vaughan, A. Stapleton, E. Sesa, N. P. Holmes, X. Zhou, P. C. Dastoor, W. J. Belcher, *Org. Electron.*, **2016**, *32*, 250.
[**166**] S. Gartner, S. Reich, M. Bruns, J. Czolk, A. Colsmann, *Nanoscale*, **2016**, *8*, 6721.
[**167**] N. Blouin, A. Michaud, M. Leclerc, *Adv. Mater.*, **2007**, *19*, 2295.
[**168**] D. H. Wang, J. K. Kim, J. H. Seo, I. Park, B. H. Hong, J. H. Park, A. J. Heeger, *Angew. Chemie Int. Ed.*, **2013**, *52*, 2874.

[**169**] J. Zhao, A. Swinnen, G. Van Assche, J. Manca, D. Vanderzande, B. Van Mele, *J. Phys. Chem. B*, **2009**, *113*, 1587.

[**170**] M. O. Reese, S. A. Gevorgyan, M. Jørgensen, E. Bundgaard, S. R. Kurtz, D. S. Ginley, D. C. Olson, M. T. Lloyd, P. Morvillo, E. A. Katz, A. Elschner, O. Haillant, T. R. Currier, V. Shrotriya, M. Hermenau, M. Riede, K. R. Kirov, G. Trimmel, T. Rath, O. Inganäs, F. Zhang, M. Andersson, K. Tvingstedt, M. Lira-Cantu, D. Laird, C. McGuiness, S. (Jimmy) Gowrisanker, M. Pannone, M. Xiao, J. Hauch, R. Steim, D. M. DeLongchamp, R. Rösch, H. Hoppe, N. Espinosa, A. Urbina, G. Yaman-Uzunoglu, J.-B. Bonekamp, A. J. J. M. van Breemen, C. Girotto, E. Voroshazi, F. C. Krebs, *Sol. Energy Mater. Sol. Cells*, **2011**, *95*, 1253.

Chapter II
PCDTBT particles by dispersion polymerization

In this work we present the synthesis of poly[N-9'-heptadecanyl-2,7-carbazole-*alt*-5,5-(4,7-di-2-thienyl-2',1',3'-benzothiadiazole] (PCDTBT) in propan-1-ol as the dispersant continuous phase in the presence of poly(vinylpyrrolidone) (PVP) used as stabilizer. Suzuki-Miyaura polycondensation of 9-(9-Heptadecanyl)-9H-carbazole-2,7-diboronic acid bis(pinacol) ester and 4,7-Bis(2-bromo-5-thienyl)-2,1,3-benzothiadiazole in alcohol dispersion yields colloidally stable nanoparticles of PCDTBT with particles size of 330-1600 nm, depending on the stabilizer concentration. Other reaction parameters are also discussed such as the amount of base or Pd catalyst.

- CHAPTER II -

PCDTBT particles by dispersion polymerization

Table of Contents

List of the figures

List of the equations

List of the tables

II.1. Introduction

The objective of this work is the synthesis of π-conjugated polymer particles in eco-friendly media to get rid of the toxic solvents usually used during the synthesis and the deposition in thin film for devices fabrication.

Typical use of such polymer particles dispersion is depicted below (see figure 1) for the fabrication of organic photovoltaic cells (OPV).

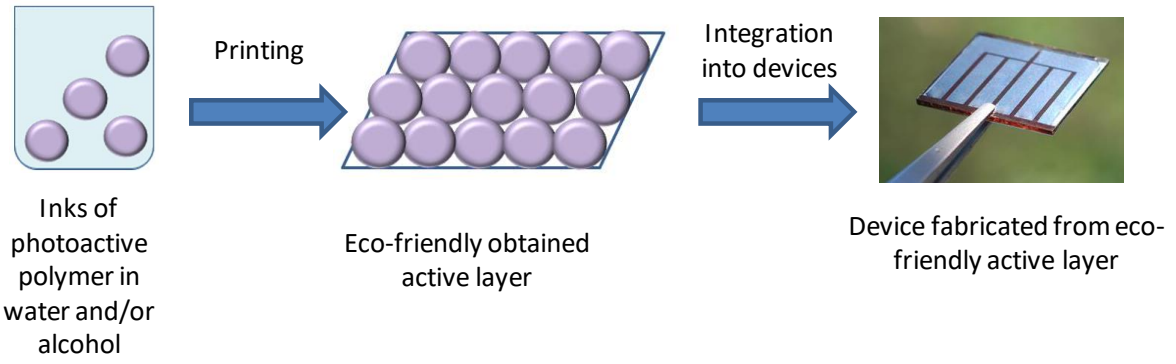

Figure 1 : Schematic of the strategy for the fabrication of OPV devices from eco-friendly active layer

II.1.1. Methodology

Dispersion polymerization was chosen as the first route to try toward the synthesis of particles in heterogeneous conditions (see figure 2).

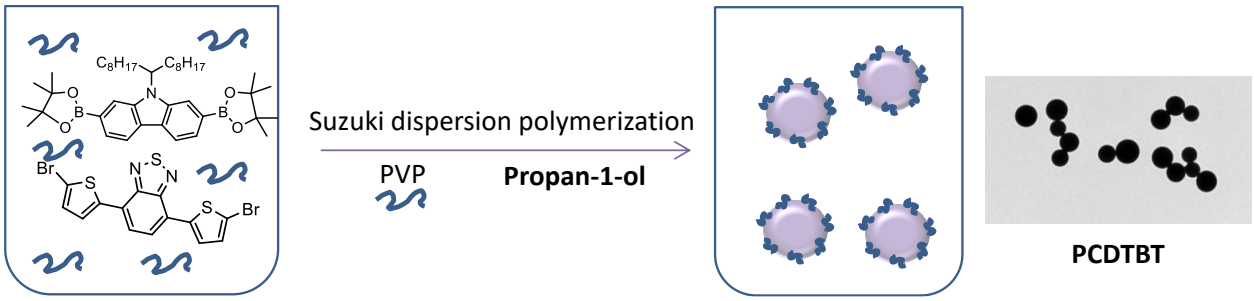

Figure 2 : Schematic of the strategy followed for the synthesis of the π-conjugated polymer PCDTBT as particles by Suzuki dispersion polymerization

The dispersion polymerization has been first introduced by Osmond *et al* and developed in the 1960's mainly by the paint industry. The mechanism has been studied by two authors Lock *et al.* and Paine *et al.*[1] Initially, the system forms one single phase[2] (see

figure 3). Once the monomer(s) have been reacting, oligomers are created. From the moment they reach a critical length, the chains will precipitate to form nuclei. This step determined the number of particles and as a consequence the size and the size distribution of the particles at the final stage.

The polymerization continues in the two media: in the continuous phase there is polymerization followed by precipitation of the chains onto the preexisting particles, and in the particles where the polymerization goes on. Most of the time the polymerization takes place mainly in the formed particles, the polymerization rate is controlled by the concentration of monomers in the particles and by the monomers diffusion in the continuous phase.

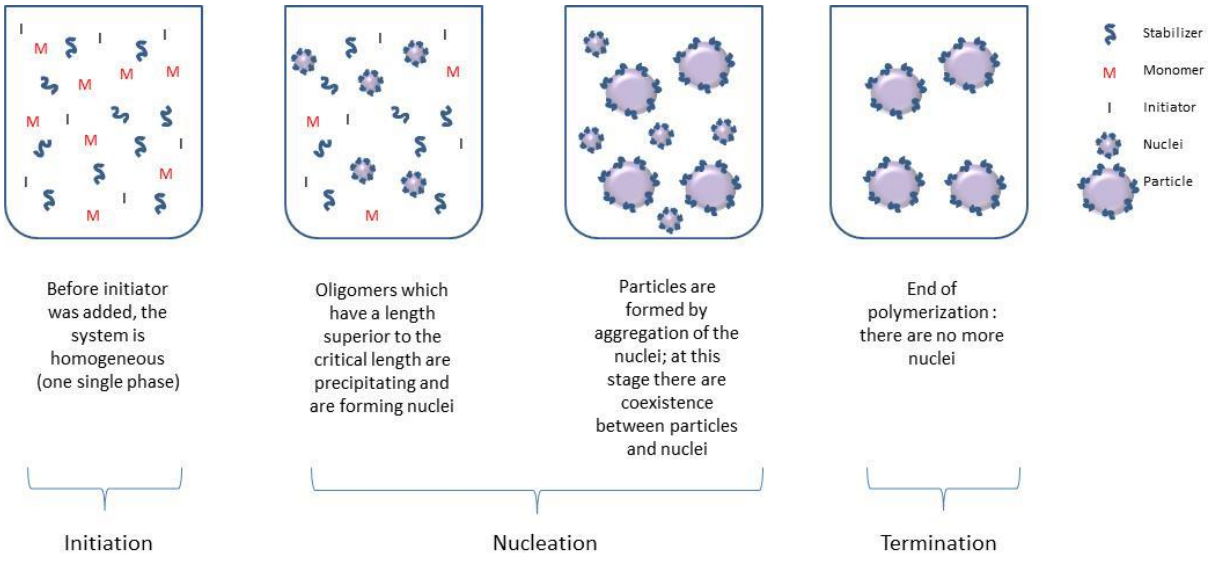

Figure 3 : Scheme of the dispersion polymerization : initial stage, nucleation and termination

The chains precipitation can be controlled by the addition of a stabilizer which is soluble in the medium and is adsorbed at the surface of the particles.

For a good stabilization, the stabilizer is composed of two parts which provide an amphiphilic behavior: a hydrophilic one (to ensure the steric barrier between the particles) and a hydrophobic one (to allow the anchoring at the surface of the particles). A high molar mass stabilizer is usually preferred because the particles will be better covered.[3]

N-polyvinylpyrrolidone (PVP) was chosen as stabilizer which is a well-known stablizer used in dispersion polymerization in water or alcoholic media (see figure 4).[4–9]

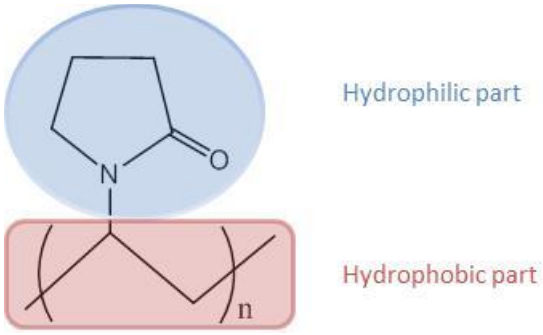

Figure 4 : Chemical structure of N-polyvinylpyrrolidone

The dispersion polymerization process has been used a lot because it enables to form various sizes in the range of 200 nm to 20 µm.

The first conjugated polymer synthesized by dispersion polymerization was polyacetylene.[10] As discussed in the chapter I, most of the conducting polymers synthesized by dispersion polymerization were made by oxidative coupling[11] of pyrrole[12,13] or aniline[14–16] or PEDOT.[3]

Polymerizations in dispersed media have the advantage to be not only restricted to polymer which are soluble in organic medium and offer a large range of particles size. This is a powerful tool to synthesize latexes which can be used in lots of applications such as paints, cosmetics, food-processing industry etc…

II.1.2. Suzuki coupling by dispersion polymerization

Suzuki coupling's mechanism has been debated. Two mechanisms have been proposed which can be seen in figure 5. The first step of the Suzuki-coupling is the oxidative insertion of $Pd^{(0)}$ into the carbon-bromine bond of the bromide compound providing an aryl $Pd^{(II)}$ intermediate. In the next step, the two mechanisms differ. In the first proposed mechanism, the base initiates the transmetallation whereas in the second, the base (hydroxide in this case) displaces the bromine from palladium. The hydroxyl group, now attached to the palladium metal, can bind to the boronic acid. This pre-coordination of the palladium hydroxide to the boronic acid facilitates the subsequent transmetallation. In the

final step, the final C-C bond is formed by reductive elimination, which regenerates the $Pd^{(0)}$ catalyst.

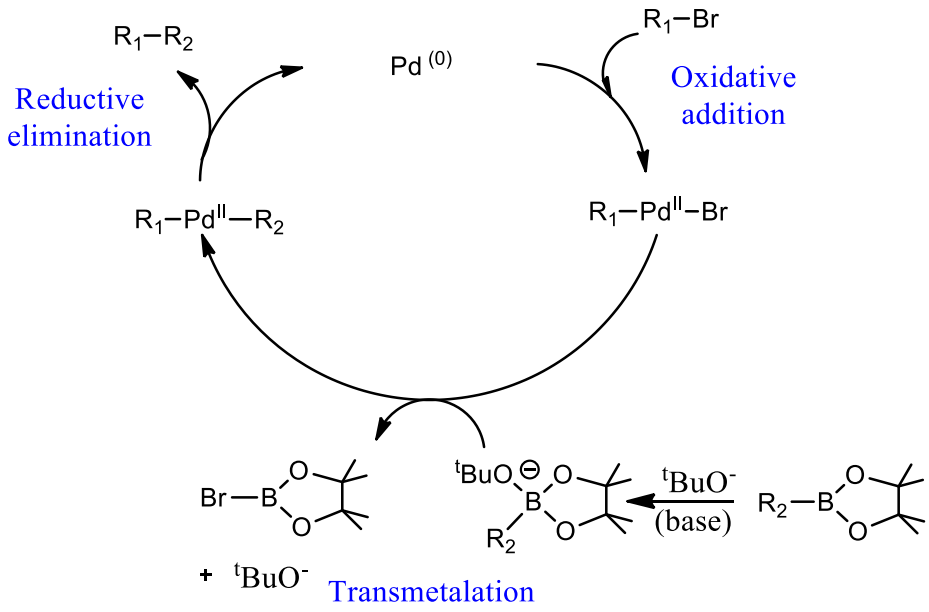

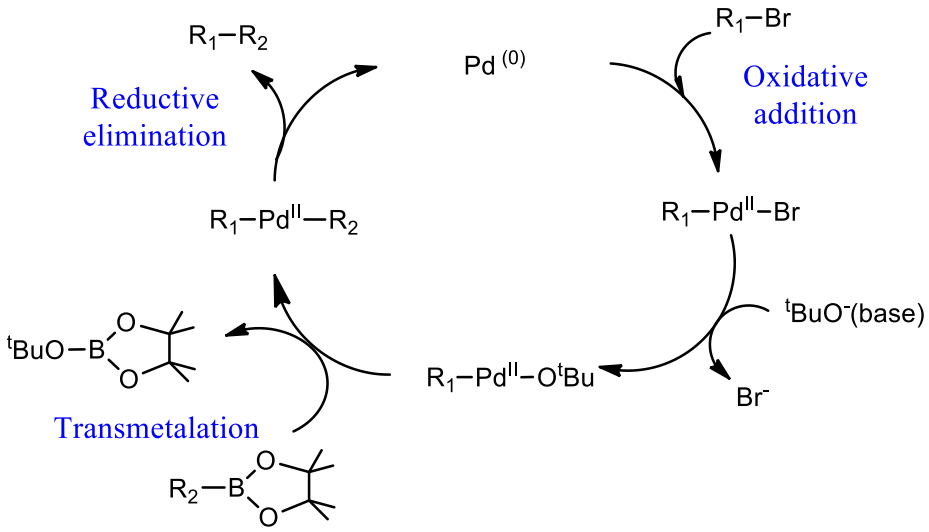

Figure 5 : Mechanistic outlines of the Suzuki coupling

In this chapter we were inspired by the work from Kuehne's team [17,18] who was the first to propose a new method for the preparation of poly(fluorene) and poly(thiophene) nanoparticles in alcohol. In 2013 they first demonstrated a Suzuki coupling dispersion polymerization, producing monodisperse particles thanks to two stabilizers : a block-copolymer poly(1-vinylpyrrolidone-*co*-vinyl acetate) (PVPVA) and a non-ionic surfactant: Triton™ X-45.

Four types of particles were synthesized with molar masses between 8.5 and 17 kDa (see Figure 6) which could be used for photonic crystals.[17]

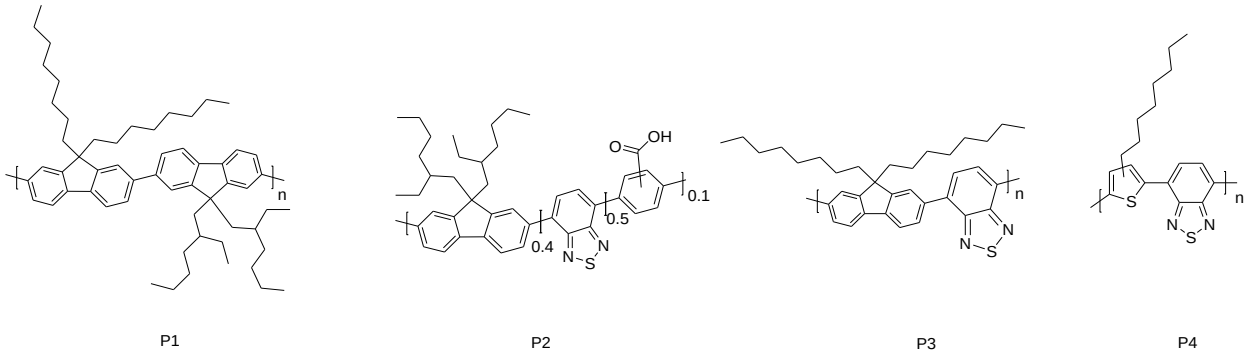

Figure 6 : Poly(dioctylfluorene-*alt*-diethylhexylfluorene) (P1), Poly(dioctylfluorene-*alt*-benzothiadiazole) (P2), Poly(diethylhexyl-*co*-benzothiadiazole-*co*-benzoic acid) (P3), Poly(thiophene-*alt*-benzothiadiazole) (P4) synthesized by Suzuki dispersion polymerization in 2013 by Kuehne and coll. [17]

Within the same year, Kuehne *and coll.* also presented three other copolymers made of fluorene and azobenzene moieties synthesized by dispersion polymerization. The molar mass obtained is 13 kDa for the two first and 50 kDa for the last one (see figure 7). These particles react with light thanks to the azobenzene moiety, finding application in photonic or labelling for biomedical.[18]

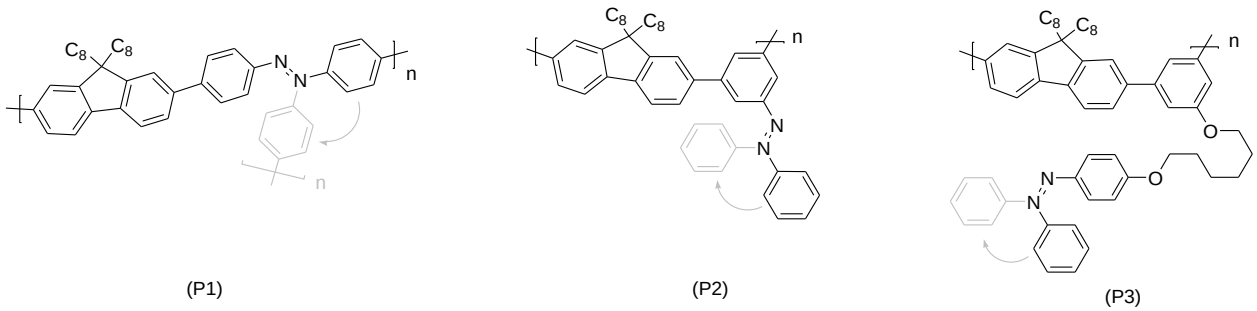

Figure 7 : Poly(fluorine-*co*-azobenzene) synthesized by Suzuki dispersion polymerization：azobenzene unit along the Polymer Backbone (P1), Perpendicular to the Polymer Chain (P2), and Electronically Decoupled from the Polymer Backbone by Means of an Alkyl-Spacer (P3) [18]

The size of the particles can be controlled by the monomers concentration within the medium even if above a typical concentration, the system was not monodisperse anymore.

II.2. Results and discussion

II.2.1. Synthesis of PCDTBT by dispersion polymerization

The main challenge was to find a good solvent for all the reactants (monomers, stabilizer, base and catalyst) which is also environmentally-friendly, in this case the propan-1-ol. Tetrakis(triphenylphosphine)-palladium$^{(0)}$ and *tert*-butoxide were chosen as the catalyst and the base respectively (see figure 8).

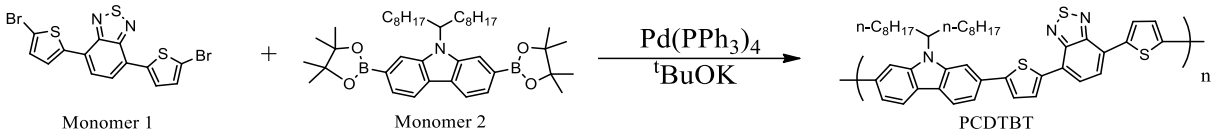

Figure 8 : Reaction scheme for PCDTBT particles during a Suzuki dispersion polymerization

Equimolar amount of 4,7-Bis(2-bromo-5-thienyl)-2,1,3-benzothiadiazole (electron-poor unit) reacts with 9-(9-Heptadecanyl)-9H-carbazole-2,7-diboronic acid bis(pinacol) ester (electron-rich unit) to obtain poly[N- 9'-heptadecanyl-2,7-carbazole-*alt*-5,5-(4,7-di-2-thienyl-2',1',3'-benzothiadiazole] (PCDTBT) in Suzuki-coupling dispersion polymerization conditions.

Completion of the reaction is confirmed by ^{1}H-NMR (see appendix figures 18 and 19), UV-visible spectroscopy and TGA (see appendix figures 20 and 21).

The reaction medium is initially transparent (figure 9a) and became milky when the particles are formed due to the light scattering (figure 9b). The color change indicates that the polymerization has started.

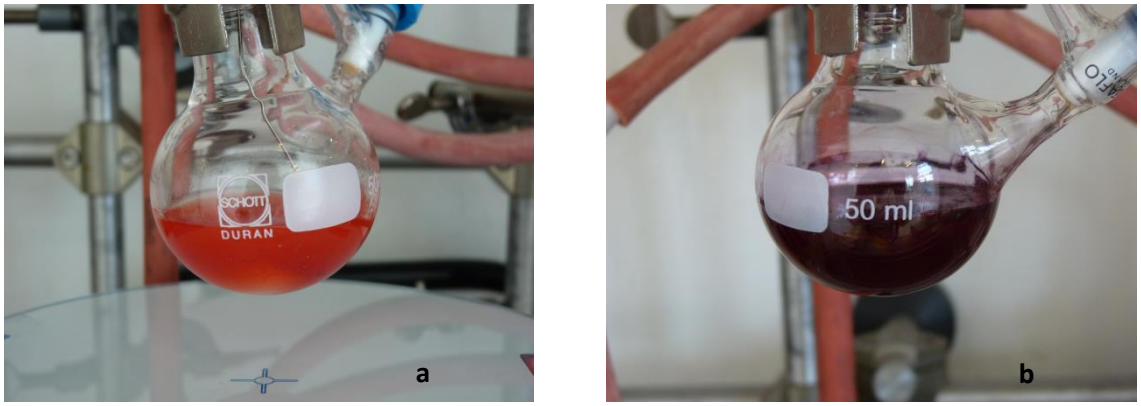

Figure 9 : PCDTBT synthesis in propan-1-ol : pictures of the solutions before the addition of the base (a) and after polymerization (b)

Suzuki-coupling dispersion polymerization allows us to reach PCDTBT particles with a relatively broad size distribution (particles'size between 500 and 670 *i.e.* PDI around 15%). Such particle size distribution will be discussed later but it happens to be an asset for a thin film formation where the smallest particles can fill the empty space between the biggest to form a more homogeneous layer.

A kinetics study was performed by measuring the size of the particles at different time scale (see figure 10). A plateau was reached at 1 hour and a half where the particle size doesn't evolve anymore. Thus in the following, reaction time was set at 90 min for the rest of experiments.

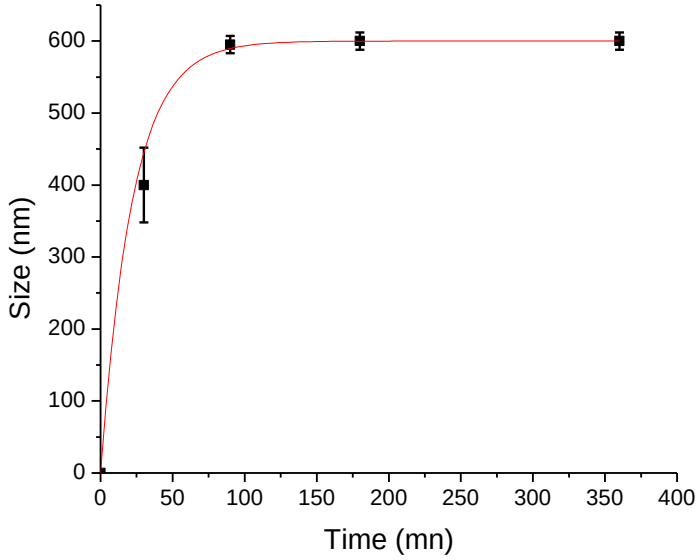

Figure 10 : Size of the particles *vs* reaction time : Suzuki dispersion polymerization of PCDTBT using entry 1 methodology in Table 1

The exponential growth rate is in agreement with step-growth polymerization and with what Kuehne *and coll* found in the case of the Heck coupling for the synthesis of poly(fluorene-*co*-divinylbenzene).[19]

Unfortunately we were not able to draw conversion *vs* time because of low amount of aliquots and NMR results were not well defined enough.

II.2.2. Reaction parameters influence on the particles size and size distribution

Different parameters of the reaction were varied to understand their impact on the size and size distribution of the particles.

The solvent quality affects the oligomers'critical length precipitation: by adding a better solvent, the size of the particles was increased.[2] Thus, if some toluene is added to the propan-1-ol (toluene is usually used for the "classical" PCDTBT synthesis as it is a relatively good solvent for the polymer), bigger particles size can be observed around 670 nm with respect to propan-1-ol sole (around 595 nm) (see figure 11 images 1 and 2).

As can be seen in table 1, the particle size could be affected by the stabilizer quantity. A high molar mass PVP (360 kDa) was used in order to increase the steric stabilization efficiency compared to a lower molar mass stabilizer.[20] By using less stabilizer than the control experiment (table 1 sample 1) particles were bigger, which could be explained by a lower coverable surface, which ends in bigger particles (see figure 11 images 1 and 3). Equivalent results have been demonstrated by Mandal *and coll* for the dispersion polymerization of pyrrole.[12]

Table 1 : Study of various conditions for the synthesis of PCDTBT particles by dispersion polymerization : effect of solvent ratio, stabilizer, monomers ratio, base and catalyst. [a)] determined by TEM

Entry	Variable	PVP *vs* monomers [wt%]	m(M2)/m(M1) [mol/mol]	Base *vs* monomers [mol%]	Catalyst *vs* monomers [mol%]	Size[a)] [nm]	PDI %
1	/	100	0.99	200	3	585	15
2	Solvent ratio	100	0.99	200	3	670	18
3	Stabilizer	50	0.99	200	3	1580	20
4	Monomers ratio	100	0.89	200	3	280	22
5	Base	100	0.99	40	3	650	28
6	Base	100	0.99	450	3	360	23
7	Catalyst	100	0.99	200	0.3	600	26

The monomers stoichiometry is an important parameter to control as in all polycondensation type reactions it affects the molar mass according to the Carothers law (see equation 1).

$$\bar{Xn} = \frac{1 + r}{1 + r - 2rp}$$

Equation 1: Carothers'law for non stoechiometric polycondensation

With r stoichiometric ratio; p the conversion rate; $\bar{X}n$ the degree of polymerization

For a total conversion of the limiting monomer, the conversion tends to 1, so the polymerization degree tends to:

$$\lim_{p \to 1} \bar{Xn} = \frac{1 + r}{1 - r}$$

Equation 2 : Carothers'law for full conversion

If one monomer *vs* the other is only 1% in excess, the stoichiometric ratio is equal to 0.99 so the limiting polymerization degree is 199 vs ∞ for equimolarity. As can be seen on table 1, below the equivalence particles are smaller, probably due to a smaller molar mass of the polymer chains (following Carothers' law). The stoichiometry has also a big influence on the dispersity because it can go up to 22% at 1.06eq of monomer 1 regarding monomer 2 (see figure 11 images 1 and 4).

In the literature, the role of the base in the Suzuki coupling mechanism is not fully understood. During the last twenty years, Suzuki and Miyaura have shown that this reaction requires two equivalents of base : one for the boronic acid quaternization and another one for the organopalladium halide metathesis into organopalladium hydroxide.[21,22] By decreasing the base quantity, the particles'size and size dispersity increased (Table 1 sample 5). Less base creates less nuclei giving rise to bigger particles (vice-versa for the sample 6, see figure 11 images 1 and 6). Stable dispersions have been obtained with lower base quantities, which goes along with what Mecking *and coll*[23] demonstrated for the miniemulsion polymerization of polyfluorene : one equivalent of base was enough for an efficient catalysis.

Finally the catalyst quantity has been varied as well. As expected, the particles'size increases when the catalyst quantity decreases because fewer chains are created which leads to bigger particles (see table 1, sample 7 and figure 11 images 1 and 7).

To sum-up, PCDTBT particles were synthesized by dispersion polymerization in propan-1-ol and the size and size distribution can be tuned by the synthesis parameters.

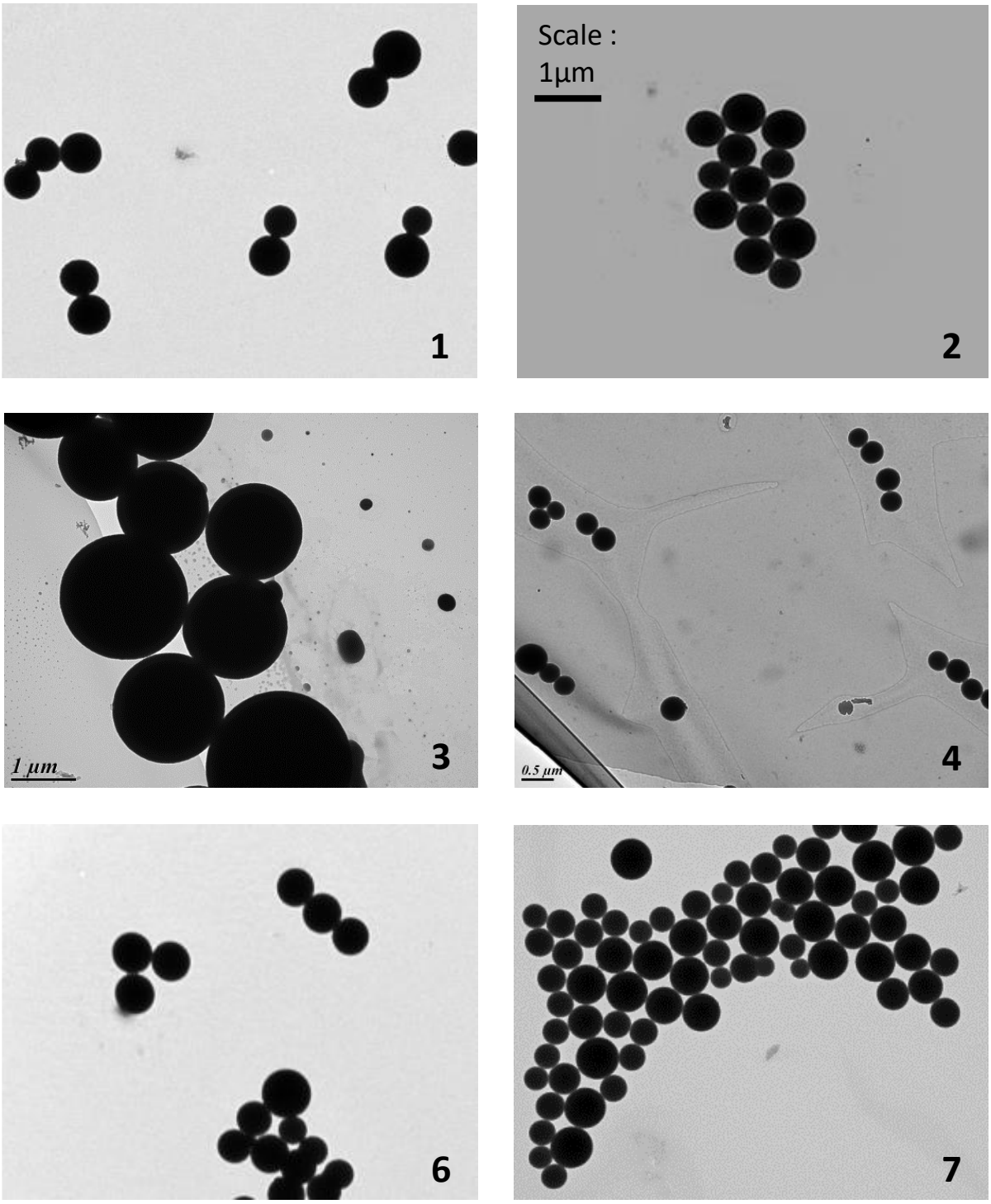

Figure 11 : TEM images of the PCDTBT particles synthesized by dispersion polymerization in propan-1-ol (the number corresponds to the entry number in Table 1)

II.2.3. Optoelectronic properties of PCDTBT particles

Absorption spectra were measured on particles in propan-1-ol (see figure 12 a), on particles dissolved into chloroform and on PCDTBT synthesized by a "classical" way called bulk PCDTBT (see figure 12 b) for the sake of comparison.

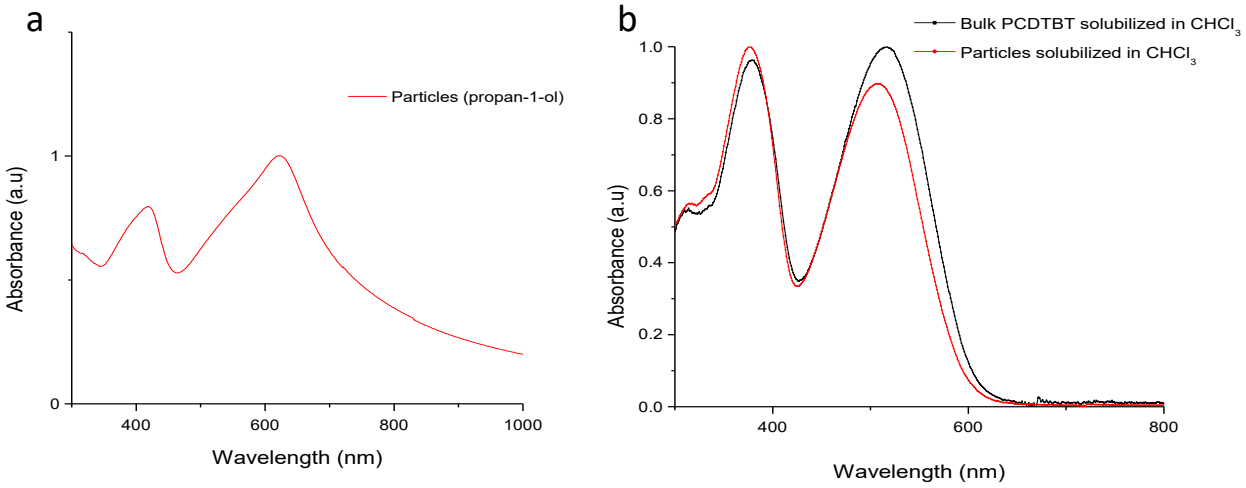

Figure 12 : Absorbance spectrum of PCDTBT particles in propan-1-ol (a) and PCDTBT synthesized by "classical" way (black curve) and by dispersion dissolved in chloroform (red curve) (b)

From figure 12 a, broad absorption peaks can be noticed with shouldering at 400 and 550 nm compared to particles solubilized into chloroform (figure 12 b). We checked that the shouldering was not due to light scattering by measuring the absorbance at different concentrations and with a smaller cuvette (following the Beer-Lambert law).

By comparing figure 12 a to b differences can be observed such as a shift of the peaks towards higher wavelength for the particles and a broadening when the polymer is under the form of particles (figure 12 a) with respect to the dissolved polymer (figure 12 b red curve). This is a well-known phenomenon due to the aggregation as reported previously for poly(3-hexylthiophene) (P3HT)[24] and poly(naphthalene diimide) (PNDI).[25]

It can be noticed that black curve in figure 12 b is in agreement with reported data from Leclerc and coll.[26]

The main reasonable explanation for this important shift towards higher wavelengths when the polymer is under the form of particles is the doping with the base or the catalyst. Simulations on dimer species (2 representative units) have been conducted and the absorbance spectra showed that negative or positive doping (addition of 1 extra electron or

removal of 1 electron to the molecule) creates a large red-shift (see figure 13). Molecular structures were optimized at the DFT level using the hybrid functional B3LYP and the 6-311G(d,p) basis set. For the UV-vis spectra, the long range corrected functional CAM-B3LYP was used with the 6-31g(d,p) basis set under the TD-DFT level.

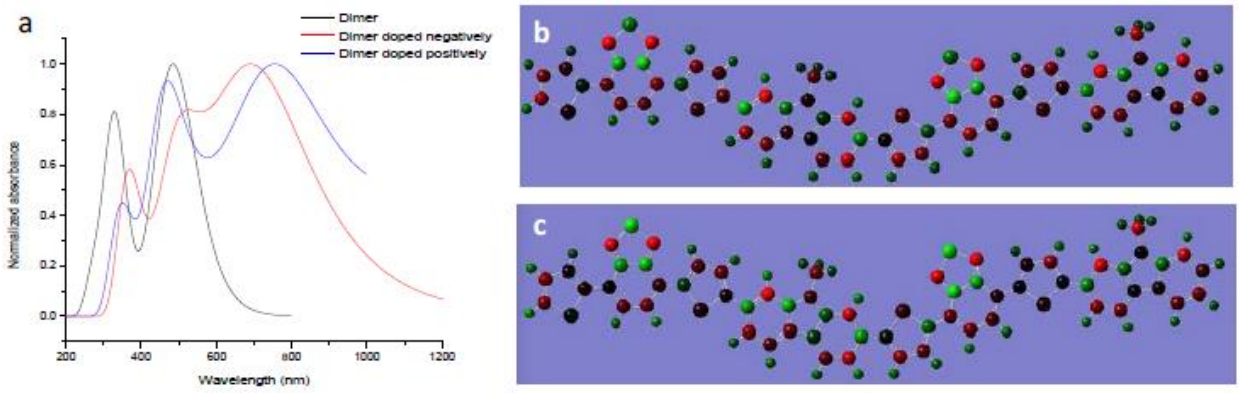

Figure 13 : Absorbance spectra obtained from simulation on undoped dimer and doped using TD-DFT cam-B3LYP/6-31g(d,p) (a), distribution of the charges in case of negatively charged dimer (b) and positively charged dimer (c). The greener an atom is the more positive it is, the redder it is, the more negative it is

Cyclic voltammetry was also performed in order to verify the PCDTBT electronic characteristics whatever the technique used "classical bulk polymerization" (figure 14 a) versus dispersion polymerization (figure 14 b).

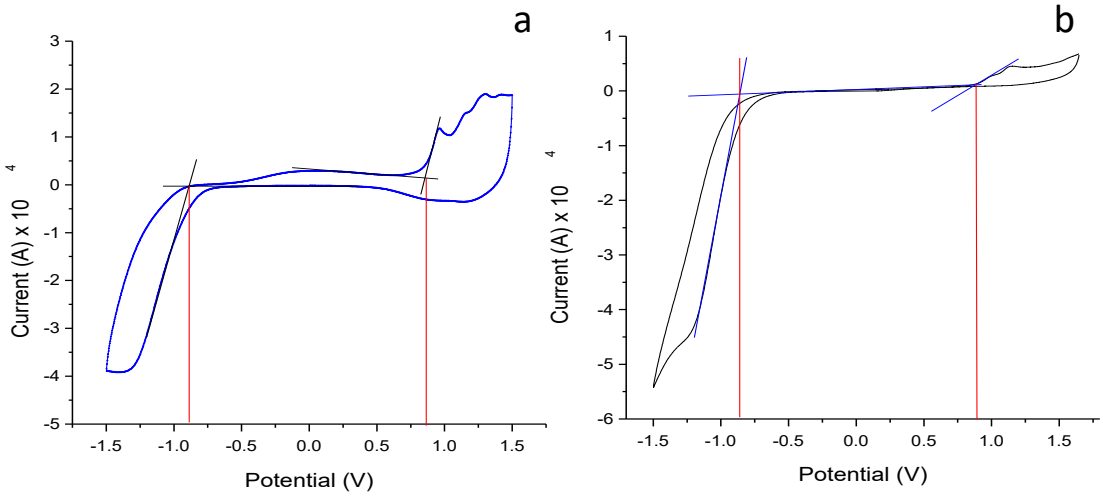

Figure 14 : (a) Cyclic voltammetry of bulk PCDTBT film, (b) cyclic voltammetry of particles film synthesized by dispersion polymerization in 0.1 M of tetrabutylammonium tetrafluoroborate (Bu_4NBF_4) in acetonitrile

Table 2 : Energy levels of particles and bulk made polymer obtained from cyclic voltammetry [a] determined by cyclic voltammetry, [b] determined by onset of the absorption peak

	E_{HOMO} eV	E_{LUMO} eV	E_{gap}^{elec} eV[a]	E_{gap}^{opt} eV[b]
Particles	-5.44	-3.69	1.75	1.91
Bulk	-5.42	-3.64	1.78	1.90
Literature[26]	-5.45	-3.60	1.85	1.88

The particles as well as the polymer synthesized by classical way should present good air stability because their oxidation potential are below the air oxidation level of -5.27eV (see table 2). The LUMO energy level is a bit different from the one of the literature[26] probably due to an experimental error, the reduction peak being hardly distinguished. The HOMO and LUMO levels are close to those of the bulk polymer which proves that they can be used as p-type material for photovoltaic.

II.2.4. Molecular characteristics of PCDTBT

It is well known that the PCDTBT forms aggregates into chloroform and THF.[27] The "real" molar masses of the PCDTBT polymers were measured by Size Exclusion Chromatography (SEC) in trichlorobenzene (TCB) at high temperature (150°C).

By comparison of the two chromatograms of the particles solubilized in TCB and bulk made polymer solubilized in TCB (overlay in figure 15), a shift towards smaller molar masses (towards higher retention volume) for the particles can be noticed.

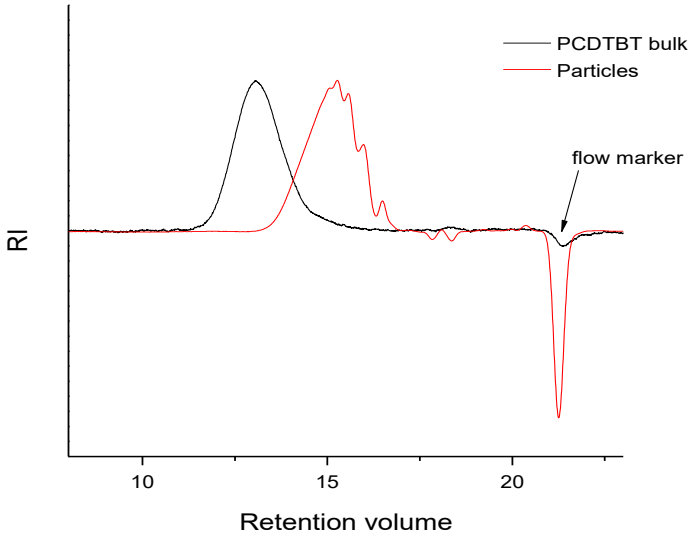

Figure 15 : Overlay of SEC chromatograms of particles and bulk made PCDTBT in TCB at 150°C

It is noteworthy that for the PCDTBT prepared by dispersion polymerization several peaks appeared at higher elution time representative of a low molar mass polycondensation products which is in agreement with a step growth mechanism such as reported in the literature for Heck coupling dispersion polymerization.[19]

The dispersion polymerization synthesis (entry 1, table 1) led to molar masses around 5 kDa (6 repeating units), whereas the bulk synthesis led to 20 kDa (30 repeating units) polymer (see Table 3).

Table 3 : Molecular characteristics of PCDTBT synthesized in bulk or in dispersion polymerization determined by SEC in TCB at high temperature (150°C)

	$\overline{M}n$ (Da)	$\overline{M}w$ (Da)	Đ
PCDTBT Particles	4 500	9 400	2.1
Bulk PCDTBT	22 000	44 000	2

With less base during the particles'synthesis (entry 5, table 1), the molar mass was increased up to 7.7kDa. This can be explained by the creation of less palladium-hydroxyl complex (4 in the mechanism outline figure 5) so the chains are longer.

These relatively low molar masses can be explained by a probably very low critical molar mass of precipitation, the precipitation occuring at early stage. Moreover in Kuehne's papers, the monomers used had alkyl chains, boronated functions or carboxylic acids which prevent from early precipitation because these functions provide a bigger solubility as compared to the monomers we used.

Another explanation for the low molar masses obtained can be the stoichiometry which can be difficult to achieve in a dispersed system because each monomer has its own solubility. Nevertheless, as already mentioned it is a key issue for step-growth polymerizations in order to achieve high molar masses.[28]

Summary of the properties:

Table 4 : Molecular, optical and electronic characteristics of PCDTBT synthesized in bulk or in dispersion polymerization compared to what is reported in the literature

Sample	$\bar{M}n$ (kDa)	Đ	Solvent	λmax sol (nm)	λmax film (nm)	ΔE_{opt} (eV)	E^{ox}_{onset} (V)	E_{HOMO} (eV)	E^{red}_{onset} (V)	E_{LUMO} (eV)	ΔE_{ec} (eV)
PCDTBT bulk	22	2	$CHCl_3$	516	586	1.90	0.875	5.42	-0.90	3.64	1.78
PCDTBT dispersion	5	x	propanol	622	540	1.91					
PCDTBT dispersion	5	2.1	$CHCl_3$	508	540	2.16	0.90	5.44	-0.85	3.69	1.75
Literature[29]	36	1.54	TCB	530	580	1.88	x	5.45	x	3.60	1.85

II.2.5. Integration of PCDTBT particles into inverted bilayer photovoltaic device

Even if the molar masses of the particles were not comparable to the molar mass of the PCDTBT synthesized by classical polymerization for the production of high efficiency photovoltaic cells,[30–32] we wanted to assess the efficiency of our particles once integrated into a device.

Inversed solar cells in bilayer were made, one layer being composed of the electron acceptor [6,6]-Phenyl C_{71} Butyric acid Methyl ester ($PC_{71}BM$) and the other layer of the PCDTBT particles in propan-1-ol (see figure 16). The stacking in bilayer is far from being ideal to reach good efficiencies because the number of interfaces where the exciton can be separated is very limited. However, as the $PC_{71}BM$ is not soluble into propan-1-ol, it was the only way to see if the PCDTBT particles could provide some current.

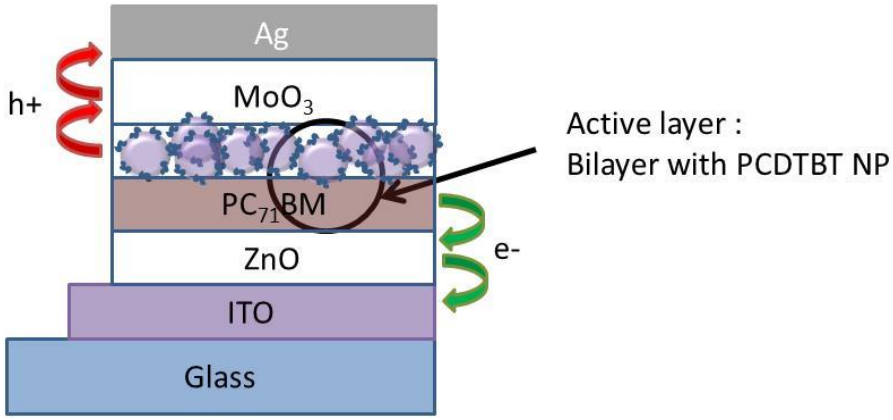

Figure 16 : OPV cell integrating the PCDTBT particles synthesized by dispersion polymerization using inverted architecture

In the dark (see figure 17 black curve), the cells have, as expected, a diode behavior. Unfortunately, when they are exposed to light we can notice a deviation towards negative currents when the voltage is negative (see figure 17 red curve). Table 5 in the appendix gathers the properties of the solar cells made from PCDTBT particles synthesized by dispersion polymerization. Such low OPV performances are a consequence of high series resistance (R_s) and low shunt resistance (R_{sh}) probably due to the presence of PVP interfaces. Moreover the low OPV performances as gathered in table 5 could be explained

by the low molar mass of PCDTBT[29] synthesized through dispersion polymerization and also by the particles size which is too big in regards to the ideal diffusion length for the excitons.

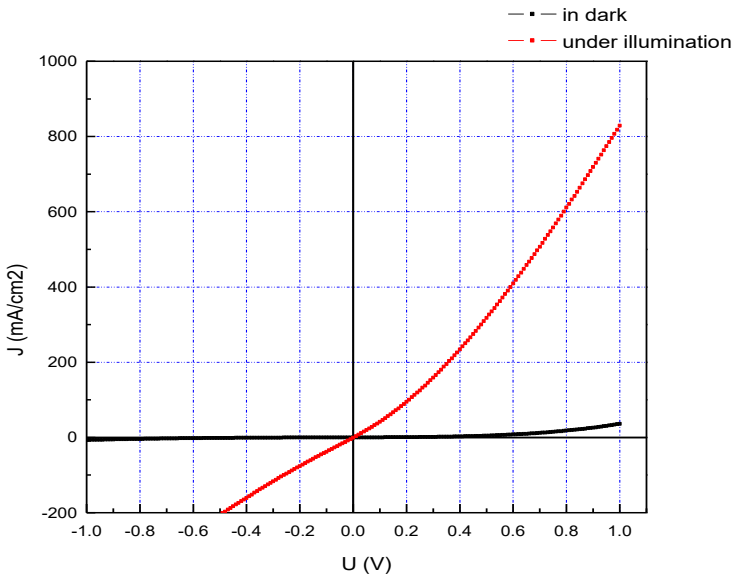

Figure 17 : J-V curves of the OPV cells integrating the PCDTBT particles synthesized by dispersion polymerization measured in dark (black curve) and in light (red curve)

II.3. Conclusion

In this chapter, we have investigated dispersion polymerization features in order to tune the size and size distribution of PCDTBT particles. Depending on the synthesis conditions PCDTBT particles with tunable sizes and good optoelectronic properties were obtained. However dispersion polymerization does not seem to be adapted towards the production of PCDTBT inks for a photovoltaic purpose because the molar mass was low. This is a critical parameter on the photovoltaic cells efficiency as reported by Leclerc's team who studied the efficiencies of solar cells based on PCDTBT depending on the molar masses, for example for a molar mass of 10 kDa the efficiency was 2.26% whereas the one for 19kDa was 4.15%.[29]

Dispersion polymerization is a method of choice for the synthesis of nanometer particles because it can be used for a large range of polymerizations : radical, ionic, oxidative coupling, metathesis, group transfer and even polycondensations. However the monomers have to be chosen carefully to allow a persistent solubility for oligomers with a high molar mass of precipitation for the polymer particles to be used for photovoltaic applications.

In the following other dispersion methodologies will be studied such as miniemulsion post polymerization (chapter III and IV) and nanoprecipitation (chapter V) in order to lower the particle size of high molar masses polymers.

II.4. References

[**1**] A. J. Paine, W. Luymes, J. McNulty, *Macromolecules*, **1990**, *23*, 3104.
[**2**] J.-C. Daniel, C. Pichot, *Les Latex Synthétiques*, **2006**.
[**3**] M. Mumtaz, A. de Cuendias, J.-L. Putaux, E. Cloutet, H. Cramail, *Macromol. Rapid Commun.*, **2006**, *27*, 1446.
[**4**] C. M. Tseng, Y. Y. Lu, M. S. El-Aasser, J. W. Vanderhoff, *J. Polym. Sci. Part A Polym. Chem.*, **1986**, *24*, 2995.
[**5**] H. Bamnolker, S. Margel, *J. Polym. Sci., Part A Polym. Chem.*, **1996**, *34*, 1857.
[**6**] S. Shen, E. D. Sudol, M. S. El-Aasser, *J. Polym. Sci. Part A Polym. Chem.*, **1993**, *31*, 1393.
[**7**] D. Wang, V. L. Dimonie, E. D. Sudol, M. S. El-Aasser, *J. Appl. Polym. Sci.*, **2002**, *84*, 2692.
[**8**] Q. Ye, Z. Zhang, H. Jia, W. He, X. Ge, *J. Colloid Interface Sci.*, **2002**, *253*, 279.
[**9**] E. Bourgeat-Lami, J. Lang, *J. Colloid Interface Sci.*, **1998**, *197*, 293.
[**10**] B. Vincent, *Polym. Adv. Technol.*, **1995**, *6*, 356.
[**11**] J. Pecher, S. Mecking, *Chem. Rev.*, **2010**.
[**12**] T. K. Mandal, B. M. Mandal, *J. Polym. Sci. Part A Polym. Chem.*, **1999**, *37*, 3723.
[**13**] R. B. Bjorklund, B. Liedberg, *J. Chem. Soc. Chem. Commun.*, **1986**, 1293.
[**14**] J. Stejskal, P. Kratochvíl, S. P. Armes, S. F. Lascelles, A. Riede, M. Helmstedt, J. Prokeš, I. Křivka, *Macromolecules*, **1996**, *29*, 6814.
[**15**] S. P. Armes, M. Aldissi, *J. Chem. Soc. Chem. Commun.*, **1989**, 88.
[**16**] K. Mallick, M. J. Witcomb, A. Dinsmore, M. S. Scurrell, *Macromol. Rapid Commun.*, **2005**, *26*, 232.
[**17**] A. J. C. Kuehne, M. C. Gather, J. Sprakel, *Nat Commun*, **2012**, *3*, 1088.
[**18**] N. Anwar, T. Willms, B. Grimme, A. J. C. Kuehne, *ACS Macro Lett.*, **2013**, *2*, 766.
[**19**] S. Ciftci, A. J. C. Kuehne, *Macromolecules*, **2015**, *48*, 8389.
[**20**] D. Napper, *Polymeric Stabilization of Colloidal Dispersions*, London, **1983**.
[**21**] A. Suzuki, *J. Organomet. Chem.*, **1999**, *576*, 147.
[**22**] N. Miyaura, A. Suzuki, *Chem. Rev.*, **1995**, *95*, 2457.
[**23**] C. Negele, J. Haase, A. Leitenstorfer, S. Mecking, *ACS Macro Lett.*, **2012**, *1*, 1343.
[**24**] T. Yamamoto, D. Komarudin, M. Arai, B. Lee, H. Suganuma, N. Asakawa, Y. Inoue, K. Kubota, S. Sasaki, *J. Am. Chem. Soc.*, **1998**, *120*, 2047.
[**25**] R. Steyrleuthner, M. Schubert, I. Howard, B. Klaumünzer, K. Schilling, Z. Chen, P. Saalfrank, F. Laquai, A. Facchetti, D. Neher, *J. Am. Chem. Soc.*, **2012**, *134*, 18303.
[**26**] N. Blouin, A. Michaud, D. Gendron, S. Wakim, E. Blair, R. Neagu-Plesu, M. Belletete, G. Durocher, Y. Tao, M. Leclerc, *J. Am. Chem. Soc.*, **2008**, *130*, 732.
[**27**] S. Beaupre, M. Leclerc, *J. Mater. Chem. A*, **2013**, *1*, 11097.
[**28**] M. C. Baier, J. Huber, S. Mecking, *J. Am. Chem. Soc.*, **2009**, *131*, 14267.
[**29**] S. Wakim, S. Beaupre, N. Blouin, B.-R. Aich, S. Rodman, R. Gaudiana, Y. Tao, M. Leclerc, *J. Mater. Chem.*, **2009**, *19*, 5351.
[**30**] K. X. Steirer, P. F. Ndione, N. E. Widjonarko, M. T. Lloyd, J. Meyer, E. L. Ratcliff, A. Kahn, N. R. Armstrong, C. J. Curtis, D. S. Ginley, J. J. Berry, D. C. Olson, *Adv. Energy Mater.*, **2011**, *1*, 813.
[**31**] Y. Sun, J. H. Seo, C. J. Takacs, J. Seifter, A. J. Heeger, *Adv. Mater.*, **2011**, *23*, 1679.
[**32**] Y. Sun, C. J. Takacs, S. R. Cowan, J. H. Seo, X. Gong, A. Roy, A. J. Heeger, *Adv. Mater.*, **2011**, *23*, 2226.
[**33**] N. G. Connelly, W. E. Geiger, *Chem. Rev.*, **1996**, *96*, 877.

II.5. Appendix

^{1}H NMR and TGA analysis showing the success of PCDTBT synthesis *via* dispersion polymerization :

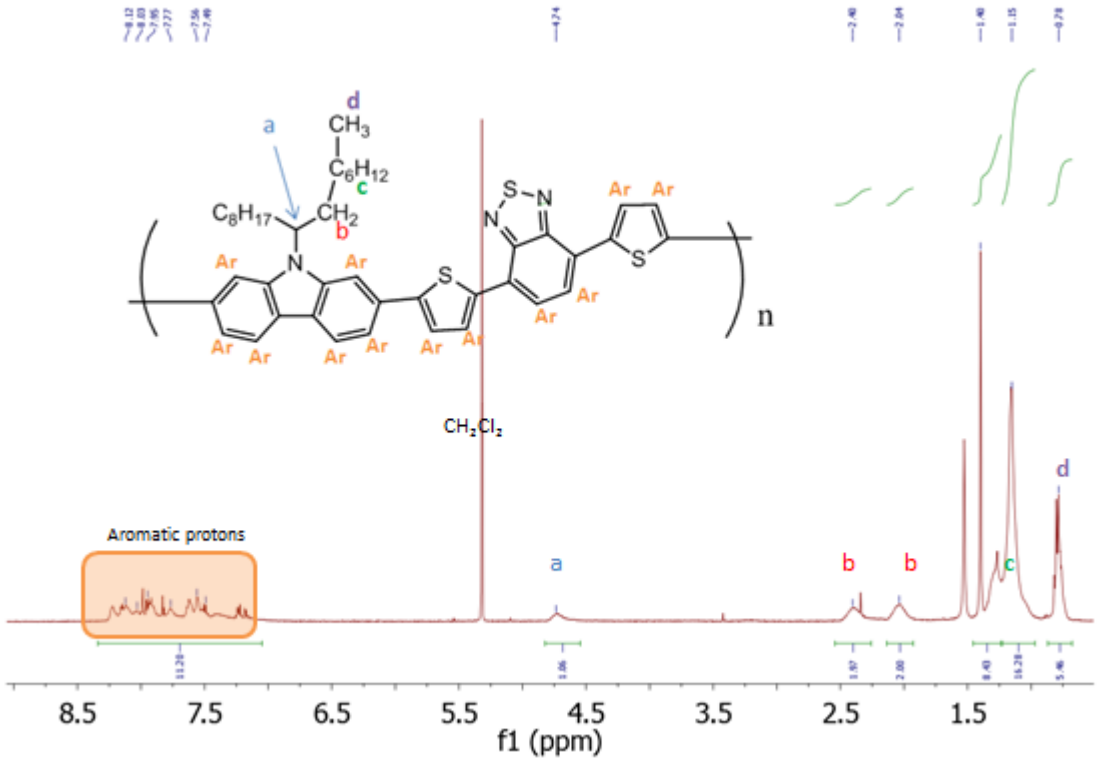

Figure 18 : ^{1}H NMR of PCDTBT particles dried and dissolved in CD_2Cl_2 at 400 MHz

^{1}H NMR (400 MHz, CD_2Cl_2, ppm): 8.3-7.1 (br, 12H, ArH); 4.74 (br, 1H); 2.40 (br, 2H); 2.04 (br, 2H); 1.45-1.23 (br, 8H); 1.23-1.00 (br, 16 H); 0.78 (br, 6H), in agreement with what Leclerc *and coll* reported for PCDTBT synthesized by classical polymerization[29] (the integrals values represent each repeating unit)

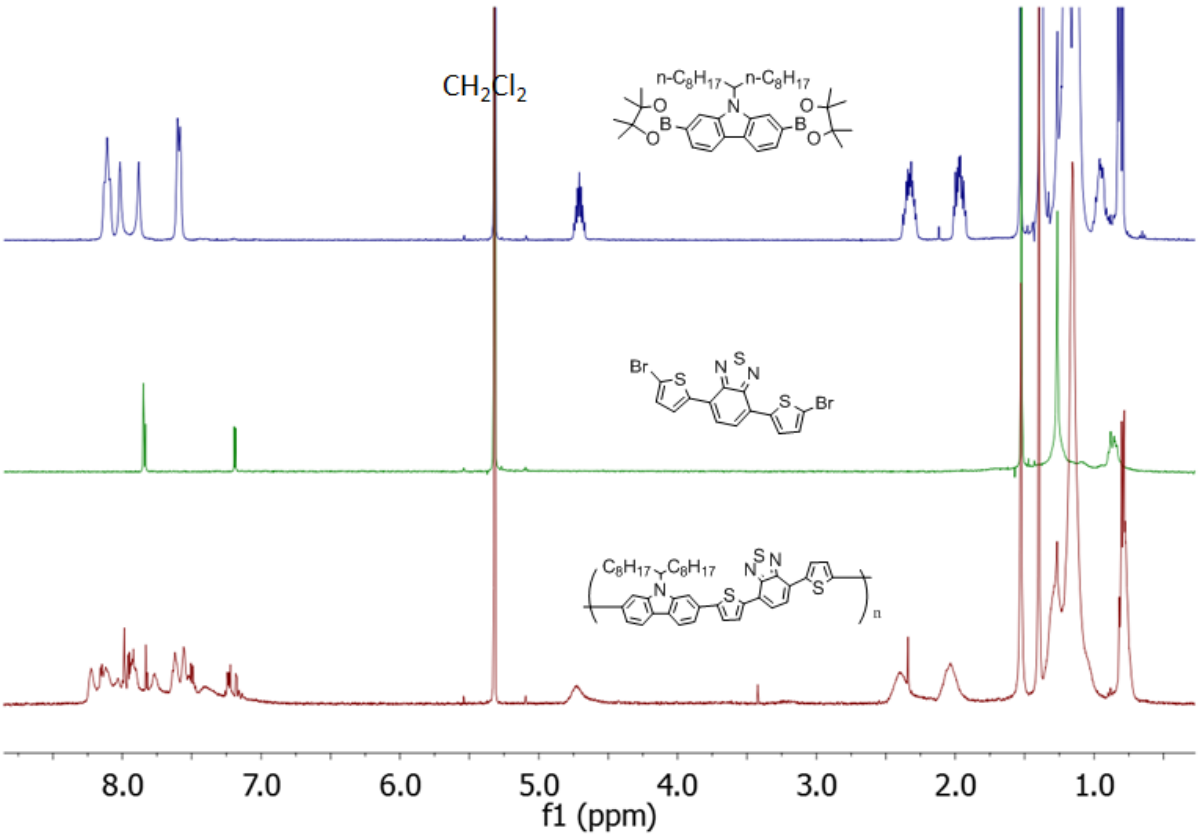

Figure 19 : ^{1}H-RMN of the two purified monomers and of PCDTBT particles solubilized in CD_2Cl_2 at 400 MHz

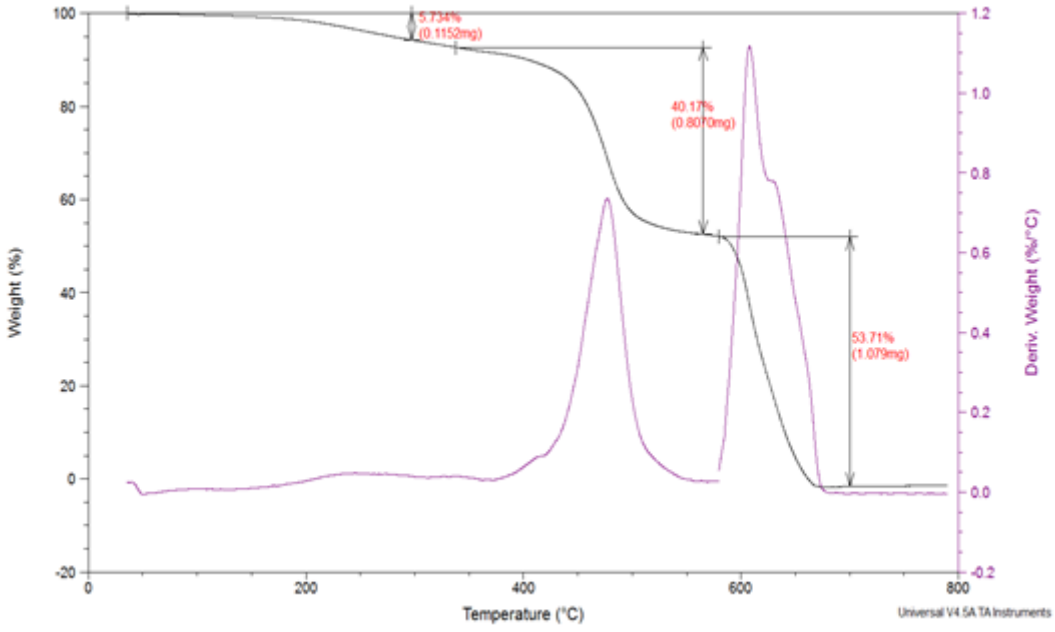

Figure 20 : Thermogravimetric analysis of PCDTBT particles dried, O_2 flow after 600°C

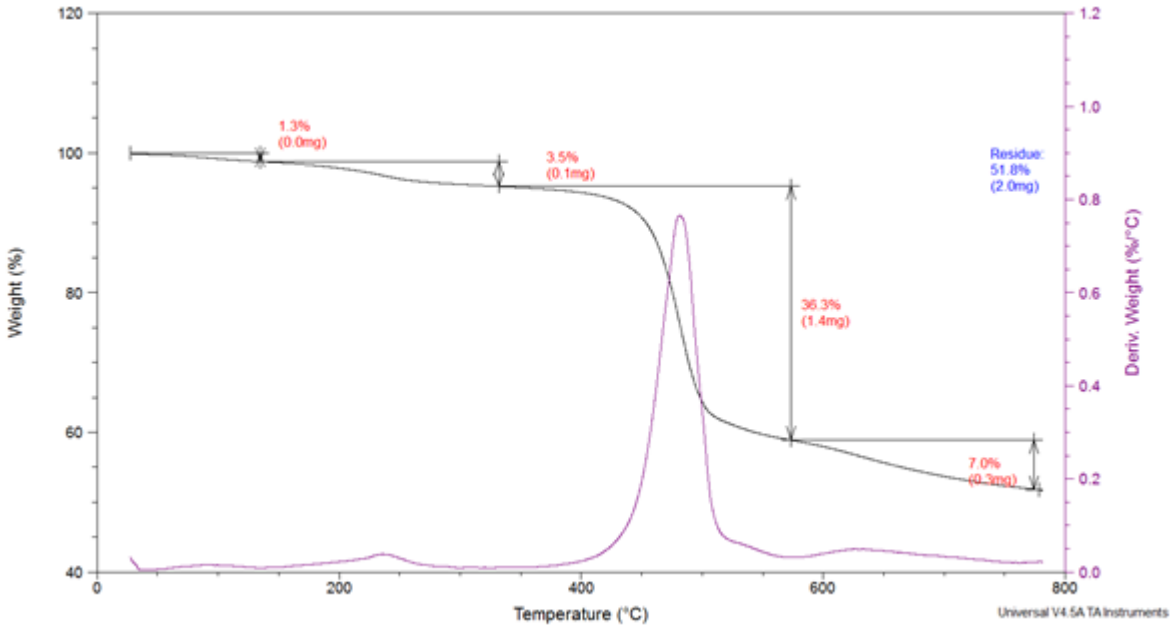

Figure 21 : Thermogravimetric analysis of PCDTBT synthesized by classical polymerization

In the dried particles, no residual monomers can be observed (their degradation temperature being before 200°C). The particles' degradation temperature is almost the same than the one of the polymer synthesized by classical polymerization.

Table 5 : Properties of the solar cells made from PCDTBT particles synthesized by dispersion polymerization and P3HT bulk as comparison

	Jsc (mA/cm²)	Voc (V)	FF	PCE (%)	R_s (Ω.cm²)	R_{sh} (Ω.cm²)
PCDTBT(particles): $PC_{71}BM$	4.43E-01	1.01E-02	2.38E-04	1.07E-06	4.05E+02	1.26E+01
P3HT:PCBM	1.31E+01	5.10E-01	5.20E-01	3.43E+00	9.11E+00	3.56E+02

II.6. Experimental Section

II.6.1. Materials

Tetrakis(triphenylphosphine)palladium (99%) and potassium *tert*-butoxide (97%) were purchased from Alfa Aesar, 9-(9-Heptadecanyl)-9H-carbazole-2,7-diboronic acid bis(pinacol) ester (97%), 4,7-Bis(2-bromo-5-thienyl)-2,1,3-benzothiadiazole (99+%), Poly(vinylpyrrolidone) K90 (Mw=360 000 $g.mol^{-1}$) and propan-1-ol (99+%) were purchased from Sigma Aldrich. All chemicals were used as received unless otherwise stated.

II.6.2. Synthesis

The reactions were performed under an Argon atmosphere using standard schlenk techniques.

II.6.2.a. Monomers purification

The two monomers were purified as reported in the literature[29] : 9-(9-Heptadecanyl)-9H-carbazole-2,7-diboronic acid bis(pinacol) ester was recrystallized twice in methanol:acetone (10:1 v/v) and 4,7-Bis(2-bromo-5-thienyl)-2,1,3-benzothiadiazole was recrystallized in *o*-dichlorobenzene.

II.6.2.b. Typical procedure for the dispersion polymerization in propan-1-ol

A 50-mL glass flask was charged with a magnetic stirrer and 40 mg of PVP (same mass than monomers). Equimolar amount of 9-(9-heptadecanyl)-9H-carbazole-2,7-diboronic acid bis(pinacol) ester and the 4,7-bis(2-bromo-5-thienyl)-2,1,3-benzothiadiazole were weighted, as well as 1 mg of the catalyst ($Pd(PPh_3)_4$), they were poured into the reaction flask, then the flask was sealed with a rubber septum and degassed propan-1-ol was added. The solution was mechanically stirred and some argon was bubbled in order to degas the medium. Once the solution has been degassed for 15-20 minutes, the flask with a condenser was transferred into an oil bath. As soon as every reagent has been dissolved the degassed-base solution was added under argon flow.

Heating to reflux temperature during one hour and a half affords the polymerization and leads to a stable dispersion, confirmed by ^{1}H-NMR, Absorption and emission spectra and TEM pictures.

II.6.2.c. Kinetics

After the beginning of the reaction (after addition of the base), aliquots of 0.5 mL were taken from the reaction medium with time and quenched in cold propan-1-ol. The size was then measured by DLS and reported as a function of the time.

II.6.2.d. Typical procedure for the polymerization of 9-(9-Heptadecanyl)-9H-carbazole-2,7-diboronic acid bis(pinacol) ester and 4,7-Bis(2-bromo-5-thienyl)-2,1,3-benzothiadiazole in bulk

Bulk made PCDTBT was synthetized according to the literature[29]

In a flame-dried flask, 654.4 mg (0.966 mmol) of 2,7-bis(4,4,5,5-tetramethyl-1,3,2-dioxaborolan-2-yl)-N-9-heptadecanyl-carbazole, 458.8 mg (1.00 mmol) of 4,7-di(2'-bromothien-5'-yl)-2,1,3-benzothiadiazole, 4.2 mg (0.0046 mmol) of tris(dibenzylideneacetone)dipalladium(0) and 6.1 mg (0.020 mmol) of tri(o-tolyl)phosphine were dissolved in 10 mL of degassed toluene and 3.4 mL of degassed 20% aqueous tetraethylammonium hydroxide. The reaction mixture was vigorously stirred and heated up to 95°C at a heating rate of 1°C per minute.

After 3 h, bromobenzene (110 mL, 1.0 mmol) was added to the reaction which was kept at 95°C for one hour, then phenylboronic acid (120 mg, 1.0 mmol) in hot toluene (3 mL) was then added and reacted for another hour to allow the end-capping. The reaction mixture was poured in methanol/water (10:1) solution and the polymer was filtered.

The crude material was washed with acetone and heptane using a Soxhlet apparatus during one day for each solvent.

The remaining solid was extracted with chloroform (300 mL) for sereval days. Then the solution was concentrated using rota-evaporator to about 50 mL and the polymer solution was precipitated in cold methanol (500 mL). The polymer was recovered by filtration and dried under vacuum.

II.6.3. Methods

Dynamic light scattering (DLS) on diluted dispersion samples was performed on a Cordouan Particle Size Analyzer Vasco. The autocorrelation function was analyzed using the Cordouan dispersion technology software algorithm to obtain number-weighted particle sizes.

NMR spectra were recorded on a Bruker Avance III 400 spectrometer at 400 MHz for ^{1}H nucleus.

Size exclusion chromatography (SEC) was performed in $CHCl_3$ at 30°C with a flow rate of 1 $mL.min^{-1}$ using TSK Gel HXL Multipore column (size 30 x 7.8, pore size 5 µm) and a guard-column from Tosoh and in trichlorobenzene at 150°C at a flow rate of 1 $mL.min^{-1}$ performed in Lyon at LCPP. The elution times were converted into molar masses using a calibration curve based on low dispersity polystyrene standards.

Thermogravimetric measurements were carried out with TA Instruments Q50 from room temperature to 800°C with a heating rate of 10°$C.min^{-1}$. The analyses were performed under nitrogen atmosphere.

Absorption spectra were measured using a Shimadzu spectrophotometer UV-3600 and *emission spectra* were measured using a Horiba Scientific Fluoromax-4 spectrofluorometer.

TEM images were obtained on Formvar grids (accelerate voltage 120 kV). Dispersed polymers were cleaned by several centrifugation-redispersion cycles before TEM analysis to remove any unreacted monomer, base and stabilizer and deposited onto a copper grid.

Cyclic voltamograms (CV) were recorded on a VersaSTAT3 potentiostat AMETEK using polymer film on ITO as a working electrode and platinum electrode as counter electrode at a scan rate of 50 mVs^{-1} and a Ag nanowire reference electrode in an anhydrous and argon-saturated solution of 0.1 M of tetrabutylammonium tetrafluoroborate(Bu_4NBF_4) in acetonitrile.

The HOMO and LUMO levels were estimated from oxidation and reduction onset from the CV spectra assuming SCE electrode to be -4.4 eV from vacuum and using the following equations. All values were corrected with ferrocene reference assuming his oxidation potential was 0.4 V versus SCE[33], in our conditions, the oxidation potential (Eox) of ferrocene was 0.26 V versus Ag/Ag+. We used Ecorrection $Ag \rightarrow SCE\ (Ferrocene)$= 0.14 V

Equation 3 : HOMO and LUMO levels calculated from cyclic voltametry

$$E_{HOMO} = \left(E_{ox\ vs\ Ag} + Ecorrection_{Ag \rightarrow SCE\ (Ferrocene)}\right) + 4.4$$
$$E_{LUMO} = \left(E_{red\ vs\ Ag} + Ecorrection_{Ag \rightarrow SCE\ (Ferrocene)}\right) + 4.4$$

Devices fabrication: Bilayer inverted solar cells have been fabricated with the following structure: Glass/ITO/ZnO/$PC_{71}BM$/PCDTBT(NP)/MoO_3/Ag. The Indium tin oxide (ITO)-coated glass substrates, purchased from Vision Tek, with a sheet resistance of ~10 $\Omega.sq^{-1}$ are successively cleaned for 10 min in acetone, ethanol and isopropanol in an ultrasonic bath.

196 mg of zinc acetate dehydrate was mixed with 54 µL of ethanolamine in 6 mL of absolute ethanol and stirred at 45 °C for 2 hours. The zinc oxide (ZnO) layer was prepared by spin-coating this solution at 2000 rpm for 60 s followed by annealing at 180°C for 1 hour in air leading to a 60 nm thick layer.

$PC_{71}BM$ layer was spin-coated in air at 2000 rpm during 60 s from chloroform solution with a resulting $PC_{71}BM$ thickness of 50 nm. PCDTBT nanoparticles were deposited by spincoating, (3000rpm for 1min) in air. The films were dried at 110°C for 2 min to evaporate the solvent and then transferred into vacuum chamber for the MoO_3/Ag evaporation.

MoO_3 (10nm) and Ag (80nm) were successively thermally-evaporated at deposition rates of 0.1 $nm.s^{-1}$ and 0.2-0.4$nm.s^{-1}$ respectively under secondary vacuum (10^{-6}mbar). The solar cells' active surface area is 10 mm^2. The devices were characterized using a K.H.S. Solar Cell test-575 solar simulator with AM1.5G filters set at 100 $mW.cm^{-2}$ with a calibrated radiometer (IL 1400BL). Labview controlled Keithley 2400 SMU enabled the current density-voltage (J-V) curves measurements.

- Vue d'ensemble du chapitre II -

Ce deuxième chapitre expose la synthèse du poly(N- 9'-heptadecanyl-2,7-carbazole-*alt*-5,5-(4,7-di-2-thienyl-2',1',3'-benzothiadiazole) (PCDTBT) par couplage de Suzuki en dispersion dans un alcool (le propan-1-ol) (voir figures 1 et 2).

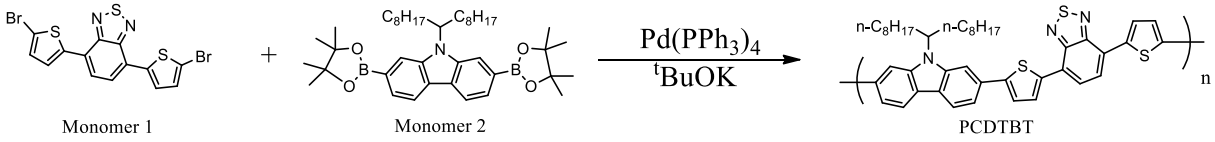

Figure 1 : Schéma réactionnel pour la synthèse du PCDTBT par couplage de Suzuki

Les particules ainsi synthétisées sont stabilisées par du poly(vinyl pyrrolidone) (PVP), adsorbé à la surface.

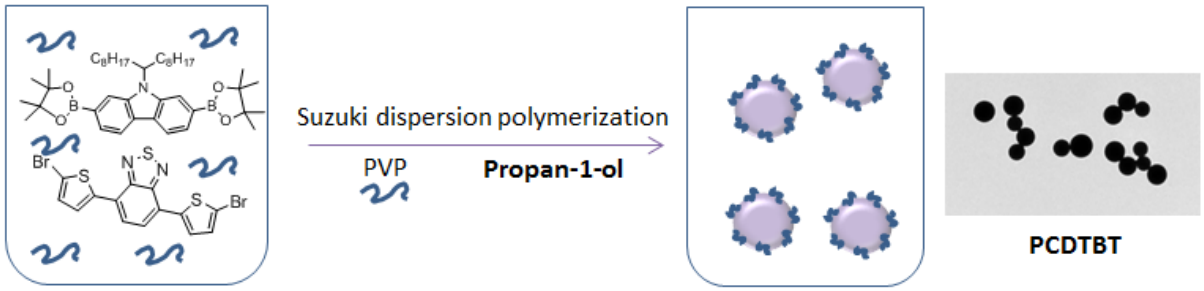

Figure 2 : Polymérisation en dispersion du PCDTBT

Tout d'abord, les paramètres de la réaction ont été étudiés pour contrôler la taille et la distribution en taille des particules tels que les quantités de base, de catalyseur, de stabilisants ou la stœchiométrie entre les deux monomères qui joue un rôle très important sur la masse molaire dans les polymérisations par étapes.

Ensuite, l'étude des propriétés opto-électroniques (absorbance UV et fluorescence (voir figure 3) ainsi que voltamétrie cyclique (voir figure 4)) a montré que ces particules pourraient être de bonnes candidates pour remplacer le PCDTBT solubilisé dans l'*o*-dichlorobenzene traditionnellement utilisé pour les cellules solaires.

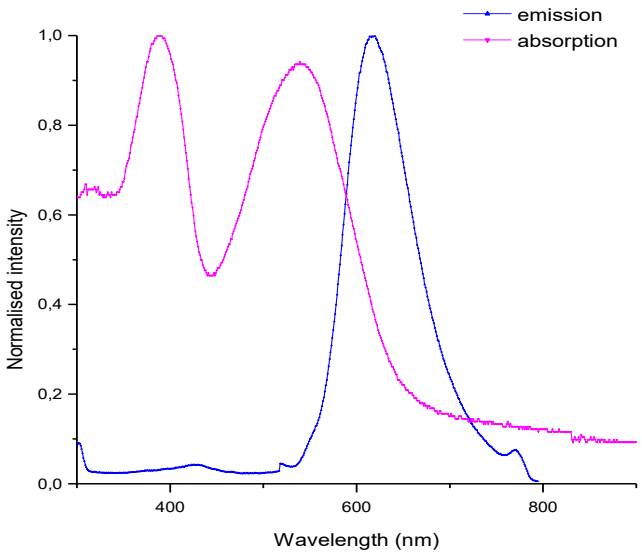

Figure 3 : Spectres d'absorption et d'émission des particules de PCDTBT solubilisées dans du chloroforme

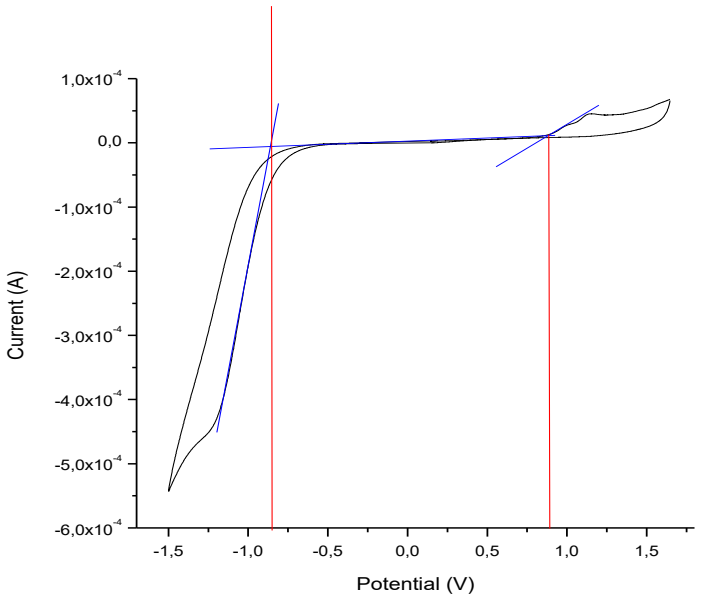

Figure 4 : Voltamétrie cyclique d'un film de particules de PCDTBT

La masse molaire des particules n'atteint malheureusement pas celle du polymère synthétisé « classiquement » en raison de conditions de polymérisation en dispersion. La plus haute masse obtenue était d'environ 7 unités de répétitions, soit 5 kDa, contre 30 unités de répétition soit 20 kDa (voir figure 5) pour un polymère donnant de bons résultats une fois intégré dans un dispositif de cellule solaire.

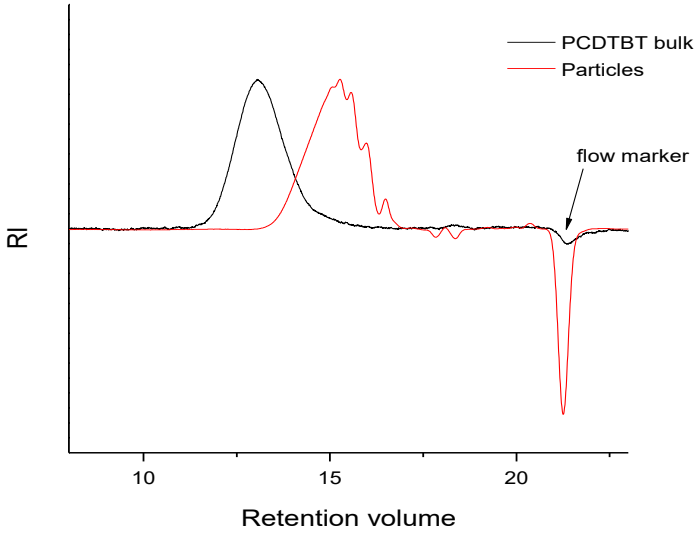

Figure 5 : Superposition des chromatogrammes des particules et du polymère PCDTBT synthétisé par la voie classique

Une très faible efficacité photovoltaïque a pu être obtenue pour les dispositifs en cellule inverse intégrant ces particules en bicouche (voir Table 1), probablement en raison de la combinaison d'une faible masse molaire et d'un stabilisant isolant créant ainsi une très grande résistance en série.

Table 1 : Propriétés des cellules solaires intégrant les nanoparticules de PCDTBT (P3HT servant de référence)

	Jsc (mA/cm²)	Voc (V)	FF	PCE (%)	Rs (Ω.cm²)	Rsh (Ω.cm²)
PCDTBT(NP):$PC_{71}BM$	4,43E-01	1,01E-02	2,38E-04	1,07E-06	4,05E+02	1,26E+01
P3HT:PCBM	1,31E+01	5,10E-01	5,20E-01	3,43E+00	9,11E+00	3,56E+02

Chapter III
PCDTBT-based particles *via* a miniemulsion post-polymerization process

In this work, composite particles of poly[N-9'-heptadecanyl-2,7-carbazole-*alt*-5,5-(4,7-di-2-thienyl-2',1',3'-benzothiadiazole] (PCDTBT) and [6,6]-Phenyl C71 butyric acid methyl ester ($PC_{71}BM$) were obtained in water from a more versatile and a ready-to-market methodology based on miniemulsion post-polymerization. Depending on experimental conditions, particles that comprise both the electron-donor and the electron-acceptor and ranging from 40 nm to 420 nm in diameter were obtained and characterized. The water-based inks were used for the preparation of the photovoltaic active layer which was then integrated in organic solar cells showing promising results.

- CHAPTER III -
PCDTBT-based particles *via* a miniemulsion post-polymerization process

Table of Contents

List of the figures

List of the tables

III.1. Introduction

With the objective of synthesizing π-conjugated polymer particles in eco-friendly media, we have seen in Chapter II that the direct processes (dispersion polymerization as well as emulsion and miniemulsion) did not allow to reach similar properties than bulk made polymer. A secondary dispersion process was therefore used in this chapter.

Eco design of π-conjugated polymer with the objective to integrate them in renewable energy devices has been the focus of some researchers recently. For instance the group of Kietzke reported the preparation of electron-donor and electron-acceptor polymers (*i.e.* Poly[(9,9-di-n-octylfluorenyl-2,7-diyl)-*alt*-(benzo[2,1,3]thiadiazol-4,8-diyl)] (F8BT) and poly(9,9-dioctylfluorene-*co*-N,N'-bis(4-butylphenyl)-N,N'-diphenyl-1,4-phenylenediamine) (PFB) respectively) via a miniemulsion post-polymerization process showing promising EQE feature. [1] The chemical structures are reported in figure 1.

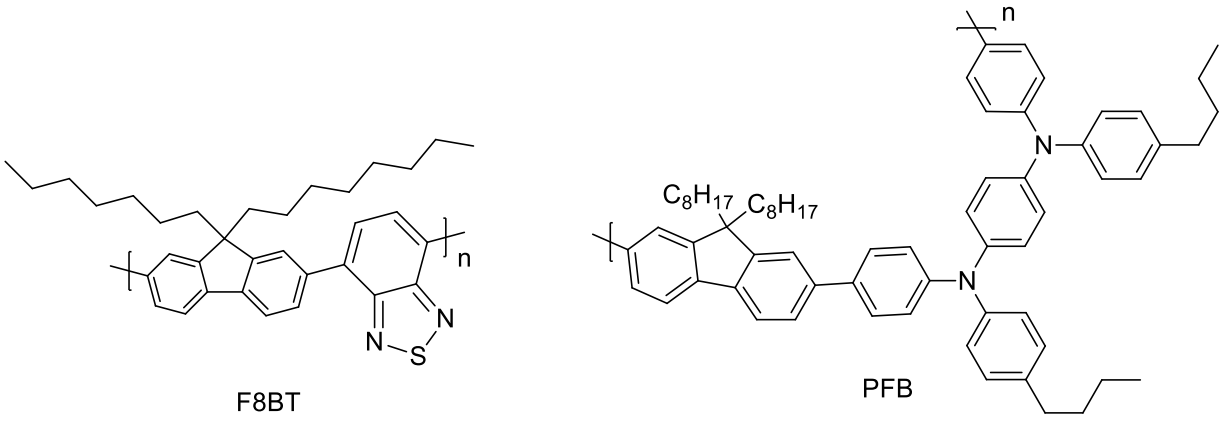

Figure 1 : Chemical structure of poly(9,9-dioctylfluorene-*co*-benzothiadiazole) (F8BT) and poly(9,9'-dioctylfluorene-*co*-bis-N,N'-(4-butylphenyl)-bis-N,N'-phenyl-1,4 phenylenediamine) (PFB) particles synthesized by miniemulsion post-polymerization reported by Kietzke and coll[1]

Following a similar methodology Andersen *et al*[2] have prepared composites of PCBM with various polymers (*i.e*. poly[4,8-bis(2-ethylhexyloxy)benzo(1,2-b:4,5-b')dithiophene-*alt*-5,6-bis(octyloxy)-4,7-di(thiophen-2-yl)(2,1,3-benzothiadiazole)-5,5'-diyl], poly[(4,4'-bis(2-ethylhexyl)dithieno[3,2-b:2-,3'-d]silole)-2,6-diyl-*alt*-(2,1,3-benzothiadiazole)-4,7-diyl], and poly[2,3-bis-(3-octyloxyphenyl)quinoxaline-5,8-diyl-*alt*-thiophene-2,5-diyl]) reaching moderate PCE of 0.07, 0.55 and 0.15% respectively. More recently Holmes *et al* have reached PCE of 2.54% with the system composed of poly[2,3-bis-(3-octyloxyphenyl)quinoxaline-5,8-diyl-*alt*-thiophene-2,5-diyl] (TQ1) and $PC_{71}BM$.[3]

III.2. Results and discussion

III.2.1. Synthesis of PCDTBT and $PC_{71}BM$:PCDTBT composite particles by miniemulsion post-polymerization

Particles of PCDTBT were synthesized by dissolving the polymer in chloroform to form the organic phase ("oil" phase of the emulsion), and sodium dodecyl sulphate (SDS) surfactant was dissolved in water to form the aqueous phase. A miniemulsion was then formed by combining the organic and aqueous phases using ultrasonication for 2 minutes with the use of an ice bath to prevent overheating. The miniemulsion was then transferred immediately to a hotplate stirrer (70°C, 800 rpm) to evaporate the chloroform from the emulsion droplets to form the nanoparticle dispersion. Remaining surfactant in the aqueous continuous phase was then partially removed by centrifugal dialysis. Following the centrifugal dialysis the final nanoparticle ink volume was 1 ml with a 3 wt% solid content.

Composite particles were synthesized using the same methodology starting with a chloroform solution of both active materials (PCDTBT electron-donor and $PC_{71}BM$ electron-acceptor). After having checked that PCDTBT and $PC_{71}BM$ were both forming particles, we focused on inks based on these two components. The particles solution was afterwards washed by dialysis to get rid of excess of SDS. The SDS quantity which was left in the continuous phase was evaluated by following the surface tension *via* the pendant-drop measurements after each washing.

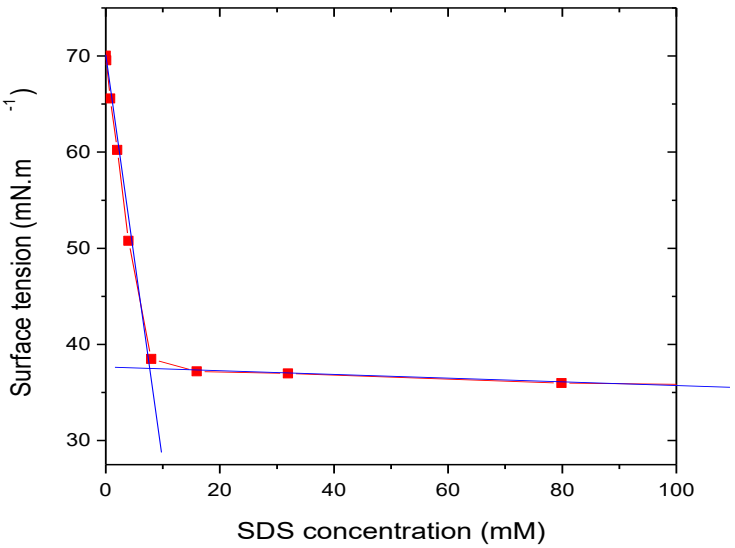

Figure 2 : Surface tension of sodium dodecyl sulfate (SDS) solution as a function of the SDS concentration in water

First a calibration curve was made by measuring the surface tension of solutions with different SDS concentration (see figure 2). This curve was in agreement with the literature, the critical micellar concentration being 8.2 mM *i.e* 2.36 $mg.mL^{-1}$ of water.[4] With this curve, by measuring the surface tension of the continuous phase, we can deduce how much SDS is left in it. The solution was washed until its surface tension was superior to 65 $mN.m^{-1}$, which means that less than 0.2 $g.L^{-1}$ of SDS is left in the aqueous phase. This quantity has to be minimized because the SDS is presumably an insulating and detrimental material for devices.

III.2.2. Experimental parameters that influence the particles size

Particles of $PC_{71}BM$:PCDTBT (80:20) with a diameter that could be tuned from 40 to 150 nm were synthesized according to the procedure described above (see also experimental part). For this study, we set the ratio at 80:20 wt% according to the best results obtained for this proportion in a bulk heterojunction (BHJ) device (solar cell).[5,6] As can be seen in Table 1, the size could be adjusted by the experimental parameters such as the concentration of the active materials (entries 1, 2 and 3, figure 5 TEM images 1 and 3). The latter has indeed a direct impact on the size of the particles, such as by increasing the concentration of the mother solution from 5 $mg.mL^{-1}$ to 50 $mg.mL^{-1}$ the particles' size went from 20-50 to 240-420 nm. This behavior was already demonstrated by Landfester *et al* for Me-LPPP [7] and Pras *et al* for PFFO. [8]

Sonication is another parameter that can be varied in order to play on the particle size.[8] For instance, longer sonication from 2 to 5 min (Table 1 entries 1 and 4, figure 3 TEM images 1 and 4) gave rise to smaller particles from 80-140 to 50-60 nm respectively. Smaller particle size distribution was also improved in these conditions. The intensity of the emulsification can also play a major role in the particles' size: from 20% to 30% intensity, the size went from 80-140 to 40-50 nm (Table 1 entries 1 and 6, figure 3 TEM images 1 and 6). This is also in agreement with a previous study reported in the literature.[8]

Table 1 : Size of the $PC_{71}BM$:PCDTBT composite particles (80:20) prepared by miniemulsion post-polymerization process as a function of the experimental parameters

Sample	Polymer/PCBM concentration in $CHCl_3$ ($mg.mL^{-1}$)	Time of sonication (min)	Probe intensity (%)	SDS concentration in water ($mg.mL^{-1}$)	Particles' size [a] (nm)
1	30	2	20	10	80-140
2	50	2	20	10	240-420
3	5	2	20	10	20-50
4	30	5	20	10	50-60
5	30	2	20	30	50-60
6	30	2	30	10	40-50

[a] determined by TEM

The particles' size could also be tuned by playing on the amount of surfactant, knowing that by increasing the amount of sodium dodecyl sulfate (SDS) allows for a higher surface coverage. It gave rise to smaller particles (Table 2 entries 1 and 5, figure 3 TEM images 1 and 5). Nevertheless, it is noteworthy that such a parameter (*i.e.* the amount of surfactant) has to be tuned with caution in regards to the photovoltaic application. Indeed, surfactants can be considered as insulating materials that have to be used in small amounts. In fact, a compromise has to be determined for the quantity of surfactant needed for an appropriate photoactive ink considering the final application.

We can assume that the size-dispersity is not an important parameter for OPV application. Indeed with a relatively broad size distribution (as can be seen on TEM images (see figure 3) and DLS curve (see figure 4), the small particles could fill the gap between the bigger ones and a more uniform film could thus be obtained.[9]

In the case of nanoparticles, the size of the domains in the active layer is limited by the size of the particles, which can be controlled in the miniemulsion post-polymerization process by playing on the parameters described previously. Thus in regards with the processing of inks of appropriate particles for solar cells one has to deal with the combination of different parameters such as concentration in active matter, concentration in surfactant and sonication time. In the following we chose to copy the conditions used for sample 6 for the production of composite particles.

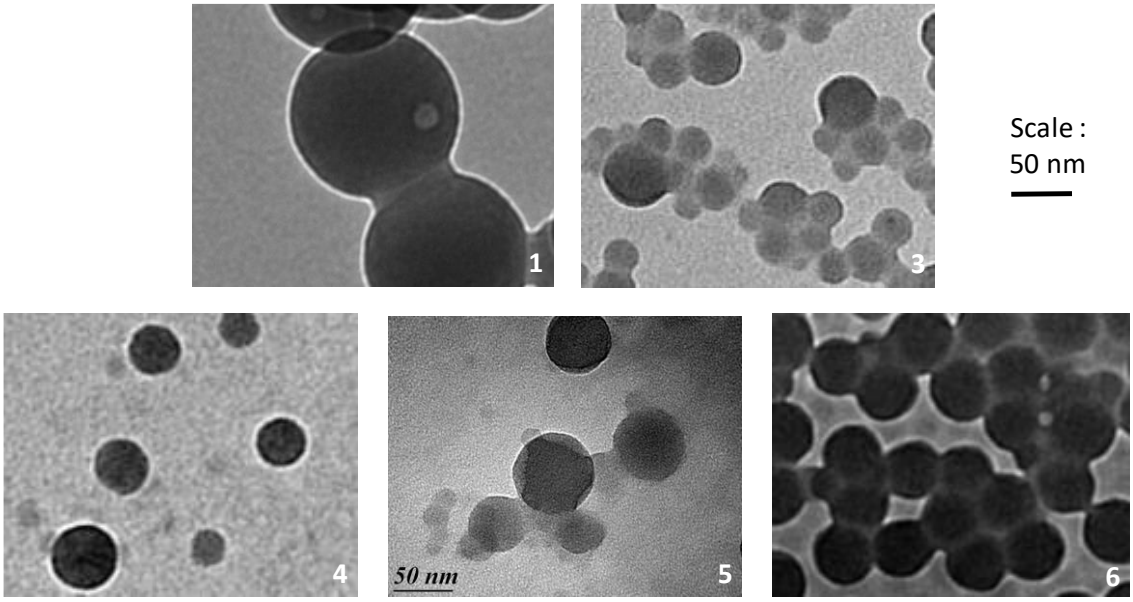

Figure 3 : TEM images of the composite particles of $PC_{71}BM$:PCDTBT (80:20) prepared by miniemulsion post-polymerization process, numbers correspond to entries in Table 1

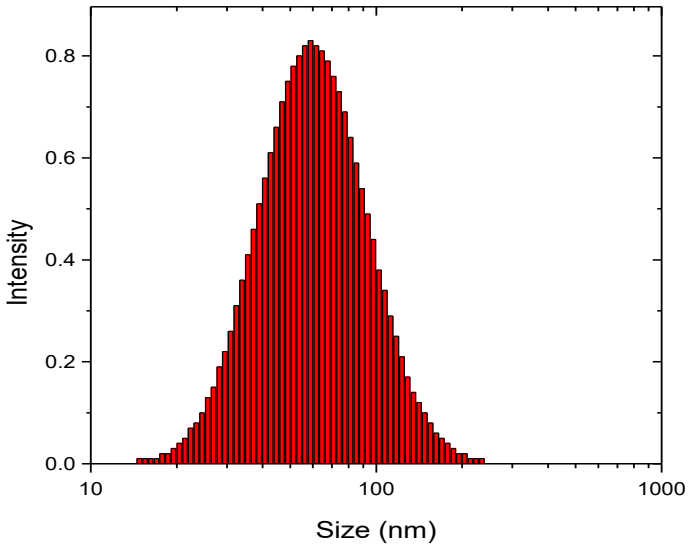

Figure 4 : DLS curve of sample 4 in Table 1 : composite particles of $PC_{71}BM$:PCDTBT (80:20) prepared by miniemulsion post-polymerization process using 5 min of sonication

III.2.3. Stability of inks of composite particles

A key feature of such materials for further development concerns the stability of the inks. Indeed, after their fabrication, they have to be stable during transport and storage until the deposition. While, usually such inks are formulated, we decided to study the raw materials' stability. The later was assessed *via* zeta potential measurements. This was determined by measuring the electrophoretic mobility of the colloidal particles in the solution when a voltage was applied. As the zeta potential depends on the magnitude of the electrostatic interaction between the particles, it can be used as a characterization tool for the colloidal stability. The zeta potential of composite particles was found around -58 ±15 mV (see figure 5) which is in agreement with the literature for a stable ink, repulsion forces being high enough to prevent aggregation upon ageing.[10]

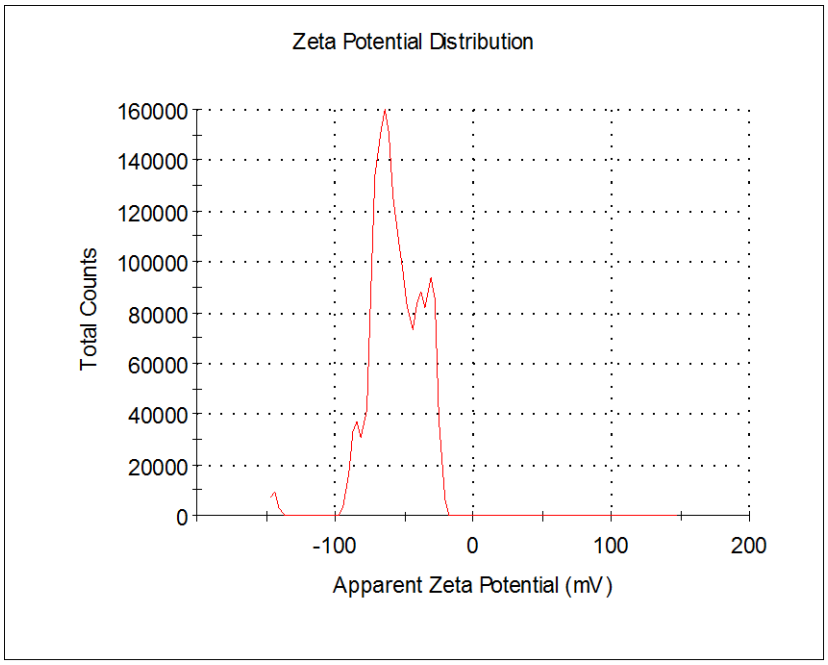

Figure 5 : Zeta potential of the composite particles $PC_{71}BM$:PCDTBT (80:20) prepared by miniemulsion post-polymerization process using 30% of sonication probe intensity (sample 6 in Table 1)

III.2.4. Optoelectronic properties of $PC_{71}BM$:PCDTBT composite particles

The optical properties of these particles have been studied by UV-visible absorption and fluorescence. In figure 6 the absorption spectra obtained in water (nanoparticles, figure 6 a) and $CHCl_3$ (solubilized components, figure 6 b) for various compositions are presented.

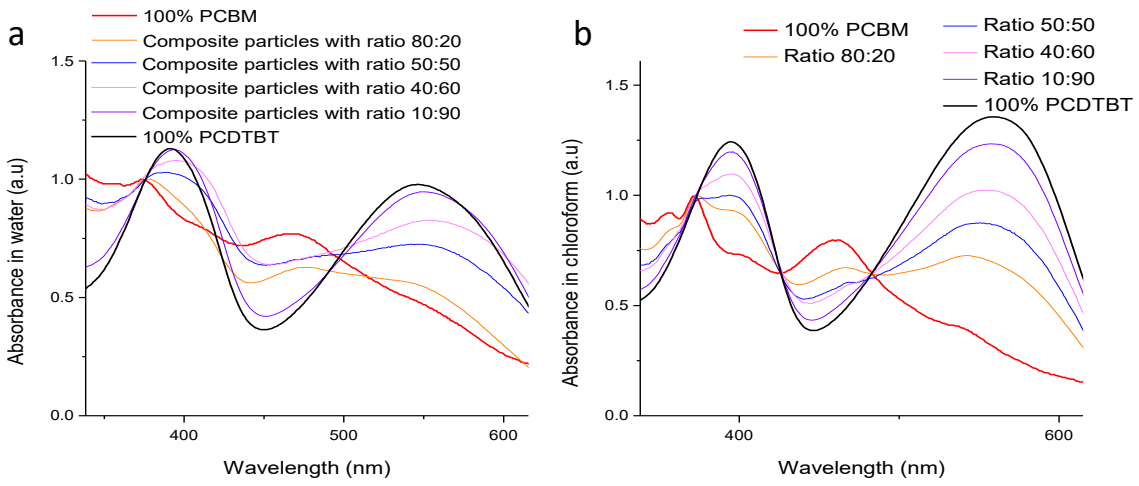

Figure 6 : Absorption spectra of composite materials at different $PC_{71}BM$:PCDTBT ratio in water (particles, spectra a) and in chloroform (spectra b)

The two graphs show different behaviors in regards with the solvent of analysis. Indeed spectra in water are of lower intensity than the ones in chloroform. This result is consistent with changes induced by aggregation, as it has been previously reported for other polymers such as poly(3-hexylthiophene) (P3HT)[11] and poly(naphthalene diimide) (PNDI).[12]

Moreover, the absorption spectra recorded in $CHCl_3$ for the blend solution (80:20 $PC_{71}BM$:PCDTBT) result from the addition of the spectra of the pure materials in the same solvent, taking into account the relative weight fractions. This suggests that $PC_{71}BM$ and PCDTBT molecules are well dissolved in $CHCl_3$ and do not interact with each other. Besides, in case of composite particles in water (NP composed of 80:20 $PC_{71}BM$:PCDTBT), the absorption spectra cannot be deconvoluted in the parent spectra of $PC_{71}BM$ and PCDTBT : as can be seen in figure 7, the spectrum of a 80:20 composite particle is not the same as the one of a water dispersion composed of 80wt% of $PC_{71}BM$ particles + 20wt% of PCDTBT particles. Indeed, the major peak at 468 nm corresponding to the $PC_{71}BM$ absorption has a weaker intensity once the particles are composite suggesting that the $PC_{71}BM$ is hidden by the PCDTBT. Moreover the 'shoulders' at 392 and 548 nm

corresponding to the PCDTBT absorption appear with a slightly stronger intensity for the composite particles compared to the mixed particles. This result suggests that the two materials are in intimate contact within one single particle.

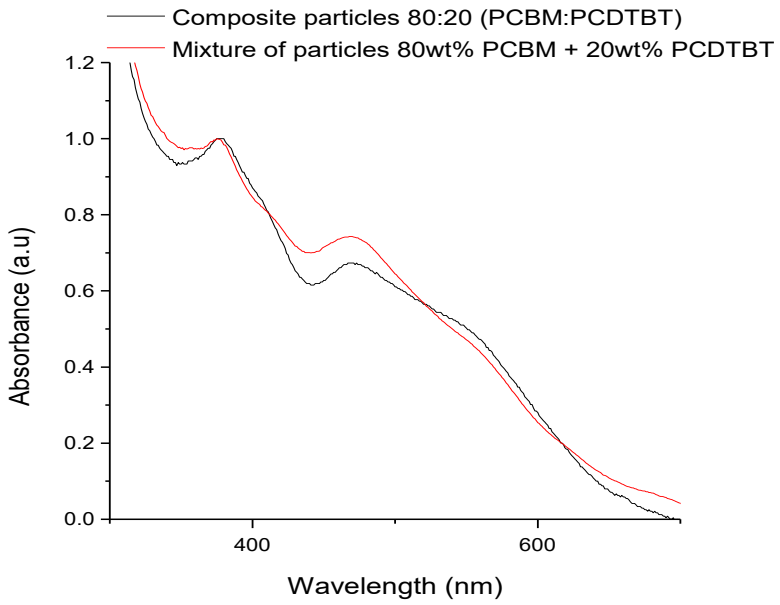

Figure 7 : Absorption spectra of 80:20 composite particles and mixture of particles (80wt% of PCBM + 20wt% PCDTBT) in water

Fluorescence spectroscopy provides further insight that both $PC_{71}BM$ and PCDTBT are co-existing in one single particle in water, as illustrated in figure 8 showing the emission spectra of particles in water (top) and emission spectra of $CHCl_3$ solutions at excitation wavelength of 395 nm, corresponding to the maximum absorption of PCDTBT. In both cases, for pure PCDTBT, an emission peak is observed between 600 and 800 nm (black curve). In water, when $PC_{71}BM$ is added in the NP composite, the fluorescence of the polymer is quenched in any composition (even when 10wt% of $PC_{71}BM$ is used almost total quenching is reported) which is not the case in $CHCl_3$ as we do observe an emission peak for the two compositions (80:20 and 10:90). This result is consistent with the fact that the two components (i.e. $PC_{71}BM$ and PCDTBT) are in intimate contact within one single particle in the composite particles.

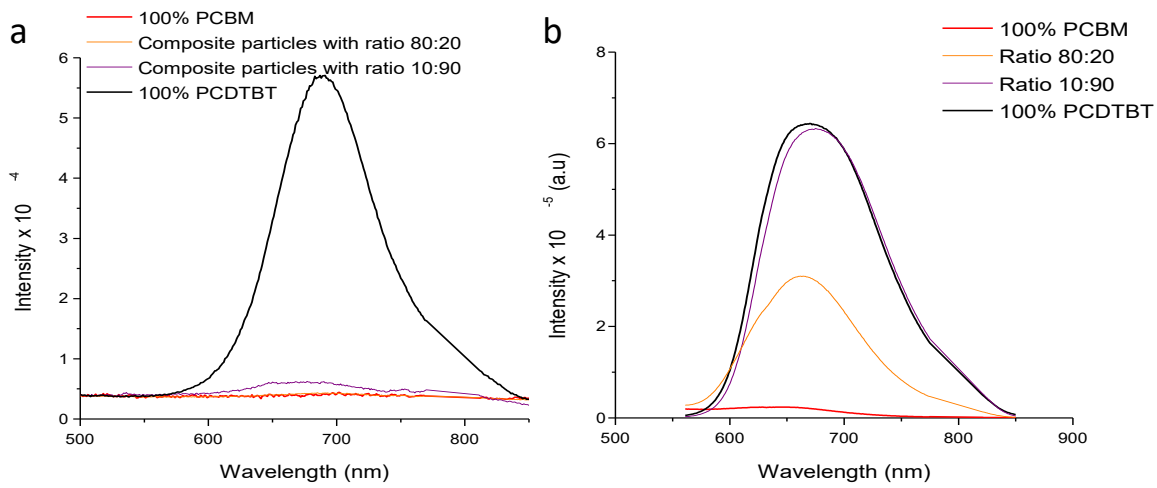

Figure 8 : Photoluminescence of the composite materials at different ratio of $PC_{71}BM$:PCDTBT in water (particles, spectra a) and in chloroform (spectra b)

Additionally, we investigated the fluorescence of a mixture of two particles (water dispersion composed of 80wt% of $PC_{71}BM$ particles + 20wt% of PCDTBT particles as above) showing a fluorescence peak centered at 700 nm characteristic of the PCDTBT in figure 9. The absence of quenching is also in favor of our previous statement confirming the cohabitation of PCDTBT and $PC_{71}BM$ in particles as synthesized *via* our post-polymerization process.

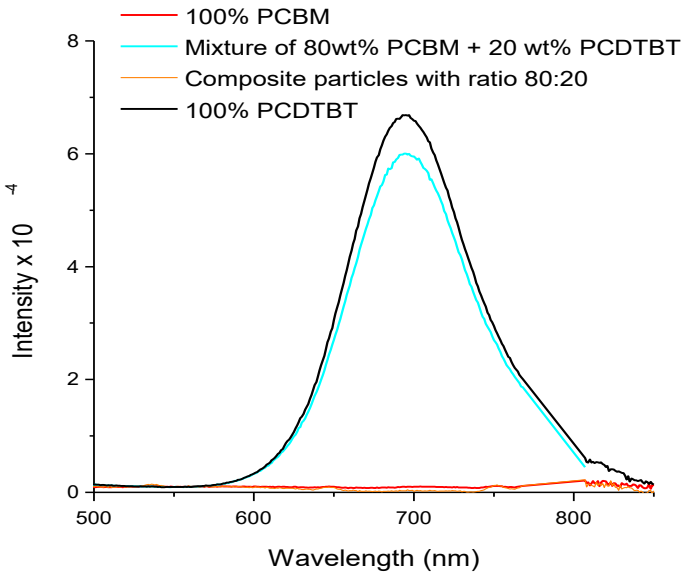

Figure 9 : Photoluminescence spectra of composite particles with ratio of $PC_{71}BM$:PCDTBT (80:20) and mixture of 80wt% $PC_{71}BM$+20wt% PCDTBT (light blue) excited at 395 nm in water

III.2.5. Study of film formation from $PC_{71}BM$:PCDTBT inks

Above described photoactive inks composed of both $PC_{71}BM$ and PCDTBT within nanoparticles were deposited as thin films using spin-coating in order to form *in fine* an active layer. Here after are some data regarding their spin-coating on a glass substrate which was heated for 2 min at 100°C to evaporate water. The films were characterized by AFM and TEM.

As can be seen on figure 10 and 11, despite the elevated temperature, still below the glass transition or melting temperature of the materials (Tg~130°C[13] and Tm~200°C[14]), after the spin-coating process the layer is formed of closely packed particles. A similar packing behavior was already described in figure 5 on TEM picture. Interestingly the rather high particles' size distribution is in favor of a good particles packing, smaller particles filling the dead space. The two colors on the phase image represent the two components which indicate that the particles are composites made of the two compounds $PC_{71}BM$ and PCDTBT.

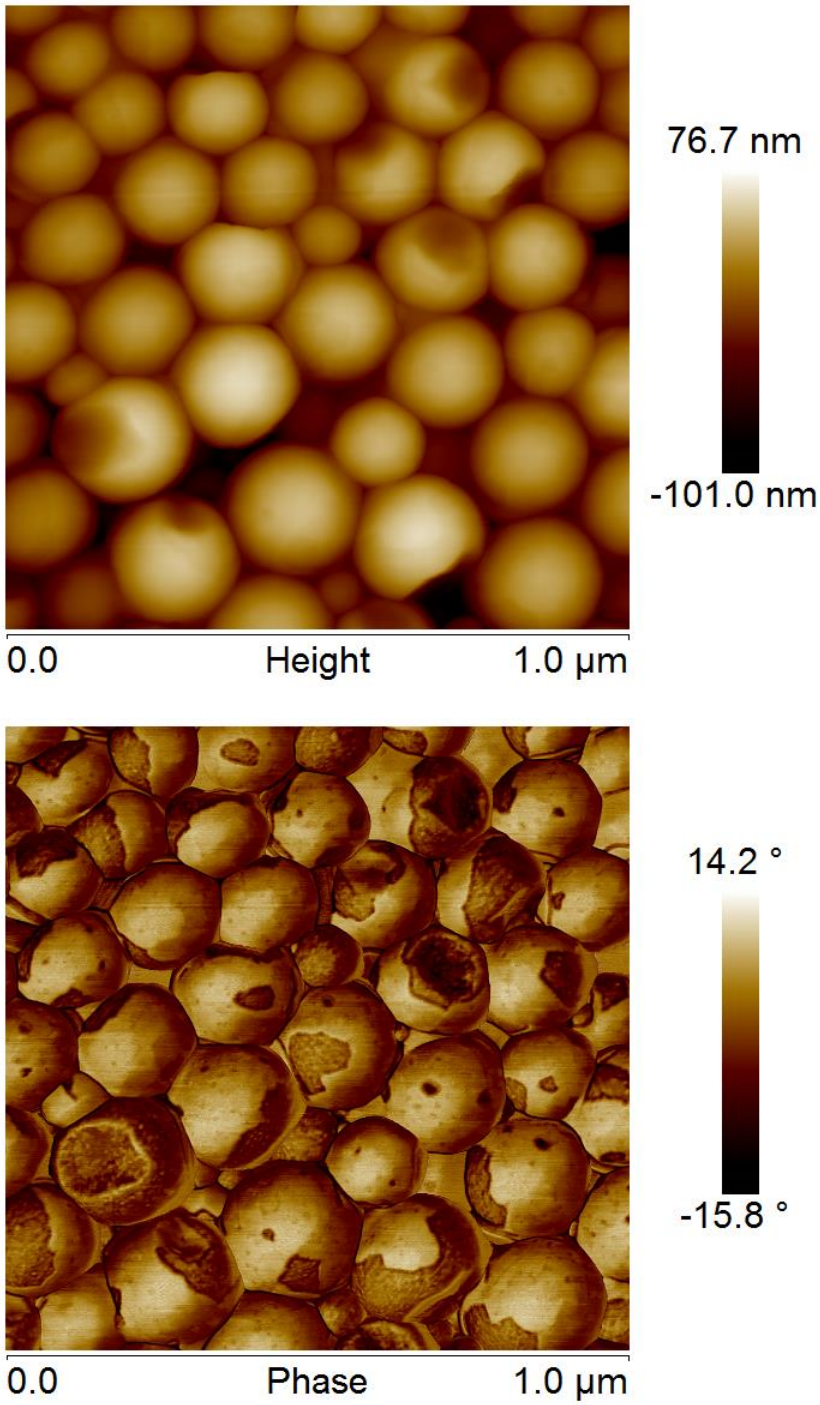

Figure 10 : AFM images height (top) and phase (bottom) of 80:20 ($PC_{71}BM$:PCDTBT) composite nanoparticles obtained through miniemulsion post-polymerization process

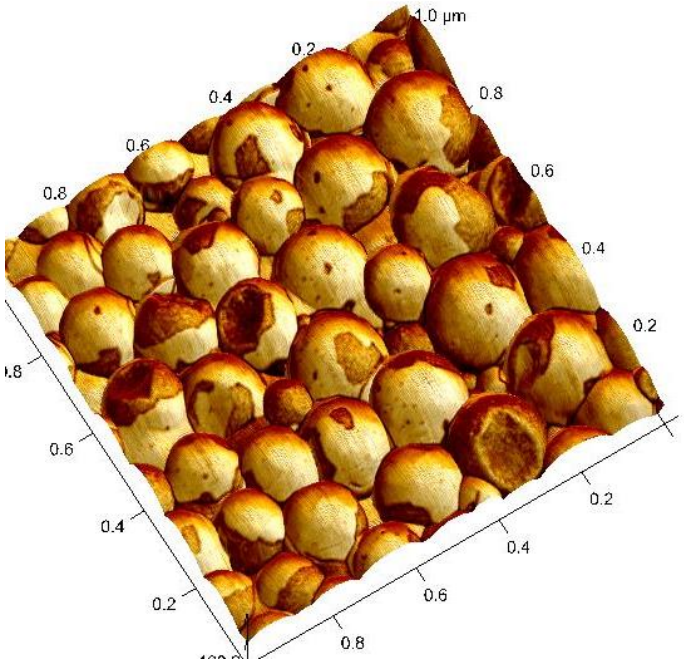

Figure 11 : 3D image: superimposition of phase and topology images of 80:20 ($PC_{71}BM$:PCDTBT) composite nanoparticles

It is noteworthy that the morphology of nanoparticles synthesized using the same methodology was reported as core-shell.[15,16] A compound segregation was proved by scanning transmission X-ray microscopy (STXM) and could be explained through thermodynamic considerations of the relative surface energies *e.g*. higher surface energy compound segregating in the core of the particles.[17] In a similar approach, surface energies (IFT) on films of pure PCDTBT and $PC_{71}BM$ were measured. For pure $PC_{71}BM$ a surface energy of 48 $mN.m^{-1}$ was measured whereas for pure PCDTBT it was 37 $mN.m^{-1}$. As the surface energy of PCDTBT is lower than that of $PC_{71}BM$, PCDTBT is expected to have preferential interaction with the external. Indeed, to minimize the total energy, the polymer should migrate to the external surface of the droplets during the chloroform evaporation and the nanoparticles formation, forming the shell of the composite nanoparticles.

$PC_{71}BM$:PCDTBT NPs were further characterized by contrast variation Small Angle Neutron Scattering (SANS) in order to get more insights on the distribution of the two materials within the nanoparticles.[18] Following the methodology reported by Richards *et al.* for P3HT NPs.[19] 80:20 NPs were dispersed into different H_2O/D_2O mixtures to probe their internal structure and heterogeneity without changing the chemical environment.[18] Scattering profiles are presented in

figure 12a for 4 different contrasts and the radius of gyration, R_g was retrieved using Gunier analysis. Interestingly the calculated radius of gyration is dependent of the changing contrast of the aqueous phase with R_g ranging from 13.2 to 14.0 nm, underlining the heterogeneous spatial distribution of the components in the NPs. Stuhrmann plot shown in figure 12b was subsequently used in order to precisely characterize the internal heterogeneity of the NPs. Following Stuhrmann analysis, the quadratic dependence of R_g on $\Delta\rho$ ($\Delta\rho = \rho_{NP} - \rho_S$ with ρ_{NP} and ρ_S the averaged NP and solvent scattering length densities respectively) can be expressed according to equation 1.[20]

$$R_g^2 = R_c^2 + \frac{\alpha}{\Delta\rho} - \frac{\beta}{\Delta\rho^2} \quad (1)$$

In which R_c is the radius of gyration of the particle at infinite contrast (*i.e.* for homogeneous particles), α is the relative distribution of scattering length density radially from the particle center of mass and β is the distance of the center of mass of the particle to the center of mass of its heterogeneous components.[19] As reported by Richards *et al*, the values of α and β allow to discriminate NPs internal heterogeneity; i.e. α and β being sensitive to the radial distribution of $PC_{71}BM$ and PCDTBT in NPs axisymmetry, respectively. [19] Consequently uniform volume distribution of $PC_{71}BM$ and PCDTBT in NPs corresponds to zero α and β, which enrichment of the lower contrast PCDTBT (ρ_{PCDTBT}=1.416x10^{-6} Å^{-2} *vs* ρ_{PC71BM}=4.464x10^{-6} Å^{-}2) at the NPs surface would lead to a negative alpha value (assuming the SDS shell contribution is negligible due to the low SDS amount incorportated at the NPs surface). A non-zero β value is related to different special position of the centers of mass and scattering length density in the NPs.

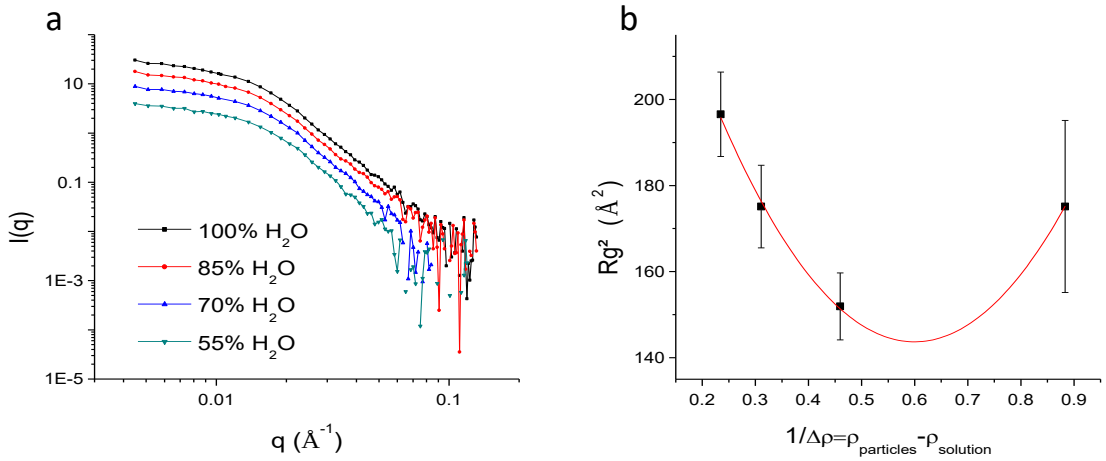

Figure 12 : (a) SANS profiles of 80:20 $PC_{71}BM$:PCDTBT NPs measured at four H_2O/D_2O different contrasts, (b) Stuhrmann plot, Rg^2 vs $1/\Delta\rho$, the red curve is the fitting allowing us to retrieve the α and β values.

Based on the Stuhrmann plot presented in figure 12b, the dependence of Rg^2 on $1/\Delta\rho$ shows that the particles are non-axisymmetric since[19] a nonzero β value of -3.91×10^{-8} ($Å^{-2}$) is retrieved. The negative α value (α= 0.047) indicates that PCDTBT is preferentially segregated at the NPs surface in accordance with surface energy consideration.

In conclusion, these particles have an enriched PCDTBT shell with an eccentric internal distribution of $PC_{71}BM$ which is in agreement with the surface energy measurements.

III.2.6. Study of thermal annealing on $PC_{71}BM$:PCDTBT films

While thermal annealing was harmfully reported for the system PC71BM:PCDTBT due to disruption of the π- π stacking and reduced hole-mobility,[5,21] it can favorably affect the morphology of film, in case of particles creating more interfaces. [3,22–25] Herein, thermal annealing was studied by AFM and TEM. For TEM, the active layer was deposited on a poly(3,4-ethylenedioxythiophene):polystyrene sulfonate (PEDOT:PSS) film, the substrate was then heated during the required time and then dipped into water in order to dissolve the underneath PEDOT layer. The active layer was then left floating and transferred onto the TEM grid. An AFM study was then carried out as a function of the temperature in order to get a better insight on the thermal annealing range.

Starting from a 80:20 composition, a temperature ramp was performed in the AFM setup and pictures of the particles were taken while heating as shown in figure 13. It is important to note that the temperature was raised stepwise from 25°C (image a) to 110°C (image b) and to

150°C (image c) while characteristic temperatures of the $PC_{71}BM$:PCDTBT materials are respectively Tm~200°C[14] and Tg~130°C[13]. As can be seen in figure 13, no change was noticed between 25°C and 110°C. Consequently, the annealing temperature should be higher than 110°C to get a more homogeneous film. When the temperature was increased to 150°C, one can notice that the particles have merged resulting from the PCDTBT transition temperature. The morphology remained unchanged when going back to room temperature (image d).

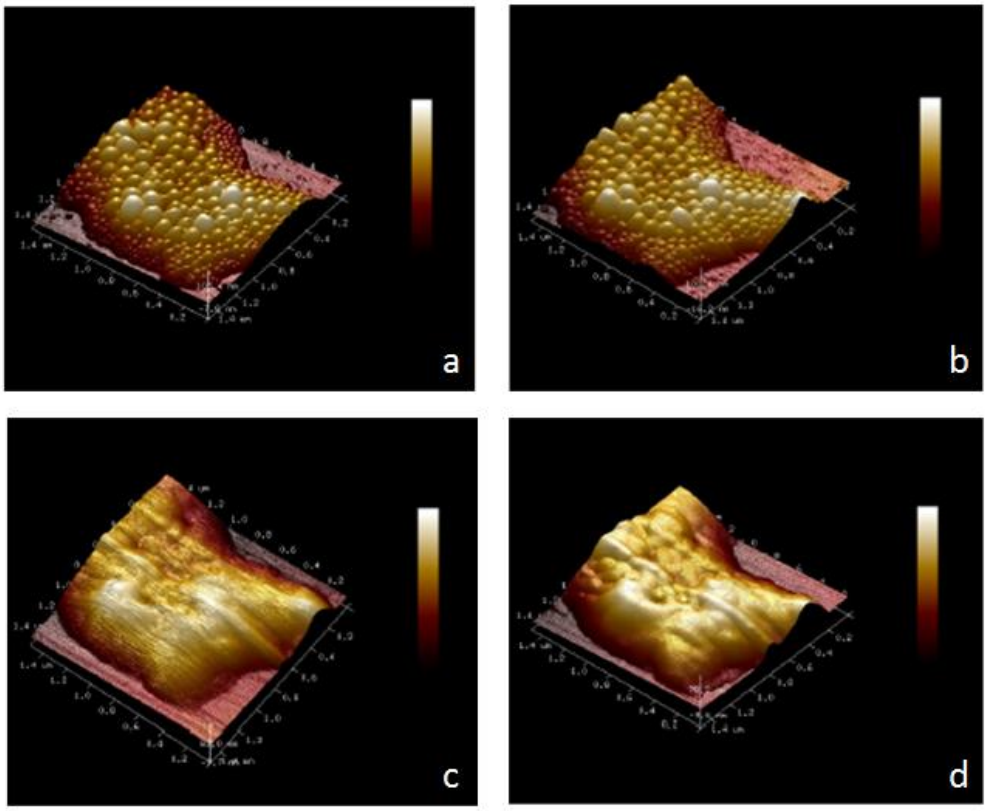

Figure 13 : AFM images during heating for 80:20 $PC_{71}BM$:PCDTBT composite particles, a: at 25°C, b: at 110°C, c: at 150°C, d: 25°C after heating at 150°C

Films of 80:20 composite particles were annealed during the same time at different temperatures, from 110°C to 150°C (we did not go higher because of dewetting). The annealing data are gathered in Table 2 based on AFM and TEM images. After annealing at 150°C, gross-phase segregation occurred, which is in disfavor of an efficient solar cell, the exciton being most probably trapped within big size domains. The roughness was decreased with the annealing

temperature up to 140°C and a more homogeneous film was created as shown on TEM image. Thus, for future experiments the annealing temperature was set at 130 or 140°C.

Table 2 : Annealing study of 80:20 $PC_{71}BM$:PCDTBT composite particles based on AFM and TEM images

Temperature and time of annealing	AFM Height	AFM Phase	TEM image	Roughness
No annealing	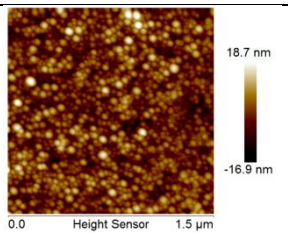	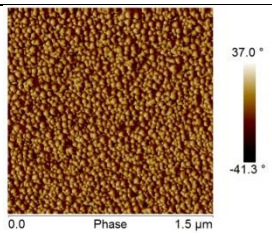	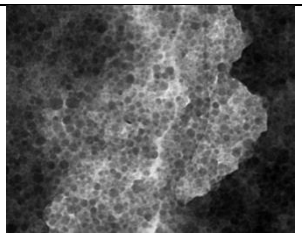	5.4 nm
110°C 4 min	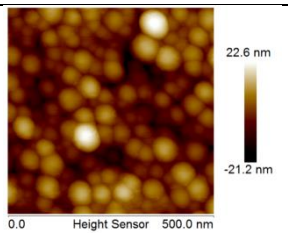	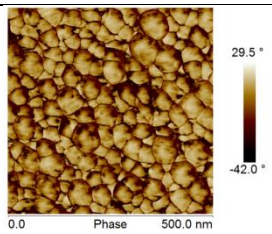	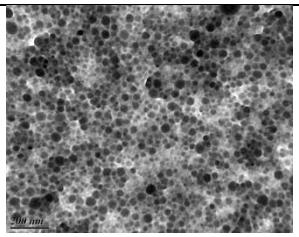	6.14 nm
120°C 4 min	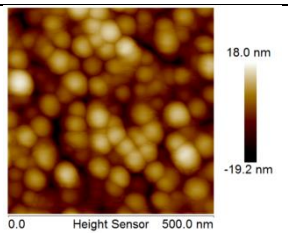	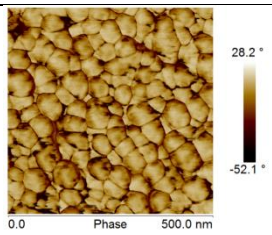	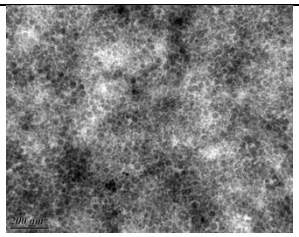	5.43 nm
130°C 4 min	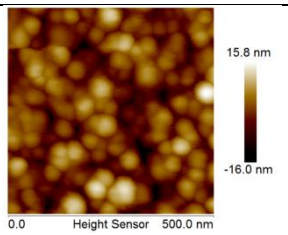	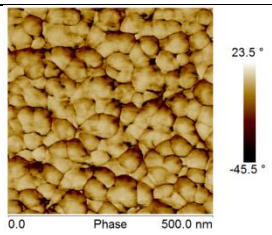	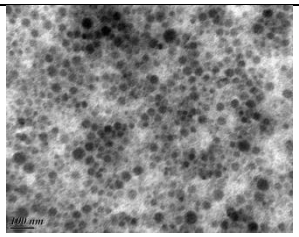	4.96 nm
140°C 4 min	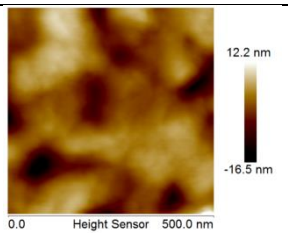	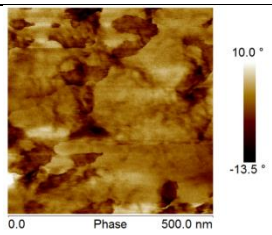	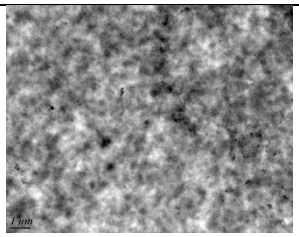	3.96 nm
150°C 4 min	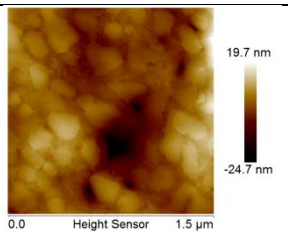	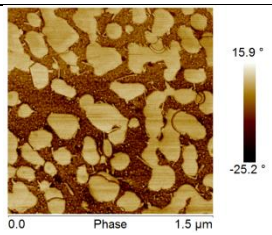		7.66 nm

From figure 13 and Table 2, thermal annealing has been shown to be beneficial for the formation of an active layer from NPs. It allows a sintering of the NPs as well as the creation of more interfaces between the p and n components. The conductivity variation can be assessed by Conductive-Atomic Force Microscopy (C-AFM) in which a voltage is applied between the tip of the AFM and the sample, generating a current image. Indeed, as shown in figure 14, prior to annealing there is almost no current variation throughout the film (no contrast on image b) due to poor contact between the NP. Instead, the annealed film at 140°C for 4 min shows domains with high (blue) and low current (yellow) (image d). These conducting pathways, due to a higher contact between particles, show local hole transport through interconnecting polymer chains[26] (image d figure 14).

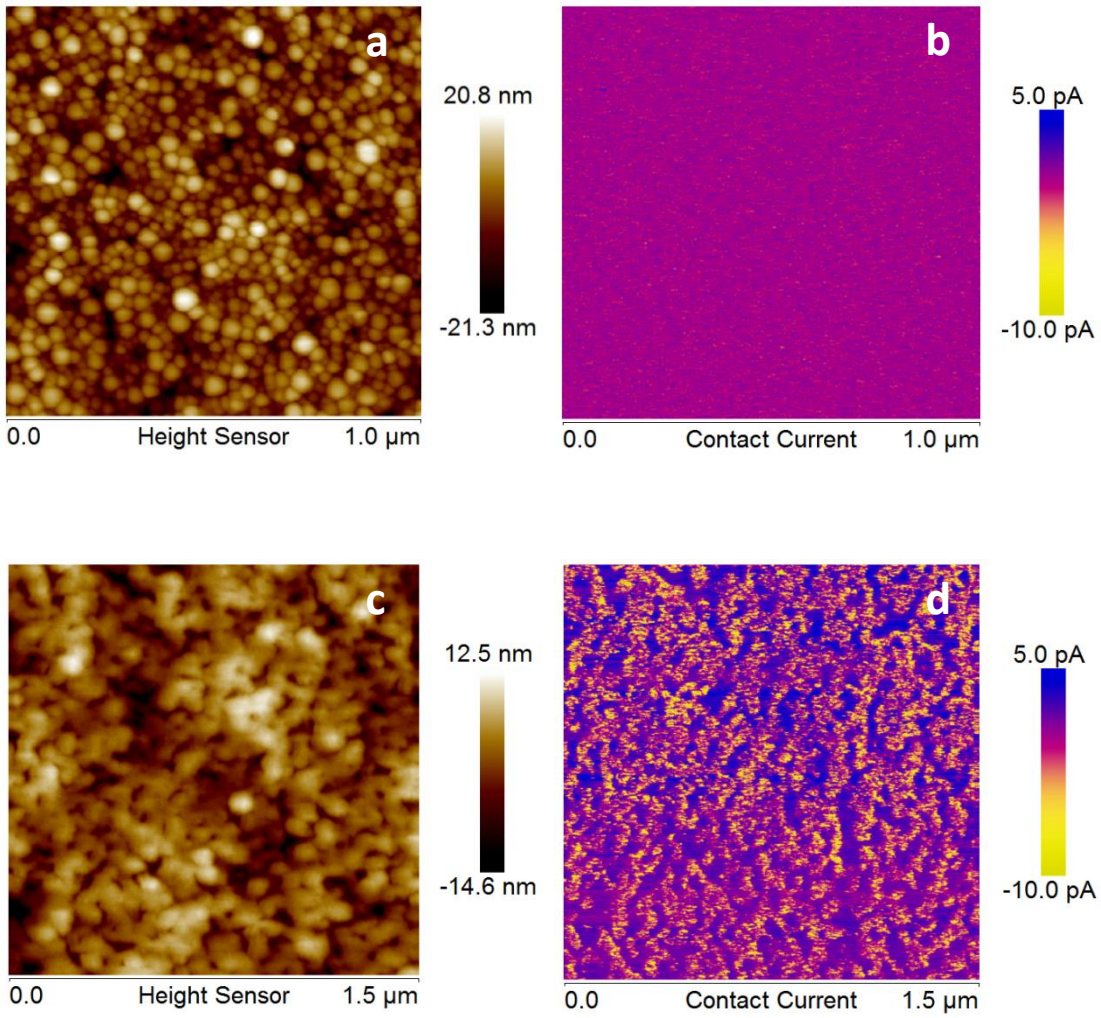

Figure 14 : Conducting- AFM, topography and contact current images of the composite $PC_{71}BM$:PCDTBT particles (80:20) without annealing (a and b) and after annealing at 140°C during 4 min (c and d) collected at +1V

III.2.7. Integration of $PC_{71}BM$:PCDTBT inks into solar cells

Above described photoactive inks composed of both $PC_{71}BM$ and PCDTBT within nanoparticles were integrated into solar cells. The inverted stack was chosen because the polymer presents a better stability[27] and the devices are air-stable using such configuration[28] *i.e.* glass/ITO/ZnO/$PC_{71}BM$:PCDTBT(NP)/MoO_3/Ag.

The surface energy of our inks and that of the substrate were then measured to study the compatibility between the two layers (see Table 3). The high surface energy of our inks deposited onto glass is attributed to the surfactant which is located at the interface between the particles and the substrate and air.[25] For zinc oxide, the surface is hydrophilic which seems appropriate for coating the composite active ink as can be seen on figures 15 and 16.

Table 3 : Surface energies of $PC_{71}BM$, PCDTBT, ZnO and 80:20 $PC_{71}BM$:PCDTBT composite particles films

	Θ_{water} (°)	$\Theta_{ethylene\ glycol}$ (°)	$\Theta_{diiodomethane}$ (°)	Surface energy (mN/m)
$PC_{71}BM$	71 ± 2	48 ± 1	11 ± 3	48 ± 0.6
PCDTBT	93 ± 2	70 ± 3	34 ± 1	37 ± 0.3
ZnO on ITO	35 ± 4	26 ± 2	36 ± 1	59 ± 0.8
$PC_{71}BM$:PCDTBT particles on glass	2.8 ± 2	10 ± 1	9 ± 0.7	69 ± 0.4

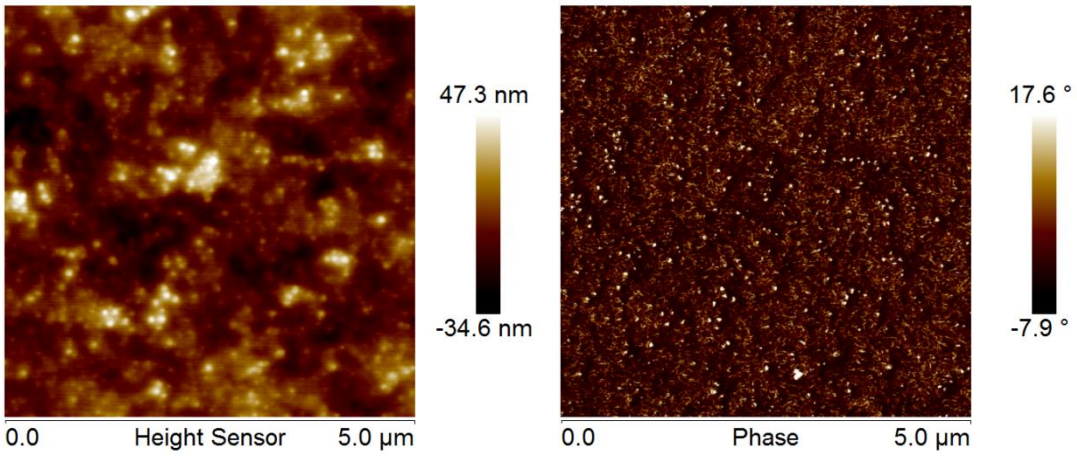

Figure 15 : AFM images of 80:20 $PC_{71}BM$:PCDTBT composite NP deposited on ZnO substrate

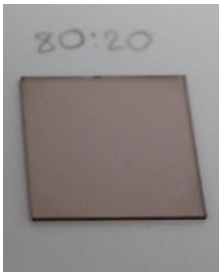

Figure 16 : Picture of the 80:20 $PC_{71}BM$:PCDTBT composite NP deposited on ZnO substrate

The non-annealed active layers were dried at 100°C during 2 min to evaporate the solvent, the other layers were annealed at 130°C or 140°C during 4 min prior thermal evaporation of MoO_3 and Ag.

As a comparison, we also made devices based on $PC_{71}BM$:PCDTBT in chloroform as BHJ with a raw PCDTBT (see figure 17 and Table 4 sample 10).

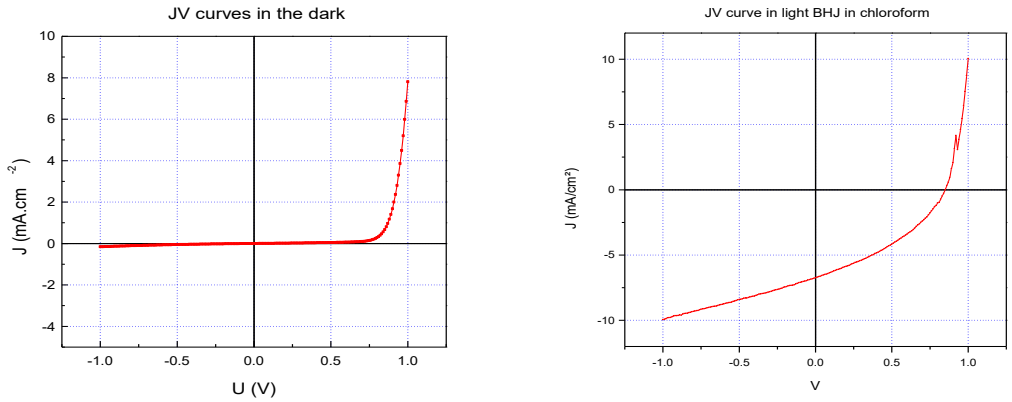

Figure 17 : JV curves in dark (left) and in light (right) of $PC_{71}BM$:PCDTBT in BHJ-based solar cell

Table 4 gathers the results obtained for three kinds of NP: 80:20 ($PC_{71}BM$:PCDTBT) and 60:40 ($PC_{71}BM$:PCDTBT) composites and a 80wt% of $PC_{71}BM$ NP+20wt% of PCDTBT NP.

Table 4 : Characteristics of the solar cells with different particles nature (composite or mixture) and different ratio of $PC_{71}BM$:PCDTBT, the temperature corresponds to the annealing during 4 min, the best results are highlighted

	Sample		J_{sc} (mA/cm)	V_{oc} (V)	FF	PCE (%)
1	NP composite (80:20)	average	1.52	6.19E-02	0.277	0.03
		best	2.27	7.00E-02	0.303	0.05
2	NP composite (80:20) annealing 130°C	average	2.28	2.16E-01	0.274	0.21
		best	5.25	2.87E-01	0.283	0.43
3	NP composite (80:20) annealing 140°C	average	3.79	6.05E-01	0.307	0.70
		best	4.49	6.87E-01	0.304	0.94
4	NP composite (60:40)	average	5.27E-03	9.20E-05	0.251	1.70E-7
		best	8.92E-03	1.30E-04	0.256	2.60E-7
5	NP composite (60:40) annealing 130°C	average	5.64E-02	5.70E-02	0.278	2.26E-4
		best	2.10E-02	1.36E-02	0.288	6.01E-4
6	NP composite (60:40) annealing 140°C	average	6.86E-01	3.68E-01	0.287	0.09
		best	1.82	4.42E-01	0.338	0.28
7	NP mixed (80+ 20)	average	2.23E-02	3.31E-02	0.259	1.95E-04
		best	2.26E-02	5.96E-02	0.262	3.53E-04
8	NP mixed (80+ 20) annealing 130° C	average	4.67E-02	1.28E-01	0.270	1.61E-03
		best	5.60E-02	1.40E-01	0.286	2.24E-03
9	NP mixed (80+ 20) annealing 140°C	average	9.84E-02	2.32E-02	0.237	5.41E-04
		best	1.04E-01	2.41E-02	0.230	5.78E-04
10	PCDTBT:PC71BM bulk	average	6.65E+00	7.83E-01	0.332	1.96
		best	6.96E+00	8.70E-01	0.416	2.48
11	PCDTBT:PC71BM bulk annealing 130°C	average	5.93E+00	4.85E-01	0.317	0.96
		best	6.09E+00	7.70E-01	0.378	1.77
12	PCDTBT:PC71BM bulk annealing 140°C	average	1.68E+00	5.04E-03	0.231	0.23
		best	1.81E+00	1.00E-02	0.264	0.49

For the 80:20 $PC_{71}BM$:PCDTBT composite NPs (which exhibits the best results in BHJ[5,6]), thermal annealing leads to an increase in the efficiencies (PCE) by one order of magnitude (see Table 4 samples 1, 2 and 3) due to a higher percolation between the particles (see conductive AFM in figure 14) and an improved intermixing of the donor and the acceptor. This increase can also be attributed to a decrease of the SDS concentration at the surface of the film as already reported in the literature[29] and observed here by surface energy measurement (see Table 5). Indeed, after annealing the surface energy of the NP film decreased from 69 $mN.m^{-1}$ to 38 $mN.m^{-1}$ which is compatible with a migration of the SDS molecules from the surface to the bulk of the film.

Table 5 : Surface energies of composite PC71BM:PCDTBT NP, bulk PC71BM:PCDTBT and SDS film

	Surface energy (mN/m)
SDS film	67 ± 1
PCDTBT:$PC_{71}BM$ NP	67 ± 0.4
PCDTBT:$PC_{71}BM$ NP annealed	38 ± 0.7
PCDTBT:$PC_{71}BM$ bulk	35 ± 0.3

In fact, the increase of PCE upon annealing results from an increase of the short-circuit current density (J_{sc}) and the open circuit voltage (V_{oc}). By overpassing the T_g of the polymer results in the merging of the particles and the formation of a more homogeneous film, it implies a better connectivity between the PCDTBT and $PC_{71}BM$ domains. Actually, increasing temperature improves inter-diffusion of the two components and, thus, the number of interfaces between the donor and the acceptor increases. Consequently, exciton dissociation is enhanced and the J_{sc} is increased. Besides, the V_{oc} increases from 0.06V for the non-annealed active layers, to 0.2V for those annealed at 130°C, to 0.6V for those annealed at 140°C, approaching gradually the reported V_{oc} value for the PCDTBT:$PC_{71}BM$ BHJ solar cells that is around 0.86V[13]. We can conclude that the morphological changes induced by annealing have a direct impact also on the V_{oc}, probably due to the decrease of the active layer's sheet resistance that follows the homogenization of the film.

For the 60:40 $PC_{71}BM$:PCDTBT composite NPs, the thermal annealing has the same effect of increasing J_{sc}, V_{oc} and consequently PCE as observed for the 80:20 NPs (see Table 4 samples 4, 5 and 6). However the efficiencies are much lower compared to those obtained for the 80:20

composite NPs. The composition seems to have the same impact on NP-based solar cells as on BHJ-based when the two compounds are blended leading to the best performance for the 80:20 ratio.[5,6]

However when similar composition is kept for a mixture of nanoparticles of each compounds (80wt% $PC_{71}BM$ NPs + 20wt% PCDTBT NPs), performance were lower (see Table 4 samples 7, 8 and 9) even after annealing, confirming the importance of nanodomains'size that are above the exciton diffusion length[30] in this case. Thus, in agreement with reported data on PFB:F8BT nanoparticles,[22] composite particles gave better results than the blended nanoparticles composed of each compound (see for instance samples 3 and 9).

Comparing to the BHJ-based devices, as discussed above, annealing led to an increase of the performance for the NP-based devices, unlike BHJ ones. In case of the BHJ devices upon annealing, the open-circuit voltage (figure 18) and the short-circuit current (figure 19) decreased and consequently the efficiency decreased too (figure 20). This implies that the NP structure may provide a more stable alternative to the standard BHJ structure as already reported by Feron *et al*[31] for P3HT-based devices.

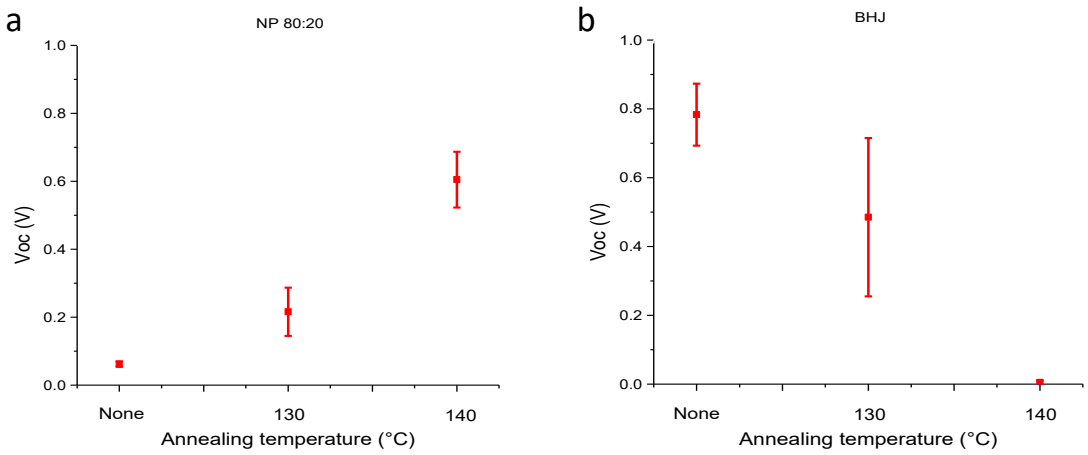

Figure 18 : Open-circuit voltage (V_{oc}) of 80:20 $PC_{71}BM$:PCDTBT composite NP-based solar cell (a) and 80:20 $PC_{71}BM$:PCDTBT BHJ-based solar cell (b) as a function of the annealing temperature

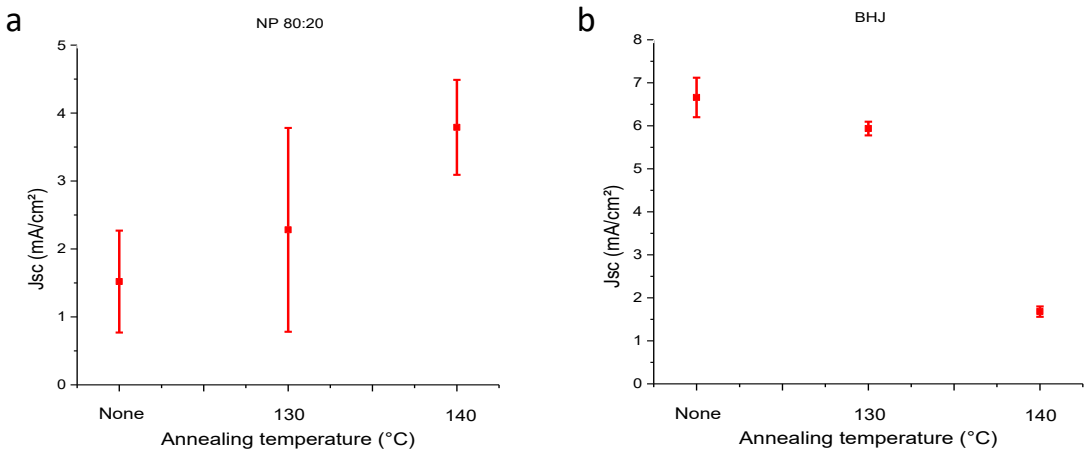

Figure 19 : Short-circuit current (J_{sc}) of 80:20 $PC_{71}BM$:PCDTBT composite NP-based solar cell (a) and 80:20 $PC_{71}BM$:PCDTBT BHJ-based solar cell (b) as a function of the annealing temperature

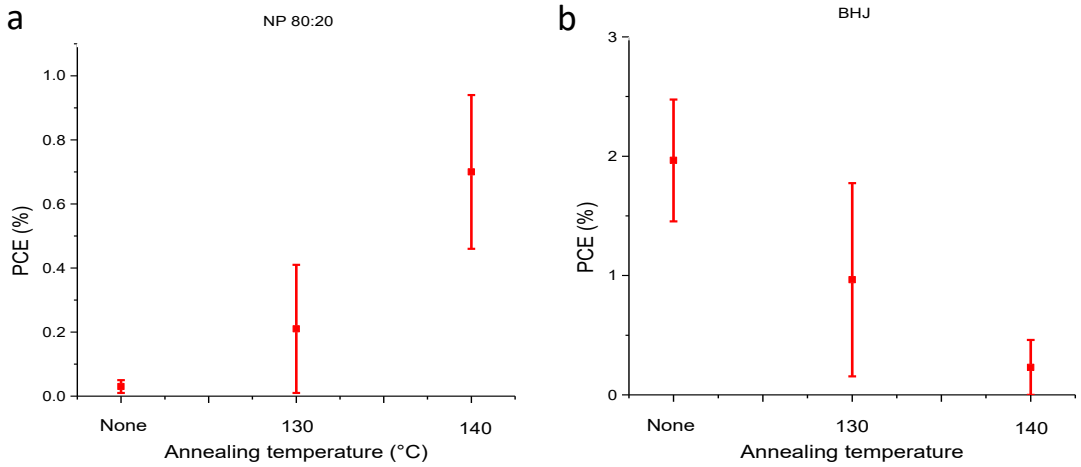

Figure 20 : Efficiency (PCE) of 80:20 $PC_{71}BM$:PCDTBT composite NP-based solar cell (a) and 80:20 $PC_{71}BM$:PCDTBT BHJ-based solar cell (b) as a function of the annealing temperature

The lower results obtained for NP-based devices compared to the BHJ ones composed of $PC_{71}BM$ and PCDTBT are probably due to the presence of insulating and charged stabilizer (SDS) used in the case of NP. Indeed, the sulfate groups and their counter ions may inhibit charge transport acting as traps and decreasing the charge mobility as reported in the literature.[32]

III.3. Conclusion

In this chapter composite NPs of $PC_{71}BM$:PCDTBT were synthesized by miniemulsion post-polymerization in the presence of a surfactant (*i.e.* SDS). The properties of the NP were studied and they were then integrated into solar cells.

The miniemulsion post-polymerization was chosen to successfully produce stable high molar mass PCDTBT particles as well as stable composite $PC_{71}BM$:PCDTBT particles with tunable size depending on the synthetic conditions in water.

Based on the optical properties, the two components are co-existing within one single particle.

The optimum thermal annealing was found at 140°C during 4 minutes to increase the contact between the particles (supported by conducting AFM) and improve the mixing, creating more interfaces. After integration into solar cells, the thermal annealing led to a strong increase in the efficiency as well as the short-circuit current and the fill factor. The best device led to a power conversion efficiency of 0.94%. These relatively low results can be explained by the presence of sodium dodecyl sulfate (SDS) which can act as trap and disturb the charge transport.

A new stabilizer could be used that will be the topic of next chapter IV. Finally, nanoparticles made without stabilizer by nanoprecipitation process will be described in chapter V.

III.4. References

[**1**] T. Kietzke, D. Neher, K. Landfester, R. Montenegro, R. Guntner, U. Scherf, *Nat Mater*, **2003**, *2*, 408.

[**2**] T. R. Andersen, T. T. Larsen-Olsen, B. Andreasen, A. P. L. Böttiger, J. E. Carlé, M. Helgesen, E. Bundgaard, K. Norrman, J. W. Andreasen, M. Jørgensen, F. C. Krebs, *ACS Nano*, **2011**, *5*, 4188.

[**3**] N. P. Holmes, M. Marks, P. Kumar, R. Kroon, M. G. Barr, N. Nicolaidis, K. Feron, A. Pivrikas, A. Fahy, A. D. de Z. Mendaza, A. L. D. Kilcoyne, C. Müller, X. Zhou, M. R. Andersson, P. C. Dastoor, W. J. Belcher, *Nano Energy*, **2016**, *19*, 495.

[**4**] E. A. G. Aniansson, S. N. Wall, M. Almgren, H. Hoffmann, I. Kielmann, W. Ulbricht, R. Zana, J. Lang, C. Tondre, *J. Phys. Chem.*, **1976**, *80*, 905.

[**5**] T. Wang, A. J. Pearson, A. D. F. Dunbar, P. A. Staniec, D. C. Watters, H. Yi, A. J. Ryan, R. A. L. Jones, A. Iraqi, D. G. Lidzey, *Adv. Funct. Mater.*, **2012**, *22*, 1399.

[**6**] V. S. Murugesan, S. Ono, N. Tsuda, J. Yamada, P.-K. Shin, S. Ochiai, *Int. J. Photoenergy*, **2015**, *2015*, 1.

[**7**] K. Landfester, R. Montenegro, U. Scherf, R. Güntner, U. Asawapirom, S. Patil, D. Neher, T. Kietzke, *Adv. Mater.*, **2002**, *14*, 651.

[**8**] O. Pras, D. Chaussy, O. Stephan, Y. Rharbi, P. Piette, D. Beneventi, *Langmuir*, **2010**, *26*, 14437.

[**9**] O. A. Ghazy, *Adv. Polym. Technol.*, **2015**, *34*, 1.

[**10**] R. H. Muller, *Colloidal Carriers for Controlled Drug Delivery and Targeting*, **1991**.

[**11**] T. Yamamoto, D. Komarudin, M. Arai, B. Lee, H. Suganuma, N. Asakawa, Y. Inoue, K. Kubota, S. Sasaki, *J. Am. Chem. Soc.*, **1998**, *120*, 2047.

[**12**] R. Steyrleuthner, M. Schubert, I. Howard, B. Klaumünzer, K. Schilling, Z. Chen, P. Saalfrank, F. Laquai, A. Facchetti, D. Neher, *J. Am. Chem. Soc.*, **2012**, *134*, 18303.

[**13**] N. Blouin, A. Michaud, D. Gendron, S. Wakim, E. Blair, R. Neagu-Plesu, M. Belletête, G. Durocher, Y. Tao, M. Leclerc, *J. Am. Chem. Soc.*, **2008**, *130*, 732.

[**14**] Y. Ning, L. Lv, Y. Lu, A. Tang, Y. Hu, Z. Lou, F. Teng, Y. Hou, *Int. J. Photoenergy*, **2014**, *2014*, 354837.

[**15**] K. B. Burke, A. J. Stapleton, B. Vaughan, X. Zhou, A. L. D. Kilcoyne, W. J. Belcher, P. C. Dastoor, *Nanotechnology*, **2011**, *22*, 265710.

[**16**] K. Feron, S. Ulum, N. P. Holmes, A. L. D. Kilcoyne, W. J. Belcher, X. Zhou, C. J. Fell, P. C. Dastoor, *Appl. Phys. Lett.*, **2013**, *103*, DOI http://dx.doi.org/10.1063/1.4829152.

[**17**] J.-S. Kim, P. K. H. Ho, C. E. Murphy, R. H. Friend, *Macromolecules*, **2004**, *37*, 2861.

[**18**] L. A. Feigin, D. I. Svergun, *Structure Analysis by Small-Angle X-Ray Scattering and Neutron Scattering*, **1987**.

[**19**] J. J. Richards, C. L. Whittle, G. Shao, L. D. Pozzo, *ACS Nano*, **2014**, *8*, 4313.

[**20**] H. B. Stuhrmann, A. Miller, *J. Appl. Crystallogr.*, **1978**, *11*, 325.

[**21**] L. Zhao, S. Zhao, Z. Xu, W. Gong, Q. Yang, X. Fan, X. Xu, *Appl. Phys. A*, **2014**, *114*, 1361.

[**22**] T. Kietzke, D. Neher, M. Kumke, R. Montenegro, K. Landfester, U. Scherf, *Macromolecules*, **2004**, *37*, 4882.

[**23**] Y. Lee, S. H. Lee, K. Kim, J. W. Lee, K.-Y. Han, J. Kim, J. Joo, *J. Mater. Chem.*, **2012**, *22*, 2485.

[**24**] A. Stapleton, B. Vaughan, B. Xue, E. Sesa, K. Burke, X. Zhou, G. Bryant, O. Werzer, A. Nelson, A. L. David Kilcoyne, L. Thomsen, E. Wanless, W. Belcher, P. Dastoor, *Sol. Energy Mater. Sol. Cells*, **2012**, *102*, 114.

[**25**] B. Vaughan, E. L. Williams, N. P. Holmes, P. Sonar, A. Dodabalapur, P. C. Dastoor, W. J. Belcher, *Phys. Chem. Chem. Phys.*, **2014**, *16*, 2647.

[**26**] P. Dutta, Y. Xie, M. Kumar, M. Rathi, P. Ahrenkiel, D. Galipeau, Q. Qiao, V. Bommisetty, *J. Photonics Energy*, **2011**, *1*, 11117.

[**27**] Z. Li, K. Ho Chiu, R. Shahid Ashraf, S. Fearn, R. Dattani, H. Cheng Wong, C.-H. Tan, J. Wu, J. T. Cabral, J. R. Durrant, *Sci. Rep.*, **2015**, *5*, 15149.

[**28**] S. K. Hau, H.-L. Yip, N. S. Baek, J. Zou, K. O'Malley, A. K.-Y. Jen, *Appl. Phys. Lett.*, **2008**, *92*, 253301.

[**29**] B. Vaughan, A. Stapleton, E. Sesa, N. P. Holmes, X. Zhou, P. C. Dastoor, W. J. Belcher, *Org. Electron.*, **2016**, *32*, 250.

[**30**] C. R. McNeill, S. Westenhoff, C. Groves, R. H. Friend, N. C. Greenham, *J. Phys. Chem. C*, **2007**, *111*, 19153.

[**31**] K. Feron, S. Ulum, E. Sesa, B. B. Gong, W. J. Belcher, X. Zhou, C. . Fell, P. C. Dastoor, *J. Appl. Phys.*, **2014**, *116*, 124502.

[**32**] J. Cho, K. H. Cheon, H. Ahn, K. H. Park, S.-K. Kwon, Y.-H. Kim, D. S. Chung, *Adv. Mater.*, **2015**, 5587.

[**33**] S. Wakim, S. Beaupre, N. Blouin, B.-R. Aich, S. Rodman, R. Gaudiana, Y. Tao, M. Leclerc, *J. Mater. Chem.*, **2009**, *19*, 5351.

[**34**] M. Bag, T. S. Gehan, L. A. Renna, D. D. Algaier, P. M. Lahti, D. Venkataraman, *RSC Adv.*, **2014**, *4*, 45325.

[**35**] D. K. Owens, R. C. Wendt, *J. Appl. Polym. Sci.*, **1969**, *13*, 1741.

[**36**] N. G. Connelly, W. E. Geiger, *Chem. Rev.*, **1996**, *96*, 877.

III.5. Appendix

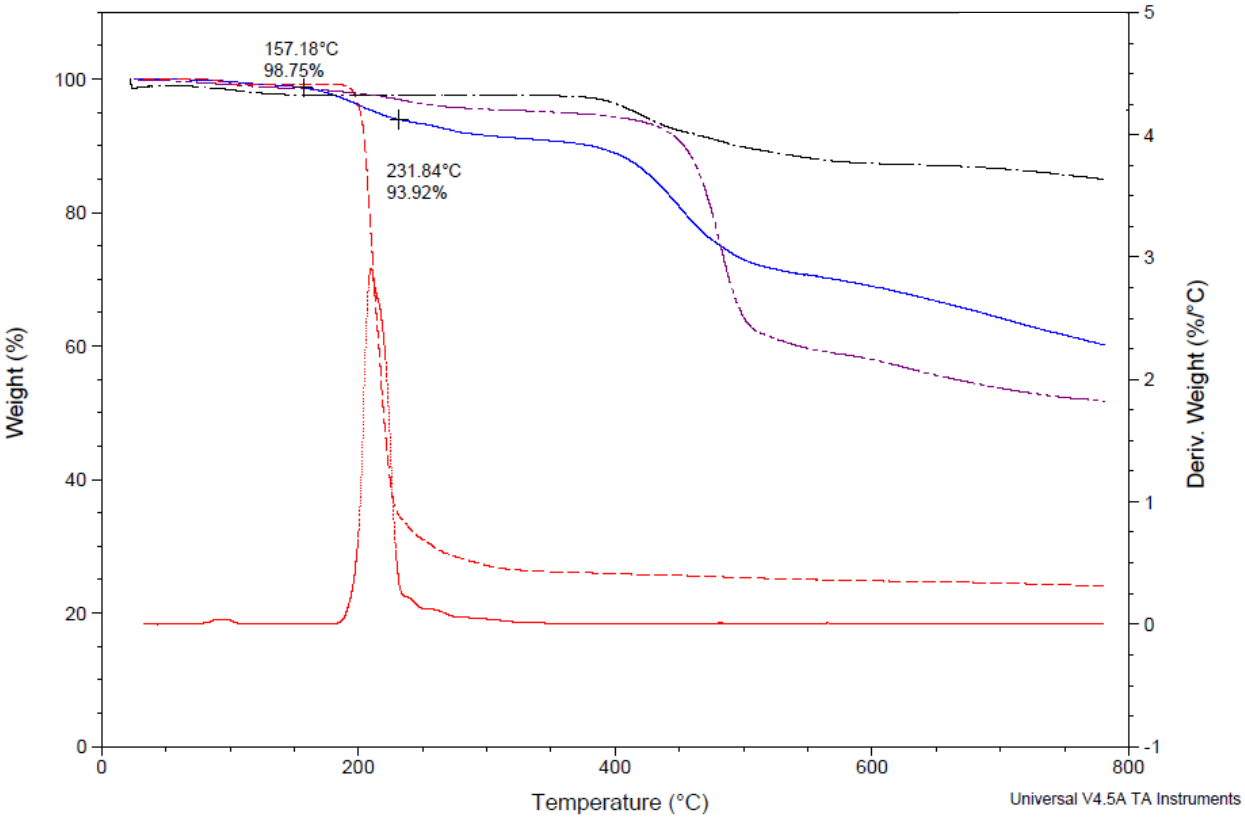

Figure 21 : Thermo-gravimetric analysis (TGA) of dried 80:20 $PC_{71}BM$:PCDTBT composite nanoparticles (in blue), raw PCDTBT as synthesized (in purple), raw $PC_{71}BM$ as bought (in black) and raw SDS as bought (in red)

The SDS corresponds to 5wt% of the total weight of the 80:20 $PC_{71}BM$:PCDTBT composite particles (in blue).

Cyclic voltammetry (CV) of synthesized PCDTBT in bulk

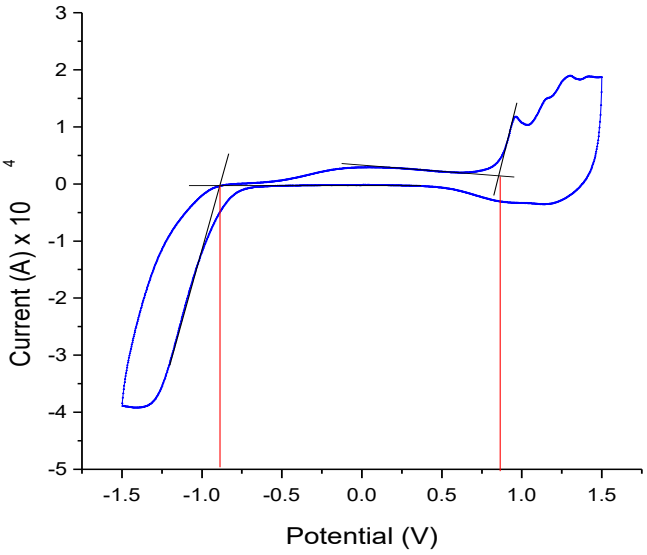

Figure 22 : Voltammogram of the synthesized PCDTBT film on ITO as working electrode, platinum as counter electrode and Ag nanowire as reference electrode in acetonitrile

Table 6 : HOMO and LUMO levels of synthesized PCDTBT calculated from CV, comparison with literature

	E_{HOMO} eV	E_{LUMO} eV	E_{gap}^{elec} eV
Bulk	-5.47	-3.73	1.74
Literature[13]	-5.45	-3.60	1.85

Table 7 : JV curves of composite or mixture particles with different $PC_{71}BM$:PCDTBT ratio and different annealing temperatures

Ratio	No annealing	130°C 4 mn	140°C 4 mn
80:20	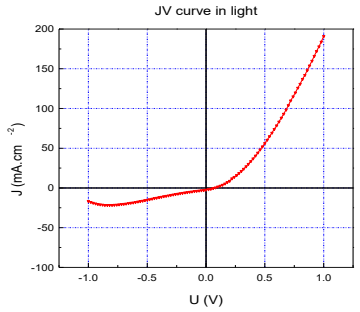	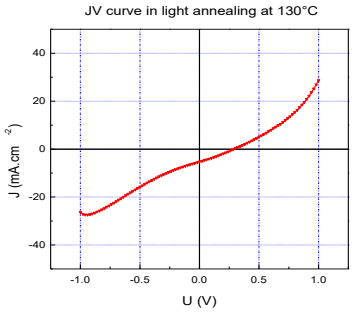	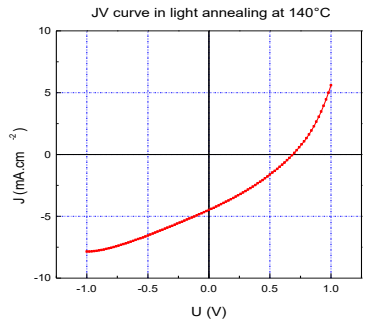
60:40	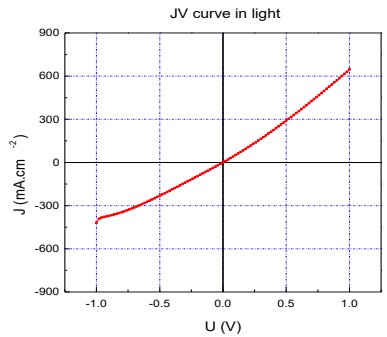	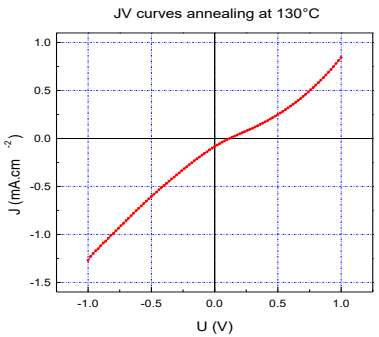	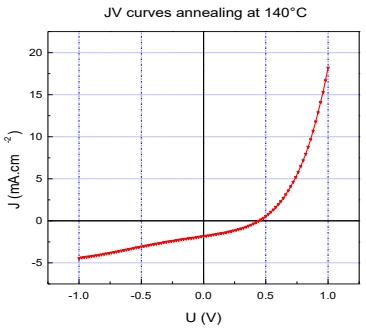
80 + 20	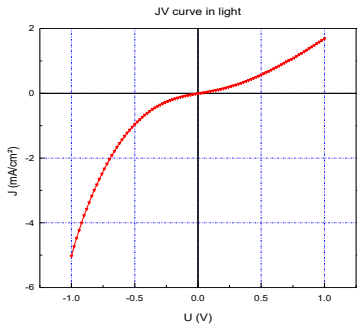	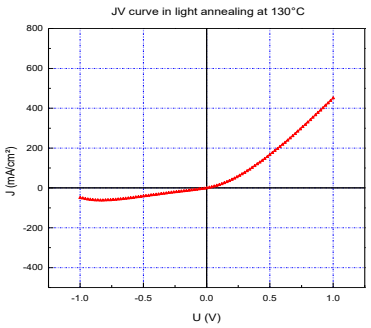	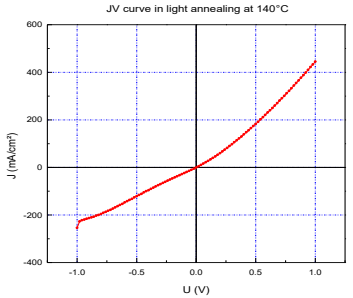

III.6. Experimental Section

III.6.1. Materials

9-(9-Heptadecanyl)-9H-carbazole-2,7-diboronic acid bis(pinacol) ester (97%), 4,7-Bis(2-bromo-5-thienyl)-2,1,3-benzothiadiazole (99+%), and chloroform (99.5+%) were purchased from Sigma Aldrich. Sodium Dodecyl Sulfate was purchased from Acros Organics (99%). $PC_{71}BM$ was purchased from Solaris (99+%). All chemicals were used as received unless otherwise stated.

III.6.2. Synthesis

The reactions were performed under an Argon atmosphere using standard schlenk techniques.

III.6.2.a. Monomers purification

The two monomers were purchased from Sigma-Aldrich and were purified as followed : 9-(9-Heptadecanyl)-9H-carbazole-2,7-diboronic acid bis(pinacol) ester was recrystallized twice in a mixture of methanol/acetone (10:1) and 4,7-Bis(2-bromo-5-thienyl)-2,1,3-benzothiadiazole was recrystallized into *o*-dichlorobenzene as reported in the literature.[33]

III.6.2.b. Typical procedure for the polymerization of 9-(9-Heptadecanyl)-9H-carbazole-2,7-diboronic acid bis(pinacol) ester and 4,7-Bis(2-bromo-5-thienyl)-2,1,3-benzothiadiazole in bulk

PCDTBT was synthesized according to the literature:[33]

In a flame-dried flask, 654.4 mg (0.966 mmol) of 2,7-bis(4,4,5,5-tetramethyl-1,3,2-dioxaborolan-2-yl)-N-9-heptadecanyl-carbazole, 458.8 mg (1.00 mmol) of 4,7-di(2'-bromothien-5'-yl)-2,1,3-benzothiadiazole, 4.2 mg (0.0046 mmol) of tris(dibenzylideneacetone)dipalladium(0) and 6.1 mg (0.020 mmol) of tri(o-tolyl)phosphine were dissolved in 10 mL of degassed toluene and 3.4 mL of degassed 20% aqueous tetraethylammonium hydroxide. The reaction mixture was vigorously stirred and heated up to 95°C at a heating rate of 1°C per minute.

After 3 h, bromobenzene (110 mL, 1.0 mmol) was added to the reaction which was kept at 95°C for one hour and then phenylboronic acid (120 mg, 1.0 mmol) in hot toluene (3 mL) was added and reacted for another hour to allow the end-capping. The reaction mixture was poured in methanol/water (10:1) solution and the polymer was filtered.

The crude material was washed with acetone and heptane using a Soxhlet during one day for each solvent. The remaining solid was extracted with chloroform (300 mL) for several days.

Then the solvent was reduced using rotary-evaporator to about 50 mL and the polymer solution was precipitated in cold methanol (500 mL). The polymer was recovered by filtration and dried under vacuum to yield number average molar mass (Mn) of 20 000 g/mol with PDI of 2.2 as determined by SEC at high temperature in trichlorobenzene.

Table 8 : Molar mass of the synthesized PCDTBT using conventional calibration (PS standards) in TCB at 150°C

$\overline{M}n$ (g/mol)	$\overline{M}w$ (g/mol)	$\overline{M}w/\overline{M}n$
20200	44400	2.20

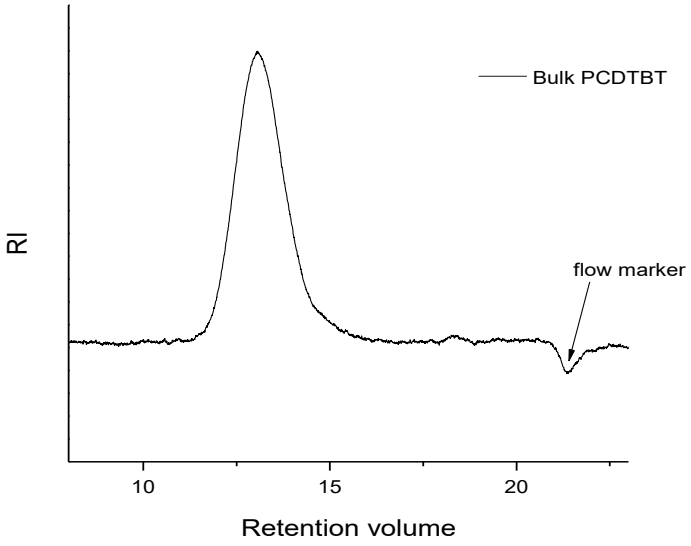

Figure 23 : Chromatogram of the PCDTBT in TCB at 150°C

III.6.2.c. Typical procedure for the $PC_{71}BM$:PCDTBT nanoparticles made by miniemulsion-polymerization

Conjugated polymer nanoparticles were synthesized using a modified mini-emulsion method.[34] PCDTBT and $PC_{71}BM$ were solubilized in 1 mL of $CHCl_3$. Aqueous SDS solution was made by dissolving 50 mg of SDS into 5 mL of MQ-water. The oily solution (chloroform) was then introduced to the stirred aqueous solution, followed by ultrasound during 5 min at 20% amplitude to form the miniemulsion. The samples were then heated to 70°C for 40 min to

evaporate off the chloroform. In order to concentrate and remove the excess of surfactant, the solution was then dialyzed with ultra centrifuge dialysis tubes purchased from Sartorium stedim vivaspin20 (10 kDa MWCO). The solution was placed into the centrifuge dialysis tube and spun at 4000 rpm for 8 min. The filtrate was then discarded and the solution diluted with 5 mL of MQ-water. The quantity of remaining SDS in the continuous phase was checked by pendant-drop measurement. The solution was washed until the surface tension reached at least 65 mN/m (at this point less than 0.2 g/L of SDS was left in the continuous phase).

III.6.3. Methods of characterization

Dynamic light scattering (DLS) on diluted dispersion samples was performed on a Cordouan Particle Size Analyzer Vasco. The autocorrelation function was analyzed using the Cordouan dispersion technology software algorithm to obtain number-weighted particle sizes.

Size exclusion chromatography (SEC) was performed in TCB at 150°C with a flow rate of 1 $mL.min^{-1}$ using Agilent PL gel MIXED C column (pore size 5 µm) and a Agilent PL gel guard-column. The elution times were converted into molar masses using a calibration curve based on low dispersity polystyrene standards.

Thermogravimetric measurements were carried out with TA Instruments Q50 from room temperature to 800°C with a heating rate of $10°C.min^{-1}$. Measurements were performed under nitrogen atmosphere.

Absorption spectra were acquired using a Shimadzu spectrophotometer UV-3600 while *emission spectra* were measured using a Horiba Scientific Fluoromax-4 spectrofluorometer.

TEM images were obtained on Formvar grids with a Transmission Electron Microscope (H7650, HITACHI (accelerate voltage 120 kV), using high contrast mode. Dispersed nanoparticles were cleaned by several centrifugation cycles before TEM analysis and deposited onto a copper grid.

Surface tension was measured using drop shape analysis technique on a pendant drop tensiometer (Krüss DSA-100) while *surface energies* were determined by measuring contact angle between three solvents: water, diiodomethane and ethylene glycol and the polymer film. The surface energy is calculated using Owens-Wendt model.[35]

Zeta potential measurements were carried out with a Zetasizer Nano ZS from Malvern. This instrument can measure zeta from -150mV to 150 mV. The cell voltage was adjusted

depending on the conductivity of the medium. The zeta potential was measured based on the Henry equation.

Small-angle neutron scattering Dispersions were prepared with the typical procedure described above using d-SDS as surfactant. Samples with four different neutron scattering contrast values in the solvent were then prepared by diluting the stock dispersion into solution of varying H_2O/D_2O content, the final concentration was 2wt%. Small-angle neutron scattering experiments were performed on the PAXY spectrometer of the Laboratoire Leon Brillouin (CEA-Saclay, France) equipped with a 2D detector made of 128 x 128 cells. Samples were measured using two configurations: the first one with a sample-to-detector distance of D=5 m and a neutron wavelength of λ=8.5 Å to cover q ranges of $2.5x10^{-3}$-$2.5x10^{-2}$ $Å^{-1}$; the second one with D=3 m and λ=6 Å to cover q ranges of $2x10^{-2}$-0.2 $Å^{-1}$. The counting time at each position was 3600 s for low q and 1200 s for high q. Sample transmission was measured at the largest sample-to-detector distance for each wavelength, and beam flux measurements were used to convert the scattering profiles to an absolute scale.

AFM Characterization: Atomic force microscopy (AFM Dimension FastScan, Bruker) was used in tapping mode to characterize the surface morphology of the samples. Silicon cantilevers (Fastscan-A) with a typical tip radius of ≈5 nm, a spring constant of 18 $N.m^{-1}$ and a cantilever resonance frequency of about 1.4 MHz were used.

Conducting AFM (c-AFM) measurements were performed with a Dimension ICON (Bruker) equipped with a PeakForce TUNA module. Platinum–iridium-coated probes (SCM-PIT, Bruker) with a spring constant of 2.8 $N.m^{-1}$ and resonant frequency of 75 kHz were used. For c-AFM measurements, a DC bias of 5V was applied between the sample and the tip.

Cyclic voltamograms (CV) were recorded on a VersaSTAT3 potentiostat AMETEK using polymer film on ITO as a working electrode and platinum electrode as counter electrode at a scan rate of 50 mVs^{-1} and a Ag nanowire reference electrode in an anhydrous and argon-saturated solution of 0.1 M of tetrabutylammonium tetrafluoroborate(Bu_4NBF_4) in acetonitrile. The HOMO and LUMO levels were estimated from oxidation and reduction onset from the CV spectra assuming SCE electrode to be -4.4 eV from vacuum and using the following equations. All values were corrected with ferrocene reference assuming his oxidation potential was 0.4 V versus SCE[36], in our conditions, the oxidation potential (Eox) of ferrocene was 0.19 V versus Ag/Ag^+. We used Ecorrection $Ag \rightarrow SCE\ (Ferrocene)$= 0.21 V

$$E_{HOMO} = \left(E_{ox\ vs\ Ag} + Ecorrection_{Ag \rightarrow SCE\ (Ferrocene)}\right) + 4.4$$
$$E_{LUMO} = \left(E_{red\ vs\ Ag} + Ecorrection_{Ag \rightarrow SCE\ (Ferrocene)}\right) + 4.4$$

Devices fabrication: Inverted solar cells have been fabricated with the following structure: Glass/ITO/ZnO/active layer/MoO_3/Ag, the active layer being composed of either $PC_{71}BM$:PCDTBT nanoparticles (NP) or $PC_{71}BM$:PCDTBT in bulk hetero junction (BHJ). The Indium tin oxide (ITO)-coated glass substrates, purchased from Vision Tek, with a sheet resistance of ~10 $\Omega.sq^{-1}$ are successively cleaned for 10 min in acetone, ethanol and isopropanol in an ultrasonic bath.

196 mg of zinc acetate dehydrate was mixed with 54 µL of ethanolamine in 6 mL of absolute ethanol and stirred at 45 °C for 2 hours. The zinc oxide (ZnO) layer was prepared by spin-coating this solution at 2000 rpm for 60 s followed by annealing at 180°C for 1 hour in air leading to a 60 nm thick layer. $PC_{71}BM$:PCDTBT solutions (for BHJ) were prepared in chloroform with a concentration of 40 $mg.mL^{-1}$ (1:4 ratio).

BHJ layers were spin-coated in a glove box at 2000 rpm during 60 s with a resulting $PC_{71}BM$:PCDTBT thickness of 80 nm.

NP layers were spin-coated in air at 600 rpm during 60 s followed by a 3000 rpm step for 3 s leading to a 70 nm thick layer. The films were dried at 100°C for 2 min to evaporate the remaining water and then transferred into a vacuum chamber for the MoO_3/Ag evaporation.

MoO_3 (10nm) and Ag (80nm) were successively thermally-evaporated at deposition rates of 0.1 $nm.s^{-1}$ and 0.2-0.4$nm.s^{-1}$ respectively under secondary vacuum (10^{-6}mbar). The solar cells' active surface area is 10 mm^2. The devices were characterized using a K.H.S. Solar Cell test-575 solar simulator with AM1.5G filters set at 100 $mW.cm^{-2}$ with a calibrated radiometer (IL 1400BL). Labview controlled Keithley 2400 SMU enabled the current density-voltage (J-V) curves measurements.

- Vue d'ensemble du chapitre III -

Ce troisième chapitre expose la synthèse de particules composite [6,6]-phenyl C71 butyric acid methyl ester ($PC_{71}BM$) :PCDTBT par un procédé de miniémulsion post-polymérisation.

Les particules ainsi synthétisées sont stabilisées par du sodium dodecyl sulfate (SDS), un tensio-actif très utilisé adsorbé à la surface (voir figure 1).

Figure 1 : Synthèse de particules composites de $PC_{71}BM$ et PCDTBT par miniemulsion post-polymérisation

Dans un premier temps, les paramètres de la réaction tels que la concentration en espèces actives, la quantité de tensio-actif et le temps d'ultrasons ont été étudiés afin d'atteindre une concentration finale suffisante pour la formation d'un film continu et une taille de particules d'environ 50 nm.

Ensuite, l'étude des propriétés optoélectroniques a montré que les deux composés (à savoir le polymère PCDTBT et l'accepteur d'électrons $PC_{71}BM$) se trouvent être en contact intime au sein d'une même particule. Ce résultat a notamment été appuyé par l'extinction de la fluorescence en solution pour les particules synthétisées à partir d'une solution mère contenant à la fois le polymère et l'accepteur d'électron (voir figure 2).

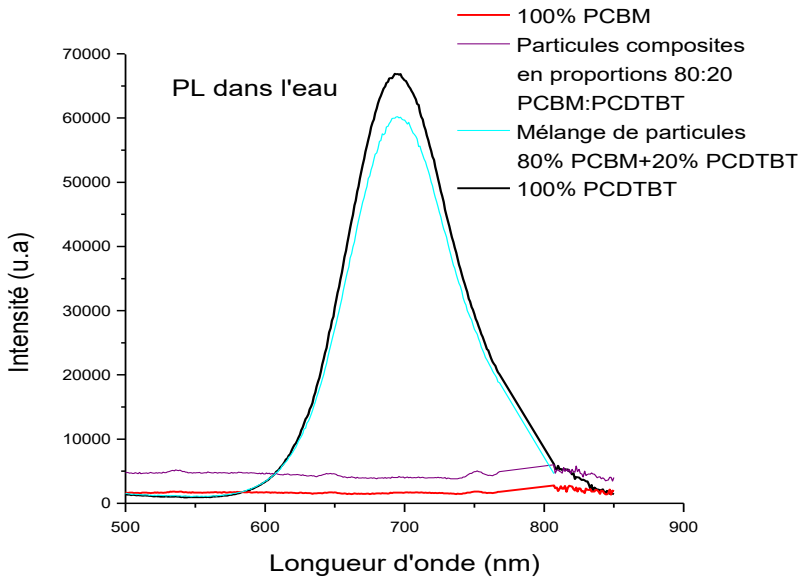

Figure 2 : Spectre de photoluminescence de particules composites en proportions 80 :20 ($PC_{71}BM$:PCDTBT) et mélange de 80% de $PC_{71}BM$+20% de PCDTBT (bleu clair) excitées à 395 nm dans l'eau

Ces encres photoactives composées de nanoparticules de $PC_{71}BM$ et PCDTBT ont été déposées par tournette en films fins. La couche obtenue est composée de particules bien empilées (voir figure 3).

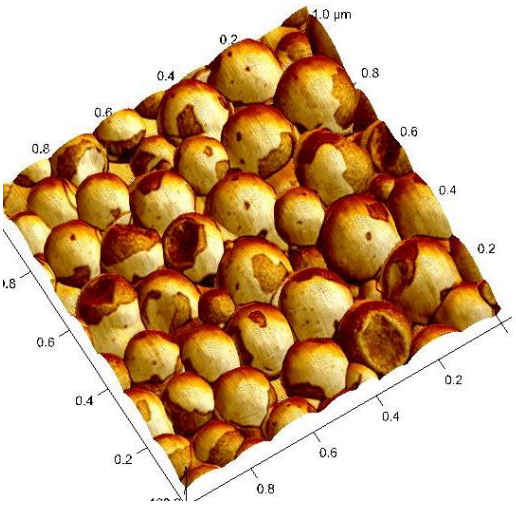

Figure 3 : Superposition des images AFM de topologie et de phase de nanoparticules composites de composition 80 :20 ($PC_{71}BM$:PCDTBT)

Un recuit thermique a été nécessaire pour augmenter le contact entre les particules, améliorer le mélange entre les deux composés et obtenir un film plus homogène. La température de recuit idéale se situe à 140°C.

Finalement, l'étude de la morphologie des films et de leur recuit a permis d'obtenir une couche active qui a par la suite été intégrée au sein d'un dispositif cellule solaire inverse. Les résultats obtenus sont résumés dans le tableau 1.

Tableau 1 : Caractéristiques des cellules photovoltaïques intégrant différentes natures de particules (composite (c) ou mélange (m)) et différentes proportions de $PC_{71}BM$:PCDTBT ainsi que une hétéro-jonction volumique à partir d'une solution de chloroforme, les températures indiquées correspondent au recuit appliqué pendant 4 min. Pour chaque échantillon les valeurs moyennes et record ont été reportées

Echantillon			Jsc (mA/cm)	Voc (V)	FF	PCE (%)
1	NP c (80:20)	moyenne	1,52	6,19E-02	0,277	0,03
		meilleure	2,27	7,00E-02	0,303	0,05
2	NP c (80:20) 140°C	moyenne	3,79	6,05E-01	0,307	0,70
		meilleure	4,49	6,87E-01	0,304	0,94
3	NP m (80+ 20)	moyenne	2,23E-02	3,31E-02	0,259	1,95E-04
		meilleure	2,26E-02	5,96E-02	0,262	3,53E-04
4	NP m (80+ 20) 140°C	moyenne	9,84E-02	2,32E-02	0,237	5,41E-04
		meilleure	1,04E-01	2,41E-02	0,230	5,78E-04
5	PCDTBT:$PC_{71}BM$ bulk	moyenne	6,65	7,83E-01	0,332	1,96
		meilleure	6,96	8,70E-01	0,416	2,48
6	PCDTBT:$PC_{71}BM$ bulk 140°C	moyenne	1,68	5,04E-03	0,231	0,23
		meilleure	1,81	1,00E-02	0,264	0,49

L'étude des paramètres photovoltaïques sur des particules de différentes natures (composites et mélangées) a permis de tirer plusieurs conclusions :

- Le recuit à 140°C permet de multiplier l'efficacité jusqu'à 20 fois pour des particules composites de composition (80 :20) (échantillon 1 par rapport au 2).
- Les particules composites offrent de bien meilleurs résultats que les particules mélangées due à la taille des domaines formés (échantillon 1 ou 2 par rapport au 3 ou 4 respectivement).
- Le recuit permet d'augmenter l'efficacité des cellules à base de nanoparticules mais c'est l'inverse qui se produit pour les cellules à base de composés solubilisés en solvant halogéné (échantillons 1 et 2 par rapport au 5 et 6 respectivement).

-

Chapter IV
PCDTBT-based particles stabilized by semi-conducting P3HT-*b*-PEO block copolymer

In this work, semi-conducting P3HT-*b*-PEO block copolymer was synthesized and used as stabilizer for the preparation of composite particles of poly[N-9'-heptadecanyl-2,7-carbazole-alt-5,5-(4,7-di-2-thienyl-2',1',3'-benzothiadiazole] (PCDTBT) and [6,6]-Phenyl C71 butyric acid methyl ester ($PC_{71}BM$) in water. Depending on experimental conditions, particles that comprise both the electron-donor and the electron-acceptor and that range from 120 nm to 400 nm in diameter were obtained and characterized. The water-based inks were used for the preparation of the photovoltaic active layer which was then integrated in organic solar cells showing promising results.

- CHAPTER IV -
PCDTBT-based particles stabilized by semi-conducting P3HT-*b*-PEO block copolymer

Table of Contents

List of the figures

List of the tables

IV. 1. Introduction

SDS is an effective stabilizer that has been extensively used to protect particles from aggregation in many processes (emulsion, miniemulsion etc).[1–5] As shown in Chapter III, SDS successfully stabilized $PC_{71}BM$:PCDTBT particles in water leading to stable inks that have been used for the production of active layer in OPV. However this surfactant is insulating and charged so it can disrupt the charge transportation once the solutions are integrated into a device. For example particles stabilized by SDS reached a charge carrier mobility around $10^{-3}cm^2.V^{-1}.s^{-1}$ versus up to 2.5 $cm^2.V^{-1}.s^{-1}$ for ethoxy and carbonated chains (C_nE_m) C_{16}-E_{10}-stabilized particles using the same polymer.[6]

In this work, semi-conducting block copolymers were designed with the objective to study their behavior as steric stabilizer for aqueous dispersion of $PC_{71}BM$:PCDTBT composite particles. The block copolymer architecture was chosen so that each block will bring different features: water solubility for the first one and conductivity for the other. In addition, it could be of interest to use a photo-active block absorbing in a complementary region of PCDTBT to allow a better coverage of the solar spectrum.

P3HT was selected as the π-conjugated segment. In fact the synthesis of well-defined functional P3HT and its copolymers via different methodologies is well documented in the literature thanks to the pioneering work of McCullough and Yokozawa teams.[7–16]

For instance, the Grignard metathesis polymerization (GRIM) developed by McCullough[9,17] allow producing well-defined end-functionalized regioregular-P3HT.[8] In this method, called *in situ* end-functionalization (see figure 1), a Grignard reagent (RMgX) is added in excess during the reaction leading to mono-functionalized P3HT (1) after reductive elimination. Ni(0)dppp can also react on 1 during oxidative addition to give (2) which can react with the RMgX to produce di-functionnalized P3HT (3).

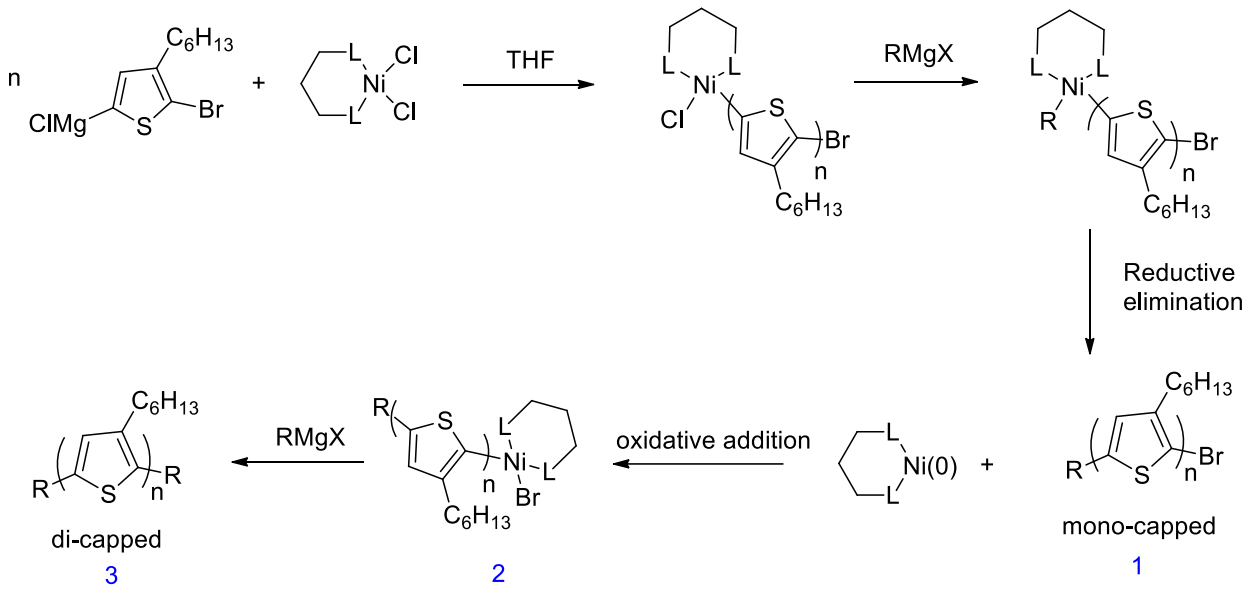

Figure 1 : General scheme for the synthesis of end-functionalized regioregular P3HT[18]

Well-defined rod-coil diblock copolymers based on P3HT have already been reported in the literature. The synthesis can be divided into two categories: divergent route where the second block is grown from the first one and the convergent route consisting in a coupling reaction between the two blocks. Controlled chain growth mechanisms were described a lot for divergent route such as Atom Transfer Radical Polymerization (ATRP)[19–21], Nitroxide-Mediated Radical Polymerization (NMRP)[22–24], Reversible Addition-Frangmentation chain-Transfer polymerization (RAFT)[25,26] or anionic polymerization[27] in which the flexible block is synthesized from a rigid macro-initiator. Similarly for the convergent method, controlled chain growth polymerizations are well suited for the preparation of well-defined blocks. For instance the two blocks can be coupled using anionic polymerization in which a “living” chain is terminated onto an aldehyde function at the end of the rigid block, click-chemistry[28–32] or esterification. The majority of P3HT-based diblocks reported so far are used as compatibilizing agent in OPV to control the phase separation[25,33,34] and very few for use as stabilizer.[35]

For the coil-block or flexible block, poly(ethylene oxide) (PEO) was used which is a water-soluble polymer and offers lots of applications from industrial manufacturing to medicine (FDA approved).

Poly(vinyl alcohol) (PVA) could also have been used, presenting excellent physical and film formation features. PVA was used for example as stabilizer to disperse carbon-nanotubes.[36,37] However this polymer is synthesized by RAFT polymerization, being hard to functionalize for a coupling afterwards. Moreover this polymer is produced from the hydrolysis of poly(vinylacetate) (PVAc) which may damage the chemical link between the water-soluble block and the π-conjugated block.

Polyelectrolyte such as poly(sodium styrene sulfonate) after hydrolysis are also water-soluble, P3HT-*b*-PSS were synthesized.[35,38] However their charge in solution could impede their use for OPV applications.

In this chapter the synthesis of rod-coil block copolymers will be presented with the rod block being P3HT a π-conjugated polymer and the coil block PEO. The copolymer will be synthesized by click chemistry from an azide functionalized PEO block and an alkyne functionalized P3HT block.[29,30,32] The chemical structure of the targeted copolymer is presented in the figure 2. The combination of these two polymers (π-conjugated polymer and water soluble polymer) under the form of diblocks offers tunable properties by controlling the volume fraction of each block. In this study, we were mainly limited by the molar mass of the PEO block since we decided to use only commercially available PEO.

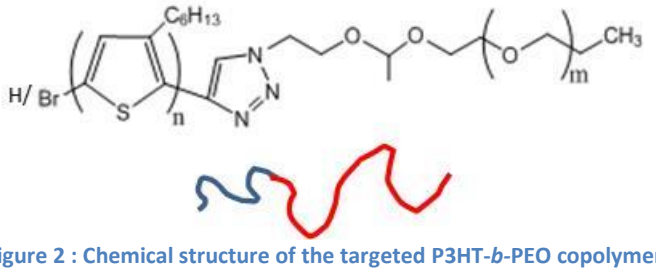

Figure 2 : Chemical structure of the targeted P3HT-*b*-PEO copolymer

IV.2. Results and discussion

IV.2.1. Synthesis of the functionalized PEO and P3HT polymers and their P3HT-*b*-PEO block copolymer

IV.2.1.a. Functionalization and characterization of the PEO block

Commercially available poly(ethylene oxide) monomethyl ether (Mn = 20000 kDa) was functionalized with an azide function to allow a click-chemistry afterwards following the Hawker *and coll* method.[39] First an acetal moiety was introduced at the chain end using 2-chloroethyl vinyl ether with a catalytic amount of pyridinium *p*-toluenesulfonate. Clickable azide group was then introduced by nucleophilic substitution of the C-Cl bond with NaN_3 (see figure 3). All detailed experimental procedures are presented in the experimental section.

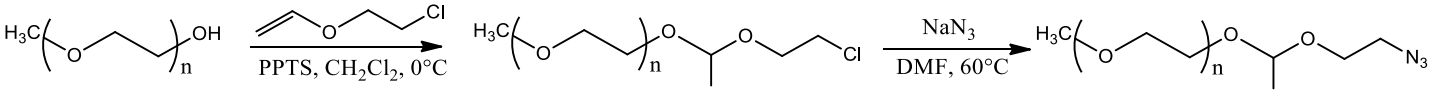

Figure 3 : Synthesis of azide-functionalized PEO (ω-N_3-PEO)

The success of the reaction was checked by ^{1}H-NMR showing appearance of c and d protons at 4.82 and 1.34 ppm respectively (see figure 4).

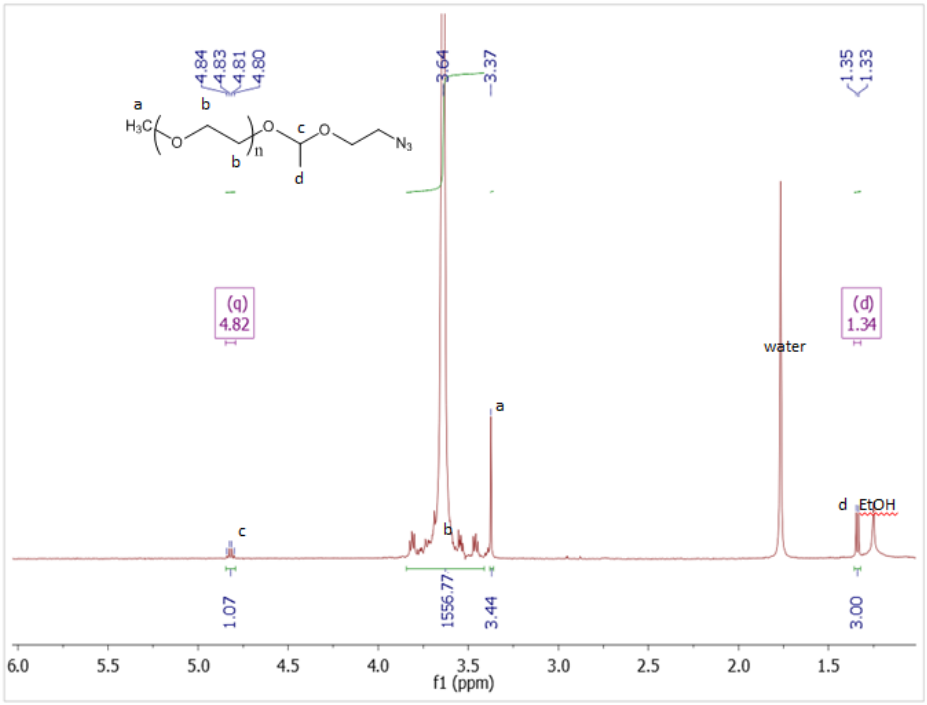

Figure 4 : ^{1}H-NMR of ω-N_3-PEO in $CDCl_3$ at 400 MHz

Infrared spectroscopy further confirmed the presence of the azide function (N_3). It has a characteristic intense signal ν (N_3) at 2100 cm^{-1} as shown in figure 5.

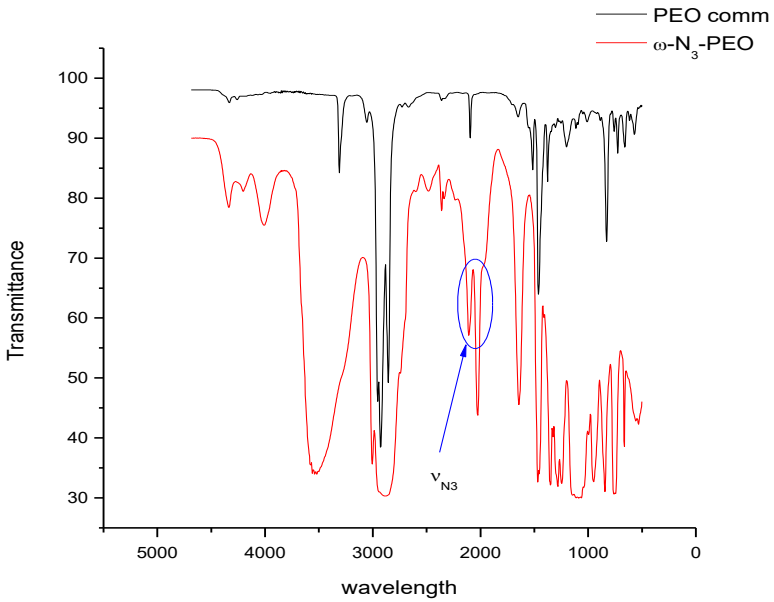

Figure 5 : FTIR using ATR mode of PEO before (black) and after functionalization with azide moiety (red)

As expected the molar mass of PEO remained unchanged after functionalization. By ^{1}H-NMR the molar mass can be calculated as following:

$$\bar{Mn}\ (NMR) = \frac{\int Hb * \ \bar{Mn}(PEO\ unit)}{4} = \frac{1557 * 44}{4} = 17000\ g/mol$$

In regards with the use of PEO-based block copolymer as a stabilizer in an oil-in-water type emulsion, we targerted a diblock copolymer with a Hydrophilic-Lipophilic Balance (HLB) [40] > 12. Knowing the molar mass of PEO we can calculate the targeted molar mass of the P3HT block.

$$HLB = \frac{wt\%\ hydrophilic}{5} = \frac{\dfrac{\bar{Mn}\ PEO}{\bar{Mn}\ PEO + \ \bar{Mn}\ P3HT} * 100}{5}$$

In case of a 20000 $g.mol^{-1}$ PEO, the synthesis of a 2000-4000 $g.mol^{-1}$ P3HT will lead to suitable HLB between 16 and 18.

IV.2.1.b. Synthesis and characterization of ω-alkyne functionalized P3HT

The monomer 2,5-dibromo-3-hexylthiophene was synthesized according to the literature and purified by several distillations under reduced pressure leading to a purity of 97%.[28]

P3HT based copolymers were synthesized following the Balsara *and coll* method.[29] First, regioregular-P3HT block was synthesized by GRIM polymerization. Using this method, the molar mass is controlled by the amount of Ni-catalyst used during the synthesis.[9] In fact, Ni(dppp)Cl_2 can be considered as an initiator, so one Ni(dppp)Cl_2 molecule can initiate one polymer chain, giving rise to the following relation :

$$DPn \propto \frac{n^0_{monomer}}{n^0_{catalyst}}$$

Equation 1 : Relationship between the degree of polymerization and the molar ratio of monomer over catalyst for P3HT synthesis

Nevertheless, it is not so trivial to predict a molar mass before the synthesis of P3HT.

As shown before, P3HT can be easily functionalized thanks to the addition of specific Grignard reagents at the end of the polymerization.

Our strategy lies on the synthesis of ω-alkyne functionalized P3HT presented in the figure 6 and already reported in the literature.[29]

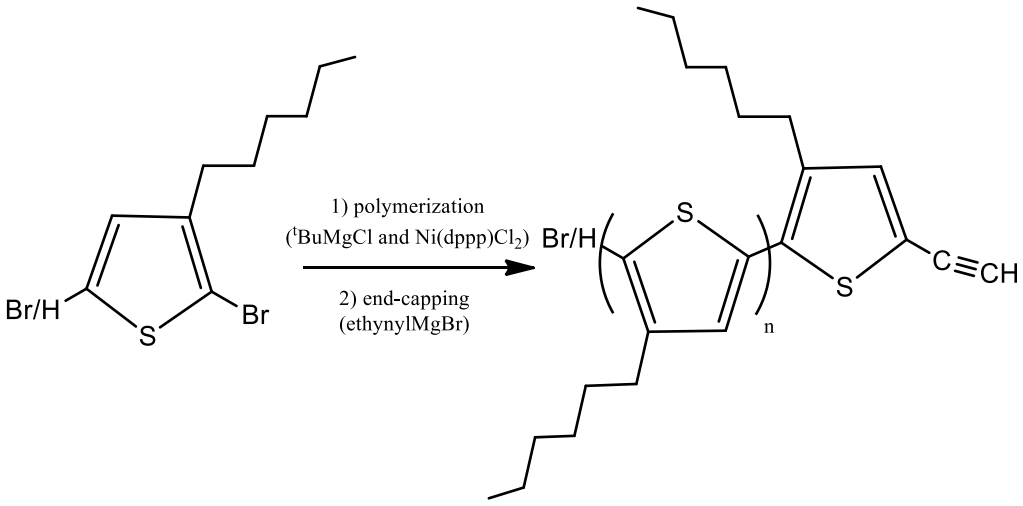

Figure 6 : Synthesis of ω-alkyne functionalized P3HT

The resulting polymer is purified by Soxhlet extraction and then characterized by ^{1}H-NMR and SEC. The appearance of characteristic peak at 3.53 ppm in the ^{1}H-NMR, which corresponds to the alkyne functional group, proves the successful addition of the end

group to the polymer (see figure 7). Based on this peak we can also calculate the molar mass of the P3HT as following:

$$Mn\ (NMR) = \frac{\int Ha * Mn(P3HT\ unit)}{\int Hb} = \frac{14 * 168}{1} = 2350\ g/mol$$

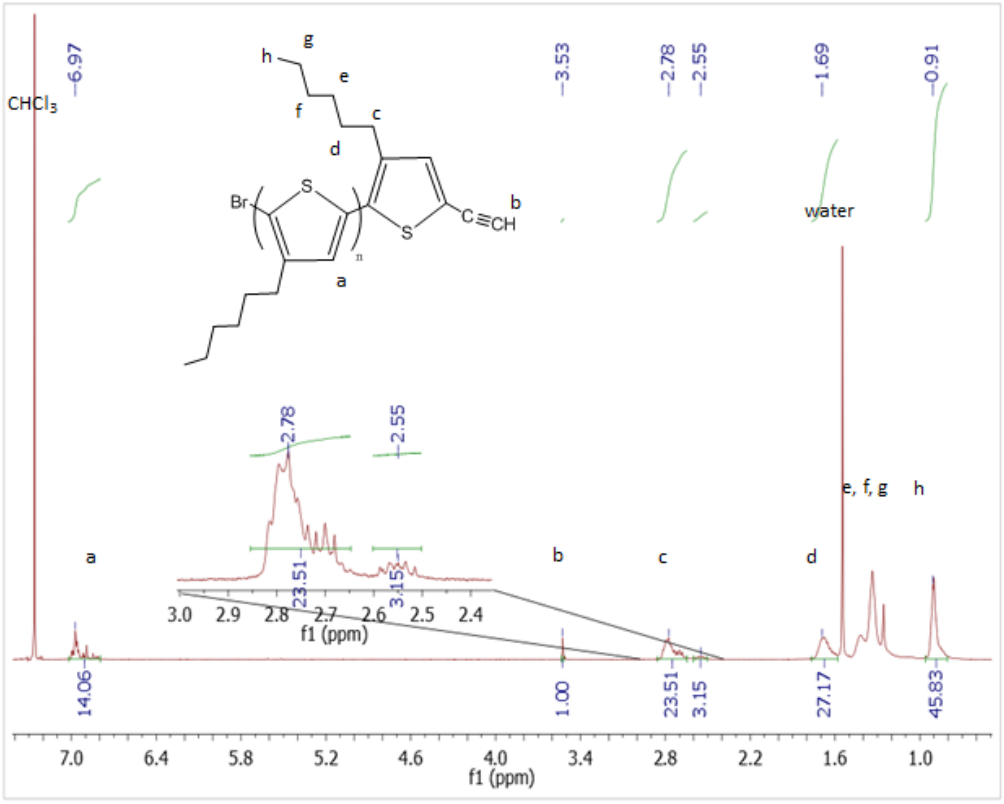

Figure 7 : ^{1}H-NMR of ω-alkyne functionalized P3HT in $CDCl_3$ at 400 MHz

The P3HT polymer was also analyzed by SEC showing a molar mass of 2500 g/mol (see Table 1).

Table 1 : P3HT molar mass based on SEC in chloroform using PS standards and on ^{1}H-NMR

$\bar{M}$n SEC (g/mol)	Dispersity (by SEC)	$\bar{M}$n ^{1}H-RMN
2500	1.2	2350

From the values of molar mass, HLB of the block copolymer was calculated at 18 which is appropriate for the use of such material as a steric stabilizer in an oil-in-water emulsion process.

Regioregularity of the P3HT block was determined by ^{1}H-NMR through the relative integration of signals from c protons at 2.78 and 2.55 ppm assigned to regioregular and non regioregular environments respectively (see figure 7). The P3HT was found 88%

regioregular which is quite below what could be expected from literature probably due to the purity of the monomer (97%).

Finally, as shown in figure 8, infrared spectroscopy further confirmed the presence of the alkyne group at 2100 cm^{-1} and 3300 cm^{-1} assigned to C≡C and C-H alkyne vibration modes respectively.

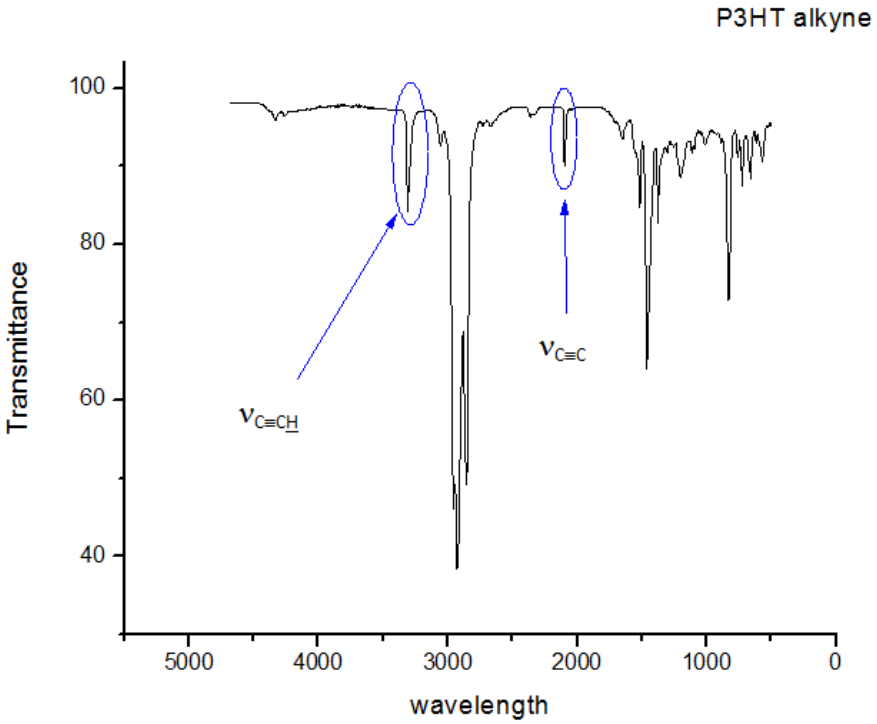

Figure 8 : FTIR using ATR mode of ω-alkyne functionalized P3HT

IV.2.1.c. Synthesis of P3HT-*b*-PEO block copolymers by Azide-Alkyne Huisgen cycloaddition

Azide-Alkyne Huisgen[41] cycloaddition has been extensively reported in the literature in organic or polymer chemistry as an efficient coupling reaction giving rise to a 1,2,3 triazole ring. It is generally named as click reaction by referring to the report from K.B. Sharpless *and coll* in 2001.[42]

Among others[29,30,32,43], this cycloaddition was chosen and reported by us to design P3HT-*b*-PS block copolymers.[28] A similar route was followed in this work targeting P3HT-*b*-PEO block copolymers of HLB of 18. It is noteworthy that literature is quite scarce on the synthesis of P3HT-based block copolymers soluble in water.

The coupling reaction (see figure 9) was performed in THF at 50°C using the catalytic system CuI/DIPEA (diisopropylethylamine). In fact, THF was found the best compromise as compared to the usual DMF (for such reaction) since it can dissolve both P3HT and PEO functional homopolymers. Sonication was also used in order to get high dissolution.

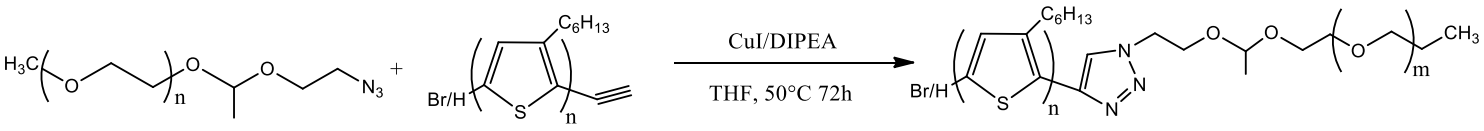

Figure 9 : Synthesis of P3HT-*b*-PEO by Click chemistry

ω–alkyne-P3HT was reacted with excess amounts (1.8 eq) of PEO according to the synthesis shown schematically in figure 9 in order to obtain the diblock copolymer P3HT-*b*-PEO. After washing with cold methanol in order to get rid of unreacted PEO introduced in excess, the product obtained was characterized by SEC and ^{1}H-NMR. Figure 10 shows the typical SEC chromatograms of homopolymers P3HT, PEO and the diblock P3HT-*b*-PEO. In the P3HT chromatogram, the shoulder towards lower elution time can be attributed to the homocoupling between two P3HT chains due to injection of MeOH not enough degassed at the end of the polymerization. The final product chromatogram shows a slight increase in the molar mass with a shift towards lower elution time due to the addition of low molar mass P3HT. The small shoulder at high molar mass region is due to a defect in the commercial PEO as can also be seen on the homopolymer trace.

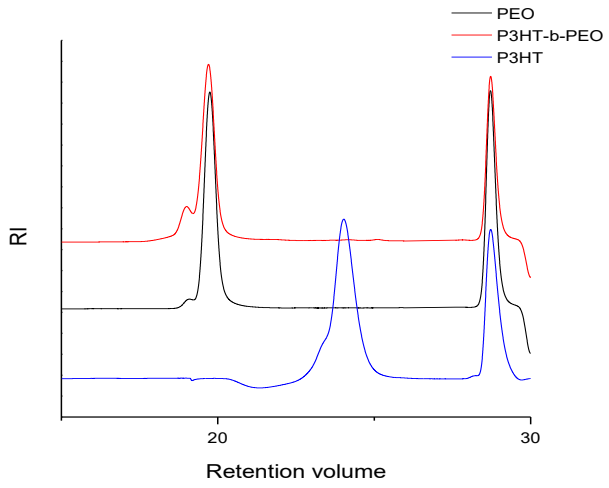

Figure 10 : Overlay of the homopolymers azido-PEO, ethynyl-P3HT and diblock copolymer P3HT-*b*-PEO chromatograms obtained by SEC in chloroform

In chloroform the molar mass of the PEO is underestimated with conventional calibration (based on PS standards) as can be seen on the table 2 by comparing the $\bar{M}n$ by SEC and by ^{1}H-NMR. In fact, chloroform is not an optimum solvent for PEO.[44]

Table 2 : Summary of the molecular characteristics obtained by SEC and NMR for the two homopolymers P3HT and PEO as well as the P3HT-*b*-PEO diblock copolymer

	$\bar{M}n$, SEC (g.mol^{-1})	Đ	$\bar{M}n$, ^{1}H-NMR (g.mol^{-1})
P3HT	2500	1.2	2350
PEO	13000	1.1	17000
P3HT-*b*-PEO	16000	1.1	19000

The efficiency of "click" chemistry coupling reaction was also confirmed by ^{1}H-NMR (figure 11). This spectrum is typical of the copolymer obtained and demonstrates the structure of expected diblock copolymer. Indeed, all peaks corresponding to P3HT and PEO are present. In addition, the peak at 7.79 ppm can be attributed to the proton a of triazole ring formed during the cycloaddition.

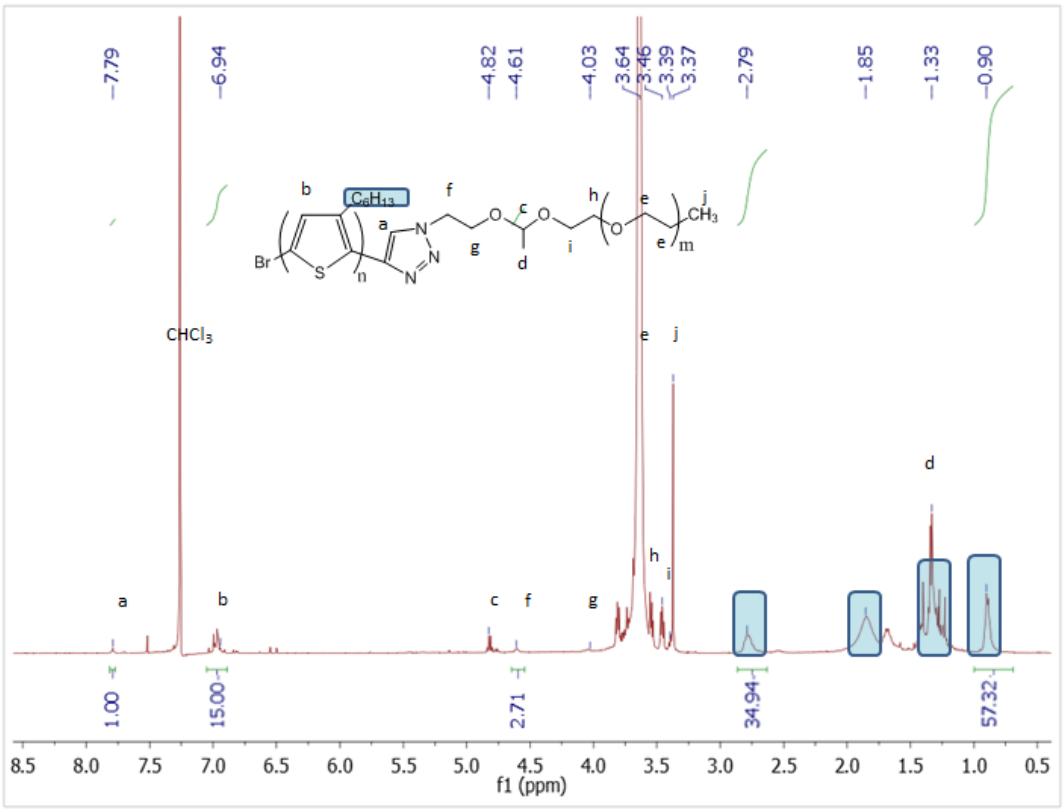

Figure 11 : ^{1}H-NMR spectrum of the diblock copolymer P3HT-*b*-PEO in $CDCl_3$ at 400 MHz

To further characterize the synthesized diblock, 2D-DOSY (Diffusion Ordered Spectroscopy) NMR was performed (figures 12, 13 and 14) to obtain the diffusion coefficient of the P3HT, PEO and P3HT-*b*-PEO copolymer.

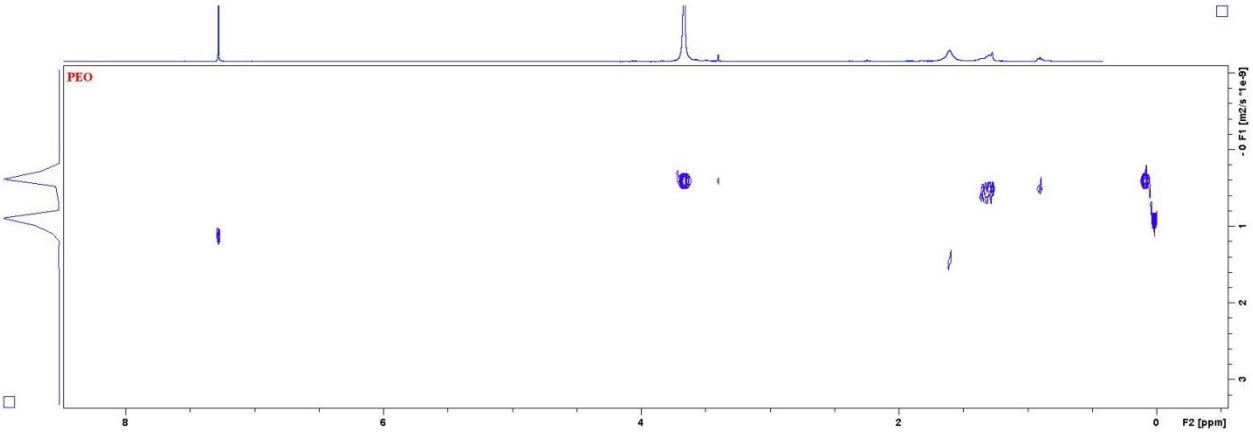

Figure 12 : 400MHZ 2D DOSY NMR spectra obtained at 298K in $CDCl_3$ solution of PEO

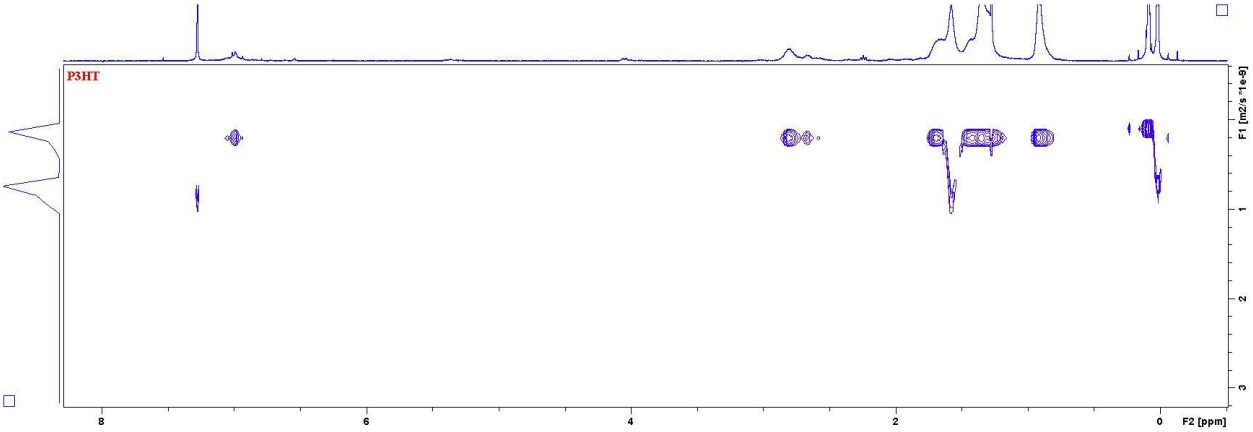

Figure 13 : 400MHZ 2D DOSY NMR spectra obtained at 298K in $CDCl_3$ solution of P3HT

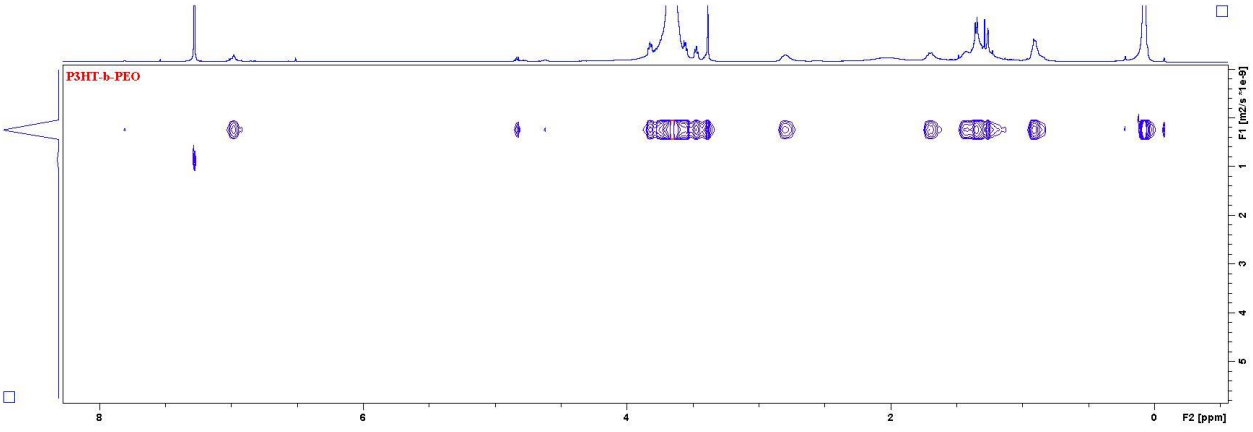

Figure 14 : 400MHZ 2D DOSY NMR spectra obtained at 298K in $CDCl_3$ solution of P3HT-*b*-PEO

Table 3 : Diffusion coefficient of the homopolymers P3HT and PEO as well as the P3HT-*b*-PEO copolymer

	Diffusion coefficient (m^2/s)
P3HT	1.58E-10
PEO	3.46E-10
P3HT-*b*-PEO	8.14E-11

On the DOSY of the diblock, we see the presence of one polymer with only one diffusion coefficient which means that the two blocks are well linked (see figure 14 and Table 3). Distinct diffusion coefficients were measured for all homopolymers and the final copolymer.

IV.2.2. Study of the P3HT-*b*-PEO diblock properties

IV.2.2.a. Self-assembly

Self-assembly behavior of P3HT-*b*-PEO block copolymer was studied for further use as oil-in-water dispersant. Indeed as shown in figure 15, such copolymer with HLB of 18 should form micelles in water.[45] Yet, this behavior needs to be investigated as function of its concentration through the determination of its Critical Micelle Concentration (CMC).

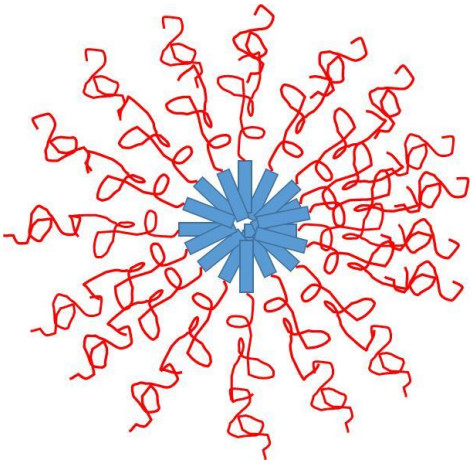

Figure 15 : Expected self-organized structure for coil-rich block copolymer in coil-selective solvent

The CMC can be determined by several methods: dynamic light scattering, fluorescence spectroscopy, surface tension measurement etc… Using P3HT as one of the two blocks, the DLS measurement was not possible due to the strong absorption of the P3HT at the laser wavelength of the DLS (632 nm). Consequently the determination of the CMC was performed by both fluorescence spectroscopy and surface tension measurement.

For the CMC determined by fluorescence spectroscopy, pyrene is considered as fluorescent probe[46,47] which detects the formation of hydrophobic microdomains. Indeed the pyrene emission varies depending on its environment (see figure 16). In the pyrene emission spectrum, the first (I_1) and third (I_3) vibronic bands were used to detect the formation of hydrophobic domains. Below the CMC, the ratio I_1/I_3 should be stable and it should decrease when hydrophobic microdomains start to form (*i.e* when micelles are formed). Aqueous solutions containing the diblock in different concentration were mixed with fixed quantity of pyrene. The excitation wavelength was fixed at 335 nm and the I_1/I_3 ratio were calculated.

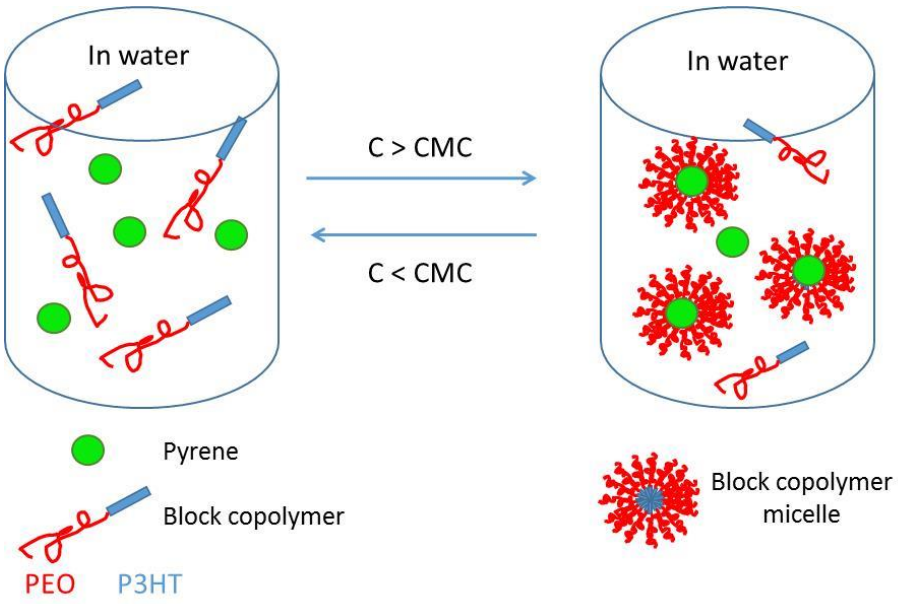

Figure 16 : Pyrene encapsulation for block copolymer CMC determination

The emission spectra of the solutions at different concentrations of P3HT-*b*-PEO diblock are presented in figure 17.

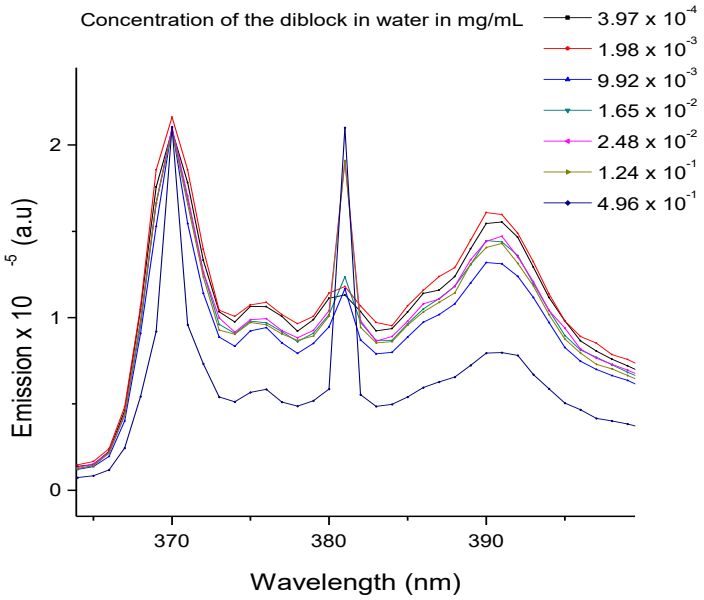

Figure 17 : Emission spectra of the pyrene with different P3HT-*b*-PEO concentrations in water

The value of I_1/I_3 is reported as a function of the copolymer concentration in figure 18. A clear drop of the ratio I_1/I_3 is observed for the copolymer concentration at 0.016 $g.L^{-1}$, indicating the formation of hydrophobic areas. The ratio remains stable for higher concentrations, allowing us to conclude that the CMC is located at 0.016 $g.L^{-1}$.

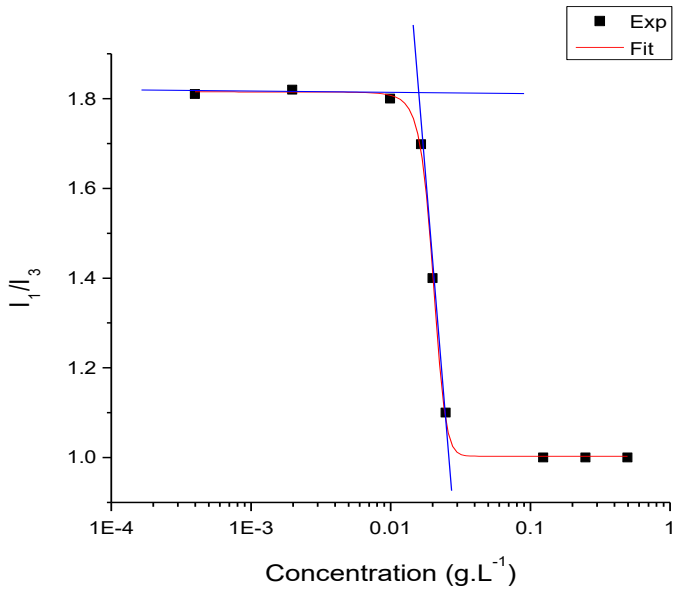

Figure 18 : Ratio of the first (I_1) over the third (I_3) vibronic bands of the pyrene emission spectra as a function of the P3HT-*b*-PEO concentration in water

Pendant drop measurements were also performed for the same copolymer concentrations in order to correlate the CMC calculated from pyrene encapsulation.

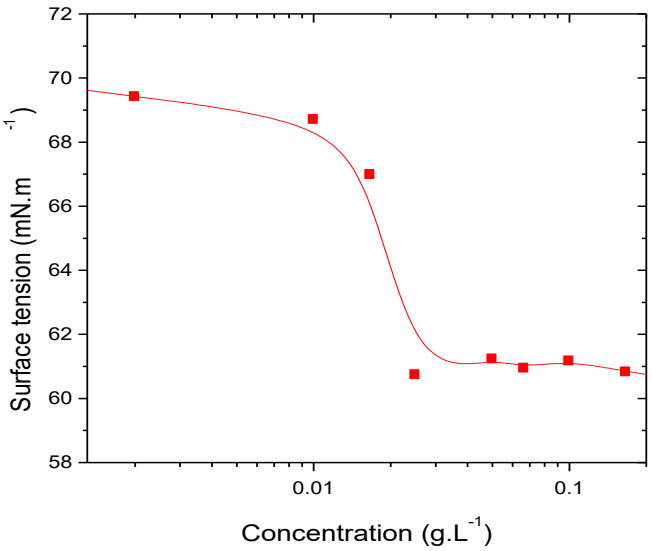

Figure 19 : Surface tension of P3HT-*b*-PEO solutions in water as a function of the concentration

As can be seen on figure 19, the surface tension decreases as long as the copolymer concentration increases until micelles are formed. Then the surface tension remains constant. In the case of the copolymer, the surface tension becomes stable around 0.025 g/L which is close to the CMC obtained with the pyrene method.

Both fluorescence and pendant-drop allow us to conclude that the P3HT-*b*-PEO self-assembles in water in the form of micelles at 0.02 g/L in water with a preferential segregation of the hydrophobic P3HT part in the core. Nevertheless, as the P3HT is absorbing in the range of the DLS laser, it was not possible to perform DLS analysis to determine the size of the micelles.

The micelles' stability was assessed via zeta potential measurements. This was determined by measuring the electrophoretic mobility of the colloidal particles in the solution when applying a voltage. As the zeta potential depends on the magnitude of the electrostatic interaction between the micelles, it can be used as a characterization tool for the colloidal stability. The zeta potential of the copolymer solution with concentration higher than the CMC was found around -15 ±5 mV (see Figure 20). In agreement with the literature, such a value allowed us to consider the micelles as unstable, repulsion forces being too low to prevent aggregation upon ageing.[48]

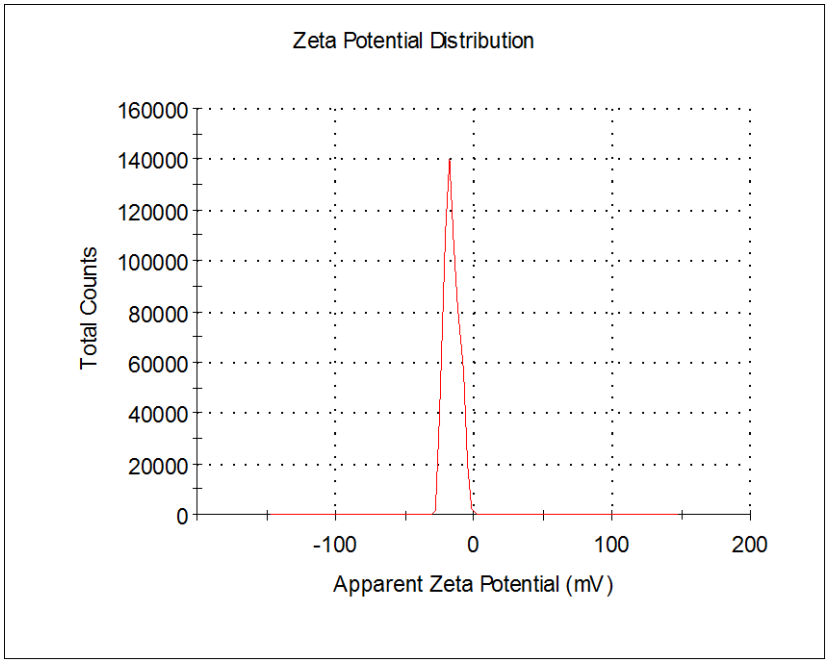

Figure 20 : Zeta potential of P3HT-*b*-PEO micelles

The self-assembling behavior of the block copolymer in aqueous medium was further investigated by Atomic Force Microscopy (AFM) on films. AFM images of solution of diblock casted on glass substrate are shown in figure 21. Rather homogeneous micelles with diameter of 20-30 nm were observed.

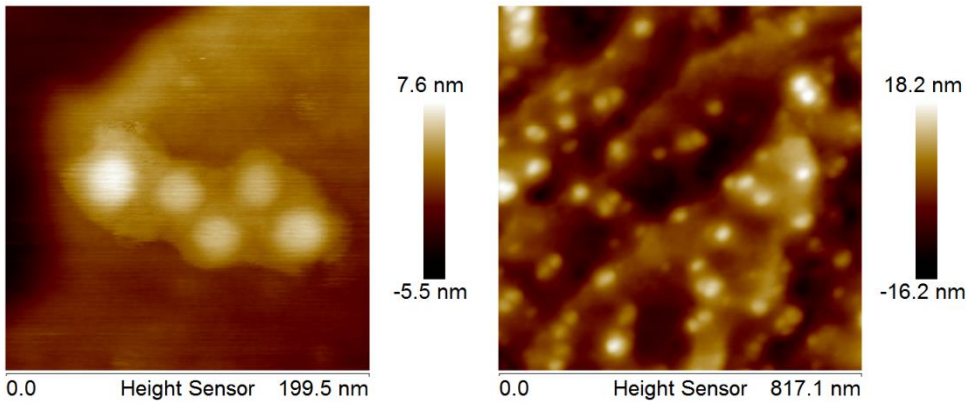

Figure 21 : AFM images of the P3HT-*b*-PEO micelles

To sum up, the rod-coil P3HT-*b*-PEO block copolymer of molar mass of 19000 g.mol^{-1} (determined by ^{1}H-NMR) self-assembles in metastable micelles in water. Its CMC was determined around 0.016-0.025 g.L^{-1} by pyrene encapsulation and surface tension

measurement respectively. AFM showed images of spherical micelles with size ranging between 20-30 nm.

IV.2.2.b. Optoelectronic properties

The self-assembly structures of the π-conjugated rod-coil block copolymers have a direct impact on the physical properties.[49] Indeed, the latter are mainly governed by the packing type of the π-conjugated rod-block (*i.e* π- π stacking).

The physical properties of the P3HT-*b*-PEO diblock were assessed via UV-visible absorption and photoluminescence using a concentration above the CMC around 0.2 g/L. Figure 22 testifies that P3HT blocks form aggregates as evidenced by the red shift of the P3HT absorbance peak from 430 nm to 460 nm when going from good solvent (THF) to bad (water or MeOH) solvent respectively.

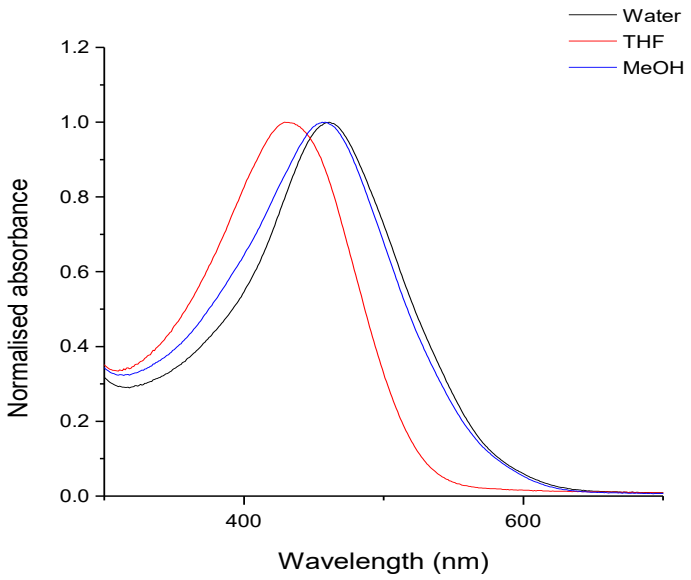

Figure 22 : Absorbance of the P3HT-*b*-PEO in different solvents : in water (black curve), in THF (red curve) and in MeOH (blue curve)

The P3HT-*b*-PEO copolymer solutions were also examined by photoluminescence spectroscopy. In figure 23, the fluorescence spectrum is presented for the three solutions: in THF, in methanol and in water. A fluorescence decrease appeared when the copolymer is in a non-solvent for the P3HT, representative of interchains couplings in the assembly.[30]

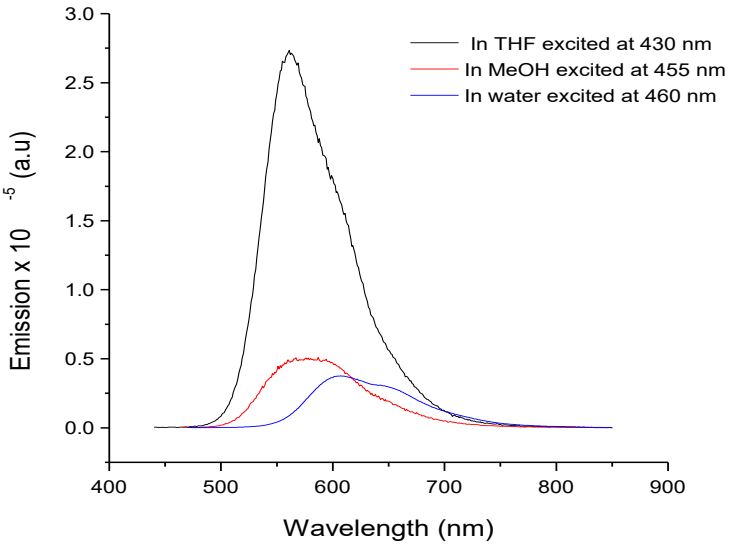

Figure 23 : Emission spectra of the diblock in different solvents

In good solvent (THF), the absorbance and PL spectra are characteristic of P3HT homopolymer, the chains being isolated. This means that the PEO linked to the P3HT does not affect the P3HT properties in a good solvent.

IV.2.3. Use of P3HT-*b*-PEO as stabilizer in a miniemulsion process

IV.2.3.a. Synthesis of $PC_{71}BM$:PCDTBT composite particles stabilized by P3HT-*b*-PEO

PCDTBT and $PC_{71}BM$ were solubilized into chloroform: toluene (1:1 v:v) and this solution was injected into water in the presence of the P3HT-*b*-PEO copolymer. Preferred π- π interactions between $PC_{71}BM$:PCDTBT and P3HT blocks are expected to occur during the dispersion phase.

The resulting dispersions were further characterized by microscopy techniques: TEM and AFM in order to visualize the nanoparticles, as well as photophysical characterizations: UV-vis absorbance and photoluminescence measurements. Finally, the dispersions were integrated as active layer into solar cells to assess their efficiency.

IV.2.3.b. Effect of reaction parameters on particles formation

Composite particles of $PC_{71}BM$:PCDTBT with a fixed ratio of 80:20 were studied with diameter that can be tuned from 120 to 400 nm by playing on the experimental parameters. As can be seen in Table 4, the concentration of the active materials has a

direct impact on the size of the particles (sample 1, 2) the lower the concentration, the smaller the size (figure 24 images 1 and 2). Indeed, by increasing the concentration from 15 mg.mL^{-1} to 30 mg.mL^{-1} the particles size goes from 180-270 to 200-400 nm as it was already demonstrated by Landfester *et al* for Me-LPPP[50] and O. Pras *et al* for PFFO using surfactant as stabilizer.[51]

Table 4 : Size of the $PC_{71}BM$:PCDTBT composite (80:20) as a function of the experimental parameters

Sample	Polymer/PCBM concentration in $CHCl_3$:toluene (mg.mL^{-1})	Time of sonication (min)	Probe intensity (%)	P3HT-*b*-PEO concentration in water (mg.mL^{-1})	Size [a] (nm)
1	15	5	20	1	180-270
2	30	5	20	1	200-400
3	15	5	30	1	150-210
4	15	5	20	20	120-190

[a] determined by TEM

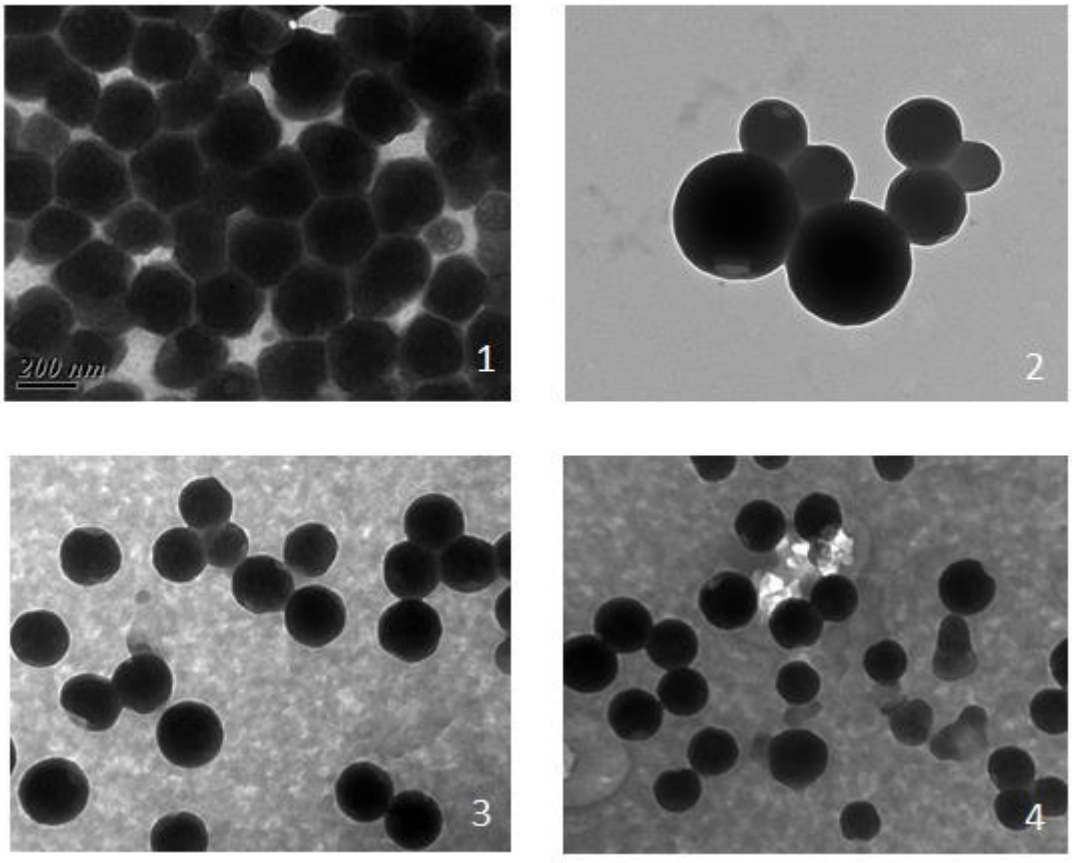

Figure 24 : TEM images of the composite particles 80:20 ($PC_{71}BM$: PCDTBT) stabilized by P3HT-*b*-PEO, the white number corresponds to the entry number in Table 4

The intensity of the emulsification can also play a major role as reported for PFFO particles.[51] In fact, smaller particles were obtained when the intensity of the probe was higher (sample 3 see figure 24 images 1 and 3).

Finally, the particles' size could be tuned with the help of the amount of copolymer. For instance by increasing the amount of P3HT-*b*-PEO (up to 20 CMC) allowed for a higher surface coverage giving rise to smaller particles (samples 1 and 4, TEM images 1 and 4). Nevertheless, it is noteworthy that such parameter (*i.e*. amount of diblock) has to be tuned with caution in regards to the photovoltaic application. Indeed, one of the block being PEO, considered as insulating materials, has to be used in small amounts. In fact, a compromise has to be determined for the quantity of diblock needed for an appropriate photoactive ink considering the final application. All the following studies use particles produced for sample 3 methodology.

The size difference comparing to SDS stabilized particles (around 50 nm) can be explained by the fact that the diblock is only stabilizing the particles by steric stabilization whereas the SDS is stabilizing by electrosteric stabilization which is detrimental for charge transportation but very efficient as already demonstrated by Rajot *and coll*[5] and Tiarks *and coll*[52] who compared ionic versus non-ionic surfactant.

IV.2.3.c. Stability

A key feature of such materials for further development concerns the stability of the inks. The dispersion's stability was assessed via zeta potential measurements. This was determined by measuring the electrophoretic mobility of the colloidal particles in the solution when a voltage is applied. As the zeta potential depends on the magnitude of the electrostatic interaction between the particles, it can be used as a characterization tool for the colloidal stability. The zeta potential of composite particles was found around -30 ±10 mV (see figure 25). In agreement with the literature, such a value allowed us to consider the inks as stable[48], repulsion forces being high enough to prevent aggregation upon ageing however the error bar being high, this information has to be taken with caution.

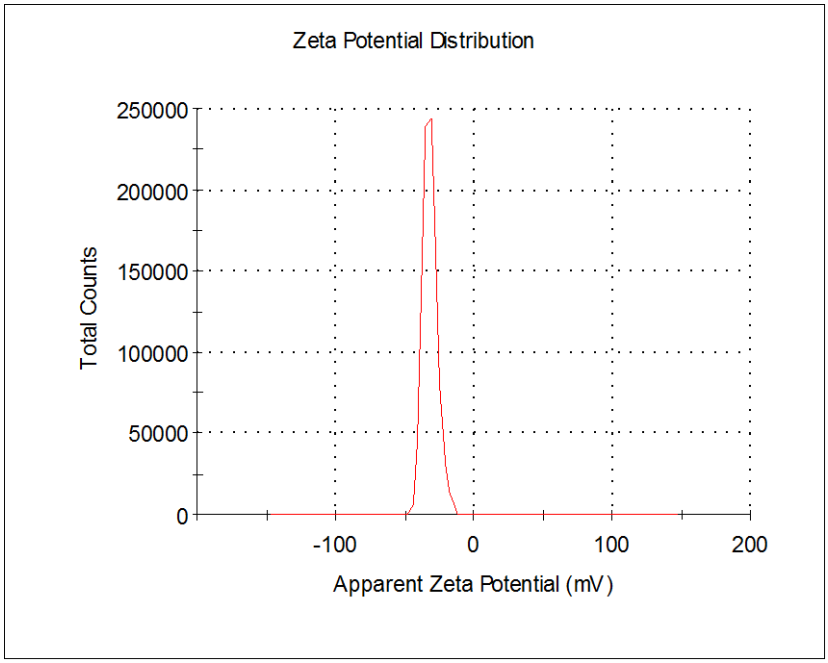

Figure 25 : Zeta potential of $PC_{71}BM$:PCDTBT particles stabilized by P3HT-*b*-PEO in water

IV.2.3.d.Optical characterization

The optical properties of these composite particles have been studied by UV-visible absorption and photoluminescence. In figure 26 the absorption spectra that were obtained in water for sole PCDTBT, sole $PC_{71}BM$ and 80:20 $PC_{71}BM$:PCDTBT composite particles all stabilized with P3HT-*b*-PEO block copolymer are presented.

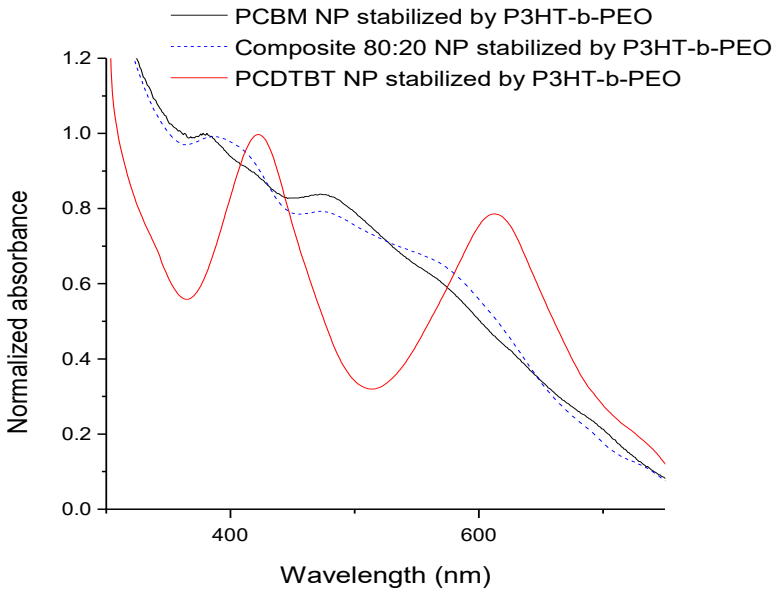

Figure 26 : Absorbance spectra of particles stabilized by P3HT-*b*-PEO in water

The copolymer P3HT-*b*-PEO was tested as dispersant of PCDTBT and $PC_{71}BM$ sole as well as composite particles. The as-synthesized copolymer successfully stabilizes the three kinds of particles.

Coexistence of $PC_{71}BM$ and PCDTBT was evidenced by fluorescence spectroscopy in figure 27 showing the emission spectra of particles in water.

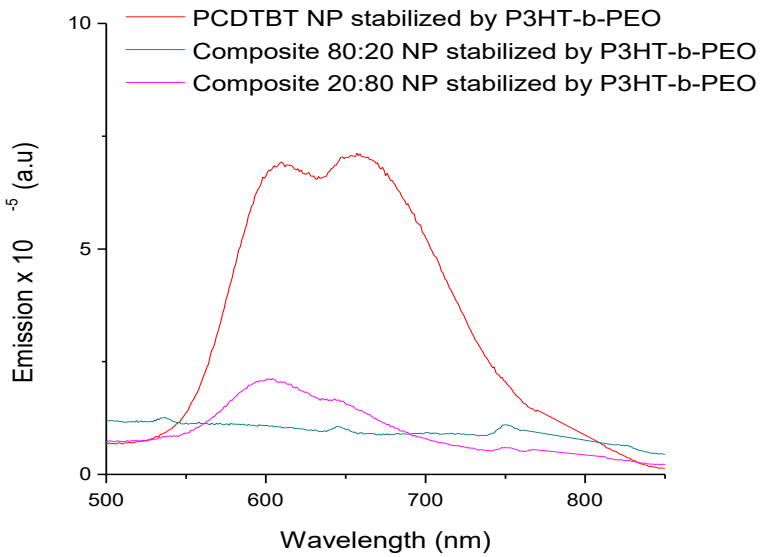

Figure 27 : Fluorescence spectra of P3HT-*b*-PEO stabilized particles in water

For pure PCDTBT nanoparticles (in red), two emission peaks are observed due to the PCDTBT and P3HT self-emission. In the 80:20 composite particles, the emission is quenched due to the presence of $PC_{71}BM$ in intimate contact. We can notice that more $PC_{71}BM$ is needed than before (when using SDS as stabilizer) to quench the fluorescence, the decrease starts at 20 wt% of $PC_{71}BM$ whereas in chapter III less than 10 wt% was enough to quench. This fact can be explained by the presence of P3HT which emits at 600 nm (as seen in figure 23). Thus more $PC_{71}BM$ is needed to quench the fluorescence of both PCDTBT and P3HT. This is in favor of the cohabitation of the three components: PCDTBT, $PC_{71}BM$ and P3HT in nanoparticles.

IV.2.3.e. Stability issue

The stability of the composite dispersions is investigated. As shown in figure 28, "sedimentation" seems to occur after 5 days on shelf at room temperature. In fact, a clear change in the dispersion could be evidenced by DLS (see figure 29) after only one day of storage; as the Gaussian shape of particles shifted to larger dimensions.

Figure 28 : Picture of the inks stabilized by P3HT-*b*-PEO as prepared and after 5 days on shelf

After only one day, the size of the particles is bigger as can be seen on DLS graph (figure 29).

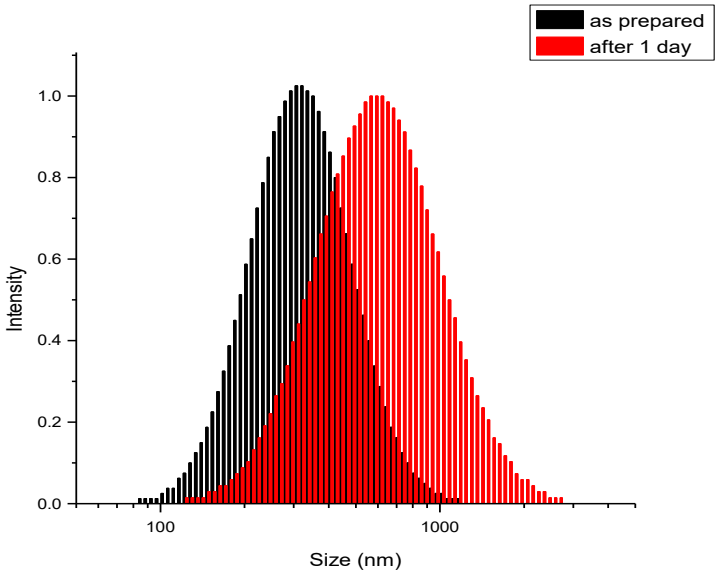

Figure 29 : DLS graphs of the inks as prepared and after one day on standing on shelf at room temperature

There are several possible mechanisms of destabilization such as creaming and sedimentation, flocculation which can lead to coalescence and Ostwald ripening.

The stability was assessed using Turbiscan® analysis at 25°C every hour for several days. This technology measures the intensity of the light scattered backward from the source

light by the sample all along the cell. Figure 30 displays the backscattering intensity as a function of the cell length (0 means the bottom of the cell). An evolution of the signal on all the height of the sample can be noticed due to an increase of the particles size coming from coalescence or flocculation. Moreover, the signal increase at the bottom of the cell is representative of sedimentation phenomenon linked to clarification at the top of the cell.

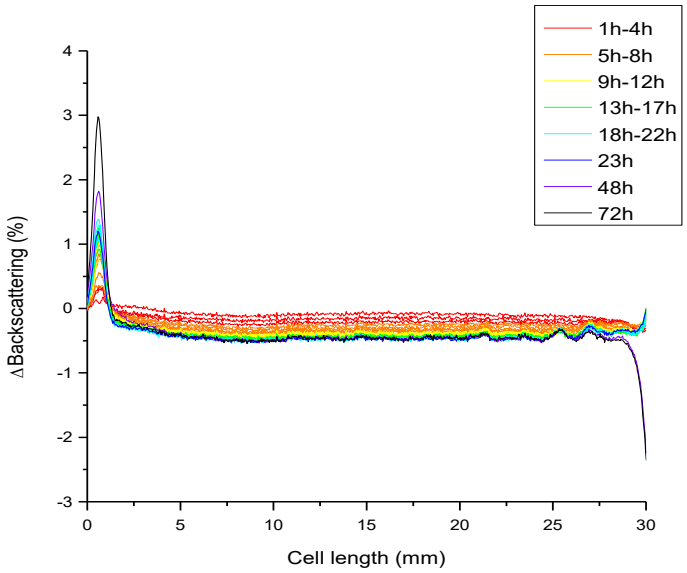

Figure 30 : Backscattering intensity of the same $PC_{71}BM$:PCDTBT dispersion stabilized by P3HT-*b*-PEO measured every hour until 3 days

To sum up, the destabilization of $PC_{71}BM$:PCDTBT NP stabilized by P3HT-*b*-PEO is linked to a combination of sedimentation and coalescence/flocculation.

IV.2.3.f. Film forming investigation from inks of $PC_{71}BM$ and PCDTBT stabilized by P3HT-*b*-PEO block copolymer

The $PC_{71}BM$:PCDTBT@P3HT-*b*-PEO inks were further used for application as active layer into inverted solar cells *i.e.* glass/ITO/ZnO/$PC_{71}BM$:PCDTBT (NP stabilized by P3HT-*b*-PEO)/MoO_3/Ag.

Spray-coating technique was used on freshly prepared inks (avoiding flocculation phenomenon). Spray-coating is an easy and fast method where the dispersion is sprayed onto a heated surface to facilitate the evaporation of the dispersant phase (see figure 31). Moreover this technique does not lead to matter losses unlike spin-coating for example.

Diluted solutions with low viscosity can be sprayed and the thickness of the films can be tuned by multiple spray steps. This method is widely used in industry as it can be applied to all surfaces and be automated. However, the main disadvantages are the poor homogeneity and high roughness of the films with the appearance of the "coffee stain effect" as the droplets are drying on the surface. Indeed, during the drying process, there is a solvent flow that drives the particles from the center to the edges leading to the formation of a ring.[53]

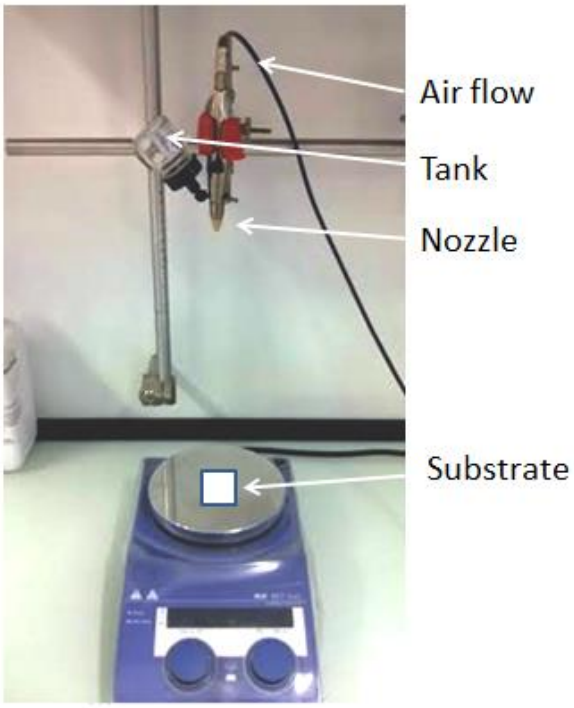

Figure 31 : Picture of the spray-coater

The surface energies were measured to assess the wettability behavior of the inks onto ZnO substrates (which will be the underlayer once integrated into solar cells):

Table 5 : Surface energies of ZnO and $PC_{71}BM$:PCDTBT inks stabilized by P3HT-*b*-PEO

	Θ_{water} (°)	$\Theta_{ethylene\ glycol}$ (°)	$\Theta_{diiodomethane}$ (°)	Surface energy (mN/m)
ZnO on ITO	35 ± 4	26 ± 2	36 ± 1	59 ± 08
$PC_{71}BM$:PCDTBT with diblock	27 ±3	21 ± 2	45 ± 1	61 ± 0.7

As can be seen in table 5, the surface energy of ZnO film on ITO and $PC_{71}BM$:PCDTBT nanoparticles stabilized by P3HT-*b*-PEO are very close, clearing the way for the ink integration into solar cells.

2 mL of inks were used to achieve 100 nm thick photoactive layer with a hot plate temperature set at 100°C. After spray-coating, the shape of the particles remains spherical as can be seen on AFM images (figure 32). However, due to the deposition method the roughness was very high (around 20 nm) compared to SDS-stabilized particles (<4nm).

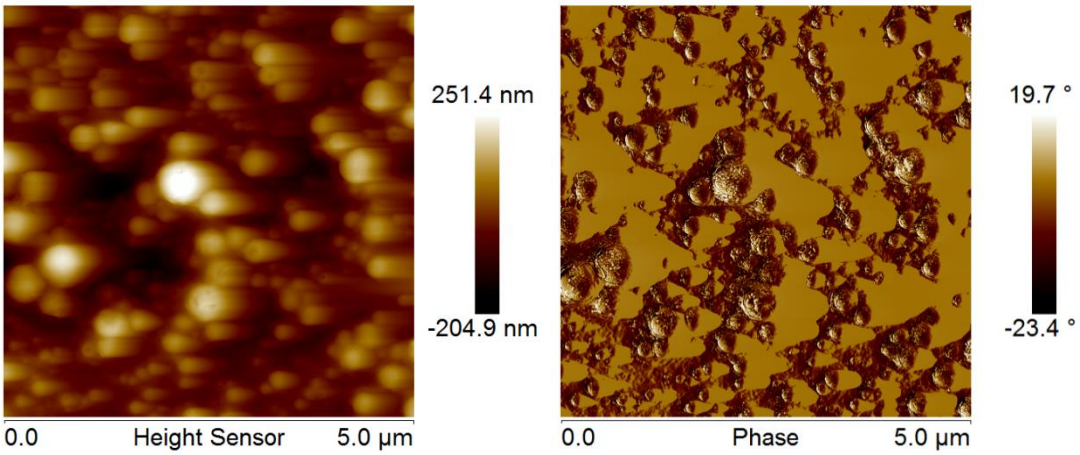

Figure 32 : AFM images of spray-coated 80:20 $PC_{71}BM$:PCDTBT NP stabilized by P3HT-*b*-PEO diblock on ZnO substrate

An annealing process was used to sinter the particles and smooth the film, as the particles are bigger than before. Comparative microscopy pictures are shown in figure 33 for the $PC_{71}BM$:PCDTBT NP stabilized either by SDS or P3HT-*b*-PEO block copolymer. Images are presented below, comparing NP using SDS with P3HT-*b*-PEO copolymer. NP using the diblock present big aggregates in film which can be smoothed by heating at 150°C during 4 min as can be seen on microscopy images (figure 33).

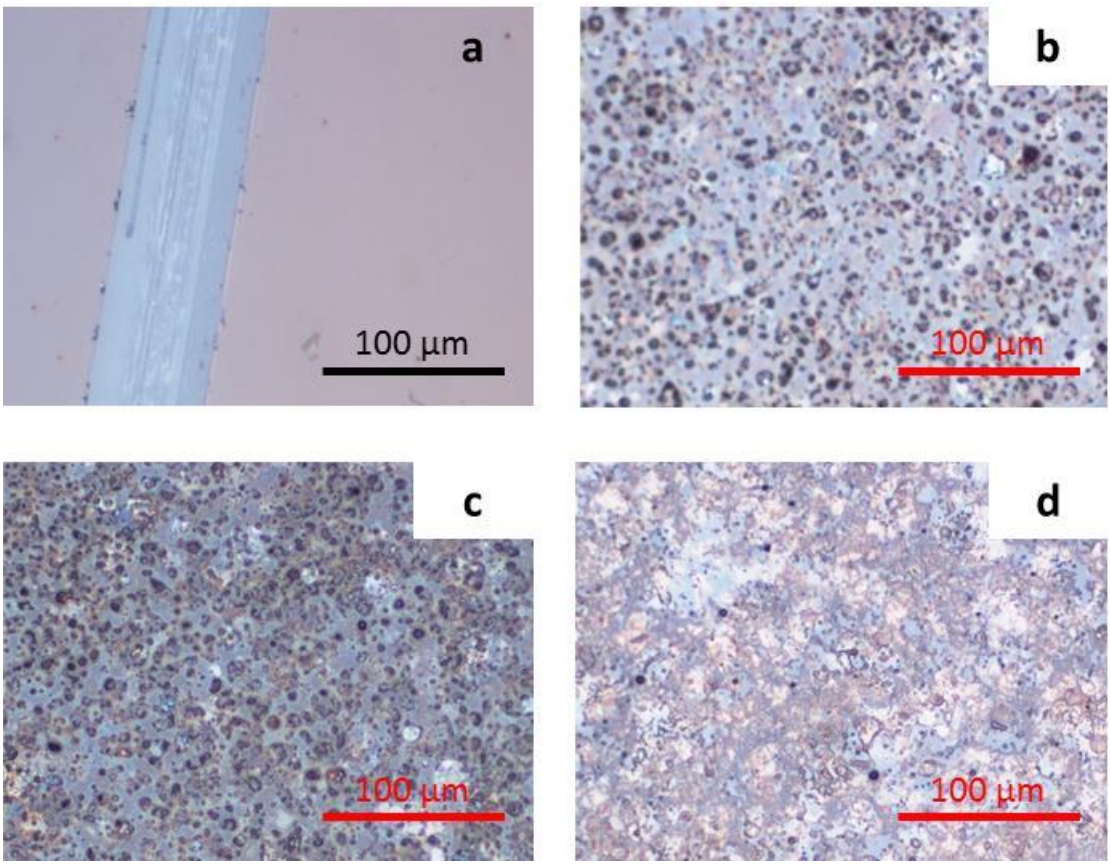

Figure 33 : Microscopy images of NP stabilized by SDS (a), NP stabilized by P3HT-b-PEO without annealing (b), annealed at 140°C 4 min (c) and 150°C 4 min

IV.2.3.g. Integration of $PC_{71}BM$:PCDTBT composite inks stabilized by P3HT-*b*-PEO block copolymer into solar cells

Despite the big aggregates found after spray-coating, the inks were integrated into inverted solar cells *i.e.* glass/ITO/ZnO/$PC_{71}BM$:PCDTBT (NP stabilized by P3HT-*b*-PEO)/MoO_3/Ag.

The non-annealed active layers were dried during the spray at 100°C during approximately 2 min, the others were annealed at 130°C, 140 or 150°C during 4 min prior to testing.

The table 6 summarizes the results obtained for the 80:20 $PC_{71}BM$:PCDTBT inks.

Table 6 : Characteristics of solar cells made from 80:20 $PC_{71}BM$:PCDTBT NP stabilized by P3HT-*b*-PEO copolymer

	Sample		Jsc (mA/cm)	Voc (V)	FF	PCE (%)
1	NP blend (80:20) $PC_{71}BM$:PCDTBT	average	1.03E+00	7.00E-02	0.217	0.02
		best	1.07+00	9.00E-02	0.230	0.03
2	NP blend (80:20) annealing 130°C	average	1.16E+00	8.75E-02	0.226	0.03
		best	1.74E+00	1.30E-01	0.231	0.05
3	NP blend (80:20) annealing 140°C	average	8.60E-01	2.53E-01	0.235	0.07
		best	1.19E+00	3.30E-01	0.276	0.11
4	NP blend (80:20) annealing 150°C	average	5.25E-01	3.10E-01	0.271	0.05
		best	5.83E-01	5.10E-01	0.281	0.08
5	$PC_{71}BM$:PCDTBT bulk in $CHCl_3$	average	6.21E+00	6.05E-01	0.332	1.50
		best	6.73E+00	8.70E-01	0.416	2.43

For the 80:20 $PC_{71}BM$:PCDTBT composite NPs (which exhibits the best results in BHJ[54,55]), thermal annealing leads to an increase in the efficiencies (PCE) (see Table 6 samples 1, 2 and 3) due to a better conductivity between the particles and an improved intermixing of the donor and the acceptor. There is an optimum on the annealing temperature based on efficiency as can be seen on Table 6, the efficiency increases with the annealing temperature up to 140°C, after this temperature the efficiency decreases.

Unfortunately, the results are lower than with SDS due to the fact that the particles are stabilized by steric repulsion which is less efficient than electrostatic repulsion (using SDS) another reason could be that the PEO block is perhaps too large. The particles are bigger than with SDS leading to domains larger than the exciton diffusion length, as a consequence lots of exciton may recombine. The stabilizer is maybe not very suitable because destabilization mechanism occurred after one day. Finally, the results can be explained by big aggregates visible by microscopy which engender high roughness (>20 nm) and poor contact between the active layer and the anode.[56]

IV.3. Conclusion

In this chapter a copolymer P3HT-*b*-PEO was synthesized, presenting self-assembly in water with a CMC determined between 0.016-0.025 g/L. From AFM images, the formation of spherical objects with a size of 20-30 nm was visualized when the copolymer was solubilized in water solutions above its CMC.

The copolymer was then tested as stabilizer for $PC_{71}BM$:PCDTBT NP. The miniemulsion post-polymerization process using P3HT-*b*-PEO as stabilizer successfully produced $PC_{71}BM$:PCDTBT NPs with a diameter ranging from 120 to 400 nm. The properties of the spray-coated films were measured and we observed that the P3HT-*b*-PEO was not stabilizing enough the particles leading to big aggregates in films. Thermal annealing reduced the roughness of the films and efficiencies up to 0.11 % were obtained against 0.03% without annealing. These results are far from the properties of bulk hetero-junction solar cells (2.43% in chloroform) due to the size of the particles which is far from the exciton diffusion length and the deposition technique which induces high roughness but they represent a promising system from environmental prospect.

IV.4. References

[1] E. Hittinger, A. Kokil, C. Weder, *Angew. Chemie Int. Ed.*, **2004**, *43*, 1808.
[2] S. J. Lee, J. M. Lee, I. W. Cheong, H. Lee, J. H. Kim, *J. Polym. Sci. Part A Polym. Chem.*, **2008**, *46*, 2097.
[3] B. G. Zanetti-Ramos, E. Lemos-Senna, H. Cramail, E. Cloutet, R. Borsali, V. Soldi, *Mater. Sci. Eng. C*, **2008**, *28*, 526.
[4] C. Negele, J. Haase, A. Leitenstorfer, S. Mecking, *ACS Macro Lett.*, **2012**, *1*, 1343.
[5] I. Rajot, S. Bône, C. Graillat, T. Hamaide, *Macromolecules*, **2003**, *36*, 7484.
[6] J. Cho, K. H. Cheon, H. Ahn, K. H. Park, S.-K. Kwon, Y.-H. Kim, D. S. Chung, *Adv. Mater.*, **2015**, 5587.
[7] R. S. Loewe, S. M. Khersonsky, R. D. McCullough, *Adv. Mater.*, **1999**, *11*, 250.
[8] A. Yokoyama, R. Miyakoshi, T. Yokozawa, *Macromolecules*, **2004**, *37*, 1169.
[9] M. C. Iovu, E. E. Sheina, R. R. Gil, R. D. McCullough, *Macromolecules*, **2005**, *38*, 8649.
[10] R. S. Loewe, P. C. Ewbank, J. Liu, L. Zhai, R. D. McCullough, *Macromolecules*, **2001**, *34*, 4324.
[11] E. E. Sheina, J. Liu, M. C. Iovu, D. W. Laird, R. D. McCullough, *Macromolecules*, **2004**, *37*, 3526.
[12] R. D. McCullough, S. Tristram-Nagle, S. P. Williams, R. D. Lowe, M. Jayaraman, *J. Am. Chem. Soc.*, **1993**, *115*, 4910.
[13] R. Tkachov, V. Senkovskyy, H. Komber, J.-U. Sommer, A. Kiriy, *J. Am. Chem. Soc.*, **2010**, *132*, 7803.
[14] E. L. Lanni, A. J. McNeil, *Macromolecules*, **2010**, *43*, 8039.
[15] V. Senkovskyy, M. Sommer, R. Tkachov, H. Komber, W. T. S. Huck, A. Kiriy, *Macromolecules*, **2010**, *43*, 10157.
[16] N. Doubina, S. A. Paniagua, A. V Soldatova, A. K. Y. Jen, S. R. Marder, C. K. Luscombe, *Macromolecules*, **2011**, *44*, 512.
[17] M. Jeffries-El, G. Sauvé, R. D. McCullough, *Macromolecules*, **2005**, *38*, 10346.
[18] M. Jeffries-EL, G. Sauvé, R. D. McCullough, *Adv. Mater.*, **2004**, *16*, 1017.
[19] M. C. Iovu, R. Zhang, J. R. Cooper, D. M. Smilgies, A. E. Javier, E. E. Sheina, T. Kowalewski, R. D. McCullough, *Macromol. Rapid Commun.*, **2007**, *28*, 1816.
[20] J. Liu, E. Sheina, T. Kowalewski, R. D. McCullough, *Angew. Chemie Int. Ed.*, **2002**, *41*, 329.
[21] H. T. Nguyen, O. Coulembier, J. De Winter, P. Gerbaux, X. Crispin, P. Dubois, *Polym. Bull.*, **2011**, *66*, 51.
[22] Q. Zhang, A. Cirpan, T. P. Russell, T. Emrick, *Macromolecules*, **2009**, *42*, 1079.
[23] A. Britze, V. Möllmann, G. Grundmeier, H. Luftmann, D. Kuckling, *Macromol. Chem. Phys.*, **2011**, *212*, 679.
[24] M. C. Iovu, C. R. Craley, M. Jeffries-EL, A. B. Krankowski, R. Zhang, T. Kowalewski, R. D. McCullough, *Macromolecules*, **2007**, *40*, 4733.
[25] C. Yang, J. K. Lee, A. J. Heeger, F. Wudl, *J. Mater. Chem.*, **2009**, *19*, 5416.
[26] K. Palaniappan, N. Hundt, P. Sista, H. Nguyen, J. Hao, M. P. Bhatt, Y.-Y. Han, E. A. Schmiedel, E. E. Sheina, M. C. Biewer, M. C. Stefan, *J. Polym. Sci. Part A Polym. Chem.*, **2011**, *49*, 1802.
[27] C.-A. Dai, W.-C. Yen, Y.-H. Lee, C.-C. Ho, W.-F. Su, *J. Am. Chem. Soc.*, **2007**, *129*, 11036.
[28] M. Urien, H. Erothu, E. Cloutet, R. C. Hiorns, L. Vignau, H. Cramail, *Macromolecules*, **2008**, *41*, 7033.
[29] A. E. Javier, S. N. Patel, D. T. Hallinan, V. Srinivasan, N. P. Balsara, *Angew. Chemie Int. Ed.*, **2011**, *50*, 9848.
[30] A. C. Kamps, M. Fryd, S.-J. Park, *ACS Nano*, **2012**, *6*, 2844.
[31] Y. Lin, Q. Wei, G. Qian, L. Yao, J. J. Watkins, *Macromolecules*, **2012**, *45*, 8665.
[32] C. N. Kempf, K. A. Smith, S. L. Pesek, X. Li, R. Verduzco, *Polym. Chem.*, **2013**, *4*, 2158.
[33] J. U. Lee, A. Cirpan, T. Emrick, T. P. Russell, W. H. Jo, *J. Mater. Chem.*, **2009**, *19*, 1483.
[34] J.-H. Tsai, Y.-C. Lai, T. Higashihara, C.-J. Lin, M. Ueda, W.-C. Chen, *Macromolecules*, **2010**, *43*, 6085.
[35] S. Yao, A. Bethani, N. Ziane, C. Brochon, G. Fleury, G. Hadziioannou, P. Poulin, J.-B. Salmon, E. Cloutet, *Macromolecules*, **2015**, *48*, 7473.
[36] P. Miaudet, C. Bartholome, A. Derré, M. Maugey, G. Sigaud, C. Zakri, P. Poulin, *Polymer (Guildf).*, **2007**, *48*, 4068.
[37] Y. Hou, J. Tang, H. Zhang, C. Qian, Y. Feng, J. Liu, *ACS Nano*, **2009**, *3*, 1057.
[38] H. Erothu, J. Kolomanska, P. Johnston, S. Schumann, D. Deribew, D. T. W. Toolan, A. Gregori, C. Dagron-Lartigau, G. Portale, W. Bras, T. Arnold, A. Distler, R. C. Hiorns, P. Mokarian-Tabari, T. W. Collins, J. R. Howse, P. D. Topham, *Macromolecules*, **2015**, *48*, 2107.
[39] K. Satoh, J. E. Poelma, L. M. Campos, B. Stahl, C. J. Hawker, *Polym. Chem.*, **2012**, *3*, 1890.
[40] W. Griffin, *J. Soc. Cosmet. Chem.*, **1949**, *1*, 311.
[41] R. Huisgen, *Proc. Chem. Soc.*, **1961**, 357.

[**42**] H. C. Kolb, M. G. Finn, K. B. Sharpless, *Angew. Chemie Int. Ed.*, **2001**, *40*, 2004.
[**43**] T. L. Benanti, A. Kalaydjian, D. Venkataraman, *Macromolecules*, **2008**, *41*, 8312.
[**44**] C. Özdemir, A. Güner, *Eur. Polym. J.*, **2007**, *43*, 3068.
[**45**] Y.-C. Tung, W.-C. Wu, W.-C. Chen, *Macromol. Rapid Commun.*, **2006**, *27*, 1838.
[**46**] K. Kalyanasundaram, J. K. Thomas, *J. Am. Chem. Soc.*, **1977**, *99*, 2039.
[**47**] O. Anthony, R. Zana, O. Anthony, *Macromolecules*, **1994**, *27*, 3885.
[**48**] R. H. Muller, *Colloidal Carriers for Controlled Drug Delivery and Targeting*, **1991**.
[**49**] B. D. Olsen, R. A. Segalman, *Mater. Sci. Eng. R Reports*, **2008**, *62*, 37.
[**50**] K. Landfester, R. Montenegro, U. Scherf, R. Güntner, U. Asawapirom, S. Patil, D. Neher, T. Kietzke, *Adv. Mater.*, **2002**, *14*, 651.
[**51**] O. Pras, D. Chaussy, O. Stephan, Y. Rharbi, P. Piette, D. Beneventi, *Langmuir*, **2010**, *26*, 14437.
[**52**] F. Tiarks, K. Landfester, M. Antonietti, *Langmuir*, **2001**, *17*, 908.
[**53**] R. D. Deegan, O. Bakajin, T. F. Dupont, G. Huber, S. R. Nagel, T. A. Witten, *Nature*, **1997**, *389*, 827.
[**54**] T. Wang, A. J. Pearson, A. D. F. Dunbar, P. A. Staniec, D. C. Watters, H. Yi, A. J. Ryan, R. A. L. Jones, A. Iraqi, D. G. Lidzey, *Adv. Funct. Mater.*, **2012**, *22*, 1399.
[**55**] V. S. Murugesan, S. Ono, N. Tsuda, J. Yamada, P.-K. Shin, S. Ochiai, *Int. J. Photoenergy*, **2015**, *2015*, 1.
[**56**] D. Darwis, N. Holmes, D. Elkington, A. L. David Kilcoyne, G. Bryant, X. Zhou, P. Dastoor, W. Belcher, *Sol. Energy Mater. Sol. Cells*, **2014**, *121*, 99.
[**57**] D. K. Owens, R. C. Wendt, *J. Appl. Polym. Sci.*, **1969**, *13*, 1741.

IV.5. Appendix

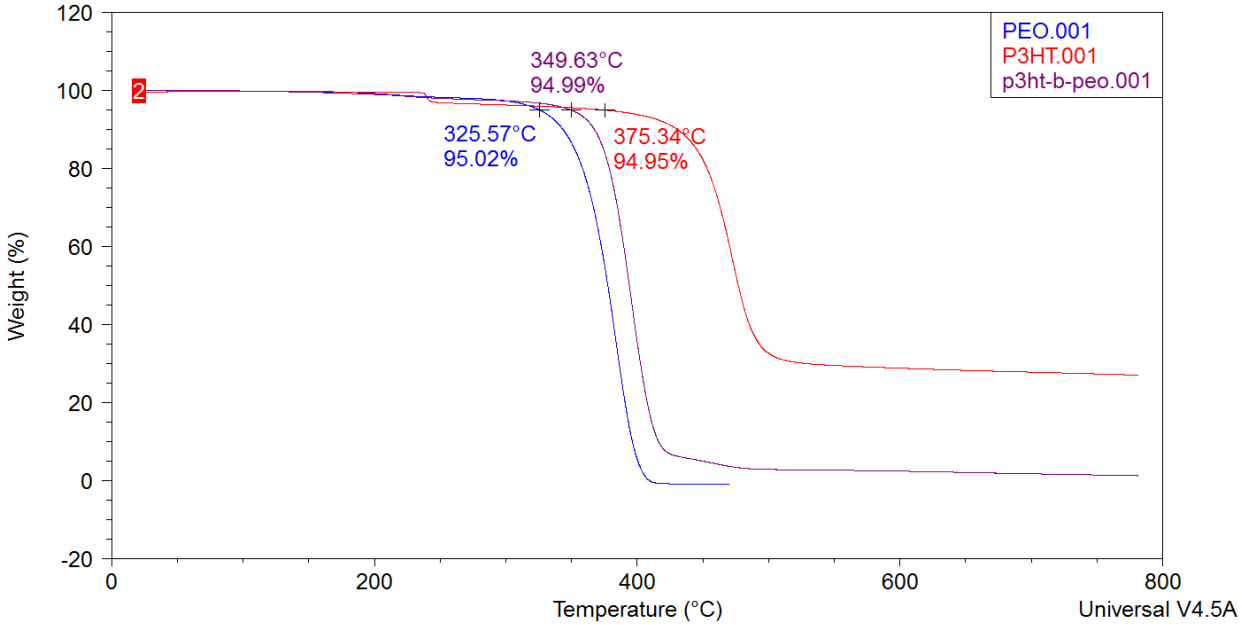

Figure 34 : Thermo-gravimetric analysis (TGA) of the P3HT (in blue) and PEO (in red) homopolymers and P3HT-*b*-PEO copolymer (in purple) under N_2 atmosphere.

IV.6. Experimental section

IV.6.1.Materials

Tert-butyl magnesium chloride (1.7 M in THF), Copper iodide (98%) and Aluminium oxide activated basic (Al_2O_3) were purchased from Acros Organic. Sodium carbonate (98%) was purchased from Alfa Aesar. 9-(9-Heptadecanyl)-9H-carbazole-2,7-diboronic acid bis(pinacol) ester (97%), 4,7-Bis(2-bromo-5-thienyl)-2,1,3-benzothiadiazole (99+%), 3-hexyl thiophene (99%), Polyethylene oxide monomethyl ether, Pyridium *p*-toluene sulfonate (98%), 2-chloroethyl vinyl ether (99%), sodium chloride (99.8+%), sodium azide (99.5+%), [1,3-Bis(diphenylphosphino)propane]-dichloronickel(II) (NidpppCl2) (97+%), Ethynyl Magnesium Bromide (0.5M in THF), N,N-Diisopropylethylamine (DIPEA) (99.5%), chloroform (99.0-99.4%) and dichloromethane (99.9+%), N,N-Diméthylformamide (99.8+%), hexane (95+%), methanol (99.6+%), THF (99.9+%) were purchased from Sigma Aldrich. $PC_{71}BM$ was purchased from Solaris (99+%) Diethyl ether (99.5%) and toluene (99%) were purchased from VWR Chemicals. All chemicals were used as received unless otherwise stated.

THF was dried over calcium hydride (CaH_2) and distilled under vacuum few hours before use.

IV.6.2.Reactions

The reactions were performed under an Argon atmosphere using standard schlenk techniques.

IV.6.2.a.Synthesis of P3HT-*b*-PEO

P3HT-b-PEO

Polyethylene oxide acetal chloride (1) 25g of commercially available Polyethylene oxide monomethyl ether (20 000 g/mol) (1.25 mmol) and 125 mg of pyridinium p-toluenesulfonate (0.5 mmol) were dissolved into 100 mL of toluene. The solvent was distilled twice to purify the two compounds by azeotropic drying. After complete drying 125 mL of dried dichloromethane was added and 2.5 mL of 2-chloroethylvinylether (25 mmol) was added dropwise at 0°C. After stirring during 30 minutes 1.5g of Na_2CO_3 in 28.5 mL of water were added to terminate the reaction (5wt%). 100 mL of dichloromethane was added to dissolve the mixture and the solution was washed with 50 mL of water followed by 100 mL of NaCl saturated solution. Each aqueous phase was extracted with 40

mL of dichloromethane and the organic phases were dried over magnesium sulfate. The solvent was evaporated and the product was dissolved with 40 mL of dichloromethane and 40 mL of THF and precipitated into 750 mL of hexanes. After filtration 24 g of polyethylene oxide acetal chloride (1) were obtained. (95% yield)

Polyethylene oxide acetal azide (2)

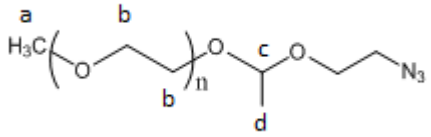

12g of polyethylene oxide acetal chloride (1) (0.625 mmol) and 1.56 g of NaN_3 (24 mmol) were dissolved into 50 mL of DMF. The mixture was allowed to react at 60 °C during 40 hours. After that, the solvent was evaporated and the compound was dissolved into 50 mL of dichloromethane. The organic phase was washed with water and brine. The solution was precipitated into hexane:diethylether (1:1), after filtration the product was redissolved into dichloromethane and reprecipitated into cold hexane. The product was finally dried under vacuum leading to polyethylene oxide acetal azide (2) (11.5g, 96% yield).[39]

δ ^{1}H NMR (400 MHz, $CDCl_3$, ppm): 1.34 (d, J ¼ 5.4 Hz, 3H, Hd), 3.37 (s,3H, Ha), 3.52–3.75 (br, 1557, Hb), and 4.82 (q, J ¼5.4 Hz, 1H, Hc)

FTIR ν(N_3) 2100 cm^{-1}

2,5-dibromo-3-hexylthiophene (3)

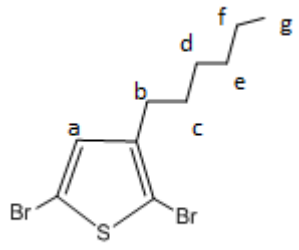

According to the literature[28] 2,5-dibromo-3-hexylthiophene was synthesized as followed : NBS (49 g, 0.275 mol) was added to a solution of 3-hexylthiophene (25 g, 0.153 mol) in acetic

acid (200 mL) and CH_2Cl_2 (200 mL). The mixture was stirred for 20 h under nitrogen. The organic layer was washed five times with water and five times with a saturated aqueous $NaHCO_3$ solution, dried over Na_2SO_4, filtered and concentrated. The crude product was recovered as a pale yellow oil by three successive secondary vacuum distillations (25 g, 60%).

δ ^{1}H NMR (400 MHz, CDCl3, ppm): 0.90 (t, 3H, Hg), 1.33 (m, 6H, Hd,e,f), 1.54 (q, 2H, Hc), 2.21 (t, 2H, Hb) and 6.78 (s, 1H, Ha)

Ethynyl-poly(3-hexylthiophene) (4)

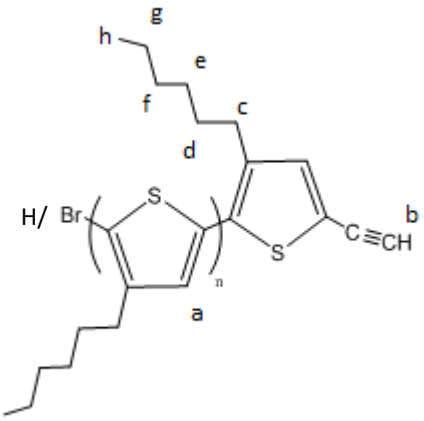

6.18 g of 2,5-dibromo-3-hexylthiophene (18.96 mmol) were dissolved with 20 mL of freshly distilled THF. After stirring during 15 min, 11.15 mL of ^{t}BuMgCl (1.7M) were added. After stirring during 2 hours the mixture was diluted with 180 mL of THF. 0.853 g of $NidpppCl_2$ (8.3% of the monomer which should lead to 2000 g/mol polymer) was then added and the solution was stirred during 10 min. 50 mL of ethynylMgBr (0.5M) (16 eq *vs* cat) was added *via* a purged syringe. After stirring during 5 min, 10 mL of degazed MeOH was added to terminate the polymerization. The solution was precipitated into 1.5L of MeOH to recover the polymer followed by Soxhlet procedure with MeOH and then chloroform to dissolve the product leading to ethynyl-P3HT recovered by precipitation in methanol. (1.9 g, 60% yield).[29]

δ ^{1}H NMR (400 MHz, $CDCl_3$, ppm): 6.97 (s,14H, Ha), 3.53 (s, 1 H, Hb), 2.78 (m, 24 H, Hc), 1.69 (m, 28H, Hd), 1.50-1.20 (m, He,f,g), 0.91 (t, 46H, Hg) Mn by NMR : signal at 0.91 ppm integrate for 3 protons, DPn=15 3HT units, Mn= 15xM(3HT)=2300 g/mol SEC: Mn=2500, Đ=1.2

P3HT-b-PEO (5)

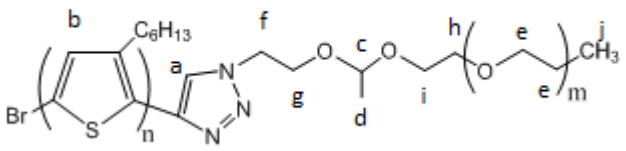

0.1 g of ethynyl-P3HT and 1.5g of azide-PEO were dissolved in 30 mL of freshly distilled THF. 76 mg of CuI and 595 µL of DIPEA were added. After N_2 bubbling during 5 min and ultrasounds to dissolve the P3HT the mixture was stirred at 50°C during 3 days. After passing through a neutral Al_2O_3 column the solution was concentrated and precipitated into MeOH leading to a red powder dried under vacuum.[29]

δ ^{1}H NMR (400 MHz, $CDCl_3$, ppm): 7.79 (s,1H, Ha), 6.94 (s, 15H, Hb), 4.82 (m, 1 H, Hc), 4.61 (m, 2H), 4.03 (m, 2H, Hf), 3.64 (m, He), 3.46(m, 2H, Hh), 3.39(m, 2H, Hi), 3.37(s, 3H, Hj), 2.79(m, 31H, $H_{alkyle\ P3HT}$), 1.85(m, 31H, $H_{alkyle\ P3HT}$), 1.33(m, 28H, $H_{alkyle\ P3HT}$), 0.90(t, 45H, $H_{alkyle\ P3HT}$)

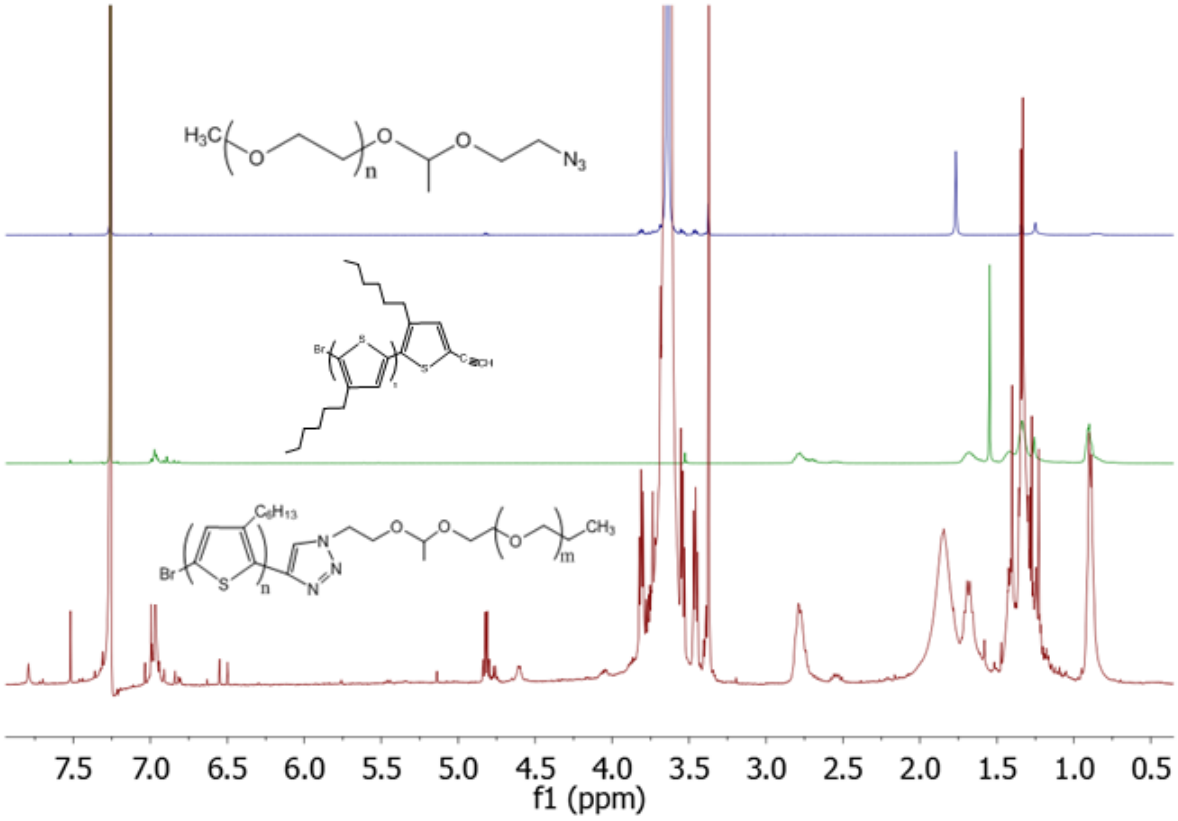

Figure 35 : ^{1}H-NMR overlay of P3HT, PEO and P3HT-*b*-PEO in $CDCl_3$ at 400 MHz

IV.6.2.b.Typical procedure for the $PC_{71}BM$:PCDTBT nanoparticles made by miniemulsion post-polymerization using P3HT-*b*-PEO as stabilizer

PCDTBT and $PC_{71}BM$ were solubilized in 0.5mL of $CHCl_3$ and 0.5 mL of toluene. Aqueous P3HT-*b*-PEO solution was made by dissolving 5 mg of copolymer into 5 mL of MQ-water. The oily solution was then introduced to the stirred aqueous solution, followed by ultrasound during 5 min at 20% amplitude to form the miniemulsion.

Nitrogen was then bubbled into the solution while heating at 70°C for 1 h to evaporate off the chloroform and the toluene.

The NPs were washed using ultra centrifuge dialysis tubes purchased from Sartorium stedim vivaspin20 (10 kDa MWCO). The solution was placed into the centrifuge dialysis tube and spun at 4000 rpm for 8 min. The filtrate was then discarded and the solution diluted with 5 mL of MQ-water. This process was repeated at least 3 times.

IV.6.3.Methods of characterization

Dynamic light scattering (DLS) on diluted dispersion samples was performed on a Cordouan Particle Size Analyzer Vasco. The autocorrelation function was analyzed using the Cordouan dispersion technology software algorithm to obtain number-weighted particle sizes.

NMR spectra were recorded on a Bruker Avance III 400 spectrometer at 400 MHz for ^1H nucleus.

DOSY (Diffusion Ordered Spectroscopy) measurements were performed at 298K on a Bruker Avance III 400 spectrometer operating at 400.33 MHz and equipped with a 5mm Bruker multinuclear z-gradient direct cryoprobe-head capable of producing gradients in the z direction with strength 53.5 $G.cm^{-1}$. Each sample was dissolved in 0.4 ml of deuterated chloroform for internal lock and spinning was used to minimize convection effects. The dosy spectra were acquired with the *ledbpgp2s* pulse program from Bruker topspin software. The duration of the pulse gradients and the diffusion time were adjusted in order to obtain full attenuation of the signals at 95 % of maximum gradient strength. The values were 3.0 ms for the duration of the gradient pulses and 100 ms for the diffusion time. The gradients strength was linearly incremented in 16 steps from 5% to 95% of the maximum

gradient strength. A delay of 3 s between echoes was used. The data were processed using 8192 points in the F2 dimension and 128 points in the F1 dimension with the Bruker topspin software. Field gradient calibration was accomplished at 25°C using the self-diffusion coefficient of H2O+D2O at 19.0 x 10^{-10} $m^2.s^{-1}$

CMC determination using pyrene encapsulation different diblock concentrations in water were prepared from 4x10^{-4} mg/mL to 0.5 mg/mL. 1 mL of these solutions was mixed with 1 µL of pyrene solution (1 mM in DMSO) and the fluorescence spectra were recorded after excitation at 335 nm in order to calculated the CMC.

Size exclusion chromatography (SEC) was performed in chloroform at 30°C with a flow rate of 1 mL.min^{-1} using TSK Gel HXL Multipore column (size 30 x 7.8, pore size 5 µm) and a guard-column from Tosoh The elution times were converted into molar masses using a calibration curve based on low dispersity polystyrene standards. *Thermogravimetric measurements* were carried out with TA Instruments Q50 from room temperature to 800°C with a heating rate of 10°C.min^{-1}. The analyses were performed under nitrogen atmosphere.

Absorption spectra were measured using a Shimadzu spectrophotometer UV-3600 while *emission spectra* were measured using a Horiba Scientific Fluoromax-4 spectrofluorometer.

TEM images were obtained on Formvar grids with a Transmission Elctron Microscope (H7650, HITACHI (accelerate voltage 120 kV), using high constrast mode. Dispersed nanoparticles were cleaned by several centrifugation cycles before TEM analysis and deposited onto a copper grid.

Surface tension was measured using drop shape analysis technique on a pendant drop tensiometer (Krüss DSA-100) while *surface energies* were determined by measuring contact angle between three solvents: water, diiodomethane and ethylene glycol and the polymer film. The surface energy is calculated using Owens-Wendt model.[57]

Zeta potential measurements were carried out with a Zetasizer Nano ZS from Malvern. This instrument can measure zeta from -150mV to 150 mV. The cell voltage was adjusted depending on the conductivity of the medium. The zeta potential was measured based on the Henry equation.

AFM Characterization: Atomic force microscopy (AFM Dimension FastScan, Bruker) was used in tapping mode to characterize the surface morphology of the samples. Silicon cantilevers (Fastscan-A) with a typical tip radius of ≈5 nm, a spring constant of 18 $N.m^{-1}$ and a cantilever resonance frequency of about 1.4 MHz were used.

Conducting AFM (c-AFM) measurements were performed with a Dimension ICON (Bruker) equipped with a PeakForce TUNA module. Platinum–iridium-coated probes (SCM-PIT, Bruker) with a spring constant of 2.8 $N.m^{-1}$ and resonant frequency of 75 kHz were used. For c-AFM measurements, a DC bias of 5V was applied between the sample and the tip.

Devices fabrication: Inverted solar cells have been fabricated with the following structure: Glass/ITO/ZnO/active layer/MoO_3/Ag, the active layer being composed of either $PC_{71}BM$:PCDTBT nanoparticles (NP) or $PC_{71}BM$:PCDTBT in bulk hetero junction (BHJ). The Indium tin oxide (ITO)-coated glass substrates, purchased from Kintec, with a surface resistance of ~10 $\Omega.sq^{-1}$ are successively cleaned in acetone, ethanol and isopropanol in an ultrasonic bath.

196 mg of zinc acetate dehydrate was mixed with 54 µL of ethanolamine in 6 mL of absolute ethanol and stirred at 45 °C for 2 hours. The zinc oxide layer is prepared by spin-coating this solution at 2000 rpm for 60 s following by annealing at 180°C for 1 hour in air leading to a 60 nm thick layer. $PC_{71}BM$:PCDTBT solutions (for BHJ) were prepared in chloroform with a concentration of 40 $mg.mL^{-1}$ (1:4 ratio).

BHJ layers were spin-coated in a glove box at 2000 rpm during 60 s with a resulting $PC_{71}BM$:PCDTBT thickness of 80 nm.

NP layers were spray-coated in air leading to a 100 nm thick layer. The films were dried at 100°C during the spray-coating process to evaporate the remaining water and then transferred into a vacuum chamber for the MoO_3/Ag evaporation.

MoO_3 (10nm) and Ag (80nm) were successively thermally-evaporated at deposition rates of 0.1 $nm.s^{-1}$ and 0.2-0.4$nm.s^{-1}$ respectively under secondary vacuum (10^{-6}mbar). The size of solar cells active area is 10 mm^2. The devices were characterized using a K.H.S. Solar Cell test-575 solar simulator with AM1.5G filters set at 100 $mW.cm^{-2}$ with a calibrated radiometer (IL 1400BL). Labview controlled Keithley 2400 SMU enabled the current density-voltage (J-V) curves measurements.

- Vue d'ensemble du chapitre IV -

Ce quatrième chapitre expose la synthèse d'un nouveau stabilisant combinant une partie semi-conductrice et une partie soluble dans l'eau. Ce stabilisant est un co-polymère à bloc poly(3-hexylthiophène)-*bloc*-poly(oxyde d'éthylène) (P3HT-*b*-PEO) utilisé pour stabiliser des particules de $PC_{71}BM$ et PCDTBT (voir figure 1).

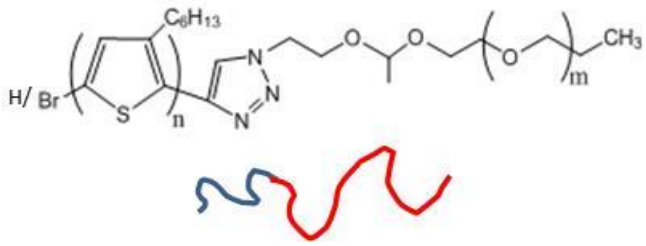

Figure 1 : Copolymère à blocs P3HT-*b*-PEO utilisé pour stabiliser des particules de PCDTBT et $PC_{71}BM$ ou des particules composites de $PC_{71}BM$:PCDTBT

L'étude de l'auto-assemblage dans l'eau a montré que ce co-polymère de masse molaire 19000 $g.mol^{-1}$ (déterminée par RMN du proton) formait des micelles sphériques métastables d'une taille d'environ 20-30 nm (voir figure 2) à partir d'une concentration micellaire critique d'environ 0,016-0,025 g/L déterminée par encapsulation au pyrène et mesure de tension de surface par goutte pendante.

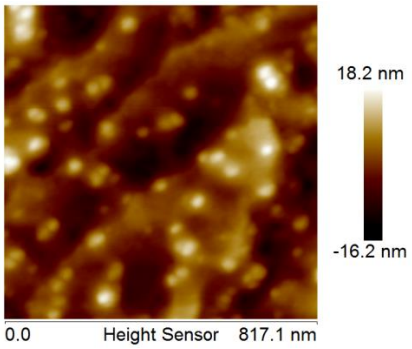

Figure 2 : Image topographique des micelles de P3HT-*b*-PEO dans l'eau

Ce co-polymère a ensuite été utilisé comme stabilisant pour la fabrication de particules de $PC_{71}BM$ et PCDTBT ainsi que de particules composites $PC_{71}BM$:PCDTBT. En

fonction de différents paramètres de synthèse (concentration en matière photo-active, ultrasons, concentration en stabilisant), la taille des particules a pu être modifiée.

Les couches actives de cellules solaires ont été fabriquées au spray à partir d'encres fraîchement obtenues. Ces couches actives ont par la suite été intégrées au sein d'un dispositif cellule solaire inverse. Les résultats obtenus sont résumés dans le tableau 1.

Tableau 1 : Caractéristiques des cellules photovoltaïques intégrant des particules composite en proportions 80 :20 de $PC_{71}BM$:PCDTBT stabilisées par un co-polymère P3HT-*b*-PEO , ainsi que une hétéro-jonction volumique à partir d'une solution de chloroforme, les températures indiquées correspondent au recuit appliqué pendant 4 min. Pour chaque échantillon les valeurs moyennes et record ont été reportées

	Sample		Jsc (mA/cm)	Voc (V)	FF	PCE (%)
1	NP composite (80:20) $PC_{71}BM$:PCDTBT	moyenne	1,03E+00	7,00E-02	0,217	0,02
		meilleure	1,07+00	9,00E-02	0,230	0,03
2	NP composite (80:20) recuit 130°C	moyenne	1,16E+00	8,75E-02	0,226	0,03
		meilleure	1,74E+00	1,30E-01	0,231	0,05
3	NP composite (80:20) recuit 140°C	moyenne	8,60E-01	2,53E-01	0,235	0,07
		meilleure	1,19E+00	3,30E-01	0,276	0,11
4	NP composite (80:20) recuit 150°C	moyenne	5,25E-01	3,10E-01	0,271	0,05
		meilleure	5,83E-01	5,10E-01	0,281	0,08
5	$PC_{71}BM$:PCDTBT bulk $CHCl_3$	moyenne	6,21E+00	6,05E-01	0,332	1,50
		meilleure	6,73E+00	8,70E-01	0,416	2,43

L'étude des paramètres photovoltaïques sur des particules stabilisées par un co-polymère à bloc photo-actif a permis de tirer plusieurs conclusions :

- Comme précédemment un recuit permet d'augmenter l'efficacité jusqu'à presque 4 fois pour des particules composites de composition (80 :20) (échantillon 1 par rapport au 3).
- Un recuit trop important a pour conséquence de diminuer l'efficacité, il existe donc un optimum de température de recuit (échantillon 3 par rapport au 4).

- Les particules obtenues ont une taille bien supérieures à celles stabilisées par du tensio-actif de type SDS (150 nm par rapport à 50) ce qui mène à la formation de domaines bien supérieurs à la longueur de diffusion de l'exciton et donc à beaucoup de recombinaisons. Par ailleurs, les faibles efficacités obtenues peuvent aussi s'expliquer par l'instabilité dans le temps des encres synthétisées. Cela se traduit par l'apparition de gros agrégats visibles au microscope qui peuvent engendrer des court-circuits. La grande rugosité engendrée par la méthode de dépôt (par spray) est aussi en partie responsable des faibles efficacités obtenues puisque de bons contacts entre la couche active et les électrodes ont été obtenus. Enfin il faudrait faire varier la masse molaire des deux blocs et en particulier celle du PEO matériau inactif pour une application photovoltaïque.

-

Chapter V
Nanoprecipitation of PCDTBT-based particles

In this work, composite particles of poly[N-9'-heptadecanyl-2,7-carbazole-*alt*-5,5-(4,7-di-2-thienyl-2',1',3'-benzothiadiazole] (PCDTBT) and [6,6]-Phenyl C71 butyric acid methyl ester ($PC_{71}BM$) were obtained in water from the nanoprecipitation process. Depending on experimental conditions, particles that comprise both the electron-donor and the electron-acceptor and ranging from 40 nm to 140 nm in diameter were obtained and characterized. Water-based inks of such nano-objects were used for the preparation of the photovoltaic active layer by using spray-coating deposition which was then integrated in organic solar cells showing promising results.

- Chapter V -
Nanoprecipitation of PCDTBT-based particles

Table of Contents

Table of Figures

List of Tables

V.1 Introduction

With the objective of synthesizing π-conjugated polymer particles in eco-friendly medium, we have seen in Chapter II and III that an insulating stabilizer can act as trap and disturb the charge transport. An alternative was to synthesize and use in chapter IV a co-polymer as stabilizer which included a semi-conducting part (*i.e.* P3HT). However, the resulting inks were not stable over time. A new strategy producing particles without any stabilizer will be the topic of this chapter.

As before, after the study of the properties, the particles will be coated onto proper electrode and integrated into solar cells to asses their efficiency.

For the synthesis of particles by heterogeneous condition using secondary dispersion we focused in this chapter on nanoprecipitation. The particles hereafter synthesized will be deposited as an active layer and then integrated into a solar cell. This process has the advantages of the secondary dispersions that is to say the conservation of the bulk made polymer properties (molar mass, chain end etc…)

In the nanoprecipitation, the components (polymer and electron acceptor if needed) are first dissolved into a good solvent. This solution is then dispersed in a big quantity of bad solvent under vigorous stirring.[1] Then, the good solvent is evaporated and leaves conjugated polymer particles dispersed in water or alcohol. This method produces nanoparticles in one step and more importantly in the absence of any stabilizer.

The strength of this process is its universality since whatever material can be processed as particles as long as they are soluble into water miscible solvent. Typically THF is used for π-conjugated polymers to nanoprecipitate in water or chloroform in ethanol, the advantage is its low boiling point which allows its evaporation without excess heating which could damage the material.

Like the previous chapters we tried to integrate the electron acceptor into the particles by synthesizing either composite particles or blend of individual particles.

The advantage of this method is the absence of stabilizer which could prevent good charge transport in case of insulating stabilizer (most of the case) as highlighted by sereval authors during the last years.

In 2006 McNeill *and coll* reported the production of poly(fluorene) particles made by nanoprecipitation with diameter of 5-10 nm. Spheres were formed because the polymer chains want to minimize the contact towards the bad solvent.[2]

The polymer solution has to be very diluted to prevent the formation of aggregates: for instance a concentration higher than 2.5wt% of P3HT led to macroscopic precipitates at the surface of water as soon as the polymer solution was added.[1]

The first devices integrating this technique were reported in 2011 by the team of Dastoor who used P3HT nanoparticles in ethanol to make the active layer of OPV devices. However, due to the low concentration, four spin-coating were needed to form a nice layer reaching very low efficiency (0.018%).

Later, P3HT particles with indene-C_{60} bisadduct (ICBA) as electron acceptor from chloroform solutions were nanoprecipitated into ethanol (EtOH) and methanol (MeOH). The deposition of several layers was needed to overcome the low concentration (up to 25 spin-coating for the ethanol solutions). Thermal annealing was then applied to reach a smoother surface. With an inverted architecture comprising of zinc oxide, 4.1% of efficiency in methanol (which however remains toxic solvent) and 3.5% for ethanol were obtained.[3]

Dr Blade and Ink Jet Printing were also used for the deposition of P3HT:ICBA NP, proving that NP are suitable for large scale production (see figure 1). Honorable results of 3.9% by Dr Blading, 2.9% by Ink-jet and 4.3% by spin-coating against 5.1% by spin-coating from *o*-DCB solution were obtained with comparable roughness.[4]

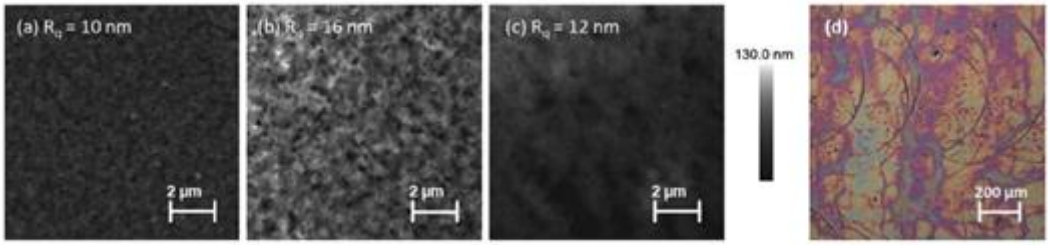

Figure 1 : AFM images of P3HT:ICBA NP deposited by spin-coating (a), doctor blading (b), and ink-jet printing (c) , (d) is the optical micrograph of (c)

V.2. Results and discussion

V.2.1. Synthesis of $PC_{71}BM$:PCDTBT composite particles by nanoprecipitation

The active components were dissolved in THF at a concentration of 0.5mg/mL by sonication during 20 min, forming the "good" solution. Particles were prepared by a modified nanoprecipitation process[5] : 4 mL of the THF solution was rapidly injected into 20 mL of stirred water at 50°C (leading to the smallest particles see figure 2). Then the THF is evaporated by placing the solution under argon flow during 2 hours to reach photo-active particles without stabilizer dispersed in water. To create composite particles both components were solubilized into THF and this solution was injected into water. For the mixed particles, each kind of particles was synthesized separately and then mixed afterwards in appropriate ratio.

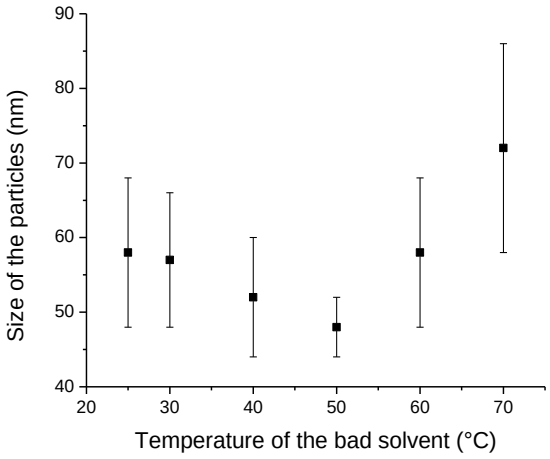

Figure 2 : Size of the composite particles depending on the water temperature (bad solvent) during injection of the THF solution (good solvent)

V.2.2. Influence of experimental parameters on the particles size

Particles of $PC_{71}BM$:PCDTBT (80:20) with a diameter that can be tuned from 40 to 130 nm were synthesized according to the procedure described in the experimental part. The smallest size was targeted in order to create small size domains which will limit the lost of exciton by recombination. For this study, the ratio was set at 80:20 wt% according to the best results obtained for this proportion in a bulk heterojunction system (BHJ). [6,7]

As can be seen in Table 1, the size of the nanoparticles could be adjusted by the experimental parameters such as the stirring speed. Indeed higher rate of stirring led to enhanced mass transfer which induced rapid nucleation to produce smaller sized nanoparticles.[8] At 250 rpm (Table 1, sample 1), the stirring is not enough intense to allow good mixing between good and bad solvent leading to bigger particles whereas at 1000 rpm (Table 1, sample 4), the speed is too intense resulting from the creation of a vortex leading to bigger particles. As a consequence, the best stirring speed is located between 500 and 750 rpm.

The concentration of the mother solution is another parameter that can be varied in order to play on the size of the NP. For instance, higher initial concentration from 0.1 mg/mL to 1 mg/mL (Table 1, samples 5 and 9) gave rise to bigger particles from 40 nm to 81 nm respectively. This increase in the particles size can be attributed to the greater number of polymer chains per unit volume of solvent which is consequently responsible for the formation of aggregates or larger particles.[8] This is in agreement with previous study reported in the literature.[9]

Table 1 : Size of the $PC_{71}BM$:PCDTBT composite (80:20) as a function of the experimental parameters

Sample	temperature	stirring speed	initial concentration in THF	final concentration in water	Size [a]
	°C	rpm	mg/mL	mg/mL	nm
1	50	250	0.5	0.006	65 ± 13
2		500			48 ± 4
3		750			44 ± 2
4		1000			74 ± 14
5	50	500	0.1	0.006	40 ± 4
6			0.25		42 ± 7
7			0.5		48 ± 5
8			0.75		66 ± 10
9			1		81 ± 11
10	50	750	0.5	0.025	44 ± 8
11				0.05	47 ± 6
12				0.1	50 ± 5
13				0.2	85 ± 11
14				0.3	133 ± 20
15				0.4	agregates

[a] determined by DLS

The particles'size could also be tuned with the help of the final concentration (the volume of the good solvent was varied). Indeed the final concentration increase gave rise to bigger particles (Table 1 samples 10 to 15) in agreement with what was reported in the literature.[9] In fact, below 0.1 mg/mL in the final solution, the concentration has low impact on the size of the nanoparticles, the variation was smaller than 10 nm. However above this value the size increases rapidly from 50 nm for a concentration of 0.1 mg/mL to 133 nm for 0.3 mg/mL until the formation of aggregates after 0.4 mg/mL.

Nevertheless, it is noteworthy that the concentrations (initial and final) have to be tuned in regards to the formation of homogeneous active layer. It was thus necessary to find a balance between a high enough concentration of active matter for the formation of a film and particles of appropriate sizes.

Here below are the experimental conditions finally used:

- temperature of 50°C (leading to the smallest particles considering all the other parameters fixed)
- speed stirring at 750 rpm
- mother solution concentration at 0.5 mg/mL in THF
- final concentration at 0.1 mg/mL in water

This procedure produces particles around 48 nm in diameter determined by TEM images (see figure 3).

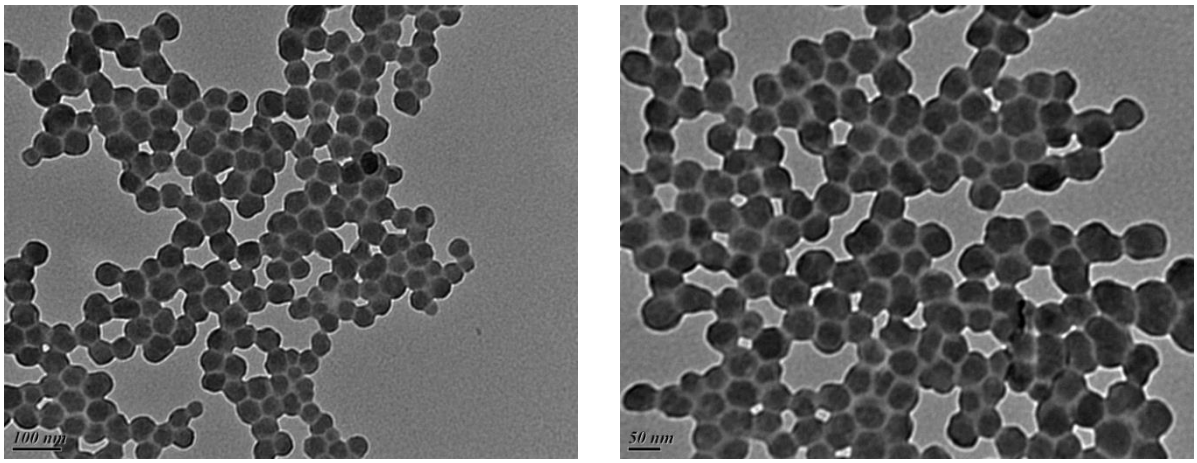

Figure 3 : TEM images of NP synthesized using optimized procedure for nanoprecipitation of 80:20 $PC_{71}BM$:PCDTBT in water

V.2.3. Optoelectronic properties of $PC_{71}BM$:PCDTBT blended particles

The optical properties of the $PC_{71}BM$, PCDTBT as well as the composite particles have been studied by UV-visible absorption and fluorescence spectroscopies. In figure 4 the absorbance spectra that were obtained in water (nanoparticles) are presented for various compositions as well as the comparison between PCDTBT as dissolved material (in THF) and as NP in water.

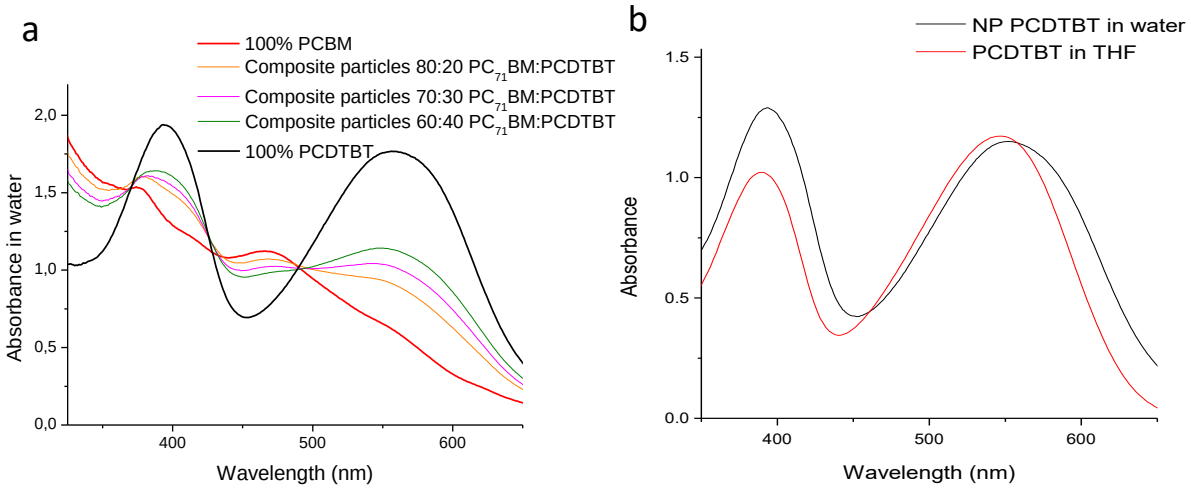

Figure 4 : Absorption spectra of composite materials in water (NP, a), comparison of PCDTBT absorption in THF (dissolved polymer) and in water (NP) (b)

The spectra b in THF and in water present some differences with respect to trace shape and intensities. The spectrum in water shows a lower peak intensity at 390 nm compared to the spectrum in THF. This result, already obtained for NP stabilized by SDS, could be attributed to change induced by aggregation as already reported in the literature.[10]

In case of composite particles in water (NP composed of 80:20 $PC_{71}BM$:PCDTBT), the absorption spectra cannot be deconvoluted in the parent spectra of $PC_{71}BM$ and PCDTBT : as can be seen in figure 5, the spectrum of a 80:20 composite particles is not the same as the one of a water dispersion composed of 80wt% of $PC_{71}BM$ particles + 20wt% of PCDTBT particles. Although the absorption peaks of the two components are apparent, their relative intensities change and there is a shift of the $PC_{71}BM$ absorption from 475 nm for the mixture of NPs to 458 nm for the composite NPs. This suggests that the two materials, just like using miniemulsion post-polymerization process, are in intimate contact within one single particle forming composite particles.

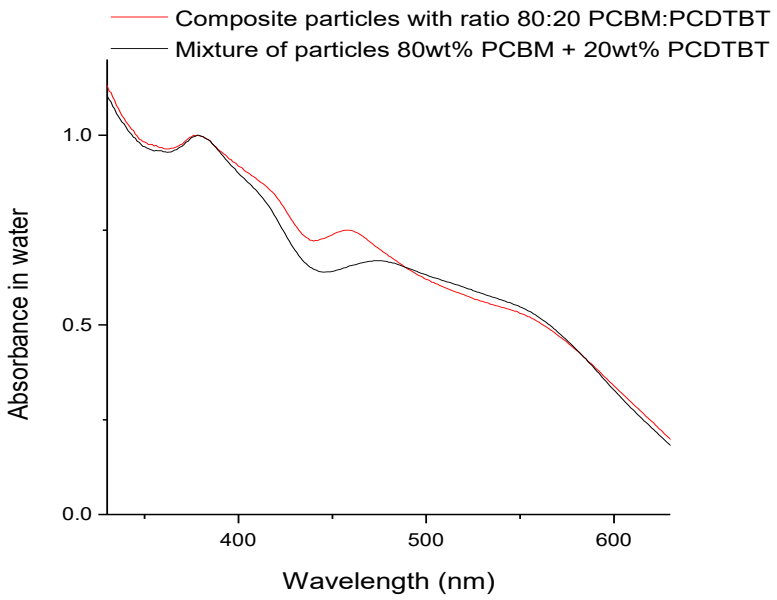

Figure 5 : Absorption spectra of 80:20 $PC_{71}BM$:PCDTBT composite particles and mixture of 80wt% $PC_{71}BM$ + 20 wt% PCDTBT particles in water

Fluorescence spectroscopy provides further proof that both $PC_{71}BM$ and PCDTBT are co-existing in one single particle in water, as illustrated in figure 6 showing the emission spectra of composite particles in water (top) and emission spectra of mixed particles (bottom). For pure PCDTBT, an emission peak is observed between 600 and 800 nm (black line). However, when $PC_{71}BM$ is added in the NP as composite, the fluorescence of the polymer is quenched in any mixture which is not the case when NP of each component are mixed as one can observe an emission peak for the 80wt% $PC_{71}BM$ NPs + 20wt% PCDTBT NPs, 70wt% $PC_{71}BM$ NPs + 30wt% PCDTBT NPs and 60wt% $PC_{71}BM$ NPs + 40wt% PCDTBT NPs. This result proves that in the composite particles the two components are in intimate contact within one single particle.

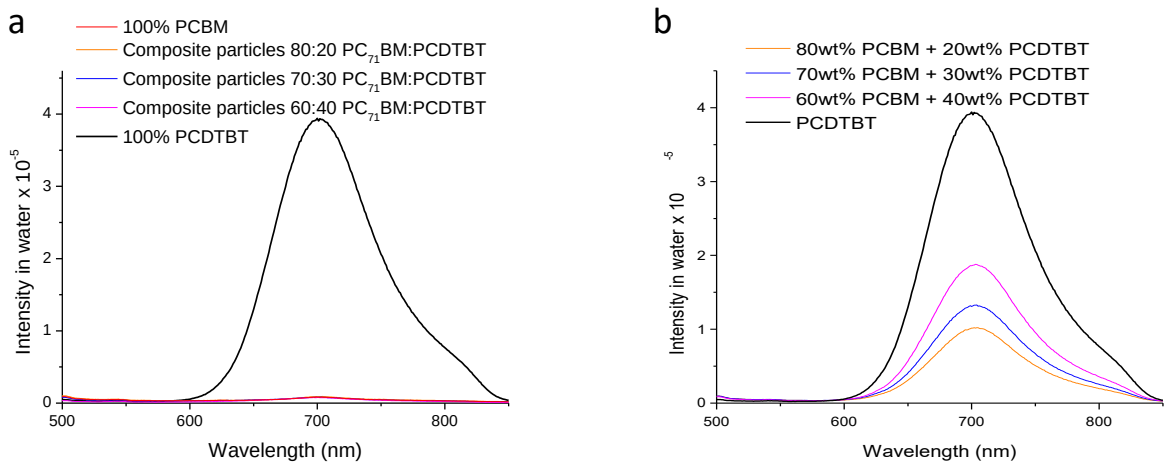

Figure 6 : Photoluminescence of the composite materials (a) and mixture of particles (b) at different ratio of $PC_{71}BM$:PCDTBT in water

To conclude, both absorbance and photoluminescence proved that the composite particles formed in water without stabilizer contained both the donor and the acceptor within one particle.

V.2.4. Study of film formation from $PC_{71}BM$:PCDTBT inks

Above described photoactive inks composed of both $PC_{71}BM$ and PCDTBT within nanoparticles without stabilizer were deposited as thin films using spray-coating deposition in order to form *in fine* an active layer. The spray-coating was chosen due to the low viscosity and low concentration of the inks allowing no matter losses unlike spin-coating. Spray-coating method was also chosen to deposit higher volume of solution (mL) in order to compensate its low concentration.[11] However, as in chapter IV the main disadvantages are the appearance of surface defects (so called "coffee stain effect"[12]) leading to high roughness. Here after are some data regarding the inks spray-coating on a glass substrate which was heated at 100°C on a hot plate during spray. The films were then characterized by AFM.

As can be seen on figure 7, despite the elevated temperature, still below the glass transition or melting temperature of the material materials (Tg~130°C[13] and Tm~200°C [14]),after the spray-coating process the layer is formed of closely packed particles with a high roughness around 30 nm due to the deposition technique. The high roughness can be attributed to the coffee stain effect as can be seen on Figure 8.

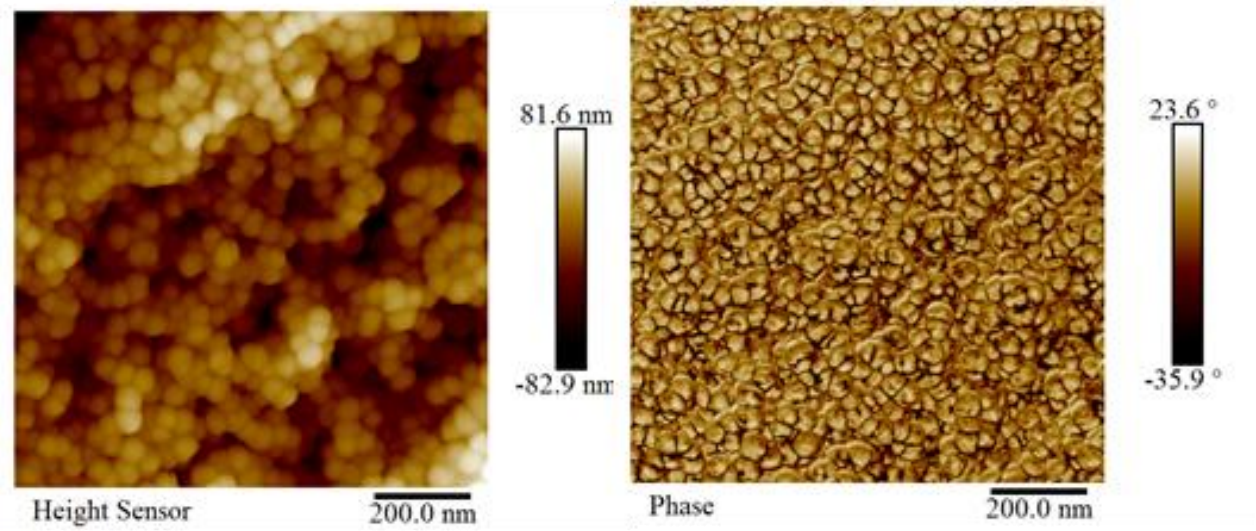

Figure 7 : AFM images height (left) and phase (right) of a composite NP with ratio of 80:20 ($PC_{71}BM$:PCDTBT)

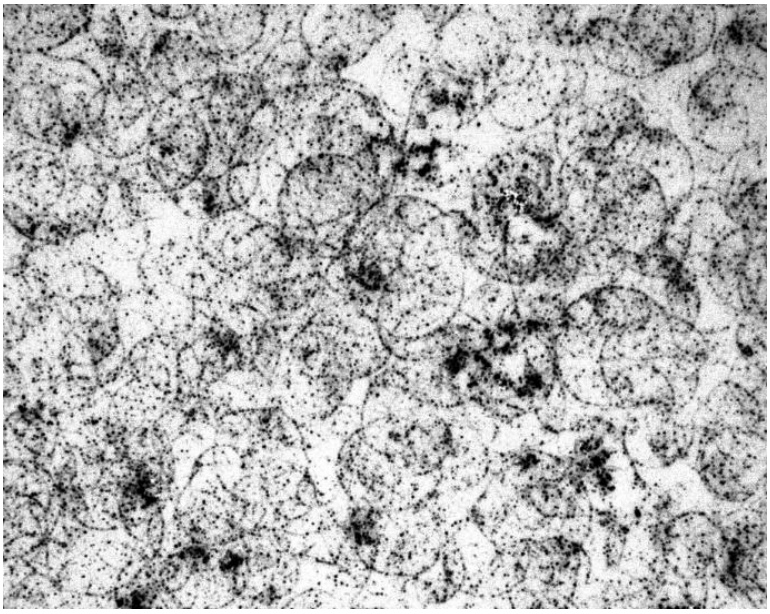

Figure 8 : Microscopy picture of spray-coated film of 80:20 composite particles using black and white filter showing "coffee stain effect"

V.2.5. Study of thermal annealing on $PC_{71}BM$:PCDTBT films

As reported in the previous chapters, annealing is a key step to improve the contact between the particles, improving the mixing between the two compounds and getting more homogeneous films.[15–19] In the literature, thermal annealing led to an increase of the efficiency on P3HT based devices made from nanoprecipitation from 0.34% to 1.09%.[20]

Thermal annealing can be used to decrease the roughness reported for our non-annealed films. Indeed, a high roughness leads to a bad contact between the active layer and the electrodes so it can be detrimental for device efficiency.[20]

Films of 80:20 composite particles were annealed during 4 min from 130°C to 180°C with a step of 10°C. The annealing study can be found in Table 2 based on AFM images. Until 140°C, the NP remained spherical and well-shaped. From 150°C, morphological modification can be noticed: the particles start to merge and to create more interfaces. The roughness decreases with the annealing temperature and reaches a minimum at 160°C. However at 180°C, well above the temperature transition of PCDTBT Tg~130°C[13], the higher roughness is attributed to large size domains.

Table 2 : Annealing study by AFM of 80:20 $PC_{71}BM$:PCDTBT composite particles made by nanoprecipitation

Temperature and time of annealing	AFM Height	AFM Phase	Roughness
NP no annealing	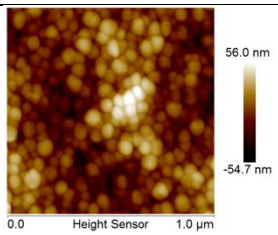	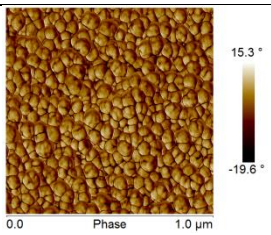	32 nm
130°C 4 min	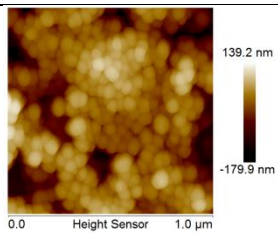	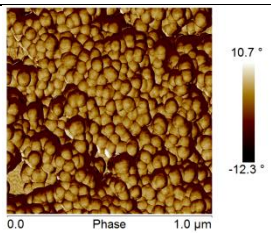	31 nm
140°C 4 min	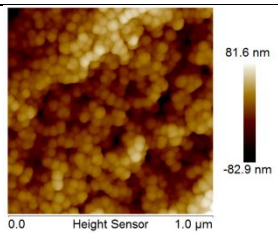	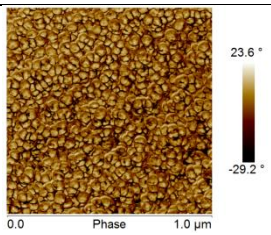	26 nm
150°C 4 min	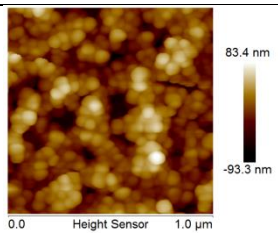	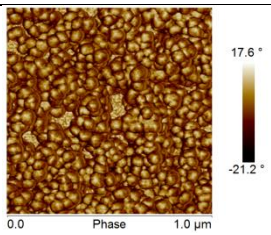	24 nm
160°C 4 min	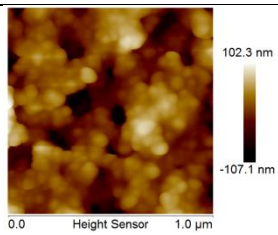	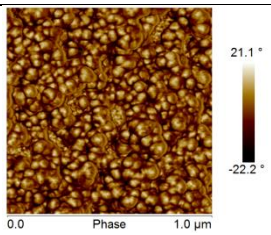	20 nm
170°C 4 min	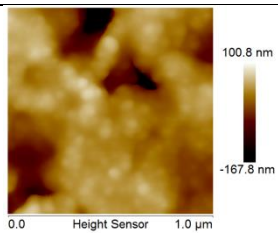	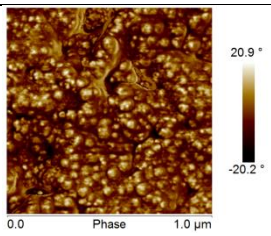	21 nm

180°C 4 min	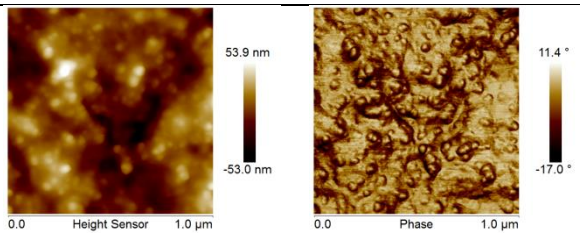	30

Annealing also increases the contact between the particles. Indeed, as shown in figure 9 without annealing, there is low current variation throughout the film measured by conducting-AFM due to poor contact between NP. Instead, an annealing process at 160°C for 4 min gave rise to domains with high (blue) and low current (yellow) (image d figure 9). These conducting pathways are due to a higher contact between particles.

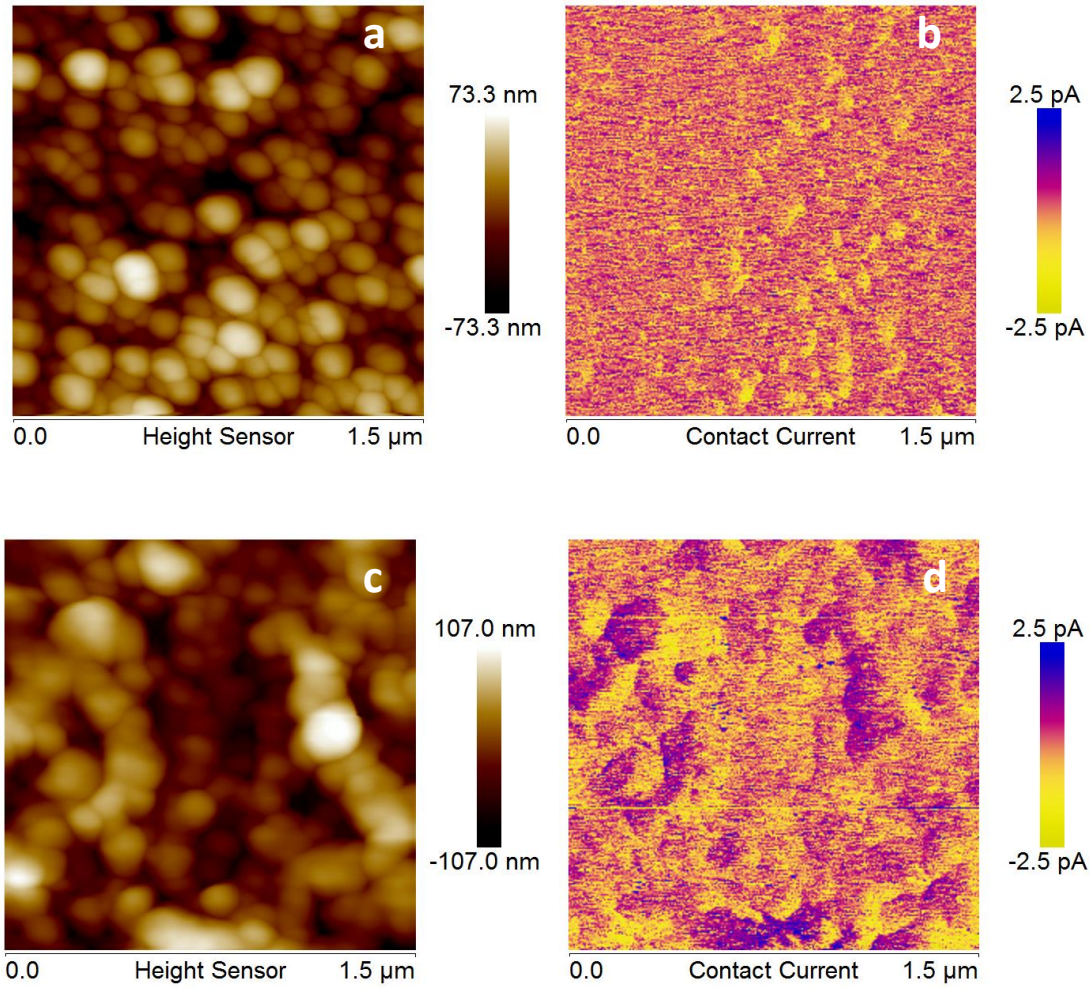

Figure 9 : Conducting-AFM, topography and contact current images of the NP (80:20) without annealing (a and b) and after annealing at 160°C during 4 min (c and d) collected at +1V

V.2.5. Integration of $PC_{71}BM$:PCDTBT inks into solar cells

Photoactive inks composed of both $PC_{71}BM$ and PCDTBT within nanoparticles made by a nanoprecipitation methodwere finally integrated into solar cells. As before, the inverted stack was chosen due to better stability[21] *i.e.* glass/ITO/ZnO/$PC_{71}BM$:PCDTBT(NP)/MoO_3/Ag.

The surface energy of the inks and of the substrate (*i.e.* ZnO) were then measured to comprehend the compatibility between the two layers (see Table 3). For zinc oxide, the surface is hydrophilic which is favorable for a good coating of such ink as can be seen on figure 10.

Table 3 : Surface energies of PCBM, PCDTBT, ZnO and 80:20 blend films

	Θ_{water} (°)	$\Theta_{ethylene\ glycol}$ (°)	$\Theta_{diiodomethane}$ (°)	Surface energy (mN/m)
$PC_{71}BM$	71 ± 2	48 ± 1	11 ± 3	48 ± 0.6
PCDTBT	93 ± 2	70 ± 3	34 ± 1	37 ± 0.3
ZnO on ITO	35 ± 4	26 ± 2	36 ± 1	59 ± 0.8
$PC_{71}BM$:PCDTBT particles on glass	90 ± 2	53 ± 1	9 ± 0.7	50 ± 0.2

Figure 10 : Picture of the NP 80:20 $PC_{71}BM$:PCDTBT sprayed onto ZnO substrate

The non-annealed active layers were dried at 100°C during spray, the other layers were annealed at different temperature during 4 min prior to thermal evaporation of MoO_3 and Ag.

Tables 4, 5, 6 and 7 gather the results obtained for four kinds of NP : 80:20, 70:30, 60:40, 50:50 composite and mixtures of NPs.

V.2.5.a. Effect of the annealing temperature

Table 4 gathers the characteristics of 80:20 $PC_{71}BM$:PCDTBT composite NP-based devices after annealing during 4 min at different temperatures.

Table 4 : Effect of thermal annealing on the properties of the solar cells using 80:20 $PC_{71}BM$:PCDTBT NP (the temperatures are the annealing temperatures during 4 min, the highlighted values are the best results for a given composition)

	Annealing temperature (°C)		Jsc (mA/cm²)	Voc (V)	FF	PCE (%)
1	no annealing	av	1.13E-01	3.54E-02	0.250	3.10E-03
		best	1.50E-01	4.27E-02	0.264	5.10E-03
2	130	av	4.90E-01	5.21E-02	0.215	5.14E-03
		best	5.10E-01	6.42E-02	0.215	5.25E-03
3	140	av	5.11E-01	5.73E-02	0.321	8.13E-03
		best	5.23E-01	1.25E-01	0.321	0.01
4	150	av	5.26E-01	8.80E-02	0.263	0.013
		best	5.35E-01	1.70E-01	0.320	0.29
5	160	av	5.63E-01	2.00E-01	0.355	0.056
		best	5.40E-01	2.63E-01	0.355	0.087
6	170	av	5.70E-01	1.50E-01	0.330	0.042
		best	1.83E+00	1.50E-01	0.330	0.049
7	180	av	8.40E-01	1.43E-01	0.265	0.033
		best	9.40E-01	2.30E-01	0.272	0.059

On 80:20 $PC_{71}BM$:PCDTBT composite NPs (which exhibits the best results in BHJ [6,7]), thermal annealing up to 160°C during 4 min increased the efficiency (PCE) (see Table 4 samples 1 to 5) due to a better conductivity between the particles (highlighted by conductive AFM in figure 9). Above 160°C the performances decreased probably due to the creation of

gross phase segregation. The fill factor (FF) also increased with the annealing temperature up to 160°C which is known to be influenced by the charge recombination.[22] The recombination is decreasing, meaning that the change in the microstructure of the film after annealing is favorable.

As discussed previously, unlike BHJ devices, $PC_{71}BM$:PCDTBT NP-based devices increase in performance upon annealing. The NP structure may provide a more thermally stable alternative to the standard BHJ structure as already reported by Feron *et al*.[23]

V.2.5.b. Influence of the materials'composition

After having found that the best annealing temperature was 160°C during 4 min for the 80:20 composite NP, the influence of the electron acceptor/polymer ratio has been evaluated. Table 5 gathers the properties of composite and blend NP based devices after annealing at 160°C during 4 min.

For the composite particles (80:20 $PC_{71}BM$:PCDTBT, 70:30, 60:40 and 50:50) thermal annealing increased the efficiency up to 160°C which produced the best results for all the composite particles (see appendix Table 8 for detailed measurement). However this behavior is different for mixed particles in which annealing at 160°C did not provide the best efficiencies (see appendix Table 9 for detailed measurement).

Table 5 : Characteristics of solar cells using different natures of NP (composite $PC_{71}BM$:PCDTBT and mixture $PC_{71}BM$+PCDTBT) annealed at 160°C during 4 min (the highlighted values are the best results for a given composition)

	160°C 4 min		Jsc (mA/cm²)	Voc (V)	FF	PCE (%)
1	80:20 $PC_{71}BM$:PCDTBT	av	5.63E-01	2.00E-01	0.355	0.06
		best	5.40E-01	2.63E-01	0.355	0.09
2	80+20	av	9.10E-01	7.42E-02	0.270	0.01
		best	9.10E-01	7.78E-02	0.270	0.01
3	70:30 $PC_{71}BM$:PCDTBT	av	1.65	3.07E-01	0.287	0.19
		best	1.76	5.60E-01	0.334	0.33
4	70+30	av	2.10	1.98E-02	0.268	0.01
		best	2.39	2.75E-02	0.268	0.01
5	60:40 $PC_{71}BM$:PCDTBT	av	1.11	4.78E-01	0.322	0.17
		best	1.17	5.50E-01	0.334	0.22
6	60+40	av	9.20E-01	8.36E-02	0.234	0.02
		best	1.91	1.12E-01	0.306	0.06
7	50:50 $PC_{71}BM$:PCDTBT	av	1.18	4.92E-01	0.322	0.14
		best	1.18	5.00E-01	0.322	0.19
8	50+50	av	1.24	1.13E-01	0.266	0.04
		best	1.40	1.20E-01	0.262	0.04

As for SDS-stabilized particles (chapter III), composite particles provided better efficiencies than mixed ones whatever the $PC_{71}BM$:PCDTBT ratio was. This result was attributed to the size of the domains (equal to the size of the particles~50 nm) created with mixed particles which is well above the exciton diffusion length (~10-20 nm).[24]

Nevertheless, the ratio 70:30 $PC_{71}BM$:PCDTBT gave the best results, which is different from BHJ devices[6,7] in which 80:20 gave the best efficiencies. The performances of 60:40 $PC_{71}BM$:PCDTBT ratio even exceeded those of 80:20 $PC_{71}BM$:PCDTBT. This result is different from what was obtained in case of SDS-stabilized particles.

In case of mixed particles annealing at 180°C for a given time of 4 minutes gave the best efficiencies as can be seen on Table 6. A higher temperature is needed to increase the number of interfaces between $PC_{71}BM$ and PCDTBT because they both have high transition temperatures (PCDTBT Tg~130°C[13] and $PC_{71}BM$ Tm~200°C).[14]

Table 6 : Characteristics of the solar cells using different mixtures of NPs ($PC_{71}BM$ + PCDTBT) annealed at 180°C during 4 min

180°C 4 min			Jsc (mA/cm²)	Voc (V)	FF	PCE (%)
1	80+20	av	6.40E-01	7.00E-02	0.279	0.03
		best	6.40E-01	8.00E-02	0.279	0.05
2	70+30	av	9.40E-01	5.00E-02	0.248	0.01
		best	9.40E-01	5.00E-02	0.267	0.01
3	60+40	av	1.74	1.03E-01	0.285	0.06
		best	2.39	1.70E-01	0.258	0.11
4	50+50	av	2.30	1.70E-01	0.258	0.10
		best	2.39	1.70E-01	0.262	0.11

V.2.5.b. Influence of the thickness of the active layer

Giving the fact that good results were obtained on an active layer based on composite NP (70:30 $PC_{71}BM$:PCDTBT composition) after annealing at 160 °C for 4 min we chose to evaluate the effect of the active layer thickness. Results are gathered in Table 7.

In fact, the thickness was varied by changing the spray-coated volume and the active layers were annealed at 160°C 4 min since it provided the best efficiencies (Table 5 and Table 8 in appendix).

Table 7 : Influence of the active layer thickness on the properties of the solar cells using 70:30 $PC_{71}BM$:PCDTBT composite NP annealed at 160°C during 4 min (the highlighted values are the best results for a given composition)

70:30 annealed 160°C 4 min			Jsc (mA/cm²)	Voc (V)	FF	PCE (%)
1	50	average	2.24	1.10E-01	0.297	0.11
		best	2.24	1.70E-01	0.302	0.11
2	75	average	2.01	2.20E-01	0.283	0.11
		best	2.64	2.20E-01	0.283	0.13
3	100	average	1.65	3.08E-01	0.287	0.19
		best	1.76	5.60E-01	0.334	0.33
4	125	average	2.05	1.73E-01	0.276	0.11
		best	2.33	4.10E-01	0.280	0.26
5	150	average	1.73	1.87E-01	0.283	0.09
		best	1.78	3.10E-01	0.283	0.15
6	200	average	0.10	5.00E-04	0.207	1.00E-04
		best	0.20	8.00E-04	0.207	1.80E-04

The thickness which provided the best efficiency was around 100 nm for 70:30 composite NP and is the same for all the different blends which have been tested (see appendix Table 10 for detailed measurements). This result was the same than what was found in the literature for BHJ-based solar cells providing the best compromise between good absorbance and low recombination.[25]

The lower performance obtained for the NP-based devices without stabilizer compared to the BHJ ones can be attributed to the deposition method which gives high

roughness even after annealing (20 nm vs <4 nm using spin-coating with SDS-stabilized particles). Most of the NP based solar cells made by nanoprecipitation are deposited by spin-coating requiring multiple steps to compensate the low concentration of the solution but leads to lower roughness.[3,26] A new process able to deposit bigger solution quantity with limited matter losses (unlike spin-coating) and producing lower film roughness has to be implemented such as Dr Blading for example whose roughness are typically in the range of few nanometers.[27] Unfortunately this technique requires a minimum viscosity of 20 mPa.s which is far from our inks viscosity close to the one of water of 1 mPa.s due to the low concentration of matter. Further formulation would there be required in that case.

Ultrasonic spray[28] is another technique that could be used to reduce the roughness of our films. In this process a tip is vibrating at an ultrasonic frequency leading to break up of the solution into uniformly sized droplets and then a N_2 gas flow directs them towards the substrate. Afterwards the droplets merge onto the substrate to form a continuous layer. After evaporation of the solvent, a continuous film is formed (see figure 11).

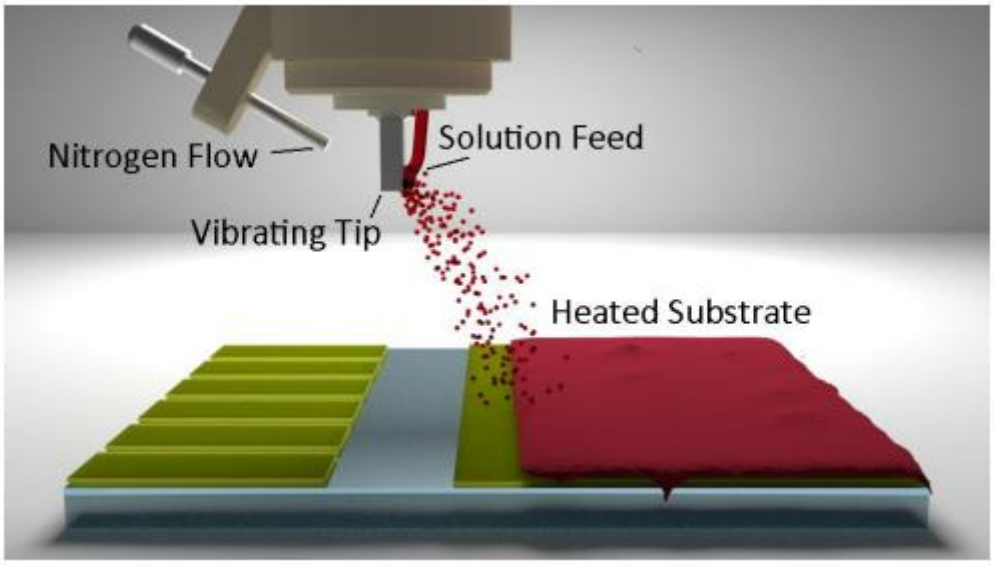

Figure 11 : Formation of a polymer film through ultrasonic spray coating

This technique led to lower roughness than using classical spray-coating : for example for P3HT:PCBM, roughnesses of 24.1 nm[29] and up to 52 nm[30] were obtained using classical spray-coating against 4 nm[31] down to 1.1 nm[32] for the ultrasonic spray.

V.3. Conclusion

In this chapter composite NP of $PC_{71}BM$:PCDTBT were synthesized by nanoprecipitation without stabilizer. The properties of the NP were studied and they were then integrated into solar cells.

The nanoprecipitation was chosen to successfully produce high molar mass PCDTBT particles as well as composite $PC_{71}BM$:PCDTBT particles without stabilizer with tunable size depending on the synthetic conditions in water.

Based on the optical properties, the two components are co-existing within one single particle.

The optimum thermal annealing was found at 160°C during 4 minutes to increase the contact between the particles (supported by conducting AFM) and improve the mixing, creating more interfaces. After integration into solar cells, the thermal annealing led to a strong increase in the efficiency as well as the fill factor. The best device composed of 70:30 composite NP led to a power conversion efficiency of 0.33%. These relatively low performances can be explained by the deposition method which produces high film roughness leading to bad contact between the active layer and the electrodes.

A new deposition method could be used to deposit bigger volume with lower roughness using ultrasonic spray for example.

V.4. References

[**1**] H. Shimizu, M. Yamada, R. Wada, M. Okabe, *Polym. J*, **2007**, *40*, 33.
[**2**] C. Wu, C. Szymanski, J. McNeill, *Langmuir*, **2006**, *22*, 2956.
[**3**] S. Gärtner, M. Christmann, S. Sankaran, H. Röhm, E.-M. Prinz, F. Penth, A. Pütz, A. E. Türeli, B. Penth, B. Baumstümmler, A. Colsmann, *Adv. Mater.*, **2014**, *26*, 6653.
[**4**] S. Sankaran, K. Glaser, S. Gärtner, T. Rödlmeier, K. Sudau, G. Hernandez-Sosa, A. Colsmann, *Org. Electron.*, **2016**, *28*, 118.
[**5**] S. Chambon, C. Schatz, V. Sebire, B. Pavageau, G. Wantz, L. Hirsch, *Mater. Horizons*, **2014**, *1*, 431.
[**6**] T. Wang, A. J. Pearson, A. D. F. Dunbar, P. A. Staniec, D. C. Watters, H. Yi, A. J. Ryan, R. A. L. Jones, A. Iraqi, D. G. Lidzey, *Adv. Funct. Mater.*, **2012**, *22*, 1399.
[**7**] V. S. Murugesan, S. Ono, N. Tsuda, J. Yamada, P.-K. Shin, S. Ochiai, *Int. J. Photoenergy*, **2015**, *2015*, 1.
[**8**] S. R. Acharya, P. R. V Reddy, *Asian J. Pharm. Sci.*, **2016**, *11*, 427.
[**9**] S. Hornig, T. Heinze, C. R. Becer, U. S. Schubert, *J. Mater. Chem.*, **2009**, *19*, 3838.
[**10**] T. Yamamoto, D. Komarudin, M. Arai, B. Lee, H. Suganuma, N. Asakawa, Y. Inoue, K. Kubota, S. Sasaki, *J. Am. Chem. Soc.*, **1998**, *120*, 2047.
[**11**] E. Lokensgard, *Industrial Plastics, Theory and Applications*, **2016**.
[**12**] R. D. Deegan, O. Bakajin, T. F. Dupont, G. Huber, S. R. Nagel, T. A. Witten, *Nature*, **1997**, *389*, 827.
[**13**] N. Blouin, A. Michaud, D. Gendron, S. Wakim, E. Blair, R. Neagu-Plesu, M. Belletête, G. Durocher, Y. Tao, M. Leclerc, *J. Am. Chem. Soc.*, **2008**, *130*, 732.
[**14**] Y. Ning, L. Lv, Y. Lu, A. Tang, Y. Hu, Z. Lou, F. Teng, Y. Hou, *Int. J. Photoenergy*, **2014**, *2014*, 354837.
[**15**] T. Kietzke, D. Neher, M. Kumke, R. Montenegro, K. Landfester, U. Scherf, *Macromolecules*, **2004**, *37*, 4882.
[**16**] Y. Lee, S. H. Lee, K. Kim, J. W. Lee, K.-Y. Han, J. Kim, J. Joo, *J. Mater. Chem.*, **2012**, *22*, 2485.
[**17**] A. Stapleton, B. Vaughan, B. Xue, E. Sesa, K. Burke, X. Zhou, G. Bryant, O. Werzer, A. Nelson, A. L. David Kilcoyne, L. Thomsen, E. Wanless, W. Belcher, P. Dastoor, *Sol. Energy Mater. Sol. Cells*, **2012**, *102*, 114.
[**18**] N. P. Holmes, M. Marks, P. Kumar, R. Kroon, M. G. Barr, N. Nicolaidis, K. Feron, A. Pivrikas, A. Fahy, A. D. de Z. Mendaza, A. L. D. Kilcoyne, C. Müller, X. Zhou, M. R. Andersson, P. C. Dastoor, W. J. Belcher, *Nano Energy*, **2016**, *19*, 495.
[**19**] B. Vaughan, E. L. Williams, N. P. Holmes, P. Sonar, A. Dodabalapur, P. C. Dastoor, W. J. Belcher, *Phys. Chem. Chem. Phys.*, **2014**, *16*, 2647.
[**20**] D. Darwis, N. Holmes, D. Elkington, A. L. David Kilcoyne, G. Bryant, X. Zhou, P. Dastoor, W. Belcher, *Sol. Energy Mater. Sol. Cells*, **2014**, *121*, 99.
[**21**] S. K. Hau, H.-L. Yip, N. S. Baek, J. Zou, K. O'Malley, A. K.-Y. Jen, *Appl. Phys. Lett.*, **2008**, *92*, 253301.
[**22**] R. C. I. MacKenzie, T. Kirchartz, G. F. A. Dibb, J. Nelson, *J. Phys. Chem. C*, **2011**, *115*, 9806.
[**23**] K. Feron, S. Ulum, E. Sesa, B. B. Gong, W. J. Belcher, X. Zhou, C. . Fell, P. C. Dastoor, *J. Appl. Phys.*, **2014**, *116*, 124502.
[**24**] C. R. McNeill, S. Westenhoff, C. Groves, R. H. Friend, N. C. Greenham, *J. Phys. Chem. C*, **2007**, *111*, 19153.
[**25**] J. Seok, T. J. Shin, S. Park, C. Cho, J.-Y. Lee, D. Yeol Ryu, M. H. Kim, K. Kim, *Sci. Rep.*, **2015**, *5*, 8373.
[**26**] D. Darwis, D. Elkington, E. Sesa, N. Cooling, G. Bryant, X. Zhou, W. Belcher, P. Dastoor, in *AIP Conf. Proc.*, **2011**, pp. 120.
[**27**] C. N. Hoth, P. Schilinsky, S. A. Choulis, S. Balasubramanian, C. J. Brabec, in *Appl. Org. Print. Electron.* (Ed.: E. Cantatore), New York, **2013**, pp. 27.
[**28**] N. W. Scarratt, The Fabrication and Scale-Up of Organic Photovoltaic Devices via Ultrasonic Spray Coating, University of Sheffield, **2015**.
[**29**] C. N. Hoth, R. Steim, P. Schilinsky, S. A. Choulis, S. F. Tedde, O. Hayden, C. J. Brabec, *Org. Electron.*, **2009**, *10*, 587.
[**30**] D. Vak, S. S. Kim, J. Jo, S. H. Oh, S. I. Na, D. Y. Kim, J. Kim, *Appl. Phys. Lett.*, **2007**, *91*, 081102.
[**31**] K. X. Steirer, J. J. Berry, M. O. Reese, M. F. A. M. van Hest, A. Miedaner, M. W. Liberatore, R. T. Collins, D. S. Ginley, *Thin Solid Films*, **2009**, *517*, 2781.
[**32**] C. Girotto, D. Moia, B. P. Rand, P. Heremans, *Adv. Funct. Mater.*, **2011**, *21*, 64.
[**33**] D. K. Owens, R. C. Wendt, *J. Appl. Polym. Sci.*, **1969**, *13*, 1741.

V.5. Appendix

Table 8 : Effect of annealing temperature on performance of composite $PC_{71}BM$:PCDTBT NP-based solar cells, the highlighted values are the best results for a given composition

Composite ratio of $PC_{71}BM$:PCDTBT NP	Annealing temperature	Jsc (mA/cm²)	Voc (V)	FF	PCE (%)
80:20 $PC_{71}BM$:PCDTBT	No	0.11	0.03	0.328	0.0031
	130	0.49	0.05	0.215	0.0051
	140	0.51	0.05	0.321	0.008
	150	0.53	0.09	0.263	0.013
	160	0.56	0.20	0.355	0.056
	170	0.57	0.15	0.329	0.042
	180	0.84	0.14	0.265	0.033
70:30 $PC_{71}BM$:PCDTBT	No	0.23	0.03	0.266	0.0092
	130	1.39	0.07	0.265	0.012
	140	1.83	0.11	0.246	0.04
	150	1.82	0.14	0.272	0.074
	160	1.65	0.31	0.287	0.1896
	170	1.28	0.48	0.322	0.1365
	180	2.56	0.04	0.242	0.0243
60:40 $PC_{71}BM$:PCDTBT	No	0.07	0.01	0.233	0.0066
	130	0.25	0.08	0.247	0.0091
	140	0.54	0.20	0.348	0.033
	150	0.86	0.17	0.307	0.052
	160	1.11	0.48	0.322	0.173
	170	1.69	0.37	0.276	0.1528
	180	1.97	0.23	0.288	0.1412
50:50 $PC_{71}BM$:PCDTBT	No	0.09	0.05	0.241	0.0012
	130	0.12	0.06	0.272	0.008
	140	0.19	0.10	0.268	0.023
	150	0.39	0.10	0.307	0.054
	160	1.18	0.49	0.322	0.1365
	170	1.21	0.42	0.329	0.107
	180	1.35	0.18	0.286	0.0803

Table 9 : Effect of annealing temperature on performance of mixture of $PC_{71}BM$ + PCDTBT NP-based solar cells, the highlighted values are the best results for a given composition

Mixture ratio of NP of $PC_{71}BM$ + PCDTBT	Annealing temperature	Jsc (mA/cm^2)	Voc (V)	FF (%)	PCE (%)
80+20	No	0.11	0.00031	0.249	0.00007
	130	0.13	0.0008	0.256	0.00025
	140	0.25	0.08	0.324	0.002
	150	0.78	0.05	0.284	0.008
	160	0.91	0.07	0.270	0.01
	170	0.68	0.057	0.285	0.022
	180	0.64	0.07	0.279	0.034
70+30	No	0.09	0.00051	0.258	0.00012
	130	0.12	0.001	0.262	0.004
	140	1.98	0.06	0.342	0.005
	150	2.31	0.02	0.284	0.007
	160	2.1	0.01	0.268	0.008
	170	1.7	0.02	0.299	0.01
	180	0.94	0.05	0.248	0.012
60+40	No	0.12	0.00014	0.260	0.00008
	130	0.13	0.005	0.271	0.006
	140	2	0.08	0.274	0.0097
	150	2.45	0.09	0.310	0.015
	160	0.92	0.08	0.234	0.02
	170	1	0.1	0.252	0.03
	180	1.74	0.103	0.285	0.058
50+50	No	0.1	0.0001	0.282	0.00007
	130	0.14	0.006	0.324	0.0065
	140	1.98	0.1	0.319	0.0134
	150	2.43	0.1	0.271	0.025
	160	1.24	0.11	0.266	0.036
	170	1.55	0.21	0.270	0.088
	180	2.3	0.17	0.258	0.103

Table 10 : Effect of active layer thickness on performance of composite $PC_{71}BM$:PCDTBT NP-based solar cells (the highlighted values are the best results for a given composition)

Composite ratio of $PC_{71}BM$:PCDTBT NP	Thickness	Jsc (mA/cm²)	Voc (V)	FF	PCE (%)
80:20 $PC_{71}BM$:PCDTBT	50	4.00E-01	5.00E-02	0.218	0.005
	75	7.90E-01	1.60E-01	0.231	0.03
	100	5.63E-01	2.00E-01	0.355	0.056
	125	8.30E-01	8.00E-02	0.246	0.016
	150	6.20E-01	9.00E-02	0.364	0.014
	200	1.00E-01	2.00E-04	0.199	0.00005
70:30 $PC_{71}BM$:PCDTBT	50	2.24	1.10E-01	0.298	0.1064
	75	2.01	2.20E-01	0.283	0.115
	100	1.65	3.08E-01	0.287	0.1896
	125	2.05	1.73E-01	0.276	0.11
	150	1.73	1.87E-01	0.283	0.0898
	200	1.00E-01	5.00E-04	0.207	0.0001
60:40 $PC_{71}BM$:PCDTBT	50	1.91	1.00E-02	0.183	0.008
	75	3.41	1.10E-01	0.284	0.1052
	100	1.11	4.78E-01	0.322	0.173
	125	3.45	7.00E-02	0.306	0.07
	150	2.31	5.00E-02	0.267	0.03
	200	1.20E-01	1.40E-04	0.214	0.00009
50:50 $PC_{71}BM$:PCDTBT	50	1.84	4.00E-02	0.293	0.02
	75	1.84	9.00E-02	0.256	0.04
	100	1.19	4.93E-01	0.322	0.1365
	125	1.31	1.40E-01	0.256	0.045
	150	9.20E-01	8.00E-02	0.234	0.02
	200	1.00E-01	1.00E-04	0.208	0.00007

V.6. Experimental Section

V.6.1. Materials

9-(9-Heptadecanyl)-9H-carbazole-2,7-diboronic acid bis(pinacol) ester (97%), 4,7-Bis(2-bromo-5-thienyl)-2,1,3-benzothiadiazole (99+%), and THF (99.5+%) were purchased from Sigma Aldrich. $PC_{71}BM$ was purchased from Solaris (99+%). All chemicals were used as received unless otherwise stated.

V.6.2. Reactions

The reactions were performed under an Argon atmosphere using standard schlenk techniques.

V.6.2.a. PCDTBT synthesis

See chapter III for the detailed synthesis

V.6.2.b. Typical procedure for the $PC_{71}BM$:PCDTBT nanoparticles made by nanoprecipitation

PCDTBT and $PC_{71}BM$ were solubilized in 10mL of THF. 4 mL of this solution were quickly introduced into 20 mL of water stirred at 50°C and 750 rpm. After 2 hours under argon flux, the THF was evaporated leading to aqueous nanoparticles dispersion.

III.6.3. Methods

Dynamic light scattering (DLS) on diluted dispersion samples was performed on a Cordouan Particle Size Analyzer Vasco. The autocorrelation function was analyzed using the Cordouan dispersion technology software algorithm to obtain number-weighted particle sizes.

Size exclusion chromatography (SEC) was performed in TCB at 150°C with a flow rate of 1 $mL.min^{-1}$ using Agilent PL gel MIXED C column (pore size 5 µm) and a Agilent PL gel guard-column. The elution times were converted into molar masses using a calibration curve based on low dispersity polystyrene standards.

Absorption spectra were acquired using a Shimadzu spectrophotometer UV-3600 while *emission spectra* were measured using a Horiba Scientific Fluoromax-4 spectrofluorometer.

TEM images were obtained on Formvar grids with a Transmission Electron Microscope (H7650, HITACHI (accelerate voltage 120 kV), using high contrast mode. Dispersed nanoparticles were deposited onto a copper grid for TEM analysis.

Surface tension was measured using drop shape analysis technique on a pendant drop tensiometer (Krüss DSA-100) while *surface energies* were determined by measuring contact angle between three solvents: water, diiodomethane and ethylene glycol and the polymer film. The surface energy is calculated using Owens-Wendt model.[33]

AFM Characterization: Atomic force microscopy (AFM Dimension FastScan, Bruker) was used in tapping mode to characterize the surface morphology of the samples. Silicon cantilevers (Fastscan-A) with a typical tip radius of ≈5 nm, a spring constant of 18 N m−1 and a cantilever resonance frequency of about 1.4 MHz were used.

Conducting AFM (c-AFM) measurements were performed with a Dimension ICON (Bruker) equipped with a PeakForce TUNA module. Platinum–iridium-coated probes (SCM-PIT, Bruker) with a spring constant of 2.8 N m^{-1} and resonant frequency of 75 kHz were used. For c-AFM measurements, a DC bias of 5V was applied between the sample and the tip.

Devices fabrication: Inverted solar cells have been fabricated with the following structure: Glass/ITO/ZnO/active layer/MoO_3/Ag, the active layer being composed of either $PC_{71}BM$:PCDTBT nanoparticles (NP) or $PC_{71}BM$:PCDTBT in bulk hetero junction (BHJ). The Indium tin oxide (ITO)-coated glass substrates, purchased from Vision Tek, with a sheet resistance of ~10 $\Omega.sq^{-1}$ are successively cleaned for 10 min in acetone, ethanol and isopropanol in an ultrasonic bath.

196 mg of zinc acetate dehydrate was mixed with 54 µL of ethanolamine in 6 mL of absolute ethanol and stirred at 45 °C for 2 hours. The zinc oxide (ZnO) layer was prepared by spin-coating this solution at 2000 rpm for 60 s followed by annealing at 180°C for 1 hour in air leading to a 60 nm thick layer. $PC_{71}BM$:PCDTBT solutions (for BHJ) were prepared in chloroform with a concentration of 40 $mg.mL^{-1}$ (1:4 ratio).

BHJ layers were spin-coated in a glove box at 2000 rpm during 60 s with a resulting $PC_{71}BM$:PCDTBT thickness of 80 nm.

NP layers were spin-coated in air at 600 rpm during 60 s followed by a 3000 rpm step for 3 s leading to a 70 nm thick layer. The films were dried at 100°C for 2 min to evaporate the remaining water and then transferred into a vacuum chamber for the MoO_3/Ag evaporation.

MoO_3 (10nm) and Ag (80nm) were successively thermally-evaporated at deposition rates of 0.1 $nm.s^{-1}$ and 0.2-0.4$nm.s^{-1}$ respectively under secondary vacuum (10^{-6}mbar). The solar cells' active surface area is 10 mm^2. The devices were characterized using a K.H.S. Solar Cell test-575 solar simulator with AM1.5G filters set at 100 $mW.cm^{-2}$ with a calibrated radiometer (IL

1400BL). Labview controlled Keithley 2400 SMU enabled the current density-voltage (J-V) curves measurements.

- Vue d'ensemble du chapitre V -

Ce cinquième chapitre discute de la synthèse de particules composite $PC_{71}BM$:PCDTBT par nano-précipitation (voir figure 1).

Cette méthode ne nécessite aucun stabilisant qui pourrait détériorer les performances une fois les particules intégrées en dispositif.

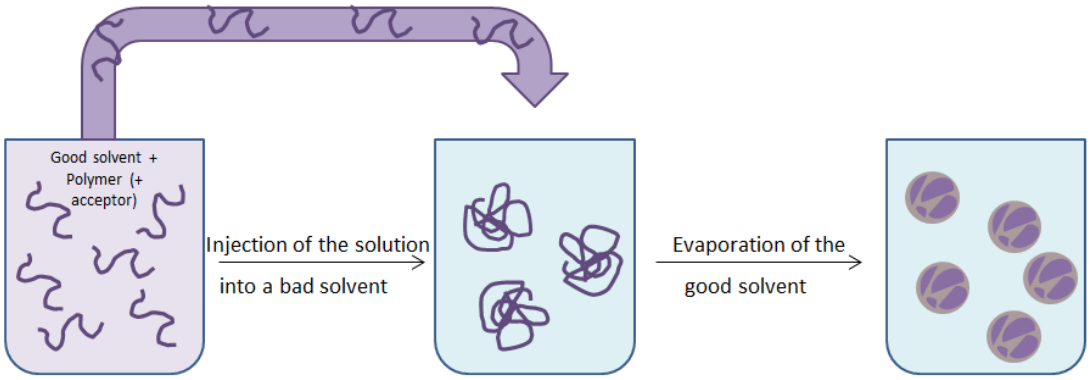

Figure 1 : Procédé de synthèse de particules de $PC_{71}BM$ et PCDTBT par nano-précipitation

Tout d'abord les paramètres du procédé tels que la concentration en espèces actives (initiale et finale), la vitesse d'agitation et la température du mauvais solvant ont été variés pour atteindre une concentration finale suffisante pour la formation d'un film continu et une taille de particules d'environ 50 nm.

Ensuite, comme dans le cas du procédé de mini-émulsion post-polymérisation, l'étude des propriétés optoélectroniques a montré que les deux composés se trouvent être en contact intime au sein d'une même particule. Ce résultat a notamment été confirmé par l'extinction de la fluorescence en solution pour les particules synthétisées à partir d'une solution mère contenant à la fois le polymère et l'accepteur d'électron (voir figure 2).

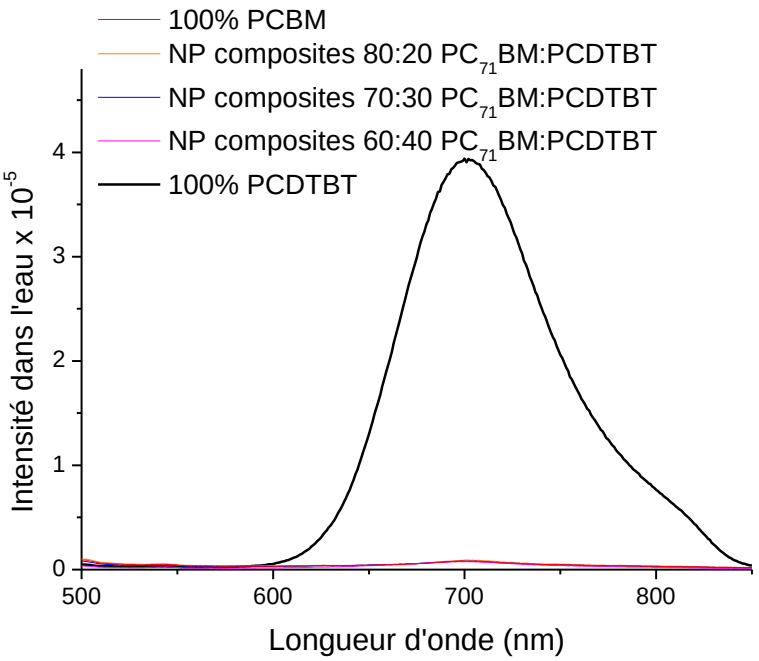

Figure 2 : Spectre de photoluminescence de particules composites à différentes proportions en $PC_{71}BM$:PCDTBT excitées à 395 nm dans l'eau

Ces encres photoactives composées de nanoparticules de $PC_{71}BM$ et PCDTBT ont été déposées par spray en films d'épaisseurs variables. Comme l'atteste le cliché d'AFM (voir figure 3) la couche active est composée d'un empilement relativement compact et homogène de nanoparticules.

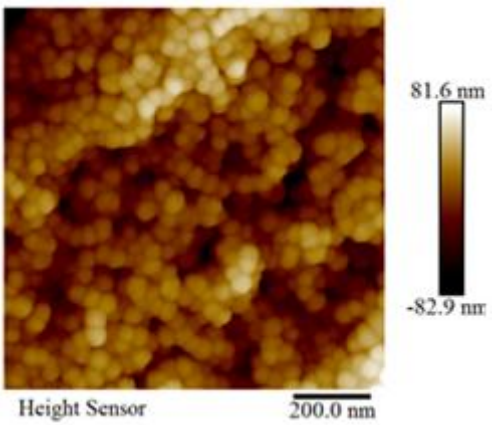

Figure 3 : Image AFM de topographie des particules composites $PC_{71}BM$:PCDTBT en proportions 80:20

Un recuit thermique a été nécessaire pour augmenter le contact entre les particules, améliorer le mélange entre les deux composés et obtenir un film moins rugueux. La température de recuit idéale se situe à 160°C.

Finalement, l'étude de la morphologie des films et de leur recuit a permis d'obtenir une couche active qui a par la suite été intégrée au sein d'un dispositif cellule solaire inverse. Les résultats obtenus sont rassemblés dans le tableau 1.

Tableau 1 : Caractéristiques des cellules photovoltaïques intégrant différentes natures de particules (composite (c) ou mélange (m)) et différentes proportions de $PC_{71}BM$:PCDTBT , les températures indiquées correspondent au recuit appliqué pendant 4 min. Pour chaque échantillon les valeurs moyennes et record ont été reportées

Echantillon			Jsc (mA/cm)	Voc (V)	FF	PCE (%)
1	NP c (80:20) (100 nm)	moyenne	1,13E-01	3,54E-02	0,250	3,10E-03
		meilleure	1,50E-01	4,27E-02	0,264	5,10E-03
2	NP c (80:20) 160°C (100 nm)	moyenne	5,63E-01	2,00E-01	0,355	0,06
		meilleure	5,40E-01	2,63E-01	0,355	0,09
3	NP c (70:30) 160°C (100 nm)	moyenne	1,65	3,07E-01	0,287	0,19
		meilleure	1,76	5,60E-01	0,334	0,33
4	NP m (70+30) 160°C (100 nm)	moyenne	2,10	1,98E-02	0,268	0,01
		meilleure	2,39	2,75E-02	0,268	0,01
5	NP c (70:30) 160°C (75 nm)	moyenne	2,24	1,10E-01	0,297	0,11
		meilleure	2,64	1,70E-01	0,302	0,11
6	NP c (70:30) 160°C (125 nm)	moyenne	2,05	1,73E-01	0,276	0,11
		meilleure	2,33	4,10E-01	0,280	0,26

L'étude des paramètres photovoltaïques sur des particules de différentes natures (composites et en mélange) a permis de tirer plusieurs conclusions :

- Le recuit à 160°C permet de multiplier l'efficacité jusqu'à 18 fois pour des particules composites de composition (80 :20) (échantillon 1 par rapport au 2).
- Les particules de composition 70 :30 présentent de meilleures efficacités que celles de composition 80 :20 (échantillon 2 par rapport au 3).
- Les particules composites offrent de bien meilleurs résultats que les particules mélangées dus à la taille des domaines formés (échantillon 3 par rapport au 4).
- L'épaisseur idéale de la couche active se situe autour de 100 nm offrant les meilleures performances photovoltaïques (échantillons 3 par rapport au 5 et 6).

Conclusion générale

Ce travail de thèse s'est inscrit dans un contexte écologique pour la fabrication de cellules solaires organiques. Mon objectif principal a été le développement de matériaux photoactifs dispersés dans des solvants non-halogénés non aromatiques afin de faciliter leur enduction.

La première étape de ce travail a consisté en la synthèse de particules de PCDTBT en milieu hétérogène par polymérisation en dispersion dans le propan-1-ol. Nous avons regardé l'influence des différents paramètres de synthèse sur la taille des particules obtenues. Malheureusement quel que soit le mode opératoire, la masse molaire obtenue est faible conduisant à des rendements de conversion énergétiques très faibles.

Nous avons ensuite synthétisé des particules composites de $PC_{71}BM$ et de PCDTBT par miniemulsion post-polymérisation dans l'eau (dispersion secondaire). Cette méthode a pour avantage d'utiliser le polymère brut synthétisé classiquement. Cette technique a permis d'obtenir une taille de nanoparticules d'environ 50 nm composées des deux entités. Le dépôt à la tournette de ces solutions suivi d'un recuit thermique a permis d'atteindre un rendement de conversion de 0,94% après 4 minutes à 140°C contre 0,05% avant recuit. Cette augmentation du rendement de conversion peut être attribuée à une meilleure conductivité entre les particules comme en atteste une mesure par AFM conductrice.

Un autre stabilisant de type copolymère semiconducteur à blocs a ensuite été développé par chimie click pour étudier son influence sur les films à base de NPs. En effet, nous avons entrepris de synthétiser un copolymère à base de P3HT semi-conducteur et de PEO pour son affinité avec le milieu dispersant polaire (eau). Des particules plus grosses de diamètre de 150 nm ont été préparées *via* miniémulsion post-polymérisation dans l'eau. Ces encres ont été utilisées pour fabriquer la couche active de cellules solaires par dépôt au spray. La taille des particules obtenues n'a pas permis d'atteindre des rendements de conversion satisfaisants (0,11% pour la meilleure cellule) en raison de trop nombreuses recombinaisons.

L'utilisation de particules sans stabilisant a aussi été étudiée par le procédé de nano-précipitation. Cette technique a permis d'atteindre des particules d'environ 50 nm avec des propriétés contrôlées comme dans le cas de la miniemulsion post-polymérisation puisque le polymère brut synthétisé classiquement est utilisé. Des encres de différentes compositions ont été déposées par spray pour fabriquer la couche active de cellules solaires. La grande rugosité engendrée par ce type de dépôt n'a pas permis d'atteindre des rendements de

conversion satisfaisants (0,33% pour la meilleure cellule) en raison de mauvais contacts entre les différentes couches.

Ce projet de recherche a montré que l'utilisation de nanoparticules dispersées dans des solvants plus respectueux de l'environnement est une voie prometteuse pour contrôler la morphologie de la couche active et s'affranchir de solvants toxiques lors du dépôt de cette dernière pour la fabrication de cellules solaires organiques. En complément de cette étude, il conviendrait de développer plus fortement la voie originale de stabilisation de particules par copolymères à blocs semi-conducteur. En effet, d'autres masses molaires et d'autres proportions pourraient être essayées pour trouver un meilleur compromis entre une bonne solubilité dans l'eau et de bonnes propriétés semi-conductrices.

Bien que cette approche soit prometteuse, il reste à valider de nombreux points avant de transférer ces méthodes sur de grandes surfaces flexibles. Il faut nécessairement atteindre des rendements de 10% minimum pour que des cellules solaires organiques soient rentables par rapport à leurs homologues à base de silicium.

Parmi les perspectives possibles de ce travail, nous pourrions proposer d'étudier l'universalité des procédés utilisés pour la fabrication de NP à base de différentes molécules/polymères photoactifs. Le PCDTBT pourrait par exemple être remplacé par un polymère à très faible largeur de bande. Nous pourrions nous demander quel impact aurait le remplacement d'hétérojonctions volumiques tout-polymères par des nanoparticules composées de deux polymères permettant d'utiliser un recuit thermique doux pour former un réseau interpénétré.

- Communications -

Publications

L. Parrenin, C. Brochon, G. Hadziioannou, E. Cloutet, "Low Bandgap Semiconducting Copolymer Nanoparticles by Suzuki Cross-Coupling Polymerization in Alcoholic Dispersed Media", **Macromolecular Rapid Communication 2015, Vol 36, Issue 20, DOI: 10.1002/marc.201500324**

L. Parrenin, G. Laurans, C. Brochon, G. Pecastaings, G. Fleury, E. Pavlopoulou, L. Vignau, G. Hadziioannou, E. Cloutet, "Photoactive composite nanoparticles dispersed in water for organic photovoltaic application" under preparation

Communications par affiches

"Photo-active polymer inks for Organic Solar Cells", **Hierarchical assembled organic materials for electronics (HOMERIC)** Fall School (2014), Latresne, France

"Synthesis of photoactive ink : toward eco-friendly fully printed organic solar cells", **Journée de l'école doctorale** (2015), Talence, France (prix du meilleur poster par l'entreprise Michelin)

« Synthesis of photoactive ink : toward eco-friendly fully printed organic solar cells" **Hierarchical assembled organic materials for electronics (HOMERIC)**, international advisory board (2015), Talence, France

Communications orales

"Synthesis and formulation of photo-active inks for photovoltaic applications", communication orale, **Workshop on Organic Electronics**, LCPO-Linköping University (Sweden) (2015), France

"Synthesis and formulation of photo-active inks for photovoltaic applications", communication orale**, Science et Technologie des systèmes pi-conjugués (SPIC)** (2015), Angers, France

"Synthesis of photo-active inks: towards eco-friendly fully printed organic solar cells", communication orale, **Material Research Society (MRS)** (2016), Pheonix, Etats-Unis

"Synthesis of photo-active inks: towards more eco-friendly organic solar cells", communication orale, **International Symposium on Flexible Organic Electronics** (2016),Thessalonique, Grèce

Titre : Synthèse et formulation d'encres polymères pour la couche active de cellules solaires organiques

Résumé :

La limitation de solvants toxiques halogénés dans les procédés de préparation de matériaux photoactifs est primordiale pour l'industrialisation des cellules solaires organiques. L'objectif de ce travail de thèse a été de préparer des nanoparticules composées de polymère π-conjugué (PCDTBT) et d'accepteur d'électron ($PC_{71}BM$) dans l'eau ou en milieu alcool. Des particules composites (PCDTBT+ $PC_{71}BM$) ont été synthétisées avec deux types de stabilisants : un tensio-actif anionique (SDS) et un copolymère à blocs P3HT-*b*-PEO, ainsi que sans stabilisant. L'intégration de ces nanoparticules dispersées en phase aqueuse dans la couche active de cellules solaires organiques a par exemple permis d'obtenir des rendements de l'ordre de 1%.

Mots clés :

Cellule solaire organique, $PC_{71}BM$/PCDTBT, nanoparticules, copolymère à blocs, dispersion, miniemulsion, nanoprécipitation

---

Title: Synthesis and formulation of polymer inks for the active layer of organic solar cells

Abstract :

The replacement of halogenated toxic solvents is fundamental in photoactive material processes to make the organic photovoltaic sector viable. Herein the use of nanoparticles made of π-conjugated polymer (PCDTBT) and electron-acceptor ($PC_{71}BM$) was targeted in order to allow for instance the control of the phase separation between the two materials. Thus composite particles of PCDTBT and $PC_{71}BM$ have been synthesized using two kinds of stabilizers: an anionic surfactant (SDS) and a block copolymer P3HT-*b*-PEO, as well as without stabilizer. As an example such nanoparticles were integrated as active layer into photovoltaic device enabling a power conversion efficiency of 0.94% from aqueous based inks.

Keywords :

Organic solar cell, $PC_{71}BM$/PCDTBT, Nanoparticles, Block copolymer, dispersion miniemulsion, nanoprecipitation

---

Laboratoire de Chimie des Polymères Organiques
UMR 5629, 16 Avenue Pey-Berland, Pessac Cedex, F-33607, France.